



**UNIVERSITY of the
WESTERN CAPE**

**Reservoir quality, structural architecture, fluid evolution and their
controls on reservoir performance in block 9, F-O gas field,
Bredasdorp Basin, offshore South Africa.**

BY

**OLUWASEUN ADEJUWON FADIPE
B.Sc (Hons); M.Sc Cum Laude (UWC)**

**A thesis submitted in fulfilment of the requirements for the degree of
Doctor of Philosophy in Applied Geology (Petroleum Option)**

**DEPARTMENT OF EARTH SCIENCES, UNIVERSITY OF THE WESTERN
CAPE; BELLVILLE,
SOUTH AFRICA.**

**SUPERVISOR: Prof. Paul Carey
CO - SUPERVISOR: Prof. Jan Van Bever Donker
Prof. Akin Akinlua**

November 2012

DECLARATION

I declare that my research work titled “**Reservoir quality, structural architecture, fluid evolution and their controls on reservoir performance in block 9, F-O gas field, Bredasdorp Basin, offshore South Africa.**” is my own work, that it has not been submitted before for any degree or examination in any other university, and that all the sources I have used or quoted have been indicated and acknowledged by means of complete references

Oluwaseun A. FADIPE

November, 2012.



.....
Signature



ACKNOWLEDGEMENTS

“The greatest task or ambition must start with a simpler act” to meet the proposed target. My arrival at this destination has been made possible only through the assistance, guidance and prayers of so many people who are hereby gratefully acknowledged. Five years ago, an email conversation with the then Dean of Science (Senior Professor Jan Van Bever Donker) started me on the path I travelled at the University of the Western Cape. Firstly, I will like to glorify Almighty God, the giver of knowledge, wisdom and privilege, for seeing me through this great journey.

To my supervisors, Professor Paul Carey, Senior Professor Jan Van Bever Donker and Professor Akin Akinlua, I say a big thank you for your provoking comments, untiring efforts and interest in this work. You introduced me to the world of petroleum and structural geology and ensured that I receive water, care and nourishment from time to time. Your self-belief in me was indeed a great motivation. To the Department of Earth Sciences, University of the Western Cape, Bellville, South Africa, the head of the department, Professor Charles Okujeni, Wasielah Davids (departmental secretary) and all the members of staff, I say a big thank you for the good and cordial working relationship I enjoyed during my studies. My immense gratitude is due to Jonathan Salomo and Anthea Davids of Petroleum Agency of South Africa for his kind assistance with respect to Kingdom suite (SMT) and ArcGis software, your friendly responses added speed to the execution of this research. Without mincing words, I would also like to thank Dr. Solomon Adekola and Dr. Omotola Babajide for creating time to review some of my chapters. Special thanks go to Dr. Segun Akinyemi and my fellow post graduate students in Lab 60, Mr. Kehinde Agbele, Ayodeji Egunlusi (intimate brother), Mr Toyin Ayodele (Designer), Ms Melisa Crowley, Chris Samakinde, Deji Adebisi and others for creating an enabling environment that contributed to the success of this study.

I am particularly grateful to Inkaba yeAfrica for financing this research work while my appreciation goes to AAPG Kenneth H. Crandall 2011 grant and SPE Star fellowship 2012 for chosen me in the Africa region as one of the few recipients for these awards. Lastly, I appreciate my parents (Mr & Mrs Lawrence Oluwafemi Fadipe), my wife and son and immediate family Ms Bola Fadipe & Mrs Modupe Adefehinti-Nee Fadipe for their continuous support and encouragement.

DEDICATION

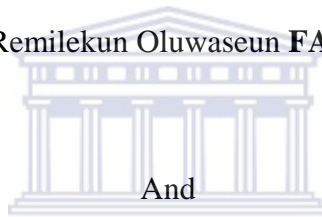
This project is dedicated to

The

Almighty God,

My lovely wife and son

Mrs Remilekun Oluwaseun **FADIPE**



UNIVERSITY *of the*
WESTERN CAPE
Demilade Louis **FADIPE**

**Reservoir quality, structural architecture, fluid evolution and their
controls on reservoir performance in block 9, F-O gas field,
Bredasdorp Basin, offshore South Africa.**

Oluwaseun A. FADIPE

Key words:

Reservoir quality

Wireline logs

Seismic interpretation

Multi-mineral analysis

Immobile water chemistry

Fluid ion ratios

Major oxides

Fluid inclusion stratigraphy

Fluid inclusion petrography

F-O gas field

Bredasdorp Basin.



ABBREVIATIONS

ICP-AES = Inductively coupled plasma-optical emission

ICP-MS = Inductively coupled plasma- mass spectrometry

IC = Ion chromatograph

XRF = X-ray fluorescence

XRD = X-ray diffraction

SEM /EDS= Scanning electron microscopy and energy dispersive spectroscopy

FIS = Fluid inclusion stratigraphy

COD = Coefficient of divergence

MIT OCW = Massachusetts Institute of Technology Open Course Ware

TSR = Thermochemical sulphate reduction

BSR = Bacterial sulphate reduction

SPWLA = Society of Petrophysical Wireline Log Analyst

PTPG = Proximal To Pay Gas

Rho = Spearman's correlation coefficient °C = degree Celsius

Mt = Million tonnes mg/kg = Milligram per kilogram

AMU = Atomic mass unit ppm = Part per million

mol/ l = Mole/litre mg/L = Milligram per litre

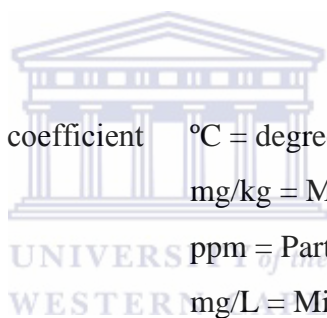
Ingress CO₂ = Ingressed carbon dioxide NO₃ = Nitrate

Ingress O₂ = Ingressed oxygen % = Percent

SO₄²⁻ = Sulphate LOI = Loss on ignition

PO₄ = Phosphate Cl⁻ = Chloride

mD = Milli darcies



ABSTRACT

The use of integrated approach to evaluate the quality of reservoir rocks is increasingly becoming vital in petroleum geoscience. This approach was employed to unravel the reason for the erratic reservoir quality of sandstones of the F-O gas field with the aim of predicting reservoir quality, evaluate the samples for presence, distribution and character of hydrocarbon inclusions so as to gain a better understanding of the fluid history. Information on the chemical conditions of diagenetic processes is commonly preserved in aqueous and oil fluid inclusion occurring in petroleum reservoir cements. Diagenesis plays a vital role in preserving, creating, or destroying porosity and permeability, while the awareness of the type of trap(s) prior to drilling serves as input for appropriate drilling designs. Thus an in-depth understanding of diagenetic histories and trap mechanisms of potential reservoirs are of paramount interest during exploration stage.

This research work focused on the F-O tract located in the eastern part of Block 9 on the north-eastern flank of the Bredasdorp Basin, a sub-basin of Outeniqua Basin on the southern continental shelf, offshore South Africa. The Bredasdorp Basin experienced an onset of rifting during the Middle-Late Jurassic as a result of dextral trans-tensional stress produced by the breakup of Gondwanaland that occurred in the east of the Falkland Plateau and the Mozambique Ridge. This phenomenon initiated a normal faulting, north of the Agulhas-Falkland fracture zone followed by a widespread uplift of major bounding arches within the horst blocks in the region that enhanced an erosion of lower Valanginian drift to onset second order unconformity.

This study considered 52 selected reservoir core samples from six wells (F-O1, F-O2, F-O3, F-O4, F-R1 and F-S1) in the F-O field of Bredasdorp Basin with attention on the Valanginian age sandstone. An integrated approach incorporating detailed core descriptions, wireline log analysis (using Interactive petrophysics), structural interpretation from 2D seismic lines (using SMT software) cutting across all the six wells, multi-mineral (thin section, SEM, XRD) analyses, geochemical (immobile fluid and XRF) and fluid inclusion (fluid inclusion petrography and bulk volatile) analyses were deployed for the execution of this study. Core description revealed six facies from the six wells

grading from pure shale (Facies 1), through progressively coarsening interbedded sand-shale “heterolithic facies (Facies 2 - 4), to cross bedded and minor massive sandstone (Facies 5 - 6). Sedimentary structures and mineral patches varies from well to well with bioturbation, synaeresis crack, echinoid fragments, fossil burrow, foreset mudrapes, glauconite and siderite as the main observed features. All these indicate that the Valanginian reservoir section in the studied wells was deposited in the upper shallow marine settings. A combination of wireline logs were used to delineate the reservoir zone prior to core description. The principal reservoirs are tight, highly faulted Valanginian shallow-marine sandstones beneath the drift-onset unconformity, 1At1 and were deposited as an extensive sandstone “sheet” within a tidal setting. The top and base of the reservoir are defined by the 13At1 and 1At1 seismic events, respectively. This heterogeneous reservoir sandstones present low-fair porosity of between 2 to 18 % and a low-fair permeability value greater than 0.1 to 10 mD. The evolution of the F-O field was found to be controlled by extensional events owing to series of interpreted listric normal faults and rifting or graben generated possibly by the opening of the Atlantic. The field is on a well-defined structural high at the level of the regional drift-onset unconformity, 1At1.

Multi-mineral analysis reveals the presence of quartz and kaolinite as the major porosity and permeability constraint respectively along with micaceous phases. The distribution of quartz and feldspar overgrowth and crystals vary from formation to formation and from bed to bed within the same structure. The increase in temperature that led to kaolinite formation could have triggered the low-porosity observed. Three types of kaolinite were recognized in the sandstone, (1) kaolinite growing in between expanded mica flakes; (2) vermiform kaolinite; and (3) euhedral kaolinite crystals forming matrix. Compositional study of the upper shallow marine sandstones in the Valanginian age indicates that the sandstones are geochemically classified as majorly litharenite having few F-O2 samples as subarkose with all F-O1 samples classified as sub-litharenite sandstone.

Most of the studied wells are more of wet gas, characterized by strong response of C₂ – C₅ with F-O1 well showing more of gas condensate with oil shows (C₇ – C₁₁) based on the number of carbon atom present. In some cases, sulphur species (characterized by the presence of H₂S, S₂, CS₂ and SO₂) of

probably thermal origin were identified while some log signatures revealed aromatic enriched sandstones possibly detecting nearby gas charges. The studied wells in the F-O field, based on fluid inclusion bulk volatile analysis are classified as gas discoveries except for F-O1 with gas condensate and oil shows. The integration of multi-mineral results and fluid inclusion studies show a dead oil stain with no visible liquid petroleum inclusion in the samples indicating the presence of quartz, kaolinite and stylolite as a major poro-perm constraint.



TABLE OF CONTENTS

DECLARATION	ii
ACKNOWLEDGEMENTS	iii
DEDICATION	iv
KEYWORDS	v
ABBREVIATIONS	vi
ABSTRACT	ix
TABLE OF CONTENTS	x - xv
LIST OF FIGURES	xv - xix
LIST OF TABLE	xix – xx

CHAPTER ONE **1 – 9**

1.0: Scientific background and state-of-the-art	1
1.1: Introduction and background information	1
1.2: Statement Problem	2
1.3: Location of study area	3
1.4: Research aims and objectives	5
1.5: Scope of work	6
1.6: General review of work on Bredasdorp Basin	6
1.7: General overview of subsurface studies	8
1.8: Exploration and production history on Bredasdorp Basin (BLOCK 9)	9

CHAPTER TWO (LITERATURE REVIEW) **10 - 32**

2.0: Literature review	10
2.1: Introduction	10
2.2: Core description	10
2.3: Well logs.....	12
2.3.1: Classification of geophysical wireline logs	14
2.3.2: Classification based on usage	14
2.3.3: Characteristics of selected wireline logs	14
2.3.4: Radioactive logs	14
2.3.5: Gamma ray logs	15
2.3.6: Neutron log	16

2.3.7: Density log	17
2.3.8: Sonic log	19
2.3.9: Spontaneous potential logs	20
2.3.10: Resistivity logs	22
2.4: Seismic interpretation	23
2.5: Depositional environments and facies discrimination	23
2.5.1: Sedimentary structures	23
2.5.2: Fossils	24
2.6: Reservoir quality predictions	24
2.6.1: Controls on reservoir quality prediction	25
2.6.2: Diagenetic studies	26
2.7: Quantitative mineralogy techniques	27
2.8: Geochemistry of pore water	29
2.9: Fluid inclusion studies	30
2.9.1: Understanding fluid inclusion stratigraphic data	31
2.9.2: Five types of FIS spectra	32
2.10: Hydrocarbon recovery	32
CHAPTER THREE	33 - 42
3.0: Geological background of Bredasdorp Basin	33
3.1: Introduction	33
3.2: Tectonic settings of Outeniqua Basin	36
3.3: Tectonic history of Bredasdorp Basin	39
3.4: Structural development of the Bredasdorp Basin	39
3.4.1: Rift phase (Mid-Jurassic - Valanginian)	40
3.4.2: Early drift phase (Hauterivian – Early Barremian)	40
3.4.3: Drift phase (Barremian – Turonian)	40
3.5: Sequence stratigraphic and chronostratigraphic framework of Bredasdorp Basin	41
3.6: Stratigraphy and sedimentary geology	42
CHAPTER FOUR	46 - 62
4.0 Materials, analytical techniques and experimental procedures.....	46
4.1: Introduction	46

4.1.1:	Wireline logs loading	47
4.1.2:	Core description procedure	48
4.1.3:	Petrophysical calculation procedures	49
4.1.3.1:	Volume of shale (V_{sh})	49
4.1.3.2:	Porosity	50
4.1.3.3:	Formation water resistivity	50
4.1.3.4:	Water saturation (S_w) and Hydrocarbon saturation (S_{hc}).....	51
4.1.3.5:	Bulk volume of water (V_b)	51
4.1.3.6:	Irreducible water saturation (S_{wir}).....	51
4.1.3.7:	Permeability (K)	51
4.1.4:	Thin section procedure	52
4.1.5:	Scanning electron microscopy procedure	53
4.1.6:	X-ray diffractometry (XRD)	54
4.1.6.1:	XRD diffractometry semi quantification procedure	55
4.1.7:	Pore water geochemistry procedure	56
4.1.7.1:	Electrical conductivity (EC) measurement	57
4.1.7.2:	Ion chromatography (IC)	57
4.1.8:	Inductively coupled plasma mass spectroscopy (ICP-MS)	59
4.1.9:	Bulk geochemical composition by x-ray fluorescence spectrometry	60
4.1.10:	Fluid inclusion stratigraphy procedure	62

CHAPTER FIVE (RESULTS AND DISCUSSION) 65 - 103

5.0:	Sedimentological, wireline logs and seismic results and discussion.....	65
5.1:	Introduction to sedimentological analyses	65
5.1.1:	Facies and depositional environment: results and discussion	65
5.1.2:	Core interpretation and sedimentological analysis of F-O1 well	68
5.1.3:	Core interpretation and sedimentological analysis of F-O2 well	71
5.1.4:	Core interpretation and sedimentological analysis of F-O3 well	74
5.1.5:	Core interpretation and sedimentological analysis of F-O4 well	75
5.1.6:	Core interpretation and sedimentological analysis of F-R1 well	78
5.1.7:	Core interpretation and sedimentological analysis of F-S1 well	80
5.1.8:	Summary of the depositional settings for the six wells in F-O field...	82
5.2:	Well log results and discussion of the F-O field	83
5.2.0:	Introduction to well log analyses	83

5.2.1: F-O1 well log interpretation	84
5.2.2: F-O2 well log interpretation	85
5.2.3: F-O3 well log interpretation	86
5.2.4: F-O4 well log interpretation	87
5.2.5: F-R1 well log interpretation	89
5.2.6: F-S1 well log interpretation	89
5.3: Cross-plot results and discussion of the F-O gas field	91
5.3.0: Cross-plotting compatible logs	91
5.3.1: F-O1 cross-plots	91
5.3.2: F-O2 cross-plots	92
5.3.3: F-O3 cross-plots	93
5.3.4: F-O4 cross-plots	93
5.3.5: F-R1 cross-plots	94
5.3.6: F-S1 cross-plots	95
5.4.0: Seismic interpretation and discussion	97
5.4.1: Introduction and brief background of the F-O gas field	97
5.4.2: Seismic profile discussion and interpretation of F93-203 line	100
5.4.3: Seismic profile discussion and interpretation of F90-149 line	100
5.4.4: Seismic profile discussion and interpretation of F80-010 line	103
5.4.5: Seismic profile discussion and interpretation of F93-201 line	103
5.4.6: Seismic profile discussion and interpretation of F93-218 line	104
5.4.7: Seismic profile discussion and interpretation of F80-055 line	104
CHAPTER SIX	111 - 163
6.0: Multi-mineral and geochemical analyses results and discussion	111
6.1: Introduction	111
6.1.1: Thin section petrography for F-O1 well	111
6.1.2: Thin section petrography for F-O2 well	114
6.1.3: Thin section petrography for F-O3 well	116
6.1.4: Thin section petrography for F-O4 well	118
6.1.5: Thin section petrography for F-R1 well	120
6.1.6: Thin section petrography for F-S1 well	122
6.2: Scanning electron microscopy (SEM) results and discussion	124
6.2.1: SEM petrography for F-O1 well	124

6.2.2:	SEM petrography for F-O2 well	126
6.2.3:	SEM petrography for F-O3 well	128
6.2.4:	SEM petrography for F-O4 well	130
6.2.5:	SEM petrography for F-R1 well	132
6.2.6:	SEM petrography for F-S1 well	134
6.3:	X-ray diffraction (XRD) results and discussion	136
6.3.1:	XRD results and discussion for F-O1 well	136
6.3.2:	XRD results and discussion for F-O2 well	138
6.3.3:	XRD results and discussion for F-O3 well	140
6.3.4:	XRD results and discussion for F-O4 well	142
6.3.5:	XRD results and discussion for F-R1 well	144
6.3.6:	XRD results and discussion for F-S1 well	146
6.4:	Geochemical analyses results and interpretation	148
6.4.1:	Immobile fluid geochemistry results and discussion	148
6.4.2:	Immobile fluid geochemistry of the studied well within the F-O gas field	148
6.4.3:	Immobile fluid ion ratios of the F-O gas field	152
6.5:	Bulk rock geochemistry results and interpretation	155
6.5.1:	X-ray fluorescence results and discussion	155
6.5.2:	Sediment maturity	159
6.5.3:	Weathering in source area	161
6.5.4:	ICV relation to recycling and weathering	162
6.5.5:	Provenance composition: Trace elements	163

CHAPTER SEVEN **166 - 179**

7.0:	Fluid inclusion stratigraphy/petrography results and discussion	166
7.1:	Introduction	166
7.1.1:	Fluid inclusion petrography of the F-O1 reservoir	167
7.1.2:	Fluid inclusion petrography of the F-O2 reservoir	168
7.1.3:	Fluid inclusion petrography of the F-O3 reservoir	169
7.1.4:	Fluid inclusion petrography of the F-O4 reservoir	169
7.1.5:	Fluid inclusion petrography of the F-R1 reservoir	170
7.1.6:	Fluid inclusion petrography of the F-S1 reservoir	171
7.2:	Fluid inclusion stratigraphy results and discussion	172

7.2.1:	Fluid inclusion stratigraphy results and discussion of F-O1 well	173
7.2.2:	Fluid inclusion stratigraphy results and discussion of F-O2 well	173
7.2.3:	Fluid inclusion stratigraphy results and discussion of F-O3 well	174
7.2.4:	Fluid inclusion stratigraphy results and discussion of F-O4 well	175
7.2.5:	Fluid inclusion stratigraphy results and discussion of F-R1 well	176
7.2.6:	Fluid inclusion stratigraphy results and discussion of F-S1 well	176
7.2.7:	Fluid inclusions stratigraphy abbreviations	178
7.3:	General diagenetic sequence of the F-O gas field	179

CHAPTER EIGHT **181 - 183**

8.0:	Conclusions and recommendations	181
8.1:	Introduction	181
8.2:	Conclusions	181
8.3:	Main scientific contributions of the dissertation	183
8.4:	Recommendations	183
8.5:	Conference contributions	183

LIST OF FIGURES

Figure 1:	Framework diagram of the thesis	3
Figure 2:	Maps showing the location of the study area and wells within Block 9	4
Figure 2.1:	Sidewall-Coring Scheme (modified from Schlumberger, 1972)	12
Figure 2.2:	Gamma ray tool (modified from Serra, 1984)	15
Figure 2.3:	(A) Schematic of Compensate neutron tool (B) Schematic trajectories of neutron in limestone with no porosity and pure water	17
Figure 2.4:	Schematic of dual-spacing density logging device	18
Figure 2.5:	Sonic Logging tool showing Receiver (R) and Transmitter (T).....	20
Figure 2.6:	Spontaneous Potential Logging tools (modified from Rider, 1996)	21
Figure 3.0:	South Africa continental margin and oceanic crust (Modified from Broad 2004)	33
Figure 3.1:	Western, eastern and southern offshore zones of South Africa (Petroleum Agency SA brochure 2003)	34
Figure 3.2:	Topography derived from satellite image showing sea floor and continental margin surrounding South Africa (modified from Broad 2004)	35

Figure 3.3: Formation of Half graben from a series of normal faults dipping in the same direction (modified from Hudson et al., 1998)	36
Figure 3.4: (a) Early drift phase in the Valanginian (1At1) – Hauterivian (6At1) showing the movement of micro plates: Falkland Plateau (FLK) Patagonia (PAT) and Maurice-Ewing Bank plates (MEB) past south coast of Africa (b) Late drift phase in the Hauterivian (6At1) onwards (modified from Broad, 2004)	37
Figure 3.5: Oblique rift half-graben sub-basins of Outeniqua Basin Bredasdorp, Pletmos, Gamtoos and Algoa (modified from Broad, 2004)	38
Figure 3.6: The rift phase in the Late Jurassic-Lower Valanginian showing the break up of Africa, Madagascar and Antarctica (modified from Broad, 2004)	38
Figure 3.7: Schematic cross-section of Bredasdorp Basin showing inverted graben (modified from PASA Brochure, 2004/05)	41
Figure 3.8: Sequence chronostratigraphic framework of the Bredasdorp Basin (PASA, 2007)	42
Figure 3.9: A: Seismic profile with identified sequence boundaries. B: Schematic cross section (modified from Broad, 2004)	43
Figure 3.10: (A) Basin floor fan canyon, (B) Channel-Levee complex on basin floor fan (C) prograding complex terminates canyon filling episode (modified from Broad, 2000)	45
Figure 4.1: The flow chart of the research methodology	47
Figure 4.2: Scanning and detection system in scanning electron microscope	53
Figure 4.3: BRUKER D8 ADVANCE XRD instrument with pw3830 X-ray generator operated at 40Kv and 40mA	55
Figure 4.4: Hanna HI991301 pH meter with portable pH/Temperature probe	56
Figure 4.5: Ion chromatography system-Dionex ICS-1600 (RFIC)	57
Figure 4.6: ICP optical emission spectrometer (Varian 710-ES)	59
Figure 4.7: Axios from PANalytical with a 2.4kWatt Rh x-ray tube	62
Figure 4.8: Fluid inclusion petrography instrument	63
Figure 4.9: Schematic diagram showing the processes involved in carrying out fluid inclusion stratigraphy	64
Figure 5.10: Cores showing sedimentary structures of the F-O field samples	66
Figure 5.11: Cores showing sedimentary structures of the F-O field samples	67
Figure 5.12a: Facies log of F-O1 well Bredasdorp basin, offshore South Africa	69
Figure 5.12b: General legend of the F-O field core graph	70

Figure 5.13a: Facies log of F-O2 well Bredasdorp Basin, offshore South Africa	72
Figure 5.13b: Facies log of F-O2 well Bredasdorp Basin, offshore South Africa	73
Figure 5.14: Facies log of F-O3 well Bredasdorp Basin, offshore South Africa	75
Figure 5.15: Facies log of F-O4 well Bredasdorp basin, offshore South Africa	77
Figure 5.16a: Facies log of F-R1 well Bredasdorp basin, offshore South Africa	79
Figure 5.16b: Facies log of F-R1 well Bredasdorp basin, offshore South Africa	79
Figure 5.17: Facies log of F-S1 well Bredasdorp basin, offshore South Africa	81
Figure 5.21: well section diagram of F-O1 well	85
Figure 5.22: well section diagram of F-O2 well	86
Figure 5.23: well section diagram of F-O3 well	87
Figure 5.24: well section diagram of F-O4 well	88
Figure 5.25: well section diagram of F-R1 well	89
Figure 5.26: well section diagram of F-S1 well	90
Figure 5.31: (A) Crossplots of neutron–density (B) Core porosity-permeability of the F-O1 gas field	91
Figure 5.32: (A, B) Crossplots of neutron–density (C, D), core porosity-permeability of the F-O2 gas field	92
Figure 5.33: (A) Crossplots of neutron–density (B) Core porosity-permeability of the F-O3 gas field	93
Figure 5.34: Crossplots of neutron–density F-O4 gas field	94
Figure 5.35: Crossplots of neutron–density F-R1 gas field	95
Figure 5.36: (A, B, C) Crossplots of neutron–density (D, E) Core porosity- permeability of the F-S1 gas field	96
Figure 5.41: Purple lines are a subset of 143 2D seismic lines in the vicinity of the study area while black thin lines are subsets of 44 2D seismic lines in the nearest vicinity of the 6 wells	98
Figure 5.42: Seismic reference reflector nomenclature of Pletmos basin historically used for Bredasdorp basin	99
Figure 5.43: Interpreted seismic profile revealing a distinct normal fault directly on the mapped base of unconformity	101
Figure 5.44: Interpreted seismic North-South revealing pronounce listric faults with a retrogradational sequence between TLVS and Top of log horizons	102
Figure 5.45: Interpreted seismic across North-Southwest showing pronounce faults with synclinal and anticlinal structures	106

Figure 5.46: Interpreted seismic Northwest-Southeast showing pronounced erosional surface beneath the seafloor	107
Figure 5.47: Interpreted seismic revealing breaks in surface layering between 22At1 and K horizon accompanied by listric faults	108
Figure 5.48: Interpreted seismic Northwest-Southeast showing progradational sequence towards Southeast section	109
Figure 5.49: Interpreted 3D view of the combined seismic profiles showing the different mapped horizons and the interconnectivity of the several mapped layers.....	110
Figure 6.11: Thin section photomicrograph of F-O1 reservoir samples.....	111
Figure 6.12: Thin section photomicrograph of F-O2 reservoir samples.....	115
Figure 6.13: Thin section photomicrograph of F-O3 reservoir samples.....	117
Figure 6.14: Thin section photomicrograph of F-O4 reservoir samples.....	119
Figure 6.15: Thin section photomicrograph of F-R1 reservoir samples.....	121
Figure 6.16: Thin section photomicrograph of F-R1 reservoir samples.....	123
Figure 6.21: Scanning electron micrograph of F-O1 reservoir samples.....	125
Figure 6.22: Scanning electron micrograph of F-O2 reservoir samples.....	127
Figure 6.23: Scanning electron micrograph of F-O3 reservoir samples.....	129
Figure 6.24: Scanning electron micrograph of F-O4 reservoir samples.....	131
Figure 6.25: Scanning electron micrograph of F-R1 reservoir samples	133
Figure 6.26: Scanning electron micrograph of F-S1 reservoir samples	135
Figure 6.31: XRD qualitative and semi-quantitative plot of F-O1 well	137
Figure 6.32: XRD qualitative and semi-quantitative plot of F-O2 well	139
Figure 6.33: XRD qualitative and semi-quantitative plot of F-O3 well	141
Figure 6.34: XRD qualitative and semi-quantitative plot of F-O4 well	143
Figure 6.35: XRD qualitative and semi-quantitative plot of F-R1 well	145
Figure 6.36: XRD qualitative and semi-quantitative plot of F-S1 well	147
Figure 6.41: pH plot of the F-O gas field	150
Figure 6.42: Eh-pH plot of the F-O field	151
Figure 6.43: Stability curve of various diagenetic minerals in terms of pH and Eh..	151
Figure 6.44a: Vertical distribution of dissolved-cations concentrations in pore water of F-O field	153
Figure 6.44b: Vertical distribution of dissolved-cations concentrations in pore water of F-O field	154

Figure 6.51: (A) Tectonic discrimination diagram (B) Alkali content of the F-O field gas sandstone	157
Figure 6.52: Classification of terrigenous sandstone using Log (Na ₂ O/K ₂ O) versus Log (SiO ₂ /Al ₂ O ₃) from Pettijohn et al., (1972), modified by Herron (1988)	160
Figure 6.53: Geochemical classification of F-O field sandstone diagram (modified from Herron, 1988)	160
Figure 6.54: Diagram showing weathering variations (Chemical index of alteration of the F-O gas field	162
Figure 6.55: Plot of Th/Sc against Zr/Sc for sandstones from F-O gas field (after McLennan et al., 1993)	164
Figure 6.56: Th/Co against La/Sc diagram for sandstone samples from F-O gas field (After Culler, 2002 in Nagaragan et al., 2007)	164
Figure 7.11: Fluid inclusion photomicrograph of F-O1 reservoir sandstone	167
Figure 7.12: Fluid inclusion photomicrograph of F-O2 reservoir sandstone	168
Figure 7.13: Fluid inclusion photomicrograph of F-O3 reservoir sandstone	169
Figure 7.14: Fluid inclusion photomicrograph of F-O4 reservoir sandstone	170
Figure 7.15: Fluid inclusion photomicrograph of F-R1 reservoir sandstone	170
Figure 7.16: Fluid inclusion photomicrograph of F-S1 reservoir sandstone	171
Figure 7.21: Bulk volatile analysis (FIS) of samples from F-O1 reservoir sand	173
Figure 7.22: Bulk volatile analysis (FIS) of samples from F-O2 reservoir sand	174
Figure 7.23: Bulk volatile analysis (FIS) of samples from F-O3 reservoir sand	174
Figure 7.24: Bulk volatile analysis (FIS) of samples from F-O4 reservoir sand	175
Figure 7.25: Bulk volatile analysis (FIS) of samples from F-R1 reservoir sand	176
Figure 7.26: Bulk volatile analysis (FIS) of samples from F-S1 reservoir sand	177
Figure 7.3: Generalized diagenetic model of F-O gas field studied wells	180

LIST OF TABLES

Table 1.0: Names and location of wells	5
Table 2.1: A classification of sedimentary structures (Selley, 1988)	17
Table 4.1: Petrophysical properties nomenclatures	52
Table 6.31: mineralogical composition of the F-O field samples from XRD.....	146
Table 6.41: Physico-chemical results of immobile water from the F-O field	150

Table 6.51: Mean composition of principal classes and average Valanginian age sandstone of the F-O gas field156

Table 6.52: Major oxide (wt %) compositions of the F-O field selected samples ... 158

Table 7.2: FIS results showing the summary of results of the F-O gas field165

Table 7.3: Summary of classification of fluid inclusion of the F-O gas field177

REFERENCES **184 - 209**

LIST OF APPENDIX **210 - 212**

Appendix 1: Mineralogical composition of F-O gas field samples from XRD 210

Appendix 2: Physico-chemical compositions of the immobile water extracts from the F-O field samples211

Appendix 3: Calculated results from major oxide analysis of the F-O field samples212



CHAPTER ONE

1.0: Scientific background and state-of-the-art

1.1: Introduction and background information

With an upbeat in hydrocarbon exploration effort in the Bredasdorp Basin, emphasis is increasingly laid on the petroleum system processes of the basin. The passive continental margins of South Africa are virtually unexplored although some potential is assumed and even proven by the F-O gas field (study area) offshore South Africa. The F-O tract is located in the eastern part of Block 9 on the north-eastern flank of the Bredasdorp Basin, a sub-basin of the Outeniqua Basin on the southern continental shelf, offshore South Africa (Mudaly, et al., 2009). The F-O field is situated 110 km from the nearest landfall and 40 km SE of the F-A platform, which supplies gas and condensate to the PetroSA GTL plant located in Mossel Bay (Mudaly, et al., 2009). A considerable work has been carried on the F-O gas field by PetroSA; however the understanding of the fluid evolution has not yet been reported in any literature.

This study involves reservoir quality prediction and the estimation of petrophysical properties such as porosity, permeability and water saturation deduced from core analysis and well logs, structural interpretation from seismic and fluid inclusion. The principle of measurement involved in core analysis and geophysical logs are well understood and the techniques have made continuous sophisticated advancement. In solving reservoir problems the focus has shifted from a single approach to an integrated approach. This is becoming highly imperative in petroleum geosciences because it has proved that it is worth it in solving pending challenges (Ketzer, 2002).

One of the most important aspects of petroleum exploration is the knowledge of the diagenetic histories of potential reservoirs because diagenesis plays a vital role in preserving, creating or impairing porosity and permeability. Upon sedimentation and subsequent burial, diagenetic reactions occur between sediments and surrounding fluids in response to increase in temperature and pressure (McLimans, 1987). Information on the physical and chemical conditions of the diagenetic processes is commonly preserved in aqueous and oil fluid inclusions occurring in petroleum reservoir cements. Basins on the Atlantic margin often display a complex history of fluid migration, the successful modelling of which is crucial to successful appraisal of

potential hydrocarbon systems (e.g. Parnell et al., 1998; Illife et al., 1999). During and after subsurface fluid migration, including oil and gas migration and charging of reservoirs, small fluid samples are encapsulated and micro-fracture annealing.

Until recently, diagenesis, fluid dynamics and sequence stratigraphy were treated as two independent disciplines in the area of sedimentary geology. In Bredasdorp Basin, there is possibility of a diagenetic alteration related to sequence boundaries which includes mechanical clay infiltration and formation which can affect the reservoir properties in a basin (Adekola, et al., 2009).

Granulation seam has also been reported by some researchers in the Bredasdorp Basin (Schalkwyk, 2005, Olajide, 2005), this seam is mostly associated with fault zone thickening in high porosity reservoir sandstone (Meadows, et al., 1997). The presence of granulation seams throughout faulted sandstones may lower the bulk permeability of the reservoir; therefore it is imperative to take into account in the course of this research work this challenging factor (granulation seam) for optimum productivity in the selected wells for evaluation.

Key petrophysical properties of reservoir sequence are determined by their individual mineral compositions and are routinely evaluated through the analysis of cores and geophysical well logs; however, mineralogical studies and fluid evolution are seldom incorporated in reservoir assessment. Routine geophysical log evaluation revealed inconsistent result when compared to core analysis data because of the influence of minerals on various logs. Hence, it is essential that mineralogical studies be included in reservoir assessment for effective log calibration (Harris, 1992, Weber et al., 1978, Hearn et al., 1984). An integrated approach involving the interpretation of seismic, log and core information, together with fluid and pressure analyses by the universities and oil companies will be a valuable base for field development studies, particularly in circumstances where major investment decisions are taken with benefit of few appraisal wells. This situation is regularly encountered in most prolific basins in the world (North Sea reservoir development, Niger Delta Basin) where major portion of capital investment is committed early in project life before significant reservoir performance has been established.

1.2: Statement Problem

The paucity of research output from producing wells in F-O gas field has made this work to be inevitable. Most of the producing wells have stopped operation due to one reason or the other such as inadequate information about the source rock

generating potential, fluid dynamics and incomplete reservoir assessment, over pressure leading to blow out, mineralogical complexities affecting the reservoir properties e.t.c. Accurate determination of hydrocarbon type within the study wells is crucial for economic assessment and production strategy design for the study area. As a result of these challenges, a study must be carried out by the University in collaboration with the oil companies/research institutes to bridge the gap and reduced the lack of information.

The application of an integrated approach engaging multi-mineral analysis, structural interpretation through seismic profiles and fluid inclusion studies will serve as techniques to understand the diagenetic processes, trap mechanisms and hydrocarbon type within the study area.

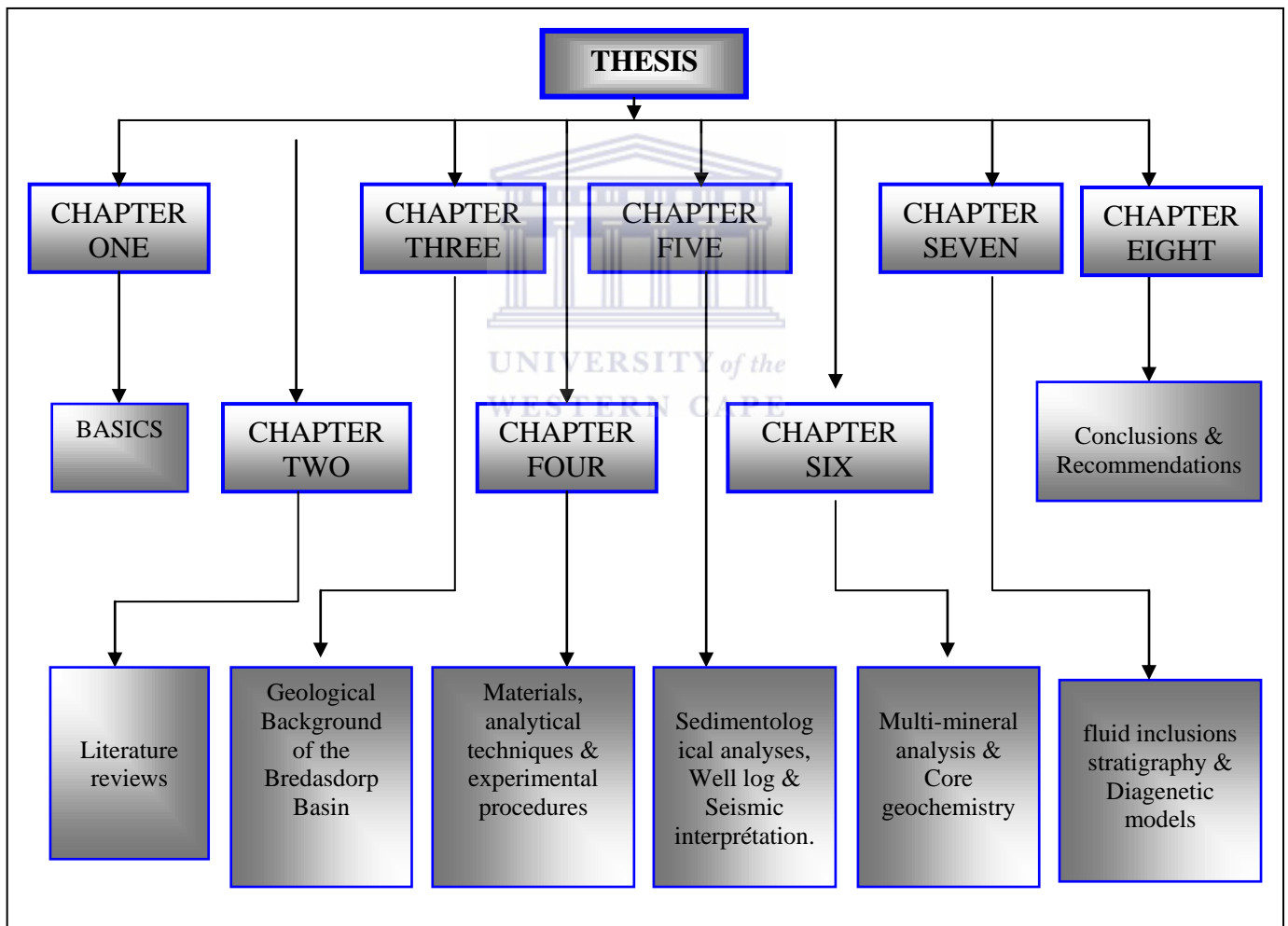


Figure 1: Framework diagram of the thesis

1.3: Location of study area

The Bredasdorp Basin is situated off the coast of South Africa, it covers approximately 18, 000 km² beneath the Indian Ocean along the Southern coast of South Africa., Southeast Cape Town and Southwest of Port Elizabeth while the F-O

field is situated 110 km from the nearest landfall and 40 km Southeast of the F-A platform, which supplies gas and condensate to the PetroSA GTL plant located in Mossel Bay (Mudaly et al., 2009). The basin covers about 18,000 sq km in general and less than 200 water depth (Wood, 1995). The study area is bounded in the west and east by geographical co-ordinates (F-O1) Lat: 35°08'54.05"S, Long: 22°31'48.45" E and (F-S1) Lat: 35°09'29.07"S and Long: 22°41'45.88"E (Table 1.0) of each studied well which are located within the PetroSA's concession block 9 F-O gas field. Figure 2 shows the location of the Block 9 and the distribution of the six selected wells for this study.

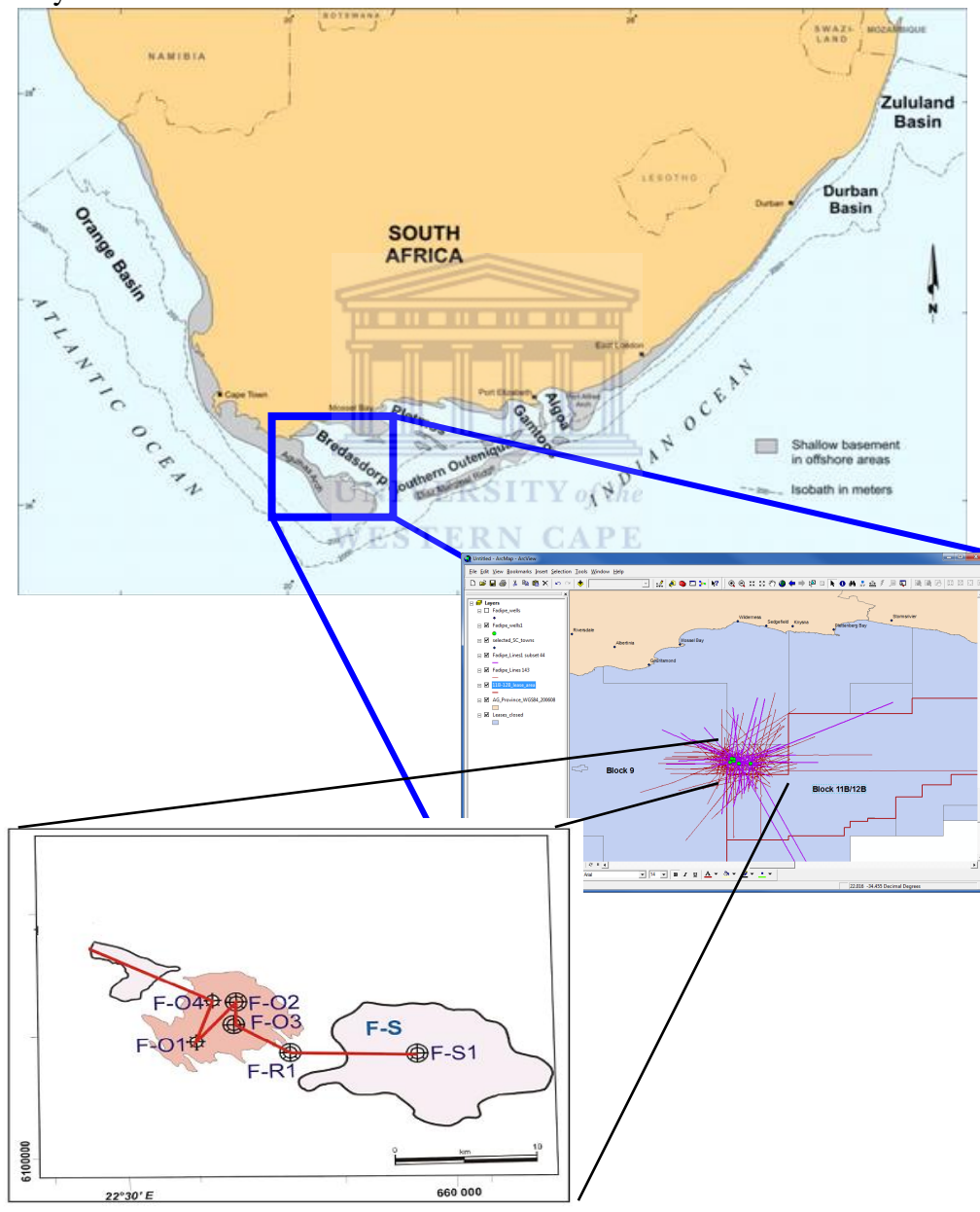


Figure 2: Maps showing the location of the study area and wells within Block 9 (Modified from Broad, 2004).

Table 1.0: Names and Location of Wells

Well Name	Location	UTM Co-ordinates	Depth (MD)
F-O1	Lat: 35° 08' 54.05" S Long: 22° 31' 48.45" E	639384.6m E 6109719m N	3914
F-O2	Lat: 35° 07' 10.99" S Long: 22° 33' 33.34" E	642088.7m E 6112853m N	3891
F-O3	Lat: 35° 08' 15.54" S Long: 22° 33' 32.46" E	642035.2m E 6110864m N	3950
F-O4	Lat: 35° 06' 59.483" S Long: 22° 32' 27.488" E	640427.123m E 6113232.902m N	3890
F-R1	Lat: 35° 09' 25.27" S Long: 22° 36' 01.98" E	645784.9m E 6108656m N	4562
F-S1	Lat: 35° 09' 29.07" S Long: 22° 41' 45.88" E	654484.9m E 6108395m N	3950

1.4: Research aims and objectives

This research is aimed at employing the broad use of different reservoir characterization methodologies to understand the fluid dynamics, to improve our knowledge of spatial distribution and internal characteristics of sediment bodies that constitute units in F-O gas field, Bredasdorp Basin. This will be achieved through identification, evaluation and characterization of the reservoir and seal rocks, understanding of the trapping mechanism coupled with the use of fluid inclusion stratigraphy to tackle the challenges within the field. The physical rock characteristics such as fluid type, lithology and hydrocarbon bearing zones were qualitatively defined while parameters such as porosity, permeability, resistivity of formation water, water saturation and hydrocarbon saturation was estimated using Interactive Petrophysics for selected reservoir intervals in all the wells. Wire line log data was be further used to identify productive zones to determine depth, thickness of zones, to distinguish between oil, gas or water in the reservoir and to estimate the hydrocarbon reserves.

The main objectives of this study is to predict the reservoir quality, evaluate samples for presence, distribution and character of hydrocarbon inclusion in order to understand the fluid history and possibly recommend more wells to be drilled based on the findings from the studied wells. The research approach shall be:
To determine the mineralogy of a range of core samples from a selected reservoir interval in the six wells.

- (i) Establish the correlation between mineralogy, geophysical log response and key rock properties.
- (ii) Use these correlations to refine the methods of petrophysical interpretations from the logs based on specific mineralogical characteristics.
- (iii) Classify the trap mechanism and establish the effect of fluid alteration on gas production.

1.5: Scope of study

The scope of this study is as follows:

- ✚ Identification of the lithologies/reservoir zones from well log character.
- ✚ Integration of conventional core analysis data where available with interpreted log sections.
- ✚ Sedimentological description and interpretation of cores from six wells (F-O1, F-O2, F-O3, F-O4, F-S1 and F-R1).
- ✚ Determination, classification and definition of sediment facies and depositional environments using macroscopic core description, petrography and wireline logs.
- ✚ Mapping of unconformities and major fault based on seismic reflection terminations and truncations
- ✚ Delineation of reservoir zones from the integration of different logs.
- ✚ Establishment of the diagenetic history of sandstones: determination of major factor controlling lateral and vertical variability in reservoir quality.
- ✚ Establishment of the hydrocarbon type through the interpretation of fluid inclusion stratigraphy (FIS).

1.6: General review of work on Bredasdorp Basin

Some studies have been carried out on Bredasdorp Basin with a few available literatures relating to the general geology, stratigraphy, paleo-geography, structural features and hydrocarbon potential of the reservoir rocks.

Considering the nature of this research, this section begins with a general overview of the various works that previous workers have carried out in the Bredasdorp Basin. The Basin is characterized by deep marine sedimentation. Sedimentary processes such as bulk emplacement, debris flow; turbidite current and slumping have put together its sequence and reservoir geometry. Accumulated terrigenous materials (land derived) on the continental slope and continental rise are delivered into deep sea by slumping

(movement of sediment piles as mass) or by turbidity currents which is the rapid movement of large slurries (mixture of sediment and water) down slope. Turbidity currents are impelled by gravity and can travel far into sea. Sediment delivery is accelerated by sea level falls during which the coast is at the shelf break making rivers empty sediment directly onto the slope (<http://geology.uprm.edu/MorelockSite/morelockonline/digbk/ContMarg.pdf>).

Turner et al., (2000) was able to identify the respective sea level falls during early Aptian and mid-Albian resulting in materials being eroded from pre-existing Highstand shelf sandstones and transported into central basin by turbidity currents from the west-southwest. Turner et al., (2000) was also able to recognize sandstone reservoir in the Bredasdorp Basin to have consist of stack and amalgamated channels and lobes. Fan lobes have coarsening-upward or blocky log motif, while channelized reservoirs are blocky or fining upward.

Frewin et al., (2000) discussed the geologic characterization of deep-marine channel lobe system. The Oribi and Oryx oil field are part of the oil fields discovered by Soekor E and P both having hydrocarbon accumulation within the turbidite system in the Cretaceous drift succession of the Bredasdorp Basin. Based on the seismic recognition of multiple unconformities within the drift successions, stratigraphic naming reflects a sequence stratigraphic approach.

According to Brown et al, (1996); sequence defined by significant unconformities recognized on seismic sections were assigned numbers (1-22) while unconformities were designated by the sequence overlying them (1A, 4B etc) and by their nature chart (Petroleum Agency SA, 2004/2005).

Southern oil exploration corporation (now PetroSA), through a comprehensive sequence stratigraphic approach which was based on seismic recognition of multiple unconformities, developed the stratigraphic nomenclature for South African offshore sedimentary successions and various structural elements such as basins, sub-basins, structural highs and faults within the drift successions. The drift succession refers to the sets of stratigraphic units, the deposition of which has been referenced to the initial and later period of the gradual west-southwest-ward plates of Southern coast of Africa. These movements led to the creation of Outeniqua sub-basins which are the Bredasdorp, Pletmos, Gamtoos and Algoa Basins. The boundary of the Pre-drift successions is marked by the drift-onset unconformity (1At1), which occurred in the Lower Valanginian. Post drift successions refer to stratigraphic units which are related

to the development of true passive margin after the cessation of transitional rift-drift in the mid Albian (Petroleum Agency SA 2004/2005).

McAloon et al., (2000) identified three lithofacies by using core, well log and dip data, it was concluded that the massive amalgamated deep-marine sandstones which make up the larger part of the E-BD reservoir, represents extensive mass flow deposits. It was further stated that the distribution of these deposits have been controlled by significant erosional feature on the regional unconformity which essentially represent easterly-trending valley on the basin floor. It is comparable to submarine canyon extending through the E-BD area and acting as conduit for sand sourced from the shelf to the west.

1.7: General overview of subsurface studies

The study of the subsurface has improved tremendously over the years with the use of geophysical methods. Measurements within a geographical restricted area are used to establish the distribution of physical properties that reflect the distinguishing characteristics of the local subsurface geology. Once these methods especially seismic have been used to locate favourable geological features for likely hydrocarbon accumulation and subsequently a possible reservoir position identified, an exploratory well will be drilled through the prospective structure to open way for various techniques of evaluating the resources. Hydrocarbon accumulation is mostly found in the pore spaces of reservoir rocks such as sandstone, limestone and dolomites. In order to have an idea of how viable economically a reservoir is, some basic petrophysical parameters need to be generated and the reservoir quality needs to be evaluated. These include porosity, permeability, hydrocarbon saturation, thickness and extent of reservoir formation and the depositional environments.

Well logging is the process of recording various physical, chemical, electrical and other properties of the rock/fluid mixture penetrated by drilling a well into the earth's crust (Crain, 2004). Petrophysics encompasses standard log analysis and various techniques of characterizing reservoir rocks through derivation of conventional reservoir parameters. It is by far one of the most important and useful field of science available to petroleum geologists. However, for a clearer and better understanding of any reservoir performance, the integration of sedimentological studies with reservoir analysis is very imperative.

In the early stages of planning exploration and development in a new area, the surface seismic survey is used to delineate prospective structural or stratigraphic traps.

Improvement in digital filtering has led to high quality results under favourable conditions. Reservoir characterization and evaluation have progressed beyond the conventional manual petrophysical analysis and their use in estimating recoverable hydrocarbons in reservoir rocks. Several windows based softwares packages for petrophysical analysis are available. Where available, well and seismic data are input in the correct format, they can be used to carry out petrophysical analysis and visualize the distribution of reservoirs parameters within a framework of 3D reservoir model. Good examples are PETREL 2011, Seismic Micro Technology (SMT), Interactive Petrophysics (IP) and Fast Tracker (FugroJason).

1.8: Exploration and production history on Bredasdorp Basin (BLOCK 9)

The Bredasdorp Basin has been the focus of seismic and drilling activity since 1980 (PASA, 2003). Exploration drilling was active from 1981 to 1991 and about 181 exploration wells have been drilled in this area. Exploration has led to the discovery of several oil and gas fields, and the commercial production of oil and gas. Presently exploration in South Africa is managed by the Petroleum Agency of South Africa (PASA), responsible for soliciting bids for offshore acreage of the southern and western coasts of South Africa (PASA, 2004/5).

Extensive exploration for more than thirty years has revealed no onshore hydrocarbons. Block 9 is located offshore South Africa within the Bredasdorp Basin. SOEKOR (Southern Oil Exploration Corporation), the state owned oil and gas exploration company, (petroleum oil and gas corporation of South Africa) discovered gas and oil deposits offshore in Block 9 in the Bredasdorp Basin. In Block 9, a total of 165 wells have been drilled, thirty-two of these wells are classified as oil and/or gas discoveries. The discoveries are relatively small and the economic viability is still being assessed. In the Bredasdorp Basin, the F-A gas and condensate fields, discovered in 1980 by Soekor are being exploited by Mossgas. Production from these fields started in 1992 and an average of 194 million cubic feet of gas and 9,500 barrels of condensate are being produced per a day. A pipeline of 91km conveys gas and condensate to the Mossgas Synfuels plant at Mossel Bay, where petrol, diesel and kerosene are produced. The EM and Satellite gas fields situated 120 km south west of the Mossel Bay, in the Bredasdorp Basin (Block 9) were discovered in 1984 in early Cretaceous sands (PASA brochure 2004/5).

CHAPTER TWO

2.0: Literature review

2.1: Introduction

The topics included in this review focused on core description, geophysical logs, depositional environments, facies and diagenetic studies. The discussion on core analysis concentrates on the possible source of errors that may arise during the analysis. Attention is also paid to the principle of various geophysical logging measurements and to the effect of different minerals on the logs and the procedures used in the evaluation of the rock properties. The review of various mineralogical techniques is limited to those most commonly used for sedimentary rocks and the discussion is based on the applicability of each technique in reservoir evaluation. An overview of the various application of mineralogy in reservoir assessment is also included.

2.2: Core description

Core analysis is the starting point for a wide range of geologic and engineering studies; it is the only tool in the reservoir assessment that directly measures many important formation properties. The analysis may aim to determine among other things porosity, permeability, and grain size distribution, grain density, and mineral composition, effect of overburden stress and sensitivity of fluid (Bateman, 1985).

Laboratory core analysis could provide very accurate measurements. Laboratory test procedure, core handling and sample preparation may introduce damage to the core if incorrectly performed (Sinclair and Duguid, 1990). Destructive processes, such as plugging may cause partial disintegration of formation and thus significantly modify the results of petrophysical property measurement. Partial disintegration of cores, due to aforementioned process (plugging) has been noted to cause highly optimistic permeability measurements (Hurst, 1987). Unnecessary breakage may also be introduced when removing the cores from the core barrel, transporting them, and laying them out in the laboratory. Laboratory procedures such as drying of the sample may drive off all the water in the clay particles (Sinclair and Duguid, 1990). This may cause misidentification of minerals on the petrophysical properties (e.g. swelling).

Core analysis has evolved from qualitative geological description to the use of sophisticated analytical tools, such as scanning electron microscope (SEM), x-ray diffraction (XRD), yet there are no uniform accepted experimental procedures or

calibration standard (Jahasz, 1990). There may be significant discrepancies in the analysis of a particular reservoir by different laboratories and the results may be valid only within set of procedures followed by each individual laboratory. For example, porosity measured in dried core plugs using humidity controlled methods has been noted to be consistently lower than those measured from oven dried core plugs (Penney and Looi, 1996). Analysis of similar set of core samples by different laboratories according to their respective procedures may thus result in considerable differences in the assessment of potential reservoir sequence. The manner of drying core samples, for examples was shown to be critical in preserving the in-situ morphology of some minerals (illite) and in understanding the differences in permeability measurements obtained by core analysis and well test data (Pallat et al., 1984). A similar observation has been noted by McHardy et al., (1982) in comparing the morphology of illite contained in samples that have undergone different drying processes. Due to lack of standards, the validity of rock properties evaluated based on particular core analysis procedures may not always be considered, and estimation of the magnitude of errors that may arise during the analysis is not possible. Thus, the errors are most likely to carry on to where core analysis results are applied. One of the serious consequence is that core analysis results may be seriously different from geophysical log data, and, in such cases, predictions from geophysical logs are sometimes doubtful without consideration of laboratory analytical procedures.

Other coring methods such as sidewall coring could be carried out when additional rock samples are required after the well has been drilled and before it has been cased. Sidewall cores are obtained with wireline tool from which a hollow cylindrical bullet is fired into the formation and retrieved after each bullet has been fired into the formation wall by free pull by wires connecting the barrel to the gun (Fig. 2.1). Core barrels are available for penetrating formations of different hardness. The type of barrel and size of charges are varied to optimize recovery in different formations. The problem with coring lies in the tendency of formation samples to undergo physical changes on its journey from the bottom of the well to the surface. More sophisticated coring mechanism that can preserve the orientation, pressure and original fluid saturations of the core samples have been developed.

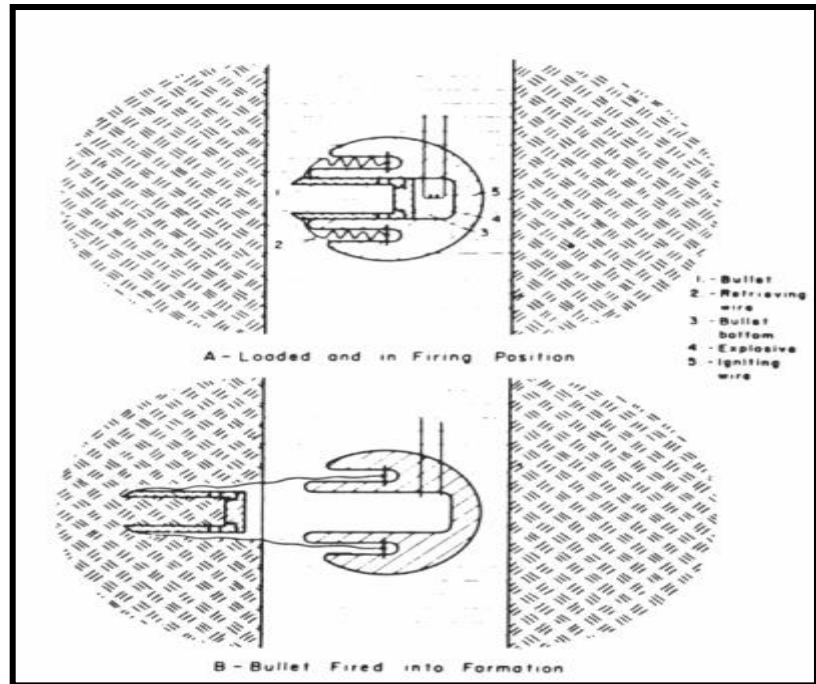


Figure 2.1: Sidewall-Coring Scheme (modified from Schlumberger, 1972).

2.3: Well logs

Well logs are class of the most useful and important tools available to petroleum geologists. They are products of survey operations consisting of one or more set of digitized data. It involves lowering a suite of petrophysical instruments down the hole. Data from the formation are transmitted to the surface and are recorded as continuous log as instrument is being pulled from the bottom of the hole to the surface. They are used to identify and correlate their physical properties and the nature of the fluids they contain. While drilling a well, little can be learned about the potential of the penetrated formation. The analyses of the returned cuttings sometimes referred to as measurement while drilling (MWD) reveals the lithology. This is already one step towards giving petrophysical information as the rock bit penetrates the formations and indeed a primitive lithological log.

Geophysical logs however are not direct measures of the petrophysical properties of the formation. Instead, the logs record different formation parameters which are then translated into properties of geological significance during log interpretation. The formation parameters measured by the logs may be inherited to the formation itself, such as natural radioactivity, or may be induced parameters such as formation's resistance to an electrical current. Logs also record mechanical parameters in the borehole, such as the hole diameter and the down-hole temperature.

Geological sampling during drilling leaves a very imprecise record of formation encountered. Mechanical coring is slow and expensive even though, geophysical logs need interpretation to bring it to the level of geological or petrophysical experience, the strong points are their precision and ability to bridge the gap between well cuttings and core samples.

The petrophysical properties determined from core and logs are not always directly comparable. The difference may be attributed, among other things, to the scale of individual measurements. Core analysis especially when done on core plugs provides point data taken from segments of a continuous but heterogeneous sequence of rocks, while log measurements can be taken over a large interval of well and cover more of variation within the rock sequence. Considerable core therefore has to be observed when comparing data from core log analysis. The conditions under which core and log measurements are obtainable also differ considerably. Well logs measure in-situ parameters and these cannot always be directly attributed to geological factors. Logging devices are also affected by the environment, temperature, overburden pressure, casing and other factors (Rider, 1996).

Although, laboratory measurements can be made under simulated reservoir conditions, restoring cores to the original confining pressure is not always successful due to irreversible expansion when cores are drilled and brought to the surface. The difference between properties derived from core measurement and geophysical log complicate reservoir assessment and there is no basis from which to estimate the validity of determinations and the degree of error in each techniques. Important information can still be obtained by comparing core and log data pertaining to some properties. The most important information is probably correcting the depth of core against the depths recorded by well logs. This can be done for example, by comparing lithology from core descriptions and from neutron-density logs. Laboratory core measurement can also be used to calibrate log values, so that the logs can be interpreted more confidently in zones where no core samples are available. Core data can also be used to extrapolate micro-scale geological information, such as mineralogy data, so that it can be integrated at a reservoir scale.

After drilling, samples are obtained by sidewall sampling; samples of fluid are also taken with formation tester for identification and measurement of their properties to aid interpretation of some of the geophysical measurements. The first log to be obtained is the drilling time logs which records the rate of drilling progress because

this depends on the nature of the formation. The chips carried to the surface are filtered from the mud examined to provide the mud log. This gives an imperfect record of the formations penetrated by the drill; this is because chips travel to the surface at rates that depend on their size and density.

2.3.1: Classification of geophysical wireline logs

Wireline logs can be classified on either the principle of operation of logging tools or their usage i.e. measurable physical parameters and deductions that can be made from them.

Based on operational principle: wireline logs can be classified as:

1. Electrical logs: Spontaneous Potential (SP) and Resistivity logs.
2. Nuclear or Radioactive logs: Gamma ray (GR), Density and Neutron logs.
3. Acoustics log: Sonic logs.

2.3.2: Classification based on usage

1. Resistivity logs: Induction, Laterolog, Deep-resistivity logs.
2. Lithology logs: Gamma ray and Spontaneous potential.
3. Porosity logs: Sonic, Density and Neutron logs.
4. Auxiliary logs: Caliper, Dip meter, Bit Size logs e.t.c

2.3.3: Characteristics of selected wireline logs

2.3.4: Radioactive logs

This log involves the use of radioactivity and is mainly to identify lithologies and help deduce the density and porosity particularly when a hole is cased, they will function with steel casing in place. Radioactivity logs belong to two groups which are:
(i) Those that passively measures the natural gamma ray radioactivity of the formation
(ii) Those that measures the induced radioactivity from strong radioactive sources in the Sonde.

The first group which uses a natural radioactive phenomenon is due mainly to potassium, thorium and uranium in lithologies (commonly present). Shale usually has the highest radioactivity, sands are intermediate, dolomite, limestone and quartz are very low. Occasionally, potash beds, ash bands and radioactive ores with higher activity than shale may be encountered. As shale is most radioactive, common sediment like shale log tool was first used primarily for identifying them. However, radioactive logs should be interpreted with utmost care for not all shales are radioactive, and not all radioactive formations are shale. Although the gamma ray

activity of shales varies widely on a world wide basis, it tends to be constant in a particular field.

This kind of log can be used in monitoring the injection of cement, depth by incorporating radioactive bullet into the collars at joints in the casing to produce sharp signals in the logs in combination tools. The spectral gamma ray is the borehole equivalent of gamma ray spectrometer. It differs from the simple gamma ray in recording separately the activities of potassium, thorium and uranium which can be used to depict the depositional environment of formations. Uranium is concentrated in marine sediments and thorium is in terrestrial sediments.

There are two types of these radioactive logs which are:

- (i) The Gamma-Gamma or formation density log which deals with densities
- (ii) The neutron or porosity logs

2.3.5: Gamma ray logs

The gamma ray log is a continuous recording of the intensity of the natural gamma radiations emanating from the formations penetrated by the borehole vs. depth. All rocks have some radioactivity. The most abundant source of natural radioactivity is the radioactive isotope of potassium ^{40}K , and the radioactive elements of the uranium and thorium series. Radioactive material originally occurred in igneous rocks. It was subsequently distributed unequally throughout sedimentary formations during erosion, transport, and deposition. In sedimentary formations, radioactive elements tend to concentrate in clay minerals which in turn, concentrate in shale (Bassiouni, 1994).

In general, sandstones, limestones and dolomite have very little radioactive content. Black shale and marine shale exhibit the highest level of radioactivity. Radioactivity is related to lithology but not directly or rigorously. A high level of radioactivity is not always associated with the presence of clay minerals hence; the use of natural radioactivity in lithology differentiation requires good knowledge of the local lithology (Bassiouni, 1994) e.g. a high gamma ray may not imply shaliness but a reflection of radioactive sands such as potassium rich feldspar, glauconitic or micaceous sandstone. The scintillation counter (Fig 2.2) is composed of a fluorescent crystal and a photomultiplier tube. When the crystal is struck by gamma radiation, it emits ultra violet or blue-light photons. These photons strike anodes placed at successively higher potentials. The scintillation counter is the most suitable instrument for radiation detection. It is characterized by fast reaction and high

detection efficiency (50% to 60%). These characteristics allow it to detect thin beds. The standard unit of measurement is API.

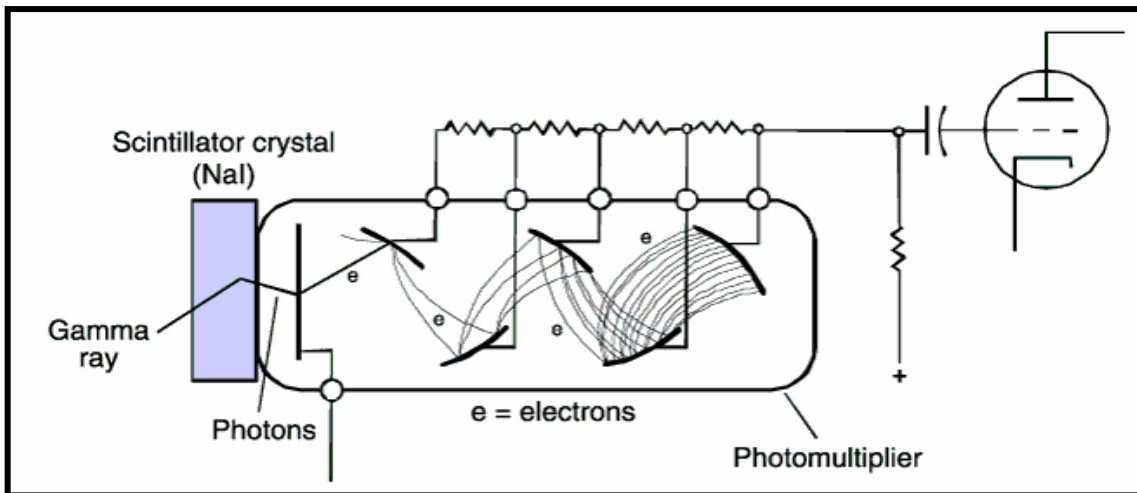


Figure 2.2: Gamma ray tool (modified from Serra, 1984)

2.3.6: Neutron log

Neutron logs are a porosity log that measures primarily the hydrogen ion concentration in a formation. In neutron, there is radioactive source from where formations are bombarded with radioactive (fast neutron rather than gamma rays). These neutrons travelling through formations only slow down significantly when they collide with atoms of similar mass i.e. Hydrogen atoms. Once they have been slowed by repeated collision, they are absorbed into the nuclei of heavier atoms present and cause them to emit gamma rays which are being recorded by counter. The number of neutron that reach the detector (neutron count) is affected by a number of factors in the borehole environment, such as hole size, mud weight and casing size (Bateman, 1985). An example of neutron tool designed to compensate environmental effects is illustrated in figure 2.3 A and B. The far detector is affected by both borehole and formation, while the near detector records signals from borehole. The ratio of the counting rates from the two detectors leaves only information from the formation, and is used to produce a record of neutron porosity index. The neutron tool however is also affected by clay minerals. Bound lattice water in the clay minerals may cause high porosity to be indicated by neutron log, but the effective porosity in such rocks may be zero due to the presence of fine clay particles in the pore spaces.

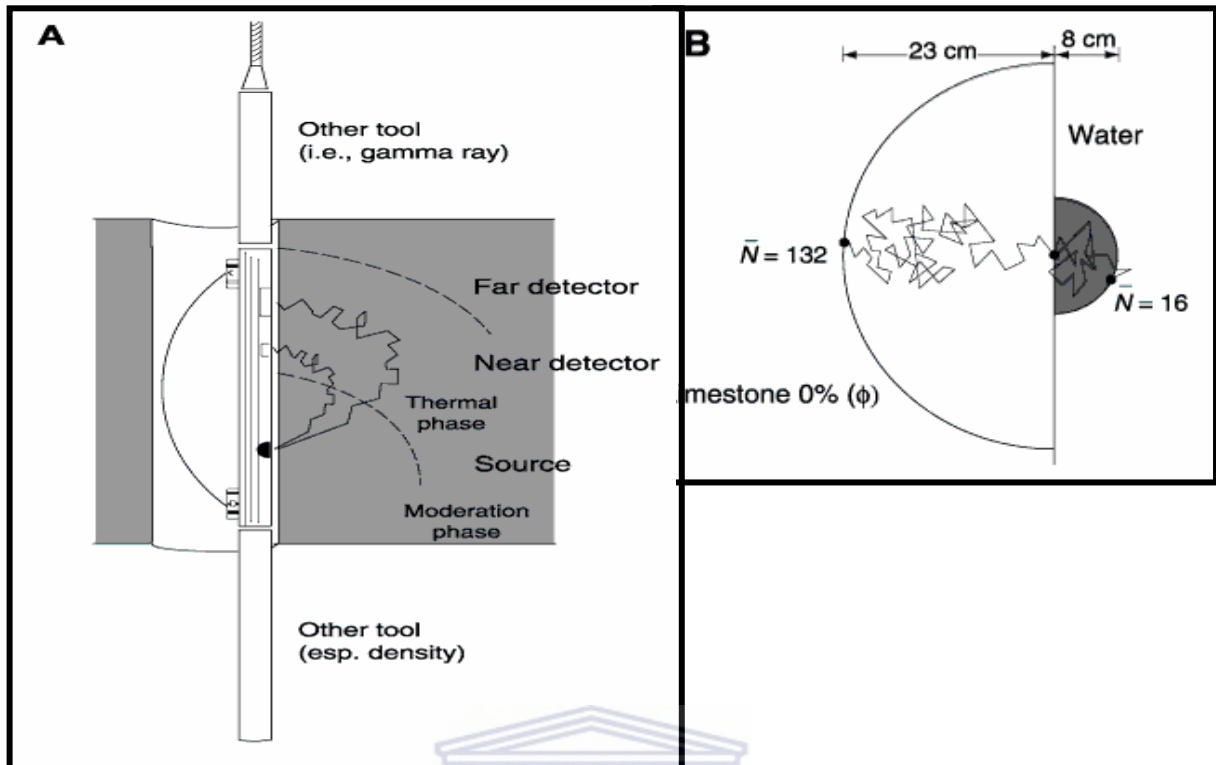


Figure 2.3: (A) Schematic of Compensate neutron tool (B) Schematic trajectories of neutron in limestone with no porosity and pure water (modified Rider, 1996).

The more rapid the neutron slows down, the nearer to the counter the gamma rays are produced resulting in stronger signal since hydrogen is an important component of both water and oil. In clean formations, where the porosity is filled with water or oil, the neutron log measures liquid-filled porosity. Whenever pores are filled with gas rather than oil and water, neutron reads low values. This occurs as a result of less concentration of hydrogen in gas compared to oil or water. The lowering of neutron porosity by gas is called Gas effect. As the two tools, gamma-gamma and neutron respond to permeability and fluid in a similar way to SP and resistivity respectively, they are used to replace them in cased holes.

2.3.7: Density log

The density log gives a record of the bulk density of the formation, which includes the density of the rock or matrix and the density of the fluid enclosed in the pores. The density log is primarily used to determine porosity, lithology and the type of fluid in the pores. The logging techniques involve exposing the formation to gamma rays, which are backscattered and absorbed by the materials in the formation. The rate of absorption and the intensity of the backscattered rays depend on the number of electrons (electron density) that the formation contains, which in turn is

closely related to the common density of the materials. Dense materials have more electrons per unit volume (electrons/cm³), with which the gamma particles can collide and lose energy. Hence, higher energy is absorbed and backscattering is lower, in dense materials. In less dense formations, which have lower electron density, more gamma particles reach the detector and more counts are recorded per unit time. The detector counts are then translated to bulk density as presented in the density log.

An illustration of a density tool is provided in Figure (2.4). The tool consists of a gamma ray source and two detectors (near or short spacing and far or long spacing). The counting rate recorded by the detector allows correction for the effects of mud cake density and thickness. The geometry of the logging tool itself is also designed to minimize the effects of the drilling mud. The source and the detectors are mounted in a plough-shaped skid and pressed against the wall of the borehole by an eccentric arm. The force exerted by the arm, and the shaped design of the skid, allows the tool to cut through the mud cake so that the tool and the formation are in perfect contact, minimizing the contribution of the drilling mud in the recorded signal. The depth of investigation is around 10 cm (Rider, 1996).

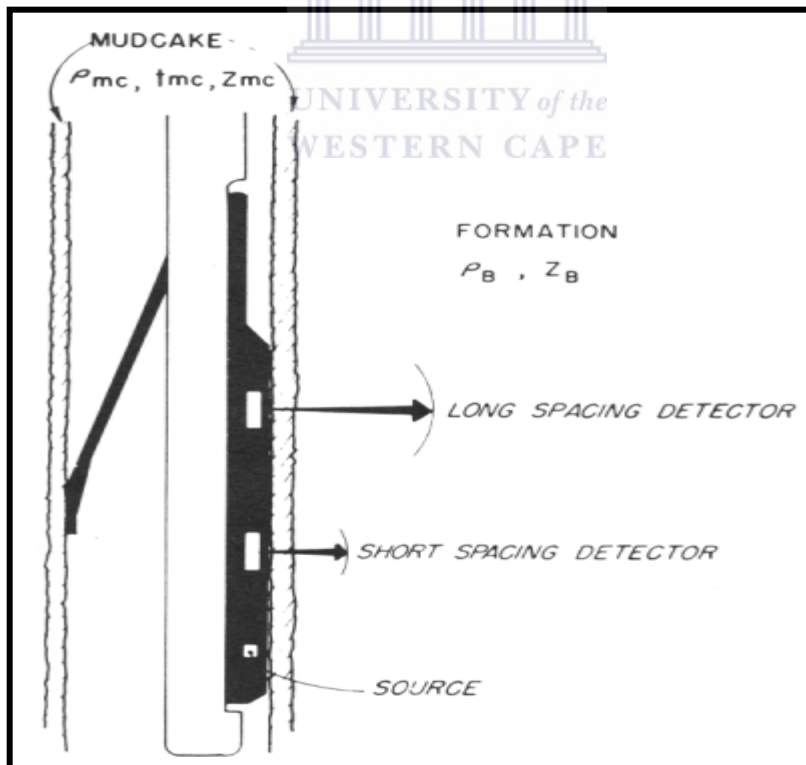


Figure 2.4: Schematic of dual-spacing density logging device (Modified from SPWLA Library, 1997)

Variations in the bulk density indicate changes in porosity, as water and hydrocarbon have lower densities than the solid (mineral or rock) materials.

The accuracy of porosity estimate from the density log depends on the choice of density values used for the matrix and the fluid in the above equation. The most reliable source of these values is from actual laboratory analysis. There is, however, a tendency to use assumed values in log analysis, especially when the lithology of formation is not known or when cores are not available. A rock density of 2.65 g/cm^3 is no longer valid. A study of Jurassic Brent group in the North Sea has shown that, for a sand of 20 % porosity, the error associated with each 1 % increase in the proportion of siderite led porosity decreases around 0.8 of one porosity percent if not accounted for in the matrix density values (Guest, 1990). In another study, the use of more accurate matrix density parameters giving consideration to the presence of organic matter and dense minerals resulted in least a 10 % increase in porosity values than by using the assumed value of 2.65 g/cm^3 (Herron and Herron, 2000). The error in the porosity values incurred with incorrect choice of matrix density is approximately 50 times the error in the matrix value (Granberry et al., 1968). For example, an error of 0.01 g/cm^3 in grain density will produce error of 0.5 % in porosity. The implications are that errors in matrix density parameters may have profound effects in the evaluation of reservoirs. When cores are not available to verify the calculated density log porosity and if the matrix density value used is too low, the calculated porosity will also be low and the potential of the reservoir could be seriously under-estimated.

In similar argument, the fluid density values usually assumed in density log analysis is that of water (1 g/cm^3) but the actual fluid density may be lower when the reservoir is saturated with gas or light hydrocarbons. Evaluation from the density log may thus result in an excessively high porosity estimate.

2.3.8: Sonic log

A sonic log measures the velocity at which the formation transmits sound waves. It is used primarily to estimate porosity and to identify the lithology and the type of fluid in the pores. The tool principally records the time (interval Transit time) it takes for sound waves to travel through one foot of the formation. Interval transit time is the reciprocal of velocity of the sound wave.

The sonic tool consist if transducers and receivers. The transducers translate electrical signal into ultrasonic vibrations while the receivers convert pressure waves into electromagnetic pulses, which can be amplified to produce the logging signal. An example of sonic tool array is shown in Figure (2.5). It consists of a number of both

transducer and receiver, which are separated by specific distances. Averaging the interval transit time recorded by each receiver reduces unwanted borehole effects such as the effect of Sonde tilt and borehole size.

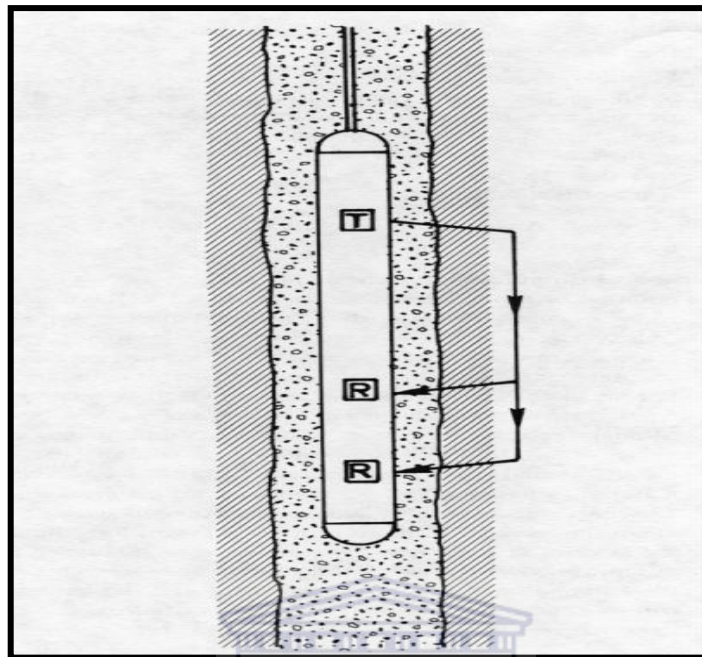


Figure 2.5: Sonic Logging tool showing Receiver (R) and Transmitter (T) (modified from http://www.spwla.org/library_info/glossary)

When the sonic log is being run, many acoustic waves interfere with the measurements. The first arrival or compressional wave is the one being amplified and measured by the tool. It is the wave pulse that has travelled from the transducers to the formation, has been refracted at the borehole wall, travelled within the formation and then travelled back to the receivers as a fluid pressure wave (Schlumberger, 1982).

The sonic log is used in combination with other logs (e.g. density and neutron logs) for porosity, shaliness and lithology interpretation. Integrating transit time is also helpful in interpreting seismic records.

2.3.9: Spontaneous potential logs

The SP log is a measurement of the natural potential difference or self potential between an electrode in borehole and a reference electrode at the surface: no artificial currents are applied in the measurements. The currents were actually called “potential spontanes” or spontaneous potentials by Conrad Schlumberger and H.G in 1936. Doll who discovered them. They originate from formation vertically (in electrical sense) when in nature they are isolated.

The principal use of SP log is to calculate formation water and to indicate permeability. It can also be used to estimate shale volume, to indicate facies and in some cases for correlation. Three factors are necessary to provoke an SP current:

1. Conductive fluid in the borehole
2. Porous and permeable bed surrounded by impermeable formation
3. Difference in salinity (or pressure) between the borehole fluid and the formation water.

SP current originate principally through the electrochemical effects of salinity differences between the borehole fluid (mud filtrate) and formation water. These differences create spontaneous currents either when the fluids themselves come into contact through a porous medium or when in contact through shale which acts as semi-permeable membrane (Rider, 1996). SP log was one of the first logs introduced for correlative purposes in sand-shale sequences, principally because certain intervals had typical log shapes. This shapes in sand-shale sequences, is related to shale abundance, the full SP occurring over clean intervals, a diminished SP over shaly zones. The relationship is considered as linear and so far shaliness is related to grain size, the SP is used to delineate both permeable and impermeable zones (Fig. 2.6) and also as good facies indicator.

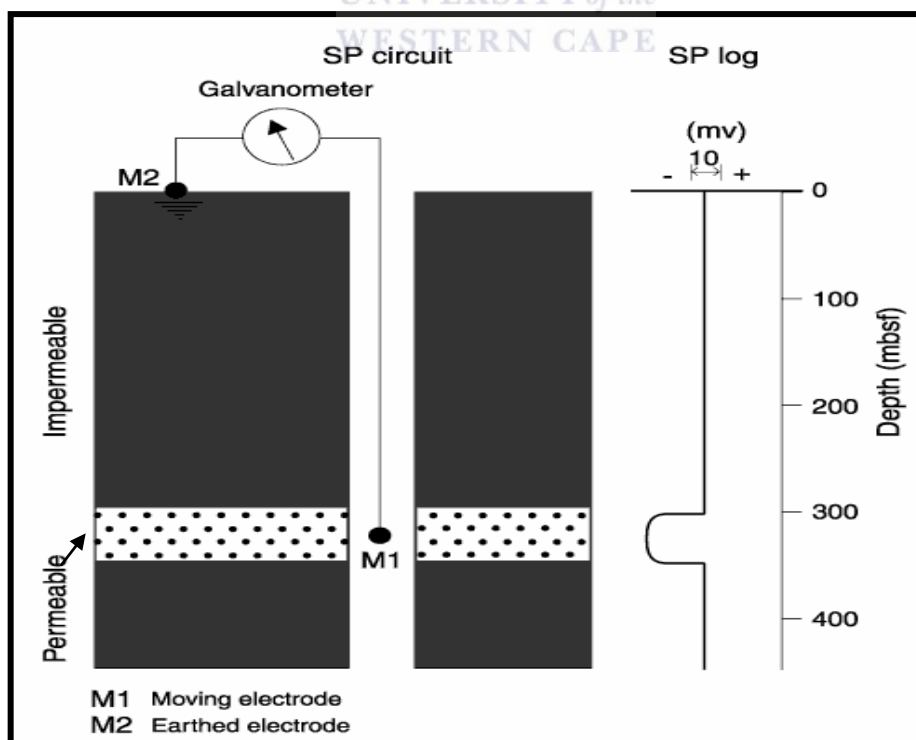


Figure 2.6: Spontaneous Potential Logging tools (modified from Rider, 1996).

2.3.10: Resistivity logs

The resistivity log is a measurement of formation's resistivity, i.e. its resistance to passage of an electric current. Conductivity logs measure a formation's conductivity or its ability to conduct an electric current but this value is generally converted directly to resistivity. Most rock materials are essential insulators, while their enclosed fluids are conductors. Hydrocarbons are the exception to fluid conductivity and on the contrary, they are infinitely resistive. When a formation is porous and contains salty water the overall resistivity will be low. When this same formation contains hydrocarbon, its resistivity will be very high. It is this character that is exploited by the resistivity logs: high resistivity values may indicate a porous, hydrocarbon bearing formation.

The resistivity logs were developed to find hydrocarbons. This is still their principal quantitative use. To interpret the geological significance of resistivity logs, it is essential to realize that the same porous bed can have a multitude of resistivity responses, depending on the fluid content.

2.4: Seismic interpretation

Conventional seismic interpretation implies picking and tracking laterally consistent seismic reflectors for the purpose of mapping geologic structures, stratigraphy and reservoir architecture. The ultimate goal is to detect hydrocarbon accumulations, delineate their extent, and calculate their volumes. Conventional seismic interpretation is an art that requires skill and thorough experience in geology and geophysics.

Traditionally, seismic interpretation has been essentially qualitative. The geometrical expression of seismic reflectors is thoroughly mapped in space and travel time, but little emphasis is put on the physical understanding of seismic amplitude variations. In recent time, seismic interpreter have put increasing emphasis on more qualitative techniques for seismic interpretation, as these can validate hydrocarbon anomalies and give additional information during prospect evaluation and reservoir characterization.

2.5: Depositional environments and facies discrimination

Study on sufficiently broad scale clearly reveals that the basic primary control of oil occurrence can be summed up in two words, "depositional environment". Environmental impact is the basic control for all the natural phenomena, whether it is the occurrence of oil or any other mineral. Our problem as oil finder is to establish

what are the products of those all important environmental factors, their relationships in the original sedimentary basin and to recognize them in the present basin.

The only direct indicator of the past basin environments is the facies which can be compared with the environment of similar facies in modern basin. The advantage in the modern basins is that the various elements that determine environment can actually be observed and measured. They include such factors as the oxidation-reduction potential (Eh), alkalinity-acidity range (pH), the salinities and other electrometric and physico-chemical conditions, the bacterial and other biochemical activities, temperature, pressure and other physical factors (Reading, 1996).

The environment and the resulting facies are in turn controlled more than anything else by the basin bottom form at the time of deposition and by the deposition rate and type of sediments (Moody, 1961). The basin bottom form varies with the type of basin and its own peculiar individual development. Other things being equal, oil occurrence is related in sequence to:

- ✚ The mechanics of the basin subsidence, which varies in general way with basin type.
- ✚ The resulting basin form, which along with supply and current determine:
 - a. The sediment distribution which further modifies the basin forms.
 - b. The environment which is largely influenced by the basin form and the rate of deposition.

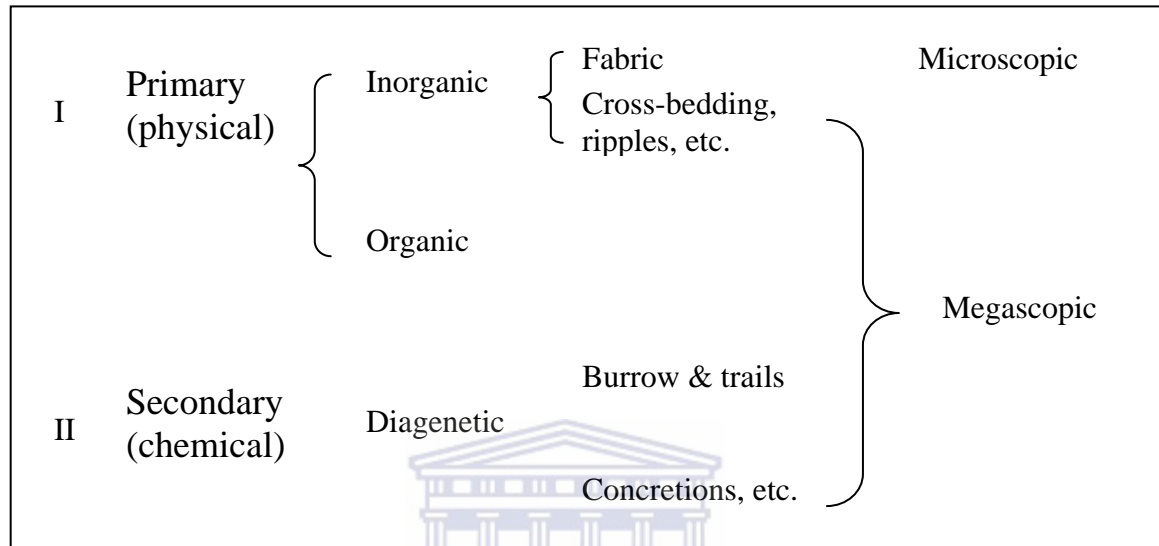
All this controls the facies distribution, alongside with the adequacy of reservoir, timeliness of traps and the efficacy of seal determines the incidence (volume and distribution) of oil (Moody, 1961).

2.5.1: Sedimentary structures

Sedimentary structures reflect the hydrodynamic processes during deposition and they are simply divided into primary and secondary classes. Primary structures are those generated in sediment during or shortly after deposition and results mainly from the physical processes (e.g. current and waves). Examples of sedimentary structures are ripples, cross bedding and slumps. Secondary sedimentary structures are formed sometimes after sedimentation and result from essentially chemical processes, such as those which lead to the diagenetic formation of concretions. Primary structures are divisible into inorganic structures and organic structures (Table 2.1) and the division between the various groups provides a useful framework on which to build the analysis of sedimentary structures (Selley, 1988).

Sedimentary structures can be studied at the outcrop and in cores taken from wells. There are two basic approaches to observe sedimentary structures. The first approach is to assume that the outcrop is a borehole and to measure a detailed sedimentological log while the second is a two-dimensional survey of all, or a major part, of the outcrop.

Table 2.1: A classification of sedimentary structures (Selley, 1988)



2.5.2: Fossils

Fossils content reflects the ecological processes at the time of deposition. Fossils are usually preserved when they are buried under the layers of sand and mud. The sand and mud become sedimentary rocks under great pressure. Minerals seep into the fossil replacing the organic matter and creating a replica in stone. This is how fossils formed. Discovered and undiscovered fossils and fossils containing in rock formations and sedimentary layers is known as the fossil record. It can be a traced fossil or a body of fossil. Body of fossil is actually organic material from animals (bone) or plant. A body of fossil is usually composed of the bones of animals. Preservation of the soft-tissue of a body is rare especially over a long period of time. Most fossils are made when an animal dies and falls, or is washed into a stream and is covered with mud.

2.6: Reservoir quality prediction

Accurate prediction of reservoir quality is, and will continue to be a key challenge for hydrocarbon exploration and development. These predictions are needed throughout the entire “life cycle” of a reservoir (Sneider, 1990). Proper assessment of reservoir quality must be continually refined from prior to exploratory drilling, to

discovery, during appraisal and development drilling, and throughout reservoir management.

At the exploration stage, the main challenge is to assess and predict the reservoir facies, its geometry, and its distribution; reservoir porosity and permeability for use in petroleum reserves calculations, seismic characteristics; migration pathways. At the appraisal, planning and development stages, it is necessary to understand and predict reservoir porosity, permeability and reservoir distribution to determine the location and optimal number of development wells, as well as to estimate economic production cut-off values, hydrocarbon pore volumes, recoverable reserves, and production rates (Sneider, 1990). The reservoir management stage involves predictability of diagenetic patterns that control reservoir quality which is used to identify bypassed and uncontacted pay, and in tertiary recovery planning and modification.

Reservoir performance has been related to the variability in sedimentary facies with a reservoir sequence, where continuous sequence of rocks with similar geological characteristics possesses comparable petrophysical properties (Hearn et al., 1984). Porosity reduction in the study of Hearn et al, (1984) was associated with particular minerals occurring in the particular sedimentary facies. The applications of mineralogy in that study were focused on two main aspects. Mineral identification was used in conjunction with other geological and well log data, to define different facies within the sedimentary sequence. Based on the facies sub-division, porosity reduction was then attributed to particular mineralogical components contained within a particular facies. Incorporation of mineralogical data in such a study is thus seen to be important, especially where the geophysical data do not provide sufficient information to describe the heterogeneity within the reservoir sequence.

2.6.1: Controls on reservoir quality prediction

Sandstone is derived mainly from erosion of a parent source and transported to its site of deposition by physical processes (Kupecz, et al., 1997). Physical parameters of sandstones (grain size, sorting, roundness etc) are used to understand and predict depositional processes and environments in which they were deposited. Siliciclastics are controlled by physical sediment supply. During relative Highstand of sea level, most coarse-grained clastics are “trapped” in fluvial systems and are not deposited in marine settings (Kupecz, et al., 1997). During relative lowstands of sea level, coarse-grained sediments are able to bypass the shelf to be deposited in basinal marine

settings. Therefore, lowstand systems tracts (LST) generally contain the most volumetrically abundant deposit of coarse-grained siliciclastics in petroleum basins.

2.6.2: Diagenetic studies

Diagenetic study is relevant to petroleum reservoir assessment because diagenesis modifies the original characteristics of the sediments through physical and chemical reactions. Diagenetic phenomena may alter rock properties such as porosity, pores size distribution and also cation-exchange capacity and also the relationship of these properties to the mineral composition of the reservoir sequence (Hurst 1984). Diagenetic study typically involves the use of x-ray diffraction, thin section petrography and scanning electron microscopy techniques (Hurst and Nadeau 1995) to determine the mineral content of the sediments. As the influence of clay mineral on reservoir characteristics are well known, study of diagenesis in reservoir sandstones often involves identifying, characterizing and quantifying the clay minerals present. A lot of substantial works are available that describe the effect of clay minerals on porosity and permeability (e.g. Ehrenberg et al., 1993; Howard, 1992; Hurst and Nadeau 1995; McHardy et al. 1982; Serra 1984; Wilson, 1992; Pittman et al. 1992).

Mineralogy of sandstones although variable, commonly consists of grains that are chemically stable in the near-surface depositional environment. Although dissolution of feldspars and lithic fragments can be locally important (Heald and Larese, 1973; Milliken et al., 1989; Milliken, 1992; Bloch and Franks, 1993: among others), changes in porosity and permeability are not generally sufficient to significantly improve the overall quality of a reservoir (Bloch, 1994). Meteoric diagenesis in sandstones is a controversial topic. Much of the controversy has focused on the generation of secondary porosity. The complexity of the processes involved precludes any prior assumptions as to the quantitative importance or even presence of secondary and enhanced porosity associated with meteoric diagenesis (Bloch, 1994). Furthermore, identification and quantification of secondary porosity often rely on subjective criteria. Even when positive evidence exists, such as partially dissolved grains and/or cements, it may be difficult to prove a meteoric origin for mineral dissolution. Giles and Marshall (1986), in a review of secondary porosity in sandstones, made a plausible case for the involvement of meteoric water dissolution in some settings. More recently, Emery et al. (1990) have furnished strong evidence using a combination of wireline log, core analysis, thin section, isotope geochemical and seismic acoustic impedance data to highlight meteoric water dissolution of

sandstones beneath an unconformity. The possibility that meteoric water can penetrate deep into a basin and still influence the course of diagenesis has been demonstrated from analysis of oxygen and hydrogen/deuterium isotope ratios in authigenic minerals (Gluyas et al., 1997). Burial diagenesis and its effects on the quality of petroleum reservoirs is a much researched topic. The range of minerals that can reduce the quality of reservoir is large: quartz, carbonate minerals, clays, zeolites and others (Primmer et al., 1997). The application of quantitative petrographic, geochemical and isotopic analyses to authigenic minerals during the past decade has allowed scientists to date minerals, determine the temperature of precipitation and characterize the pore waters from which precipitation occurred (Emery and Robinson, 1993; Williams et al., 1997). When such data coupled with analysis of the thermal and burial history information, powerful descriptions of diagenetic processes have emerged (Glasmann et al., 1989; Kupecz and Land, 1994; Robinson and Gluyas, 1992, Hogg et al., 1993; Walderhaug, 1994a).

The timing of development and the distribution of diagenetic minerals within a reservoir sequence also influence some of the variations in petrophysical characteristics (Al-Ramadan et al., 2005). The implication of diagenetic studies in reservoirs is that they allow prediction of porosity and permeability, in this way they serve to proffer possible and lasting solutions as regards the appropriate well treatment methods to be adopted for the wells

2.7: Quantitative mineralogy techniques

The choice of mineralogical evaluation as a complementary tool in the analysis of rock properties is constrained by the cost of the analysis and the time frame to meet the completion of the well. Among the quantitative mineral evaluation techniques used in some core laboratories are thin section, x-ray diffraction analysis, x-ray fluorescence spectrometry, infrared spectroscopy. Mineralogical analysis in reservoir description typically includes combination of methods; thin section petrography and x-ray diffraction are the most common (Hurst and Nadeau, 1995).

Thin section petrography can provide much information on mineralogical composition, sediment provenance, petrofabric and diagenesis (Harwood, 1988). Quantitatively, the technique requires counting of at least 500 points to cover mineral components present in small proportions (Van der plas and Tobi, 1965). This increases the time and cost needed for analysis. The technique also does not provide a true evaluation of mineralogy, since it treats poly-mineralic particles, such as detrital

rock fragments and matrix component as separate phases, rather than determining the percentages of individual minerals involved. With the limited resolution of the ordinary petrographic microscope, fine particles such as clay minerals and other closely inter-grown phases may be inadequately identified or even overlooked. Clay mineralogy however is of particular concern in evaluating reservoir properties. Electrical, radioactive and nuclear logging techniques, for example are all affected by different clay minerals. Significant proportions of these minerals may also provide drilling, completion and production problems in potential reservoir rocks (Frost and Fertl, 1981). Clay minerals however are difficult to quantify or even to identify by optical microscopy techniques. Hence, there is need for an alternative approach that could provide a detailed and quantitative evaluation of mineralogy including the clay components. Point counting analysis may also be affected to some extent by three-dimensional heterogeneities in mineral distribution, due to limitations imposed by small area embraced in a thin section, thereby limiting the applicability of the technique to reservoir studies concerned with larger volumes of investigation or more heterogenous lithological materials. Operator preferences during the analysis have been shown to produce consistent differences in point counting results performed on similar sets of samples (Swanson, 2001). Thus, point count analysis does not always yield accurate and reproducible results. The technique has nevertheless been used in reservoir description, mainly in research on diagenetic effects applied to porosity and permeability issues (Baker et al., 2002, Rossi et al., 2002).

The x-ray diffraction (XRD) technique is based on the diffraction of x-rays by atomic layers within the crystalline phases (minerals) of the rock sample. Because each crystalline material has distinct set of atomic layer spacing (d-spacings), all of the crystalline materials in a sample can be identified from XRD scan. The analysis requires finely powdered samples, packed in a sample holder and directly inserted into the XRD instrument. Powdered based techniques have advantage over thin section studies of being able to include a split from larger, more representative sample in the analysis, to cover any compositional variability. Such capability is important in studies of sedimentary rocks which may be very heterogenous. In reservoir applications, the inclusion of more representative samples in the analysis is important to complement geophysical log data, which typically cover a larger volume of rock than single thin section. Identification and quantification of clay minerals can also be performed using XRD techniques, either by powder analysis or by preparation of

oriented slides from the fine fraction of sample. A more detailed discussion of the XRD techniques and their interpretation, including the technique used in the present study is given in Chapter 4. X-ray diffraction has been applied in reservoir sandstone studies involving the assessment of effects of clay minerals on porosity (Ramm, 2000; Ramm and BjØlykke, 1994). The technique has also provided valuable information to facilitate log interpretation (Cannon and Coates, 1990). Understanding of the mineralogical factors affecting petrophysical properties is traditionally based on thin section petrography included as part of routine core analysis. However, this provides a petrographic rather than true mineralogical analysis (the mineralogy of poly-mineralic components such as rock fragments and matrix is not taken into account), and thus does not always provide sufficient information to address the need for understanding of mineralogical influences on reservoir properties.

Traditionally, x-ray diffraction (XRD) is used to identify minerals of core samples from oil well. The qualitative aspects of infrared spectroscopy are one of the most useful techniques to complement XRD technique. Over the years, much has been published in terms of fundamental absorption frequencies (also known as group frequencies) which are the key to unlocking the structure-spectral relationships of the associated molecular vibrations. Currently, bulk mineralogical analysis relies heavily on x-ray diffraction (XRD) which tends to be supported by data from infrared spectroscopy, chemical analysis and electron microscopy (Środoń and Clauer, 2001) therefore, this technique will be used to complement the petrographic results (Thin section, SEM and XRD). Infrared spectroscopy has not been utilized significantly in the identification of minerals and in structural studies (Xu, 1999, Moore et al., 1989). Analysis of rock chemistry by x-ray fluorescence (XRF) is based on the characteristic of radiation spectra emitted by the different elements on exposure to x-ray radiation. A wide range of elements can be identified with high precision. The technique however, cannot analyse elements with atomic weight less than that of fluorine, and there is also some difficulty in analysing some trace elements with high molecular weights (Lewis and McConchie, 1994).

2.8: Geochemistry of pore water

Deposited sediments also have high water content if accumulated under water. The sediments progressively lose water (with time) after burial and become lithified due to diagenetic changes (Gerhard, 2000). Mechanical diagenesis caused by overburden of younger sediments and tectonic stresses expel pore water and lead to a

rearrangement of sediment particles. Chemical diagenesis involves dissolution and recrystallization of primary minerals, as well as precipitation of cement in pore space. Dissolution and cementation may take place at different depths within the sediments. The effects of mechanical and chemical diagenesis in various sediment types are quite complex but can be investigated using various proxies in which pore water is one of the most important proxy. pH is so important as it can drastically change equilibrium state and speed of many reactions (<http://www.chembuddy.com/?left=pH-claculation&right=pH-scale>). It is well established through field observations, experiments, and chemical models that (redox) reaction and pH exert a strong influence on the speciation of dissolved components and the solubility of minerals in hydrothermal fluids (<http://www.chembuddy.com/?left=pH-claculation&right=ionic-strength-activity-coefficients>).

2.9: Fluid inclusion studies

When a crystal grows in the presence of a fluid phase, some of the fluid may be trapped as imperfections in the growing crystal to form fluid inclusions. The trapped fluid may be liquid, vapor, or superficial fluid, and the composition of the trapped fluid may include essentially pure water, brine of various salinity, gas or gas-bearing liquids and silicate, sulfide or carbonate melts among others. As noted by Roedder (1984), some researchers use the term fluid inclusion to describe only those inclusions that have trapped a fluid and have remained in the fluid state during cooling to ambient temperatures. Fluid inclusions are a common feature of minerals. In fact, it is much more common to find crystals with optically-resolvable fluid inclusions than it is to find crystals with no visible fluid inclusions. Even gemstones which are sought after because of their beauty and apparent perfection often contain large inclusions that are in some cases characteristics of area or mine where they were found (Roedder, 1986).

Fluid inclusions are small relicts of fluid trapped in natural minerals during their growth from hydrothermal solutions (primary inclusions), or during later deformation (secondary inclusions). They are the most direct record of chemical and physical properties of ancient fluids trapped deep in the Earth's crust and they provide essential information about the formation of hydrothermal deposits (Gunther et al, 1998). Nevertheless, the physical and chemical conditions that might lead to formation of fluid inclusions are many, and some are limited to certain minerals or even specific crystal faces in individual minerals (Watanabe, 1987).

In addition to conventional fluid inclusion studies, fluid inclusion stratigraphy (FIS) is a bulk volatile analysis technique that allows pore fluids trapped in inclusions to be chemically characterized in cuttings and core, in large numbers of samples (Hardley, et al, 1997). This technique can determine the quantity and specific types of petroleum fluid trapped in pores in mineral grains, their stratigraphic and spatial pattern of organic compounds which in turn will yield valuable information on migration pathways, pay delineation/proximal pay detection, petroleum type (oil vs. gas, oil type) and fluid compartmentation.

Fluid inclusion stratigraphy (FIS) is a patented technique that involves the rapid, complete analysis of volatiles trapped as fluid inclusions in cuttings, core or outcrop samples using quadrupole mass analyzers attached to an automated high-vacuum sample introduction system (<http://www.fittulsa.com/fis.php>; accessed on 06/04/2012). The technique documents the presence and relative bulk abundance of geologically important inorganic species as well as organic species with 13 carbon atoms or less. FIS methodology and theoretical framework are result of long-standing research and development effort.

2.9.1: Understanding fluid inclusion stratigraphic data

There are two parts to conventional fluid inclusion data sets:

- ✚ Stratigraphic profile of critical species and species ratios with depths.
- ✚ Individual mass spectra for each sample.

A mass spectrum is a graphical display of the log of the ion current (measured on the mass spectrometers detectors) as a function of the mass-to-charge ratio (m/z) of the detected ions. The amplitude of the ion current is proportional to the quantity of each type of ion, which in turn is proportional to the abundance of the species in the original gas mixture. Discrete peaks occur because the charged substances have discrete masses and discrete charges ((FIT#FI020073a-Middleton-www.fittulsa.com: accessed on 01-07-2012). Complex volatile mixtures have mass spectra characterized by multiple, interfering ions on a given m/z , making it difficult or impossible to find a “clean peak” indicative of a specific species. Generally, higher m/z positions display more interference, but even low m/z has these overlaps. Nevertheless, similar compounds give similar fragmentation patterns that tend to be distinct from other classes of compounds. Because of this, the major classes of organic species (paraffins, naphthenes and aromatics) can be distinguished and their relative abundance estimated. Similarly, it is useful to consider the assemblage of anomalous peaks in a given mass spectrum, as

these will often indicate the presence of compounds that are concentrated by similar subsurface processes (e.g. the water soluble species benzene, toluene and acetic acid as the primary indicators of “proximal pay”). It is these assemblages that are most useful for distinguishing among major types of FIS mass spectra, as well as inferring the presence of specific compound even where interfering ions are possible (FIT#FI020073a-Middleton-www.fittulsa.com: accessed on 01-07-2012).

2.9.2: Five types of FIS spectra

FIS mass spectra can be classified into five end member types

1. Non-hydrocarbon FIS mass spectra
2. Gas-range enriched FIS mass spectra
3. Liquid-range enriched FIS mass spectra
4. Sulphur-compound enriched FIS mass spectra

Mixture and gradations among these ideal end members are common. In considering the fragmentation patterns of organic species, it is useful to keep in mind the general formulas for three dominant hydrocarbon classes:

1. Paraffins: C_nH_{2n+2}
2. Naphthenes: C_nH_{2n}
3. Aromatics: C_nH_{2n-6}

2.10: Hydrocarbon recovery

Optical microscopy, x-ray diffraction and scanning electron microscopy have been applied in a study of clay mineral diagenesis in sandstone of the Niger Delta (Lambert-Aikhionbere and Shaw, 1982). In this study, possible problems that may arise in the recovery of hydrocarbons from the reservoirs because of the friable nature in the sandstone were that could have provided a source of silica cement, which in turn could have strengthened the sediment framework of sandstone clay mineralogy in this study will be considered important not only because of the effect of clay minerals on permeability, but also for assessing the best means to enhance hydrocarbon recovery. The use of clay mineralogy has also been suggested in designing water injection facilities for friable reservoir sands, where the swelling capacities and fine kaolinite particles might reduce permeability and possibly cause irreversible formation damage (Morris and Shepperd, 1982). Information provided by scanning electron microscope and x-ray diffraction was considered as useful addition to flow test data for predicting clay reactions during drilling and well completion (King, 1992).

Chapter Three

3.0: Geological background of Bredasdorp Basin

3.1: Introduction

The rapid growing South African petroleum upstream sector is playing an important role in the evolution of South African oil industry. South Africa has a long coastline of about 3000 km in length. This includes the western coast, which is about 9000 km starting from Orange River to Cape point and more than 200 km long moving Cape point further round southern coast up along the eastern coast through Durban and Zululand Basins to the Mozambique border (Petroleum Agency SA Brochure, 2004/05). Beyond the coastline is the continental margin which constitutes the South African offshore environments. The immediate relatively shallower area is about 20 - 160 km wide off the western coast, 50 – 200 km wide off the southern coast and averaging 30 km wide on the eastern coast. The continental slope connects the shelf area with the deep marine environment it follows a similar trend in width and fairly wide on the west and south coast but become narrower to the eastern coast (Fig. 3.0).

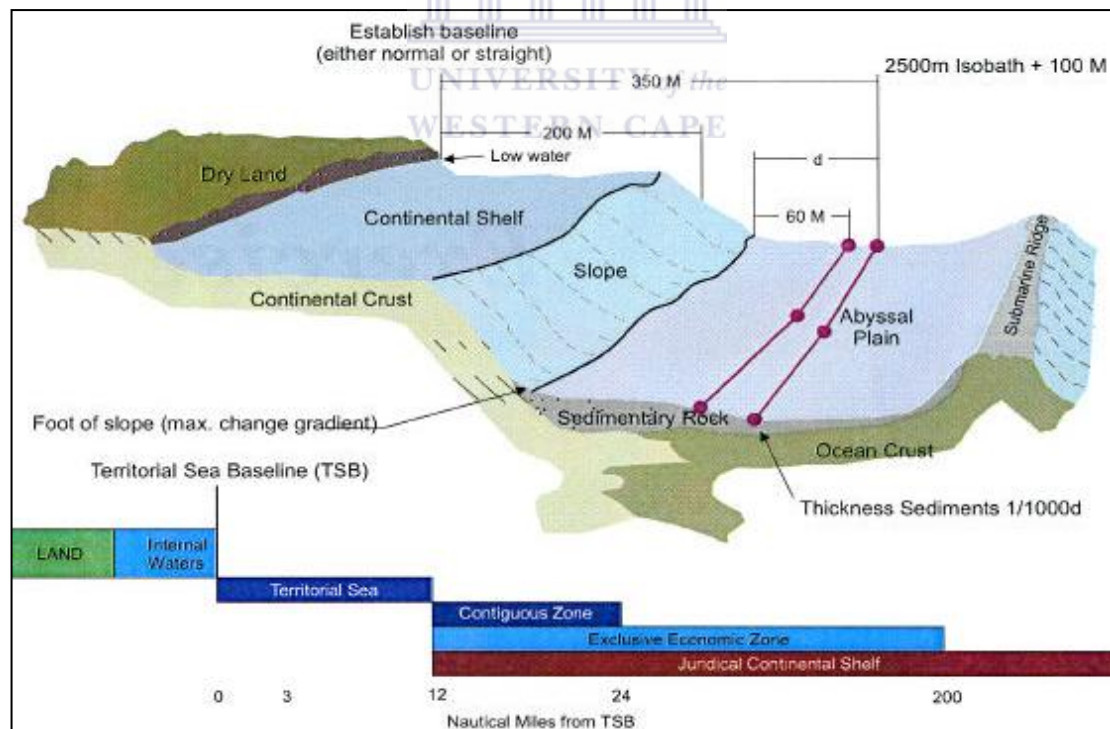


Figure 3.0: South Africa continental margin and oceanic crust (Modified from Broad 2004).

The Bredasdorp Basin which is the subject of this study has a number of economic to marginal economic discoveries of oil, gas and condensate (Oribi, Sable and Oryx fields). The estimated recoverable reserves of the Oribi, Sable and Oryx fields are 23, 25 and 7 million barrels (MMbbl) respectively (Petroleum Agency SA, Brochure, 2003/04). Wells drilled offshore has gas shows and tested good gas flow rates and provided good evidence for a gas province. South Africa's prospect for natural gas production increased recently with the discovery of offshore reserves. Exploration is being carried out in Bredasdorp Basin with the aim of assessing the extent of these available reserves and determining their economic potentials.

The offshore basins of South Africa have been divided into three distinct tectono-stratigraphic zones: western, southern and eastern offshore (Fig. 3.1). These basins have developed in the Permo Triassic-Jurassic period or earlier. The western zone known as Orange Basin is a divergent plate margin with graben structures trending sub-parallel to coastline (Jikelo, 2000). It is related to the opening of south Atlantic in the early cretaceous. A narrower passive margin describes the eastern offshore which is part of the African rift system formed as a result of breakup of Africa, Madagascar and Antarctica in the Jurassic (Fig. 3.2). Unlike the western and southern margin, this zone has limited deposition with only the Durban and Zululand basins containing an appreciable sedimentary succession.

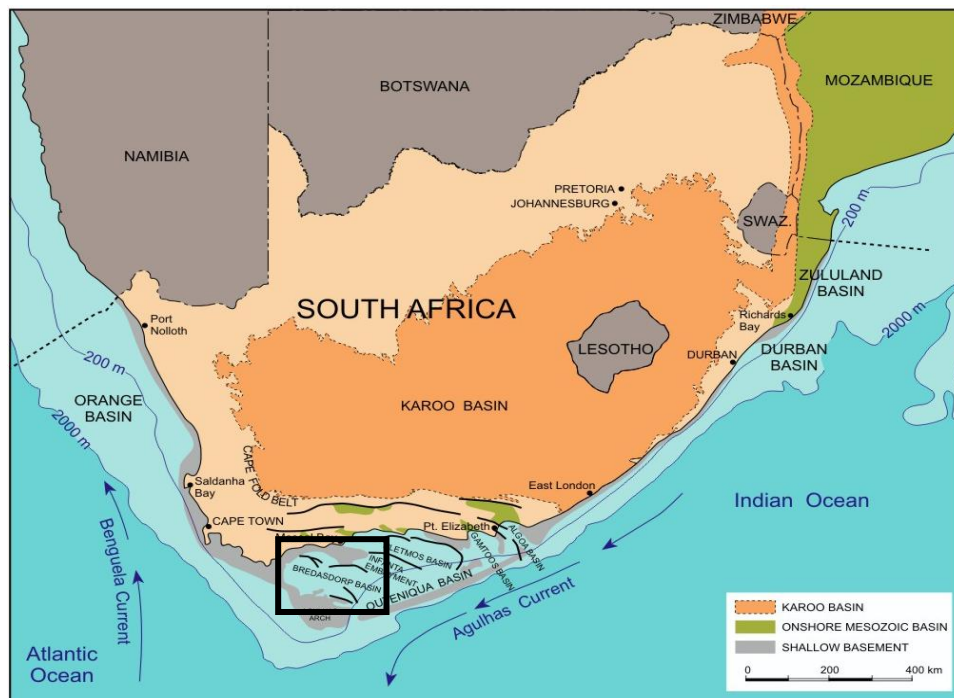


Figure 3.1: Western, eastern and southern offshore zones of South Africa (Petroleum Agency SA brochure 2003).

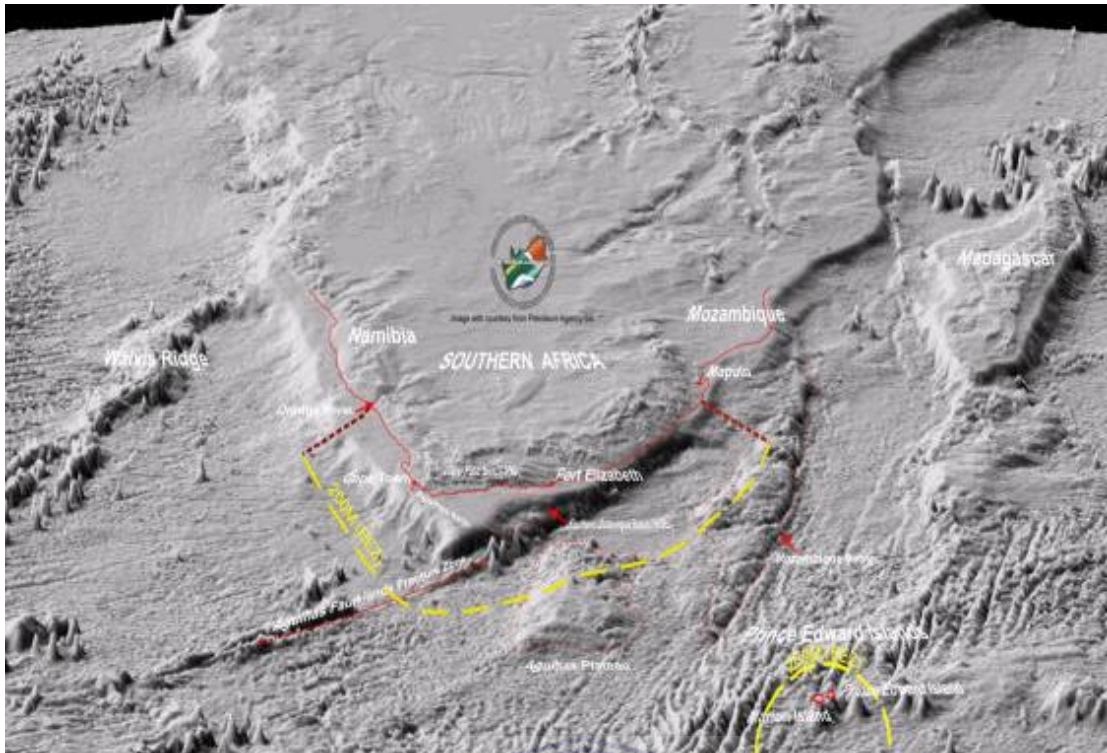


Figure 3.2: Topography derived from satellite image showing sea floor and continental margin surrounding South Africa (modified from Broad 2004).

The Southern offshore (Fig. 3.1) region is a large composite intra-cratonic rift basin known as the Outeniqua Basin; it shows a history of strong strike-slip movement during the Late Jurassic Early Cretaceous break-up and separation of Gondwana (PASA Brochure, 2005). The Outeniqua Basin comprises of rift sub-basin from east to west, the Algoa, Gamtoos, Pletmos, Infanta and the Bredasdorp basins with the satellite image showing the topography of the basin in relation to the other onshore and offshore basin (Fig 3.2). Each of these basins comprises of rift half-graben overlain by variable thickness of drift sediments and the deepwater extensions of these basins merge into the Southern Outeniqua Basin. Half graben feature is formed when normal faults within a sedimentary basin are dipping in the same direction making adjacent fault blocks to slip down and tilt relative to the fault next to it (Fig. 3.3).

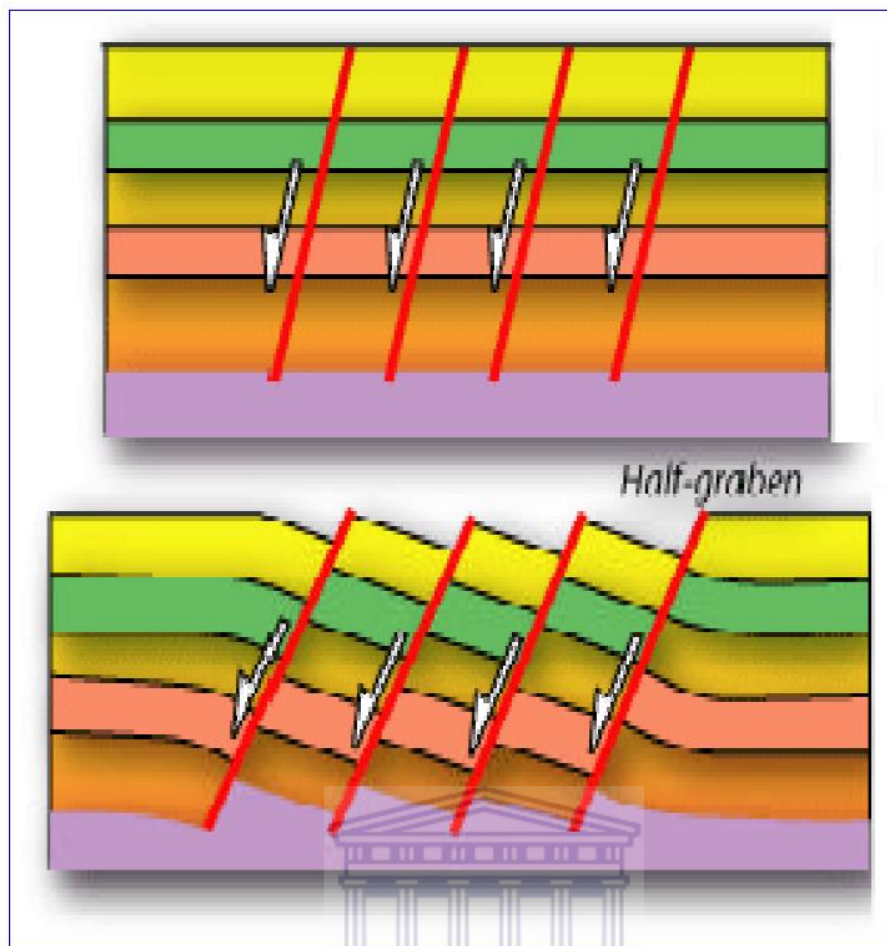


Figure 3.3: Formation of Half graben from a series of normal faults dipping in the same direction (modified from Hudson, 1997)

3.2: Tectonic settings of Outeniqua Basin

The Outeniqua Basin comprising of four sub-basins (Bredasdorp, Pletmos, Gamtoos and Algoa) was formed from dextra shearing processes of South African margin which began in the Early to Mid-Cretaceous. The rift phase of the South coast ended in the Lower Valanginian which is associated with a drift-onset unconformity (1At1) (PASA Brochure 2004/05). The drift-onset unconformity is simultaneously to the earliest oceanic crust in the South Atlantic. A complex series of micro-plates such as the Falkland Plateau gradually moved west south-westwards, past the southern coast of Africa (Fig 3.4a). These movements created some oblique rift half graben sub-basins including the Bredasdorp basin which may be regarded as failed rifts. It is the youngest in the west and oldest in the east (Fig. 3.5).

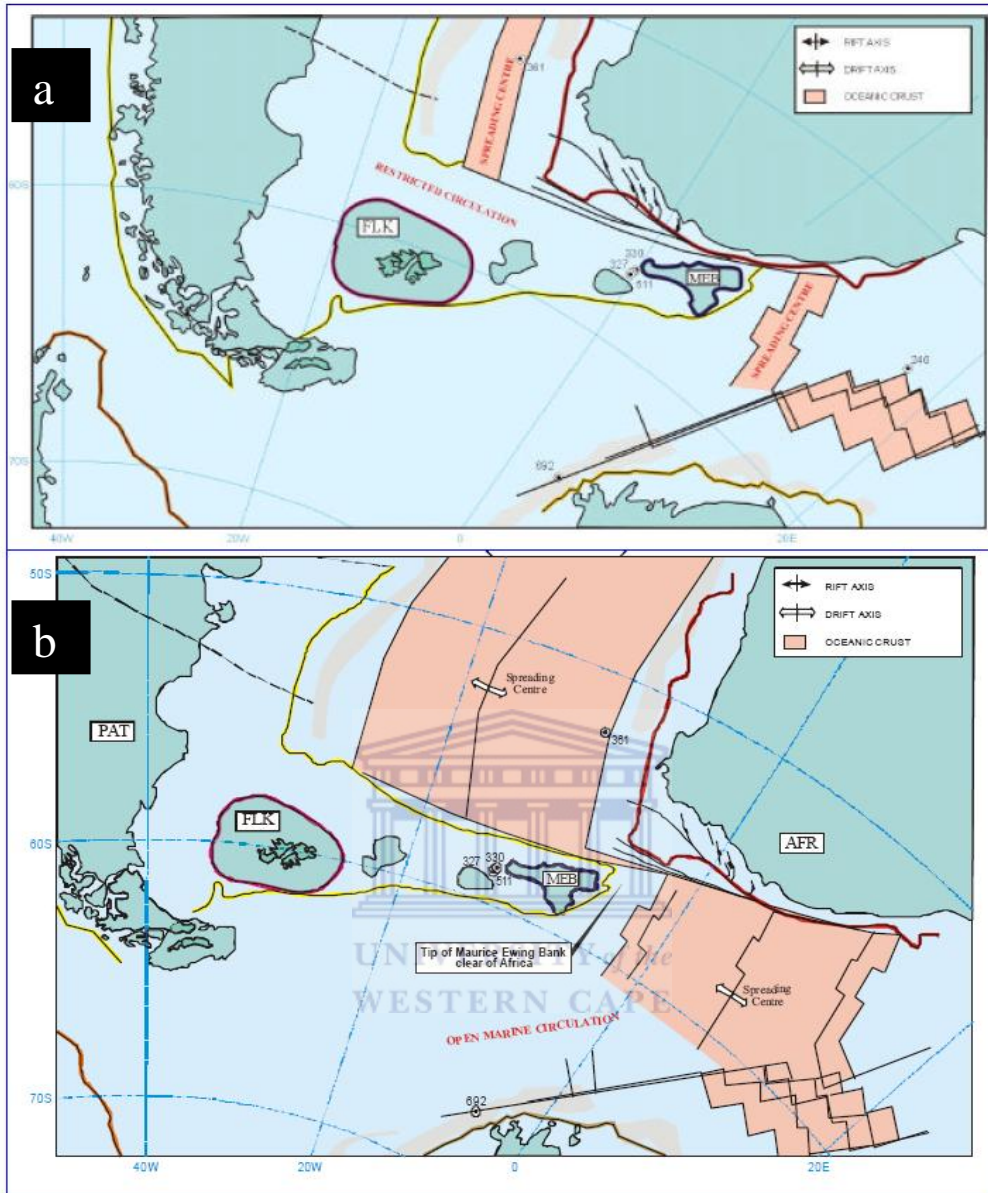


Figure 3.4: **(a)** Early drift phase in the Valanginian (1At1) – Hauterivian (6At1) showing the movement of micro plates: Falkland Plateau (FLK) Patagonia (PAT) and Maurice-Ewing Bank plates (MEB) past south coast of Africa (Modified from Broad, 2004). **(b)** Late drift phase in the Hauterivian (6At1) onwards (modified from Broad, 2004).

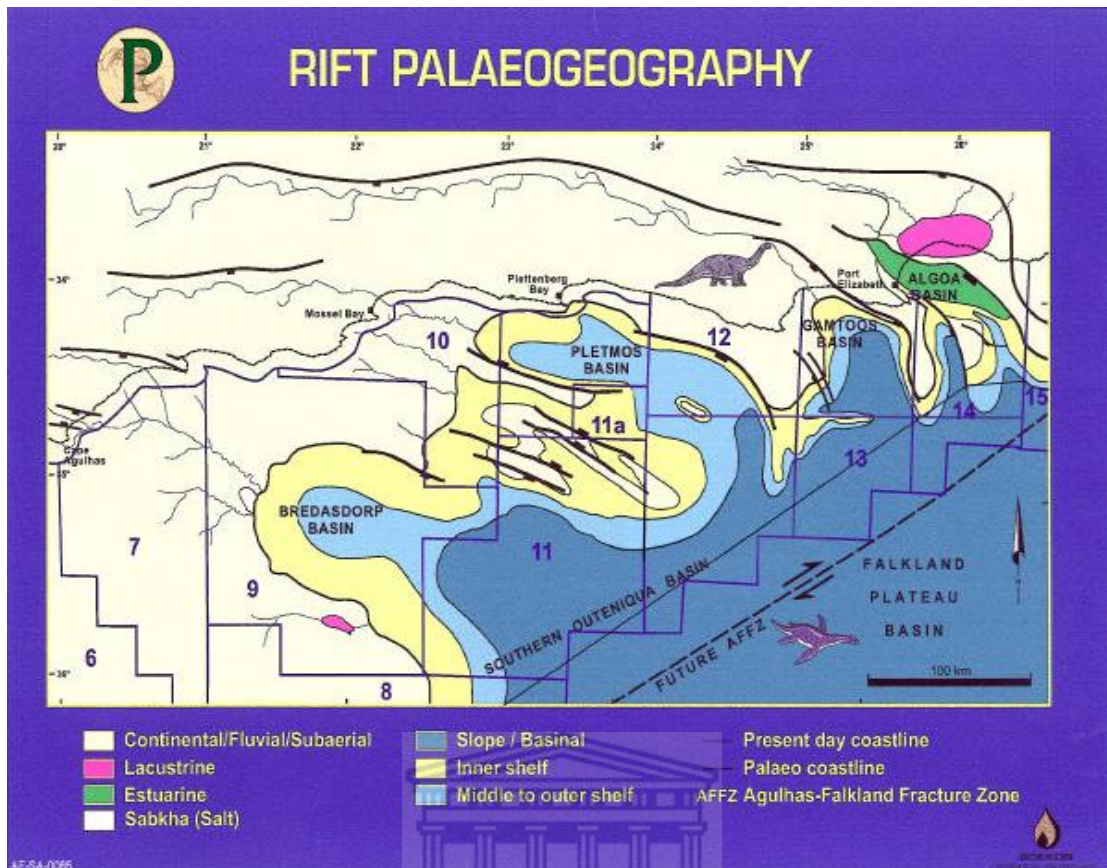


Figure 3.5: Oblique rift half-graben sub-basins of Outeniqua Basin Bredasdorp, Pletmos, Gamtoos and Algoa (modified from Broad, 2004).



Figure 3.6: The rift phase in the Late Jurassic-Lower Valanginian showing the break up of Africa, Madagascar and Antarctica (modified from Broad, 2004).

3.3: Tectonic history of Bredasdorp Basin

The Bredasdorp as well as the adjacent Pletmos and Gamtoos basins experienced onset of rifting during the Middle-Late Jurassic. Dextral trans-tensional stress which was produced by the breakup of Gondwanaland which occurs to the east between the Falkland Plateau and the Mozambique Ridge, initiated normal faulting north of the Agulhas-Falkland fracture Zone (Schalkwyk, 2005).

The principle of normal fault bound elongate synrift graben and half graben basins up to ~10 km wide. Deposition of thick synrift continental and marine sediments continued within the rift basin until ~126 Ma when most of extensional faulting ceased, the synrift deposition started and initiate post rift tectonics erosion and deposition.

After the above mentioned took place, widespread uplift of major bounding arches and less within the horst blocks in the region resulting in enhanced erosion of lower Valanginian drift onset second order unconformity (Schalkwyk, 2005). Subsidence and deposition during the initial post rift super cycle that is composed of third order cycle were concentrated within the most central parts of Bredasdorp Basin. Distribution of early post-rift Bredasdorp embayment closely coincides with the distribution of late synrift basins which continued to subside slowly along the rift faults during most of the super cycle (Schalkwyk, 2005).

Bredasdorp Basin resembles a well developed systems tract and type 1 erosional unconformities (Schalkwyk, 2005) in which the super cycle ended with the final movement of Falkland Plateau westward past the Agulhas platform. During the remainder of the Cretaceous, the Bredasdorp Basin experienced four principle episode of subsidence ranging from 9-12 Ma, each terminating by uplift of basin margins and sub-aerial erosion.

3.4: Structural development of the Bredasdorp Basin

The Bredasdorp Basin has no onshore equivalent, although it does lies between two anticlinally dominated basement highs at Cape Infanta Agulhas. Dingle et al., (1983) described Bredasdorp Basin as a wide basement depression and its cross-section is asymmetrical (Fig. 3.7). The Southern boundary of the Bredasdorp Basin formed as a result of faulted and gently northward titling flank of Agulhas Arch, it can be traced as a major subsurface feature to the southwest of Cape Agulhas. The upper division of the arch is exposed of post-Paleozoic rocks and is composed of Table Mountain Group quartzite and Bokkeveld shales over granite core. The floor is

relatively flat except the western part and it also dips generally to the North-west such that the deepest part of the basin lie close to its northern margin (Dingle et al., 1983). In the Northern part of Bredasdorp Basin, the basement descends rapidly through several small boundary faults from the Infanta Arch. The northern edge linearity which is broken by small deep grabens forms embayment onto the Infanta Arch and at least three horst, which project southeast and southwards into the Basin. These horsts stand above the general level of basin floor and are bounded by short curved faults. These horsts stand above the general level of basin floor and are bounded by short curved faults. These horsts have been targets for hydrocarbon exploration drilling. The western portion of the Bredasdorp basin does not extend onshore but breaks up into small narrow, northwest-southeast horsts and graben, which extend to the coast linking Cape Agulhas and Cape Infanta (Dingle et al., 1983).

3.4.1: Rift phase (Mid-Jurassic - Valanginian)

Extension-driven subsidence and synrift basin fill characterized rift phase. Isostatic uplift both flanks of the half graben resulted in erosional truncation of the late-rift sediments. Extreme marginal uplift and erosion of the northern flank removed the entire synrift sequence in places (PASA Brochure, 2004/05).

3.4.2: Early drift phase (Hauterivian – Early Barremian)

Before onset of rapid thermal subsidence, continued uplift resulted in erosion truncation on the southern flank. Rapid subsidence and deposition of deep water sequence (source rocks) occurred within the graben (PASA Brochure, 2004/05).

3.4.3: Drift phase (Barremian – Turonian)

Regional subsidence was driven by thermal cooling and sediment loading with continued minor movement on the Arniston fault. In early Paleozoic oil prone source in the half graben reached the main stage of generation. Continued minor subsidence until early Tertiary when alkaline intrusive affected the southern flank resulting in uplift and erosion (Turonian – Present Day; PASA Brochure, 2004/05).

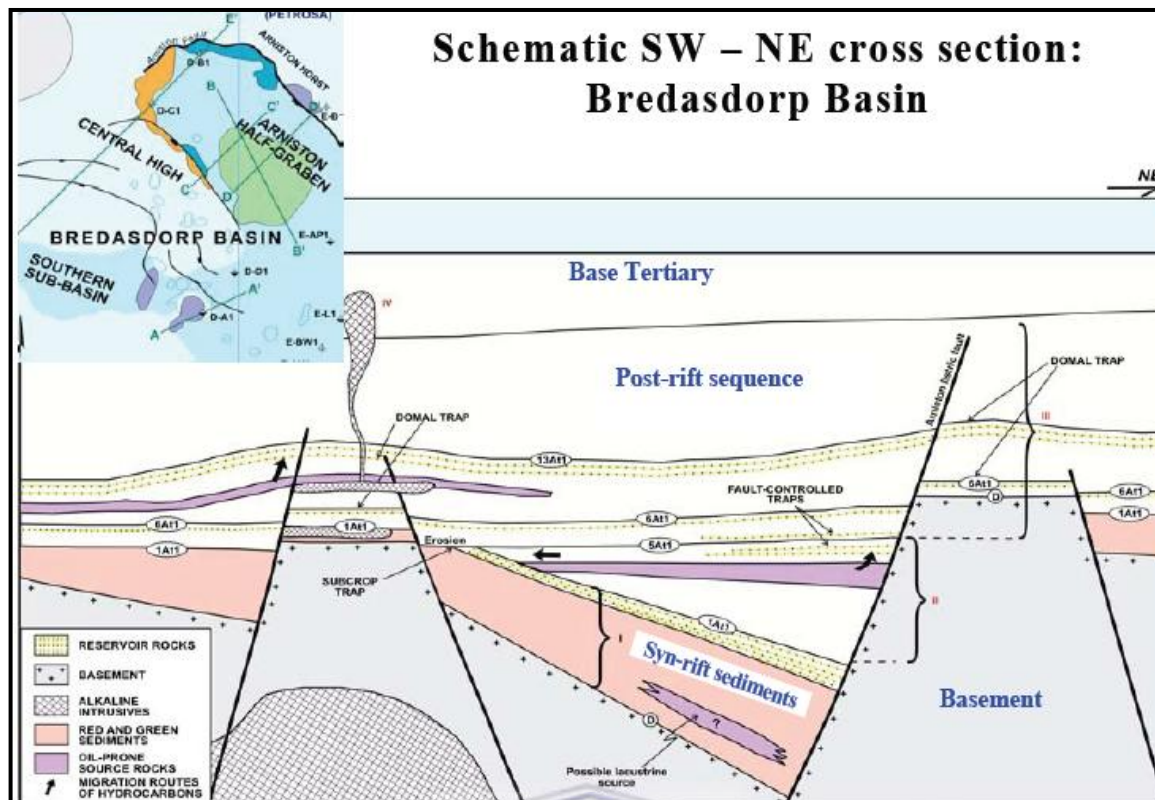


Figure 3.7: Schematic cross-section of Bredasdorp Basin showing inverted graben (modified from Petroleum Agency SA Brochure, 2004/05).

3.5: Sequence stratigraphic and chronostratigraphic framework of Bredasdorp Basin.

Utilizing the principles of sequence stratigraphy, the drift successions in South Africa's offshore basins have been divided into unconformity – bounded sedimentary sequences. Each sequence is interpreted to have been deposited in response to world wide (eustatic) relative changes of sea level and is defined at its base by type 1 unconformity, as defined by Van Wagoner et al., (1988). Each sequence is associated with a sea level Lowstand followed by Highstand flooding event. The methodology and principles of the sequence stratigraphic process and their application to the South African offshore are describe by Brown et al., (1996).

The chronostratigraphic correlation chart (Fig. 3.8) is based on these studies and utilizes the time scale of Haq et al. (1988) to provide a geological time framework, which is useful for understanding the distribution of lithofacies through space and time. The sequence stratigraphic approach has relevance for understanding and predicting the occurrence of petroleum source rocks and reservoirs.

GENERALISED CHRONOSTRATIGRAPHY FOR THE BREDASDORP, INFANTA, PLETMOS AND SOUTHERN OUTENIQUA BASINS

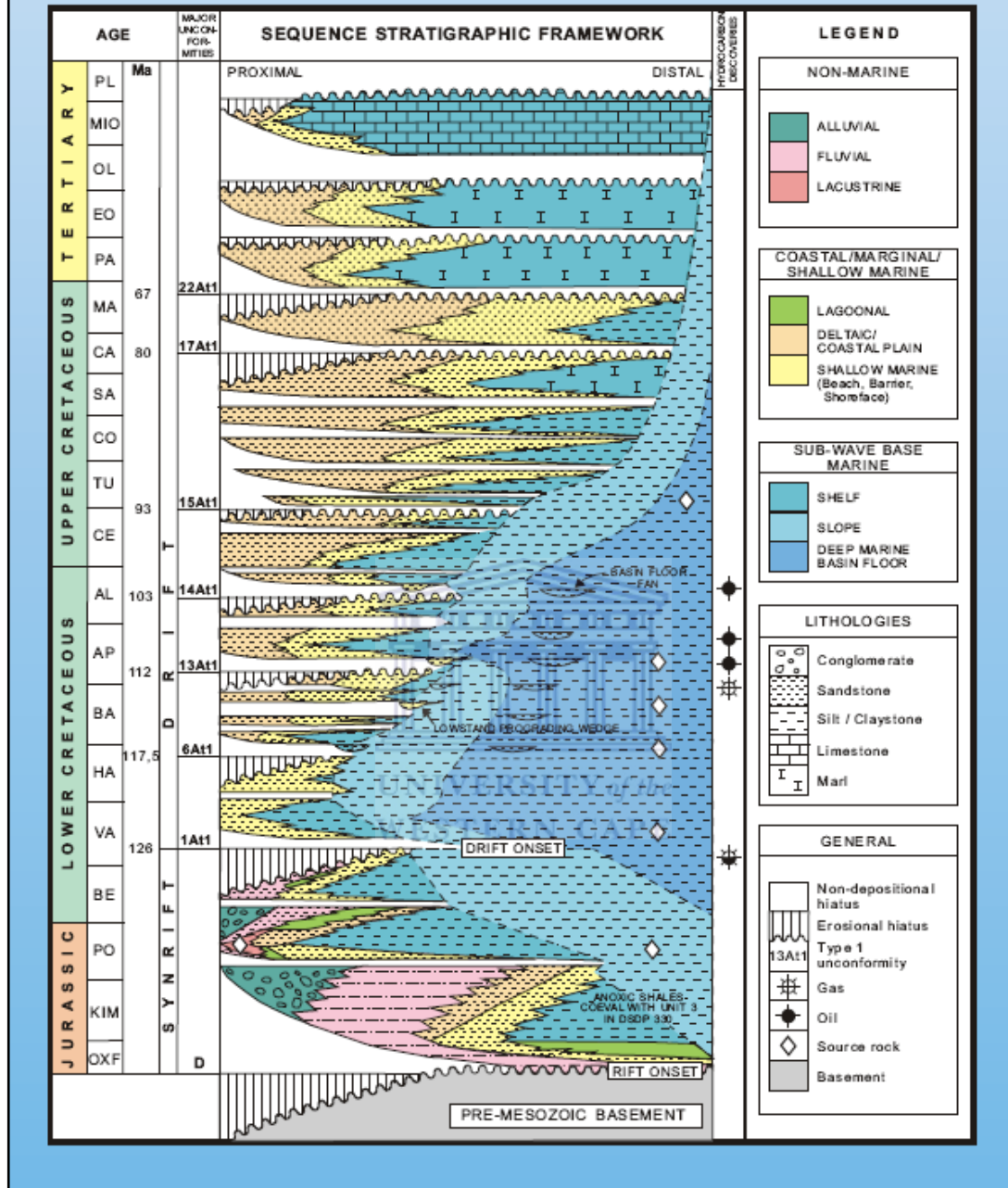


Figure 3.8: Sequence chronostratigraphic framework of the Bredasdorp Basin (PASA, 2007)

3.6: Stratigraphy and sedimentary geology

Hydrocarbon exploration in the offshore South African rift basins within structural synrift plays yielded limited success. In 1987, after the first oil discovery in post rift sediments in the Bredasdorp Basin, sequence-stratigraphic concepts were applied to the lower Cretaceous post rift sequences to permit correlation of depositional system tracts and related facies throughout the Basin. The interaction of rift tectonics, thermal

cooling and eustatic variations in global sea level produced a distinguishing series of cyclical depositional sequences. Within resolution limits of regional seismic profiles, about 10 cyclic sequences and mega sequences, deposited between the mid-Valanginian and lower Santonian can be recognized (Fig. 3.9; Broad, 2000).

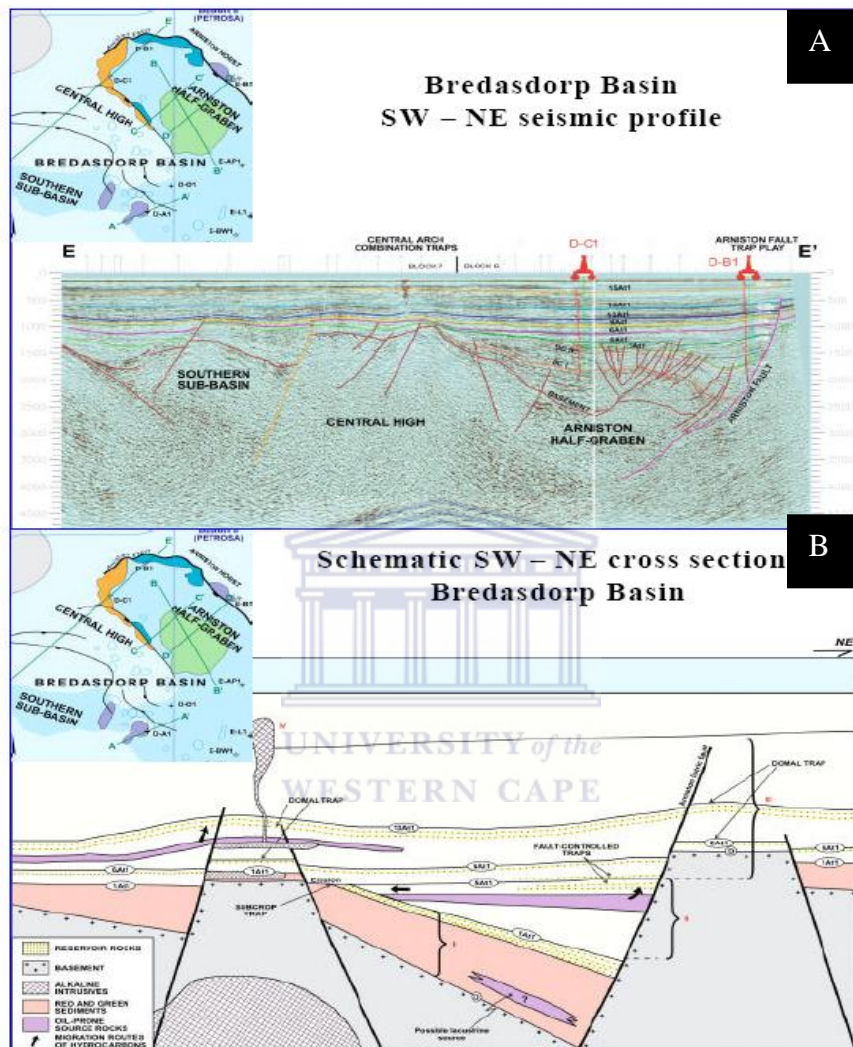


Figure 3.9: A: Seismic profile with identified sequence boundaries. B: Schematic cross section (modified from Broad, 2004).

The basin fill consists of cyclic sequences deposited in response to relative changes in sea level. Cyclic sequence concepts were applied to mark out hydrocarbon plays, a process that does not depend upon a global system. However, once the sequences were recognized, mapped, and placed within a chronostratigraphic framework (Fig. 3.8) using age dating, these cycles were compiled with Exxon’s global system. Thus, although processes of global cyclicity as proposed by Exxon can be observed in the Bredasdorp Basin, local tectonics has overprinted this global effect to produce a unique sedimentation history (Broad, 2000).

Various elements of low-stand systems tracts within these sequences appear to contain potential reservoirs. High erosional (type-1) unconformity, exhibiting incised valleys and Canyons (Fig. 3.10A), provide surfaces on which:

- ✚ Mounded and sheet-like submarine/basin floor fans,
- ✚ Submarine channel fill and associated mounds and fans, and
- ✚ Prograding deltaic/coastal low stand wedges were deposited.

These fans, channel fill, and wedges are top sealed and sourced by transgressive shales and marine condensed sections deposited at a time of regional transgression of the shoreline. Discovery wells and various reservoir-quality sandstones occurring at predicted stratigraphic levels support the application of the sequence-stratigraphic concepts to hydrocarbon exploration. A seismic-stratigraphic study of Cretaceous strata in the Bredasdorp Basin has evaluated potential stratigraphic hydrocarbon plays in a classic post-rift Basin where structural traps are rare (Broad, 2000).

In a terrigenous clastic basin such as the Bredasdorp, lowstand system tracts are interpreted as being composed of basin floor turbidite fans, channels and/or sheets. These features formed contemporaneously with the erosion of incised valleys and submarine canyons, followed by channelized slope fans and deltaic/coastal low stand wedges that prograded during a relative sea level rise (Fig. 3.10B). Subsequent flooding of the shelf as relative sea level rises accelerated resulted in poorly defined transgressive system tracts. With the relative sea level at highstand, extensively developed deltaic/coastal systems progrades basin-ward exhibiting a well-defined clinofolds (Fig. 3.10C). The major hydrocarbon plays in the lowstand tracts occur as mounded basin-floor turbidite fans, channel fills, draped sheets and are found in the up-dip pinch-out of deltaic/coastal sandstones (Broad, 2000).

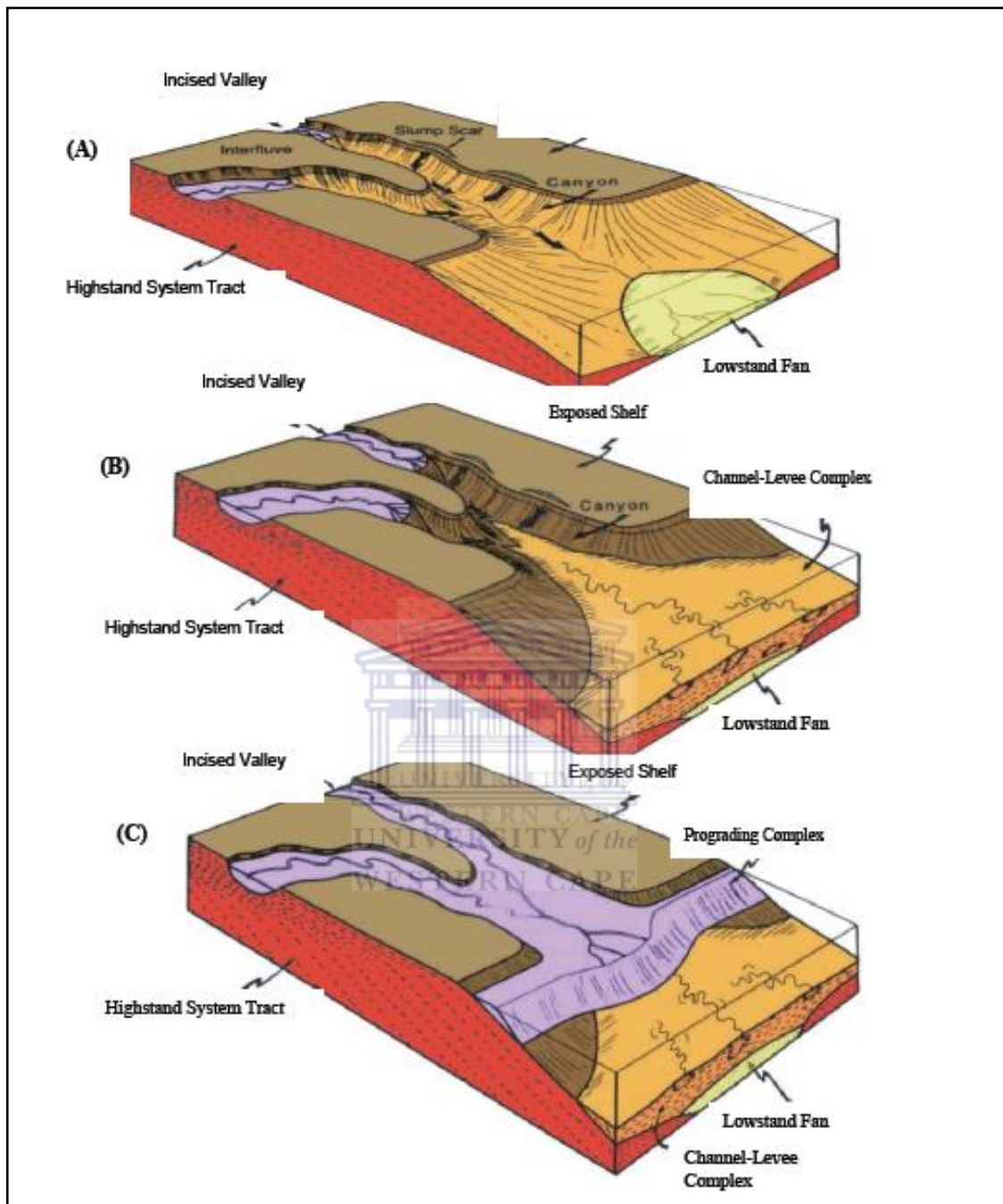


Figure 3.10: (A) Basin floor fan canyon, (B) Channel-Levee complex on basin floor fan (C) prograding complex terminates canyon filling episode (modified from Broad, 2000).

CHAPTER FOUR

4.0: **Materials, analytical techniques and experimental procedures.**

4.1: **Introduction**

This chapter gives a synopsis of the various techniques used in this study. The framework diagram in chapter one (Fig. 1.0) provides a schematic look at the methodological approach followed while figure 4.1 presents the flow chart of the various methods that were used in the course of this study. Well logs and core samples were obtained from the Petroleum Agency, South Africa and the softwares employed for this study includes Petrel 2011.1, Interactive Petrophysics, Kingdom suites (SMT) and Sedlog.

The data sets include:

- ✚ Conceptual map for the block.
- ✚ Digitized wire line log (LAS format) data and 2D seismic lines.
- ✚ Composite paper logs.
- ✚ Core data and sedimentological core logs.
- ✚ Well survey data.
- ✚ Well completion report.
- ✚ Core samples of selected depths for analysis.

The process starts with the review of previous studies and literature search in comparable oil and gas fields needed to provide information on the basin geometry, tectonic history sediment source, diagenetic history, flow units and structural features. The discussion of the quantitative mineralogy techniques includes the principle of measurement, sample preparation and analytical programs used in the study. The textural similarities and elemental geochemistry of some interested depth and section are carried out. This is supported with the use of wire line logs to pick out the depths of interest for correlation purpose. The core mineralogy was measured by whole rock x-ray diffraction (XRD) for the purpose of validating modeling result from the EDAX analysis. The multiminerall analysis study would create a geologic model which will be used to enhance the characterization of the reservoir especially where clay is present. The internal architecture of reservoir rock of interested sections was determined with SEM to reveal the diagenetic history of each well. The data collection segment has list of all the data collected from petroleum Agency SA, which is used in this thesis. They

are being loaded into the softwares used to display the log curves reference to Kelly bushing (RKB).

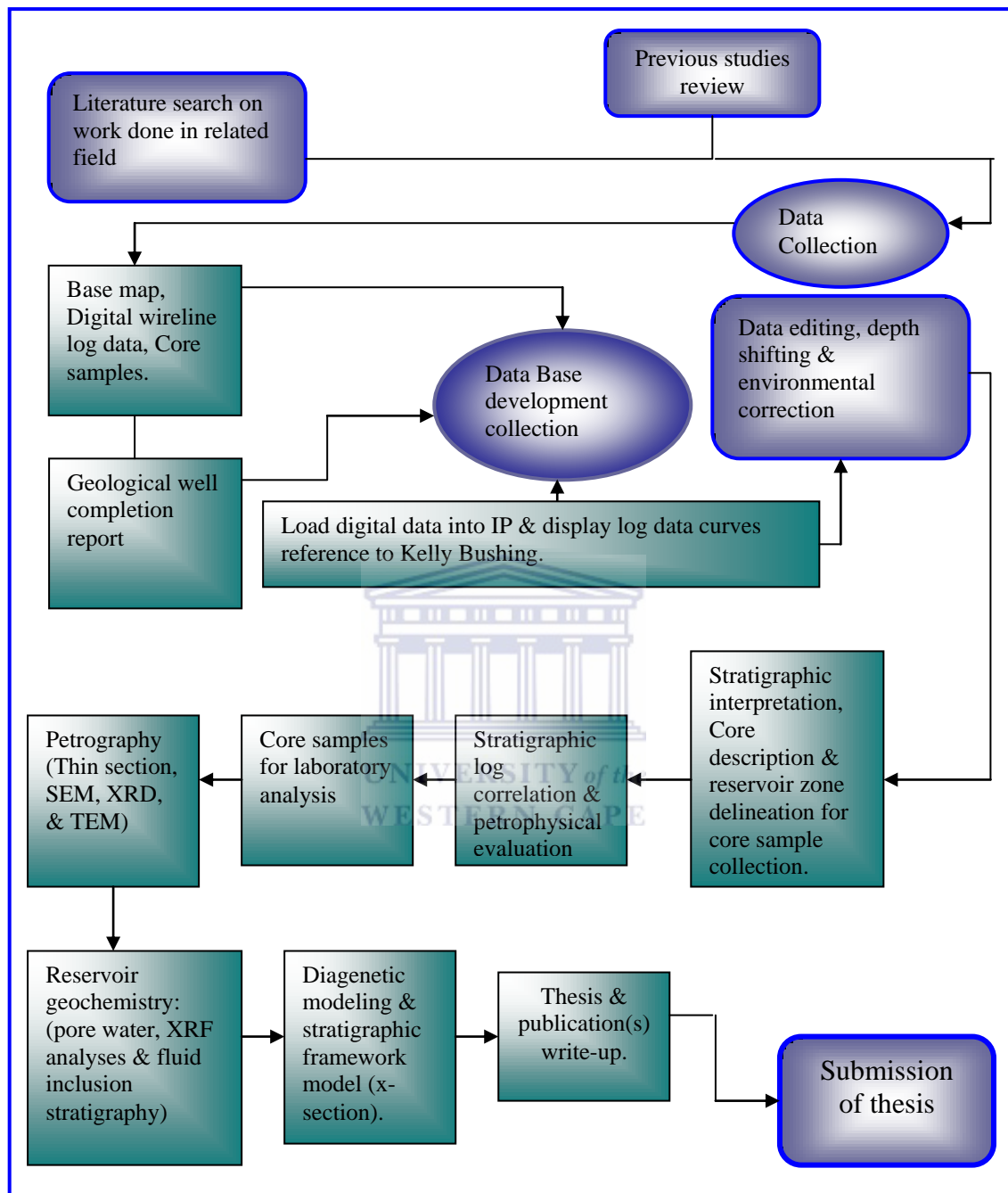


Figure 4.1: The flow chart of the research methodology.

4.1.1: Wireline logs loading

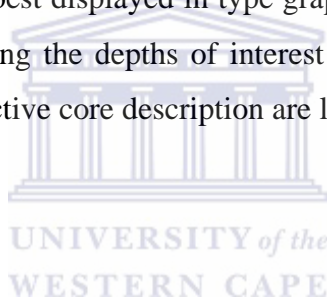
Interactive Petrophysics (IP) and Petrel 2011.1 were used for the loading to display of the log curves, the data were received in LAS format and were loaded directly into the Interactive Petrophysics workstation where depth shifting was done based on the core description along with necessary environmental corrections. This data was exported from Interactive Petrophysics in “ASCOUT” format and converted

into ASCII word-pad format loadable into Petrel. Proper quality control was performed and reservoir zones were identified using the appropriate well logs. Interactive Petrophysics and Petrel were chosen to model this reservoir because they are window based softwares for 3D visualization with a user interface based on the windows Microsoft standards as well as shared earth modelling. A data base was created within Interactive Petrophysics and Petrel clearly delineating the different information and data needed to complete this project. The geophysical, geological and petrophysical data was imported to Interactive Petrophysics within the main data base through this it was possible to generate and visualize the imported data in 2D and the core data crossplots in 3D.

4.1.2: Core description procedure

Core description comprises a combination of quantitative and qualitative data, which needs to be concisely recorded. The quantitative information varies continuously down hole and best displayed in type graphic plot. The core description processes started by identifying the depths of interest and then laying out of cores. The equipments used for effective core description are listed below:

- ❖ Digital Camera
- ❖ Tape rule
- ❖ Log sheet
- ❖ Microscope
- ❖ Sample bags
- ❖ Pyrex spot plate
- ❖ Hammer
- ❖ Water bottle and foam
- ❖ Small Clip board
- ❖ Hand lens
- ❖ Grain size standard chart



After the laying out of the core, the total depth was established as well as the log format. The samples were laid out in compartmentalized trays to enable a sequence of five to ten samples be observed in a single tray. The samples were laid in a stack of five-cell trays with the depths marked on the trays. Ten metres or more of the samples were scanned to observe the lithologic “breaks”. The samples were then re-examined for more detailed study in order identify other properties. Wetting the samples not

only cleans off mud and other contaminants, but also brings out the rock characteristics that are not apparent in the dry samples.

Critical visualization was done by observing the following parameters: rock type, sedimentary structures and grain size variation, packing pattern, fossils assemblages, colour, textures, cement/matrix and the effect of HCL on the samples. During the description, the rock type was first established, after which the colour was determined using the standard geologic colour chart, then a proper examination was done to determine the grain size, texture and degree of sorting. The sedimentary structures were observed and recorded however, some of these structures cannot be seen by our naked eye thus, chips were taken out of the core samples using hammer, and examined under microscope in the laboratory. In the cause of the microscopic examination, the cement/matrix, fossil content, and some minerals were observed. The representative chips selected were etched lightly in dilute HCL (10ml) and placed in a clear pyrex spot plate and then quickly viewed again under the microscope to observe the degree of effervescence, reaction and etching in order to detect the presence of calcareous materials and possibly to identify some other minerals as well as to estimate porosity.

4.1.3: Petrophysical calculation procedures

The abbreviations used in this section can be found in Table 4.1 below. The methodological approach used in arriving at the petrophysical results was as follows:

4.1.3.1: Volume of shale (V_{sh})

The values of shale volume (V_{sh}) were derived from gamma ray log. Stieber method was used for the estimation as it has the advantage of suppressing likely initial high response of GR log to a small amount of shale (Olajide, 2005). It defines volume of shale as: Vsh =

$$\frac{I_{sh}}{(3 - 2I_{sh})} \dots\dots\dots (1)$$

Or

Clavier’s model for Older rocks given as: 0.33 (2^{2I_{sh}} - 1) or Stieber model I_{sh}/ (3-2I_{sh}).

I_{sh} is the gamma ray shale Index which varies from 0 – 1 and it is given as:

$$I_{sh} = \frac{Y_{log} - Y_{cl}}{Y_{sh} - Y_{cl}} \dots\dots\dots (2)$$

4.1.3.2: Porosity

Porosity of the selected reservoir formation is determined from the recorded porosity logs. The logs used for this research work are density (RHOB) and neutron (NPHI) logs.

Porosity from density log (Φ_D) is given as:
$$\frac{\rho_{ma} - \rho_{log}}{\rho_{ma} - \rho_f} \dots\dots\dots (3)$$

Note: The standard density for sandstone used in this calculation is 2.65g/cm³ while that of shale is 2.7 g/cm³ (Rider, 1982).

Porosity from neutron log (Φ_N) was read and then corrected with the 1972 Schlumberger chart (Fig. 5.7.2) to generate a corrected porosity from neutron log (Φ_{CNL}).

Total Porosity (Φ_T) is given by:
$$\frac{\Phi_D + \Phi_{CNL}}{2} \dots\dots\dots (4)$$

However for this research work total Porosity (Φ_T) for better estimation of gas zone was used which is given as:
$$[0.5 * (\Phi_D^2 + \Phi_{CNL}^2)]^{0.5} \dots\dots\dots (5)$$

Effective Porosity (Φ_{eff}) is given as: $\Phi_T * (1 - V_{sh})$ provided V_{sh} is determined using Stieber method.

4.1.3.3: Formation water resistivity

Formation resistivities; R_t and R_s are taken directly from the resistivity record of deep and shallow resistivity measuring devices. Invaded zone resistivities R_s were deduced directly from: Spherically Focused Log (SFLU), Shallow Laterolog (LLS), and Microspherically Focused Log while uninvaded zones resistivities or true formation resistivities R_t were recorded by: Deep induction Log (ILD) and Deep Laterolog (LLD) Formation water resistivity (R_w) was estimated from clean non shaly water filled reservoir using relationship between formation factor and shale free, water filled formation defined by Gus Archie in 1940 – 1941. In shale free, water filled formation, formation factor (F) is a constant defined by: $F = R_0 / R_w$ where $F = a / \Phi^m$

By rearranging the equation: $R_w = (\Phi_D^{m/a} * R_0)$

Note: R_w , a, m and n used for this research work evaluation were 0.09 Ωm at 200°F, 1, 1.94 and 1.80 respectively. The a and m were obtained from the electrical properties measurement from special core analysis (SCAL) from F-O1, F-O3 and F-R1 wells while the R_w was based on the pickett plot (F-O2) R_w from SP and water gradient slope from RFT pressure data obtained from the well report.

4.1.3.4: Water saturation (S_w) and Hydrocarbon saturation (S_{hc})

In a hydrocarbon bearing reservoir, the void spaces are partly occupied by formation water and remaining volume by hydrocarbon. The resistivity of hydrocarbon reservoir is function of formation factor (F), Resistivity of formation water (R_w) and its water saturation (S_w).

Using Archie's equation, water saturation (S_w) for hydrocarbon bearing reservoir is defined as: $S_w = [F * (R_w / R_t)]^{0.5}$

Where $F = a / \Phi^m$

Hydrocarbon saturation (S_{hc}) is the fraction of pore volume filled with hydrocarbon (oil and gas). It is given by: $S_{hc} = 1 - S_w$

4.1.3.5: Bulk volume of water (V_b)

This is the measure of the quantity of formation water present in a unit volume of rock. It is defined as the product of water saturation (S_w) and porosity (Φ)

$$V_b = S_w * \Phi$$

4.1.3.6: Irreducible water saturation (S_{wir})

This is the minimum saturation attainable by reservoir water when displaced from porous medium by immiscible hydrocarbons i.e. the fraction of pore volume occupied by water in the reservoir at maximum hydrocarbon saturation. It is normally used in preparation for permeability calculation.

This is defined as: $S_{wir} = \frac{V_b}{\Phi_{eff} / (1 - V_{sh}^2)}$ (5)

Note: $S_w = S_{wir}$: implies an obvious hydrocarbon bearing zone

$S_w > S_{wir}$ implies production hydrocarbon likely with some water cut

$S_w < S_{wir}$ implies error in calculation

4.1.3.7: Permeability (K)

The values of permeability of selected reservoir rocks are calculated using Coates simplified method. This method works well in shaly sands (Crain, 2004). The generated values also correlate well with values estimated from core analysis.

Coates defines Permeability (K) in millidarcies as:

$$K = G\Phi_{eff}^4 \left[\frac{[\Phi_T - (\Phi_{eff} * S_{wir})]}{\Phi_{eff} * S_{wir}} \right]^2$$

Note: $G = 65,000$ to $10,000$ for oil, 650 to 1000 for gas (Crain's Petrophysical Handbook). However G is taken to be 1000 in this study based on the gas prone potentials.

Table 4.1: Petrophysical properties nomenclatures

No	Description & symbol Units	Units
i	Shale Index (I_{sh})	API
ii	Volume of shale (V_{sh}) fraction	Fraction
iii	Total Porosity (Φ_T)	% or fraction
iv	Effective Porosity (Φ_{eff})	% or fraction
v	Resistivity of formation (R_t, R_w)	Ωm
vi	Water saturation (S_w)	% or fraction
vii	Hydrocarbon saturation (S_{hc})	% or fraction
viii	Irreducible water saturation (S_{wir})	% or fraction
ix	Bulk volume of water (V_b)	Fraction
x	Formation factor (F)	Constant
xi	Permeability (K)	millidarcies (mD)
xii	Permeability scale factor fractional (G)	Constant
xiii	Gamma ray in zone of interest (γ_{log})	API
xiv	Gamma ray for shale baseline (γ_{sh})	API
xv	Gamma ray for cleanest formation (γ_d)	API
xvi	Matrix/grain density (ρ_{ma})	g/cm^3
xvii	Fluid density (ρ_f)	g/cm^3
xviii	Porosity from density log (Φ_D)	g/cm^3
xix	Porosity from reservoir unit (ρ_{res})	g/cm^3
xx	Porosity from shale above the reservoir unit (ρ_{sh})	% or fraction
xxi	Porosity from neutron log (Φ_N)	% or fraction
xxii	Corrected Porosity from neutron log (Φ_{CNL})	% or fraction
xxiii	True formation resistivity (R_t)	Ωm
xxiv	Formation water resistivity (R_w)	Ωm
xxv	Porosity exponent (m)	Constant
xxvi	Saturation exponent (a)	Constant

4.1.4: Thin section procedure

Thin section was prepared by making a thin slice of about a centimetre thick from the sample with a diamond saw. The slice glued to glass slide and further thinned with diamond saw. The slide was thinned further by grinding with progressively finer abrasives. When the thickness has been reduced to about 0.03 mm,

a thin cover was glued to the top of the slice to complete the thin section. Thin sections were studied with a petrographic microscope fitted with a polarized light source. The effect of the passage of polarized light through the individual mineral crystals were analysed and information about the arrangement of the atoms of the crystals were obtained.

4.1.5: Scanning electron microscopy procedure

Scanning electron microscopy is a versatile and well-established complementary technique to light optical microscopy. By using a beam of electrons instead of photons, samples can be imaged at far higher magnifications. The Topcon Leo S440 at ITRI Innovation is capable of imaging up to 100,000 times magnification, although in practice magnifications of this magnitude are seldom required. The Leo S440 is also fitted with an energy-dispersive x-ray (EDX) spectrometer. This device measures the energy of x-rays that are generated by the atoms of the sample during interactions with the electron beam. The x-ray spectra formed are characteristic of the atoms that formed them, allowing the chemical composition of the sample to be determined. Pellets are prepared by using very little grams (> 0.3 g) of the samples, the pellets were first selected and the surface was covered with adhesive, after some minutes this minute sample was spread on the pellet evenly, this process was repeated for all the samples. The pellets were inserted into a carbon sputter where they were coated with carbon. After coating the pellet with carbon, it was then inserted into the SEM machine for image/EDX analysis. The diagram below explains the workability of the SEM (Fig. 4.2), the focused electron beam was deflected in x and y direction by the scanning system. The deflection is controlled such that small rectangular frame was scanned on the system's surface. The scanning system synchronised the electron beam in the microscope with the electron beam inside the monitor that is used to display the image. The intensity of the monitor was modulated by the signal that was obtained from the electron detector in the SEM.

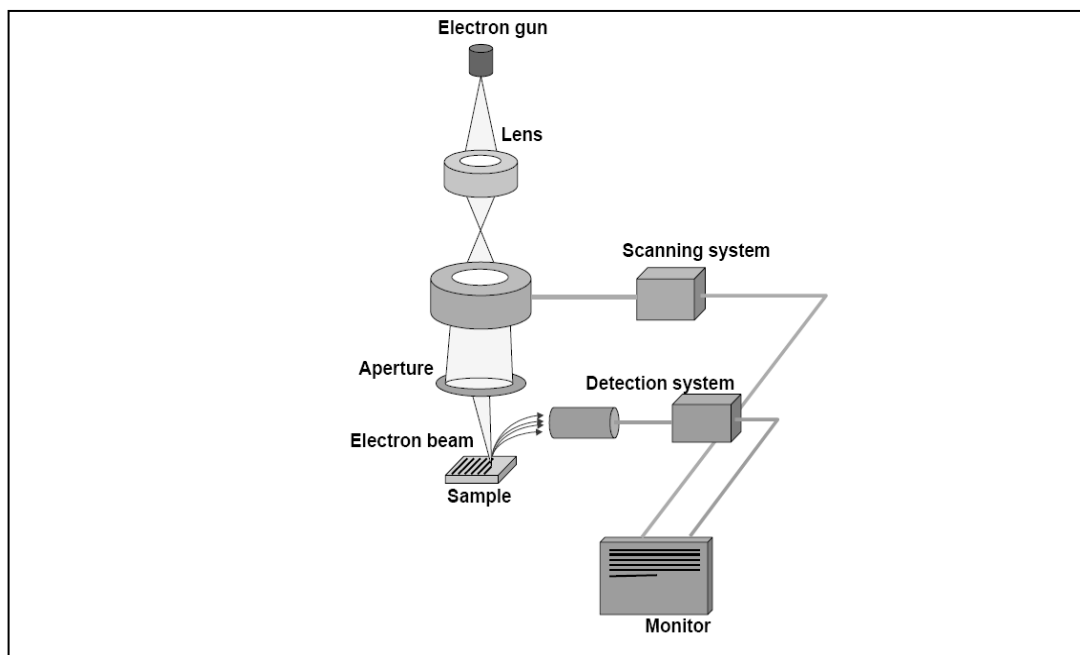


Figure 4.2: Scanning and detection system in scanning electron microscope (Theodoor, 2000).

In this way, the image was built point by point and line by line, with intensity in each point that is proportional to the signal from the electron detector. The signal from the electron detector is in turn dependent on the amount of electrons collected. The magnification is defined as the ratio of the size of the image on the monitor and the size of the frame that is scanned on the sample's surface. The magnification was increased by reducing the size of the scanning frame, which is controlled by the scanning coils.

4.1.6: X-ray diffractometry (XRD)

Diffraction measurements for phase identification were done using BRUKER D8 ADVANCE diffractometer at iThemba LABS x-ray facility (Fig. 4.3). Measurements were done using the 8 KeV Cu radiations. The X-ray generator was operated at 40 kV and 40 mA. Experimental set-up included a 3° divergence slit on the primary side and 3 ° on the secondary side. The diffracted beam was collected with a 4° window position sensitive detector, Lynx eye. Samples were measured from 2-theta start of 10 ° to 2-theta stop 85 °, with step size of 0.02 ° and step time of 0.3 s. The analysis of the data was carried out using BRUKER's Eva software.

4.1.6.1: XRD diffractometry semi quantification procedure

The samples were prepared for XRD analysis using a back loading preparation method analysed with a PANanalytical X'Pro powder diffractometer with X'Celerator detector and variable divergence and fixed receiving slits with Fe-filtered Co-K α radiation. The phase were identified using X'Pert Highscore plus software with the relative phase amounts (weight %) estimated using the Rietveld method.

The following were noted in the course of reading the results:

- ✚ Errors are on the 3 sigma level below the amount.
- ✚ Mineral names may not reflect the actual compositions of minerals identified, but rather the mineral group (i.e. “muscovite” represents the “Mica” group).
- ✚ Ethylene glycol and heating to 500 °C test were performed on some selected samples and it was established that chlorite and not smectite are present in most samples. The heating test confirmed the absence of serpentine and chlorite was used in the quantification, although traces of kaolinite may be present.
- ✚ Errors reported for phases occurring in minor amounts are sometimes larger than that of the quantity reported, indicating the possible absence of those phases.
- ✚ As the samples were pulverized to a very small particle size, it was not possible to do the clay separation.
- ✚ Amorphous phases, if present, were not taken into account in the quantification.



Figure 4.3: BRUKER D8 ADVANCE XRD instrument with pw3830 X-ray generator operated at 40Kv and 40mA.

4.1.7: Pore water geochemistry procedure

The pH, electrical conductivity (EC) and redox potential (Eh) parameter of the extracted interstitial pore water were achieved using 1:10 core sample to water ratio. 5 grams each of the core samples taken at depths of interest were weighed into a beaker and 50 ml of ultra-water was added. The mixture was then shaken thoroughly for 1 hour using a mechanical shaker, allowed to settle for 15 minutes after which the solution was filtered through whatman no 2 filter paper and the pH, EC and Eh of the supernatant recorded. After each measurement, the pH meter is preserved in potassium chloride (KCl). The pH meter was calibrated before use with buffer solution of pH 4.0, 7.0 and 10 while the procedure was duplicated for each sample at each depth at room temperature. The pH and Eh measurement was carried out using Metrohm 827 pH Lab with Metrohm pH-electrode respectively with the later using a Pt-redox electrode while the EC was measured with Jenway 4510 Conductivity meter. Anions and cations of the filtrate were measured using Ion chromatograph and ICP-MS respectively.



Figure 4.4: Hanna HI 991301 pH meter with portable pH/EC/TDS/Temperature probe.

4.1.7.1: Electrical conductivity (EC) measurement

Electrical conductivity measurements focuses on salts - or their ions when dissolved in water - which are conductors of an electrical current. Conductivity is measured by a probe that applies voltage between two electrodes, spaced a known distance apart, and records the drop in voltage. This drop reflects the resistance of the

water, which is then converted to conductivity. Thus, conductivity is the inverse of resistance and is measured as the amount of conductance over a certain distance. Electrical conductivity is normally measured in mS/cm or $\mu\text{S}/\text{cm}$, or in $\mu\text{mhos}/\text{cm}$ ($1\text{mS}/\text{cm} = 1000 \mu\text{mhos}/\text{cm}$). The electrical conductivity (EC) measurement of the samples was determined using a Jenway 4510 Conductivity meter. The meter was calibrated before use by using a standard of $12.88 \text{ mS}/\text{cm}$ at room temperature. Duplicate samples measurements were taken at room temperature.

4.1.7.2: Ion chromatography (IC)

Ion chromatography is a form of liquid chromatography where retention is predominantly controlled by ionic interactions between the ions of the solute and counter ions that are situated in, or on the stationary phase. For example, to separate organic acids, it is the negatively charged acid ions that need to be selectively retained. It follows that the stationary phase must contain immobilized positively charged cations as counter ions to interact with the acid ions to retain them. Alternately, to separate cations; the stationary phase must contain immobilized anions as counter ions with which the cations can interact (Fritz, 2005). Ion exchange stationary phases are available in mainly two forms. One form (probably the most popular) consists of cross-linked polystyrene polymer beads of an appropriate size which have been suitably treated to link ionic groups to the surface.



Figure 4.5: Ion chromatography system-Dionex ICS-1600 (RFIC).

The other form is obtained by chemically bonding ionic groups to silica gel by a process similar to that used to produce bonded phases. These materials are called ion exchange media, a term which has given rise to the term “ion exchange chromatography” as an alternative to ion chromatography. Ionic substances can also be adsorbed on the surface of a reverse phase media and act as an adsorbed ion exchanger. The mobile phase is made to contain a small percentage of a soluble organic ionic material (e.g. tetrabutyl ammonium dihydrogen phosphate or n-octyl sulphonate). These substances are adsorbed onto the surface by dispersive interactions between the alkyl groups of the agent and those of the bonded phase and act as counter ions (Dionex, 1998).

Ion chromatography is an analytical method of choice for inorganic anions and cations (Haddad, 2004). The instrument can separate and determine anions such as chloride, chlorate, nitrate, chromate sulfate, thiocyanate and perchlorate (Tyrell et al., 2009). It uses ion-exchange resins to separate atomic or molecular ions based on their interaction with the resin. Its greatest utility is for analysis of anions for which there are no other rapid analytical methods (Dionex, 1998). The instrument analyzes aqueous samples for quantities of common anions such as fluoride, chloride, nitrite, nitrate and sulphate in parts per million (ppm) and parts per billion (ppb) for common cations like lithium, sodium and potassium using conductivity detectors. The Ion Chromatography (IC) unit was first calibrated with a certified reference standard solution and then recalibrated after every 10 samples. Reference value of standards are: F = 20.07 mg/L; Cl = 30.04 mg/L; Br = 100.3 mg/L; NO₃ = 100.2 mg/L; NO₂ = 99.9 mg/L; PO₄³⁻ = 150.2 mg/L; SO₄²⁻ = 150.1 mg/L. Average values are: F = 20.05 mg/L; Cl = 29.95 mg/L; Br = 100.6 mg/L; NO₃ = 100 mg/L; NO₂ = 100.35 mg/L; PO₄³⁻ = 149.15 mg/L; SO₄²⁻ = 150.15 mg/L. Common application areas of IC include environmental analysis, clinical analysis, and industrial analysis, bio analysis (Haddad, 2004, Haddad et al., 2008) just to mention a few. The filtrates of the core samples sandstone were filtered through a 0.45 μm membrane filter with the aid of a vacuum pump to remove suspended solids. SO₄²⁻, Cl⁻, NO₃⁻ and PO₄³⁻ were analyzed in the filtrates using a Dionex DX-120 ion chromatograph with an Ion Pac AS14A column and AG14-4 mm guard column (located at Soil Science Department, University of Stellenbosch, South Africa) and Dionex ICS-1600 (Fig. 4.6; located at Chemistry Department, University of the Western Cape, South Africa).

4.1.8: Inductively coupled plasma mass spectroscopy (ICP-MS)

ICP-MS originally was designed primarily to replace atomic absorption and ICP-optical emission instrumentation for analysis of metals in aqueous and organic matrices (Geiger and Raynor, 2009). The Inductively Coupled Plasma Mass Spectroscopy (ICP-MS) was introduced commercially in 1983 (Beauchemin, 2008), the basic design is still the same today. ICP-MS gives very high sensitivity for the determination of elements and it is good at separating isotopes of the same element. It is well-suited to detecting very small amounts of material, in the parts per billion (ppb) to the parts per trillion (ppt) range. The dynamic range is typically ten orders of magnitude and data reduction is relatively simple.



Figure 4.6: ICP optical emission spectrometer (Varian 710-ES).

Rapid data acquisition and data reduction enables the measurement of large numbers of samples in a short period of time. ICP-MS is the technique of choice for trace element analysis of natural waters, and can be used in analyzing minerals and rocks after digestion. One of the major short coming of ICP-MS technique is its susceptibility to matrix effects (Beauchemin, 2008). In general, liquid samples are introduced by a peristaltic pump (brings the liquid sample in at about 1 mL per minute), to the nebulizer where the sample aerosol is formed. A double-pass spray chamber ensures that a consistent aerosol is introduced into the plasma. Argon (Ar) gas is introduced through a series of concentric quartz tubes which form the ICP. The torch is located in the center of an RF (radio frequency) coil, through which RF

energy is passed. The intense RF field causes collisions between the Ar atoms, generating high-energy plasma. Thus, the ICP portion of the technique, or the “inductively coupled plasma” aspect, continues to supply radio frequency energy to the argon gas, forming more ions, and making more plasma. The sample aerosol is instantaneously decomposed in the plasma (plasma temperature is in the order of 6000 -10000 K) to form analyte atoms which are simultaneously ionized (Wilbur, 2009). The ions produced are extracted from the plasma into the mass spectrometer region which is held at high vacuum (typically 10^{-4} Pa). The vacuum is maintained by differential pumping: the analyte ions are extracted through a pair of orifices known as sampling and skimmer cones. The analyte ions are then focused by a series of ion lenses into a quadru-pole mass analyzer, which separates the ions based on their mass charge ration.

Finally, the ions are measured using an electron multiplier, and are collected for each mass number (<http://www.chem.agilent.com/en-us/products/instruments/icp-ms/pages/gp455.aspx>; accessed on 16/12/2011). In this study, analyzed samples were filtered with 45 μm membrane filter paper to remove suspended solids and refrigerated before analysis. Major and trace elements were analyzed using ICP-OES (Varian 710-ES) (Fig. 4.7), ICP-AES (Varian Liberty) and ICP-MS (Agilent 7500ce). The inductively coupled plasma mass spectrometry (ICP-MS) and the inductively couple plasma atomic emission spectrometry (ICP-AES) were calibrated twice daily using multi-element standards, with a calibration verification standard analyzed directly after the calibration and control standards for every 12 samples run by the ICP-MS and every 20 samples for the ICP-AES. Internal standards were used to correct for instrument drift in ICP-MS.

4.1.9: Bulk geochemical composition by x-ray fluorescence spectrometry

The bulk chemical compositions of the reservoir core samples were determined with X-ray fluorescence spectrometry. XRF is ideal for rapid and accurate whole bulk elemental analysis in rock or soil samples (Akinyemi et al., 2011). The gas-flow proportional counting detector and scintillation detector, or a combination of the two, are used to cover the elements fluorine to uranium. Major oxides (Na_2O , MgO , SiO_2 , K_2O , CaO , TiO_2 , MnO , P_2O_5 , Al_2O_3 , Cr_2O_3 and Fe_2O_3) are analysed on a fused glass bead and trace elements (Cr, Ni, Zn, As, Ga, Co, V, Rb, Sr, Y, Zr, Nb, Ce, Nd, La, Th, U, Ba as well as S and Cl) are analysed on a powder briquette. A wide range of international (NIST®) and national (SARM®) standards is used in the

calibration procedures and quality assurance (accuracy) for both major and trace element analyses. Detection limits for the elements quoted, depending on the matrix (combination of elements present), are approximately 0.5 ppm for trace elements on a pressed pellet and approximately 0.001 wt% for major elements on a fused bead. A local granitic sample “HG” is used as in-house secondary process control for quality control (precision) purposes.

Loss on ignition (LOI) is a test used in XRF major element analysis which consists of strongly heating a sample of the material at a specified temperature, allowing volatile substances to escape or oxygen is added, until its mass ceases to change. The LOI is made of contributions from the volatile compounds H_2O^+ , OH^- , CO_2 , F, Cl, S; in parts also K and Na (if heated for too long); or alternatively added compounds O_2 (oxidation, e.g. FeO to Fe_2O_3), later CO_2 (CaO to CaCO_3). In pyro-processing and the mineral industries such as lime, calcined bauxite, refractories or cement manufacture, the loss on ignition of the raw material is roughly equivalent to the loss in mass that it will undergo in a kiln, furnace or smelter.

Below is the sequential approach used in carrying out the major and trace element analysis for this study.

Fusion bead method for major element analysis:

- Weigh $1.0000\text{g} \pm 0.0009\text{g}$ of milled sample
- Place in oven at $110\text{ }^\circ\text{C}$ for 1 hour to determine H_2O^-
- Place in oven at $1000\text{ }^\circ\text{C}$ for 1 hour to determine LOI
- Add $10.0000\text{g} \pm 0.0009\text{g}$ Claisse flux and fuse in M4 Claisse fluxer for 23 minutes.
- Flux type: Ultrapure Fused Anhydrous Li-Tetraborate-Li-Metaborate flux (66.67 % $\text{Li}_2\text{B}_4\text{O}_7$ + 32.83 % LiBO_2) and a releasing agent Li-Iodide (0.5 % LiI).

Pressed pellet method for trace element analysis:

- Weigh $8\text{g} \pm 0.05\text{g}$ of milled powder
- Mix thoroughly with 3 drops of Mowiol wax binder
- Press pellet with pill press to 15 ton pressure
- Dry in oven at $100\text{ }^\circ\text{C}$ for half an hour before analysing.

List of standard reference materials commonly used:

- NIM-N, -G, -S, -P, -D

- AGV-1
- BHVO-1
- GA
- GH
- GSN
- SY-2, -3
- BCR

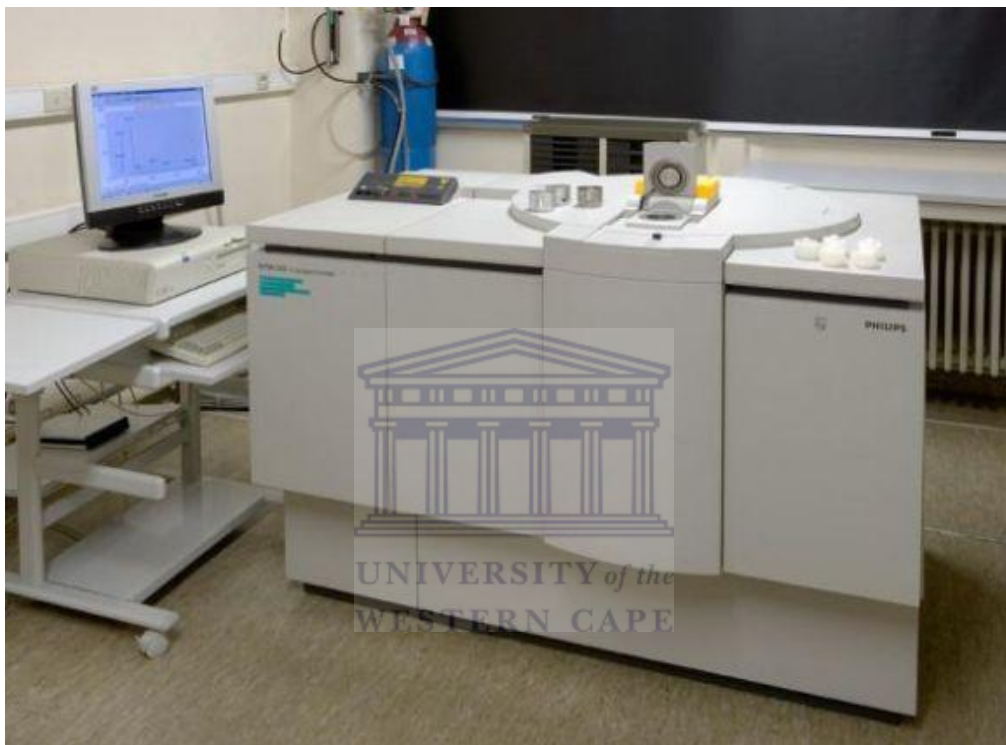


Figure 4.7: Axios from PANalytical with a 2.4kWatt Rh x-ray tube

4.1.10: Fluid inclusion stratigraphy procedure

Fluid inclusion stratigraphic (FIS) studies was carried out on forty samples for trapped volatiles within the sandstones while thirteen core and cuttings samples out of the forty analysed sample for FIS from six wells were evaluated petrographically for fluid inclusion populations, abundance, characteristics, fluorescence colours, kerogen and bitumen. The samples are polished and the slabs of rock materials are prepared and studied optically with a petrographic microscope (Fig 4.9). Samples are viewed under transmitted plane-polarized white light as well as under reflected ultraviolet or blue-violet illumination in order to verify the presence of petroleum-bearing inclusions in the rock samples and to explore textural relationships that may yield additional information on the timing of hydrocarbon migration or generation.

Aromatic species containing condensate inclusions and natural oils render them fluorescent under UV light. Hence, aqueous inclusions, non-fluorescent gas and fluorescent condensates and oils were identified and their relationship to each other, diagenetic features (e.g., physical and chemical compaction) and the rock matrix can be resolved.

Prior to fluid inclusion stratigraphic analysis, samples of rock material are freed of significant interfering contamination by washing, picking and magnetic separation as necessary to remove drilling fluids, lost circulation materials, other solid mud additives such as gilsonite, and metallic particles from the drill-string. Cleaned samples are loaded with appropriate standards into specially designed auto-samplers and are heated in a vacuum oven for a minimum of 24 hours. This is done to remove adsorbed organic and inorganic volatile materials that could interfere with the analysis. The auto-sampling device is placed in the vacuum system and evacuated to appropriate high vacuum. Bulk fluid inclusion volatiles are afterwards instantaneously released from each sample in a sequential manner by automated mechanical crushing. Volatile organic and inorganic species are dynamically pumped through quadrupole mass analyzers (DQ 1000™ mass spectrometer) where they are ionized, separated according to their mass/charge and recorded. C₁ – C₁₃ petroleum species and sulphur bearing compounds including H₂S, SO₂, COS, CS₂ and SO₂ were analyzed. The main objective is to evaluate samples for presence, distribution and character of hydrocarbon inclusions (Figs. 4.8; 4.9).

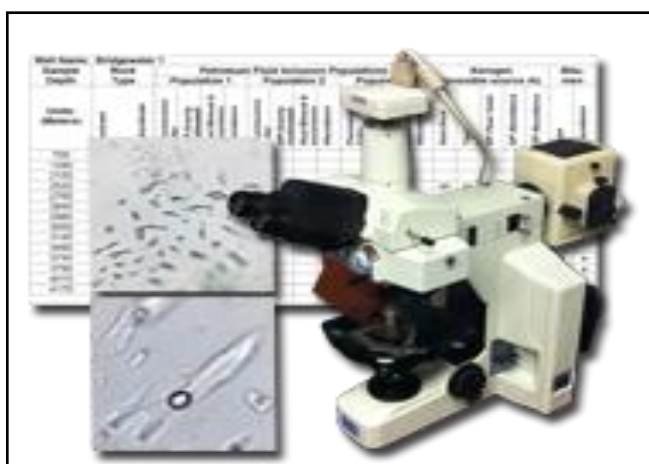


Figure 4.8: Fluid inclusion petrography instrument (www.fittulsa.com/mt_pet.php)

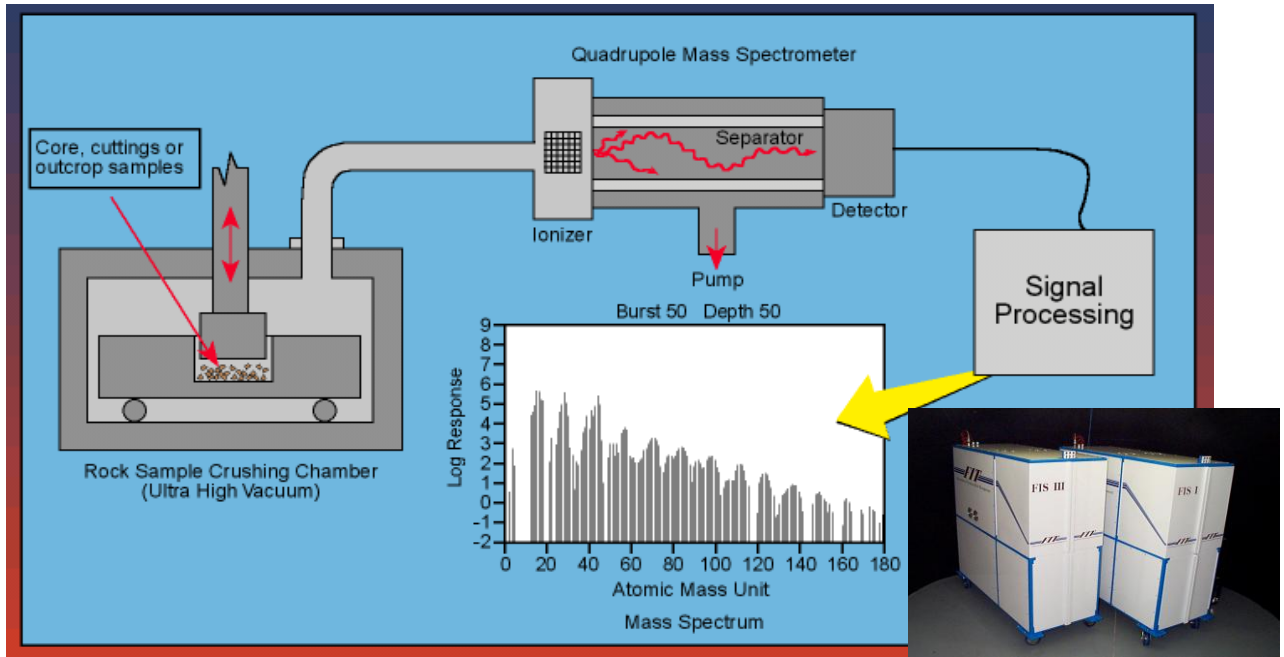


Figure 4.9: Schematic diagram showing the processes involved in carrying out fluid inclusion stratigraphy (www.fittulsa.com/mt_pet.php).



CHAPTER FIVE

5.0: Sedimentological, wireline logs and seismic results and discussion

5.1: Introduction to sedimentological analyses

Conventional sedimentological research has mainly been pre-occupied with the reconstruction of paleo-geography and external geometry of sediment bodies. The resulting depositional models which are primarily used for the exploration of hydrocarbon are therefore of qualitative nature. Less attention has been given to the quantification of reservoir architecture, internal organization, sediment body size parameters, and heterogeneities within and between the reservoir units (intra reservoir shale). These are major factors that control reservoir size and compartmentalization and reservoir performance. Accurate core description is a basic work, the foundation upon which the entire structure of subsurface investigation rests. The study of cores from both field and wildcat wells offer the opportunity to interpret subsurface rock sequences and relate them to surface sections, to calibrate mechanical logs with observed lithologies and to use these data to enhance both field development drilling and wildcat exploration.

This chapter presents core description results, wireline logs interpretation of six wells (F-O1, F-O2, F-O3, F-O4, F-R1 and F-S1) and seismic deep lines interpretation. Detailed core description is carried out to account for facies and facies associations, distribution of facies and depositional settings which includes a description of lithologies, fabrics, sedimentary structures, bedding thickness, and other pertinent features. The data are compiled and computer-drafted into a lithologic format using Sedlog software (Figs. 5.11 – 5.16) which includes other rock properties data such as mineralogical and fossil estimations. The vertical succession of texture and sedimentary structures help define the depositional facies of the sequence. The depositional facies define the geometry of the potential hydrocarbon reservoir. Lower Cretaceous is the age of interest in this study, therefore the interpreted core intervals in this chapter are all within the Valanginian age of the studied wells.

5.1.1: Facies and depositional environment: results and discussion

Six facies were recognized in the cores from the six wells (F-O1, F-O2, F-O3, F-O4, F-R1 and F-S1), grading from pure shale (Facies 1), through progressively coarsening interbedded sand-shale “heterolithic facies (Facies 2-4), to cross bedded and minor massive sandstone (Facies 5-6). There is no evidence of sub-aerial

emergence (e.g. roots, paleo-soils), but abundant evidence for fully marine salinity and tidal dominance. Figures 5.10 and 5.11 below reveals the different sedimentary structures observed during core examination on the six wells under study.

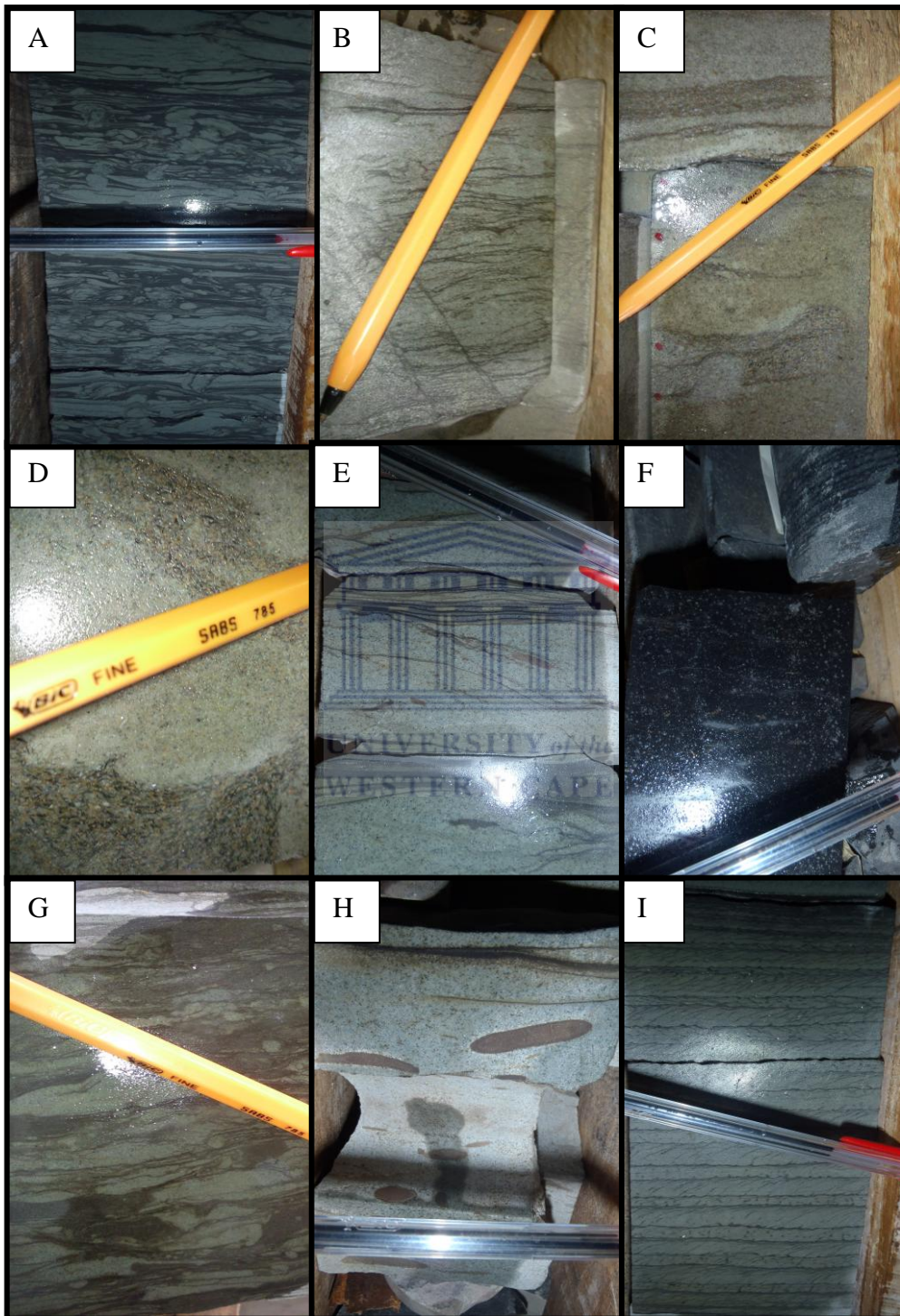


Figure 5.10: (A) Light-grey heavily bioturbated mudstone forming low density ichnofossil suite (B) Cross stratification revealed by diffused foreset mud drapes (C) Heterolithic sandstone with patchy brown coloration (probably siderite) (D) Sandstone with possibly pronounced brown coloration (probably siderite alteration) (E) Abundant ripple-scale foreset mud drapes (F) Un-slabbed dark-grey coaly mudstone (G) Bioturbated mudstone with some flaser lenses (H) Sandstone with pronounced nucleated oval shaped sideritic brown colored clast (I) Parallel laminated sandstone with sub-millimeters mud partings.

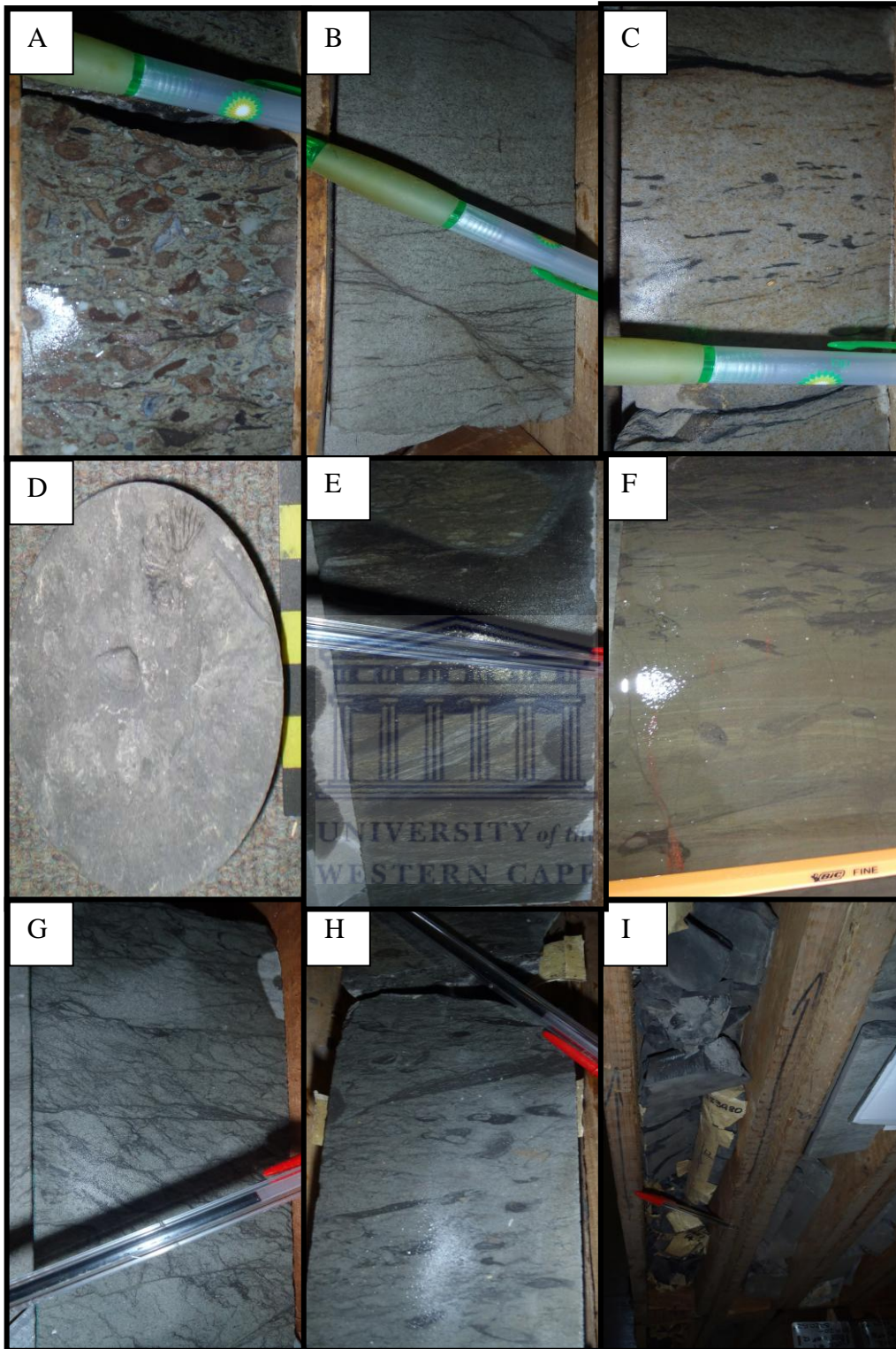


Figure 5.11: (A) Brecciated brown siderite-cemented mud (B) Herringbone cross bedding structure on sandstone (C) Decimetric massive sandstone containing mud flakes (D) Facie 1 mudstone showing ammonite (E) Dark-grey mudstone with strong evidence of concretions (patchy brown coloration) (F) Dirtying up trend of a shaly unit with some evidence of stylolite (G) Silty-shaly showing abundant foreset mud couplets (H) Silty-shale concentrically laminated mud drapes (I) Racks of shattered coaly shale (left) and strongly burrowed laminated sandstone (right).

5.1.2: Core interpretation and sedimentological analysis of F-O1 well

Four facies (F4, F5, F6, & F8) were recognized out of the generally eight delineated facies observed within the F-O field studied wells. Cored section of F-O1 well spanned from 3702 m – 3730 m with a considerable interval of sandstone (13 m) between 3714 m – 3727 m (Fig. 5.12a). The cored section generally contains mostly sandstone with few intervals of siltstone and heterolithic sand units. Different structures and features were noted within the cored section such as: stylolitized mud drapes with visible cross laminations (centimeter bands), plant concretions with evidence of alterations (Fig. 5.10D). Evidence of bioturbation is much more pronounced within the silt-stone interval (F5, F6 & F8) than in the sandstone units (F4). A non-laminated silty-stone was observed at the basal unit with floating and broken crystals (3730 m). Soft-sediment deformational structures were also noted which could have resulted from the differential compaction, liquefaction, sliding or slumping e.t.c (Li et al., 2008).

Lack of facts regarding sub-aerial emergence (e.g roots, paleo-soil, desiccation cracks indicates a permanently sub-aqueous environment. Glauconite with evidence of echinoids fragments (F4) and ammonites (F1) were noted indicating a fully marine salinity. Abundant foreset mud drapes (ripple and dune scale) coupled with lack of evidence for waves indicate deposition below fair-weather wave base i.e. not shoreface. The presence of foreset mud drapes indicates periodic slack of water i.e. tidal dominance while the evidence of a commonly double drape (Fig. 5.10E) indicates sub-low-tide-setting (always under water). The stylolite observed at the upper section (around 3705 m) could be attributed to a tidal flat shallow marine environment due to its association with mud drapes and the intense bioturbation seen. Figure 5.12b below shows the interpretation of the several lithologic symbols used in the constructed core graphs.

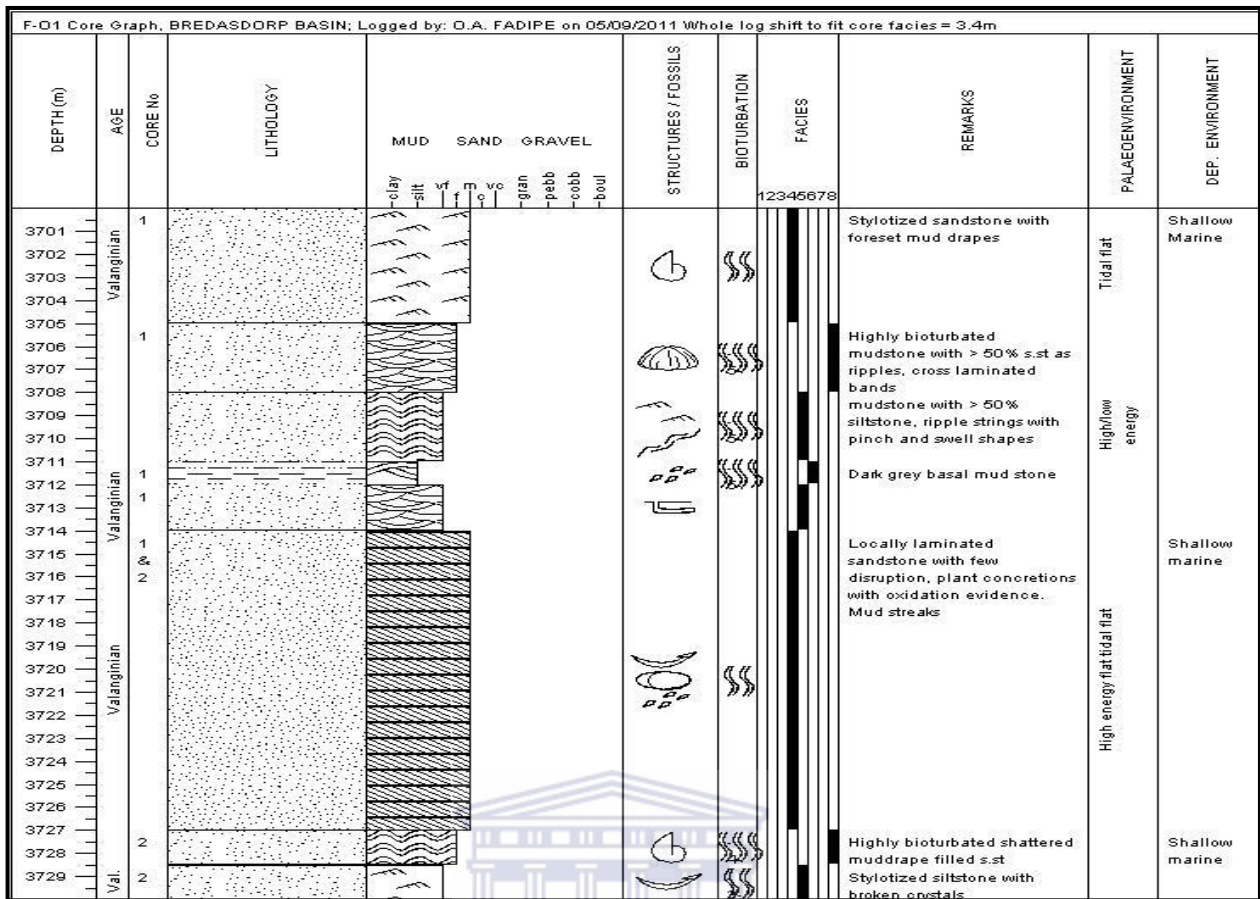


Figure 5.12a: Facies log of F-01 well Bredasdorp basin, offshore South Africa.

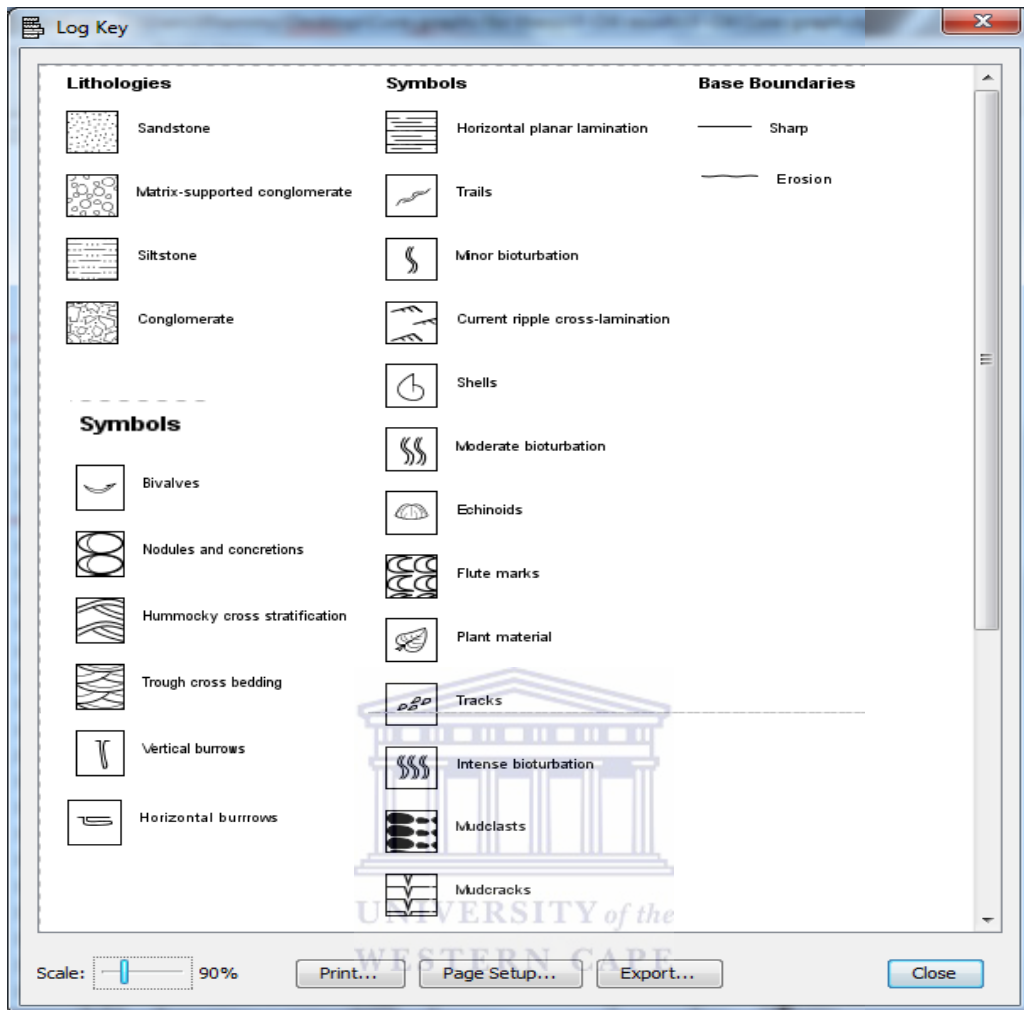


Figure 5.12b: General legend of the F-O field core graph

5.1.3: Core interpretation and sedimentological analysis of F-O2 well

Four facies (F4, F5, F6, & F8) were recognized out of the generally eight delineated facies observed within the F-O field studied wells. The F-O2 well has 4 different cored sections which ranges from 3615 m – 3746 m with a missing core noticed between 3687 m – 3725 m within core 4 (between Figs. 5.13a and 5.13b). The cored section is predominantly of sandstone with few streaks of shale and siltstone. There is strong evidence of bioturbation with imprint of micro-organism especially in F4 (Fig. 5.13a). Towards the top of the core graph, between the depth ranges of 3625 m – 3640 m are pronounced ripple marks with steep open fracture duely observed coupled with some coaly deposits, ball and pillow structures, clustering of mud drapes and cross laminations. The shally interval was accompanied with sharp-walled sand filled pseudo-borings in mud, Ophiomorpha burrows, non-laminated with silt streaks. Mud drapes cemented by siderite was also observed within the F4 which was confirmed as siderite after testing with HCl during core examination.

The clustering of mud drapes reflects spring-neap tidal cyclicity (Johnson and Baldwin 1996) while the mud drapes indicate sub-low-tide settings similar to the one observed in F-O1 well. The soft sediment deformation (ball and pillow structures) which is also observed in the cored section could have resulted from a physical shock that has been applied to the unconsolidated sediments. It could also be explained as one of the tectonically triggered deformational sedimentary structures that can be found within sedimentary basin throughout earth's history, it has been reported to have occurred in Cretaceous of Mexico (Blanc, 1998) and Cambrian shallow marine sandstone (Vik Sandstone) in Eastern Scania, South Sweden (Scholz and Obst, 2004). The local presence of preserved organic matter (coal), probably marine kerogen could be suggestive of a very slow rate of deposition in deoxygenated bottom waters.

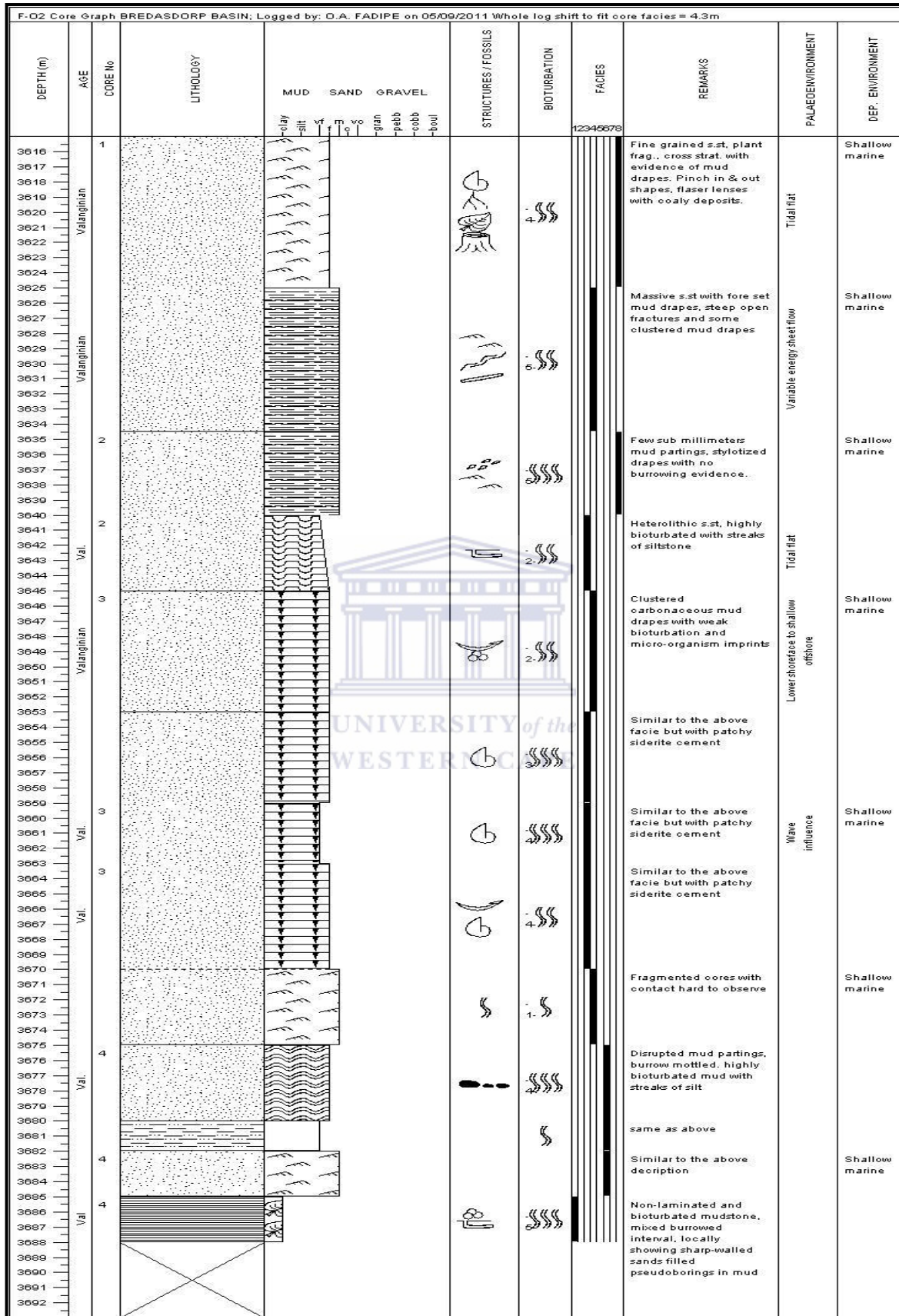


Figure 5.13a: Facies log of F-O2 well Bredasdorp Basin, offshore South Africa.

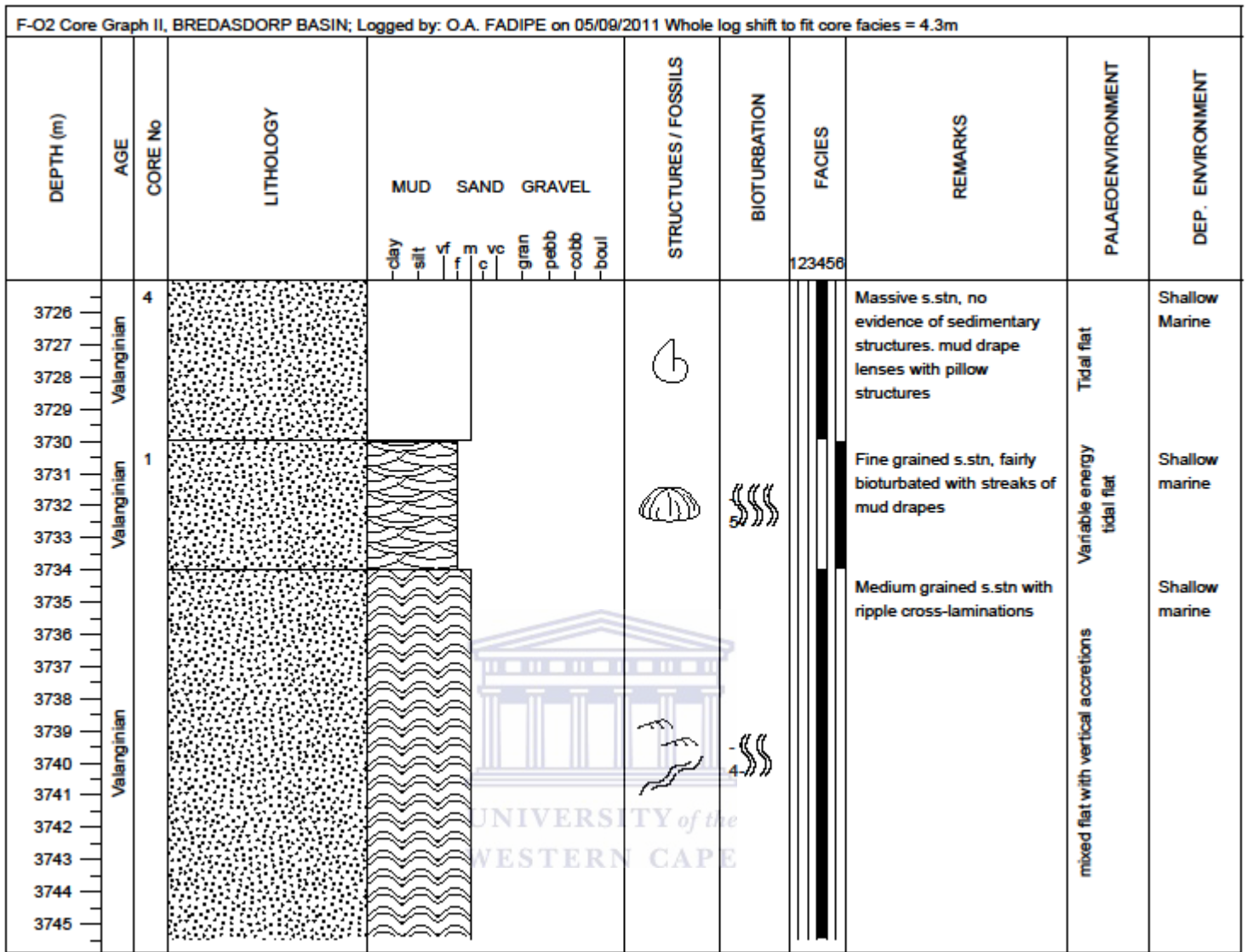


Figure 5.13b: Facies log of F-O2 well Bredasdorp Basin, offshore South Africa.

5.1.4: Core interpretation and sedimentological analysis of F-O3 well

The F-O3 well consist of five cores, these cores were examined in details as shown in figure 5.14. Six different facies categories were delineated based on distinguishable sedimentary structures, textures, grain size, primary mineralogy and environment as inferred from these characteristics. The cored section is predominantly of sandstone with few intervals of mudstone (F1) at the top of the cored section (3701 m – 3711 m) as shown in figure 5.14. Facie 1 is highly bioturbated with dark grey sand and few streaks of silts. Ammonite in figure 5.11D above was also observed in parting surfaces while facies 8 (F8) and facies 7 (F7) show very few imprint of bioturbation rather having very pronounced brecciated sandstone with mud clast. Interestingly, an igneous tuff (F2) of about 1m thickness was observed at depth range of 3726 m – 3727 m with no clear lamination but visible burrowing near sharp contacts while an heterolithic sandstone (F3) with high bioturbation and few mud clast was detailed down, clusters of foreset mud drapes and irregular surfaces was also recorded in facie 3. The tuff observed within the sedimentary terrain complicates interpretation of depositional processes because the vertical lithofacies changes in the tuff unit must have been affected by the nature depositional settings (Jeon and Sohn, 2003).

The degree of bioturbation observed in these well ranges from extreme to moderate, the degree of bioturbation is important as it introduces sand and silt and increases the vertical permeability (Cody et al., 2001). The fossil burrow that leaves traces generally parallel to bedding was evident in the cores. This fossil might be an indicator of deep water deposit (slope to basin) settings (Basan, 1978). The effect of bioturbation must have washed away most of the primary sedimentary structures like cross stratification and ripples, the period which must have provided benthic organisms with plenty opportunity to rework the sediment sometimes even in the deeper area of the shelf where life is usually sparse.

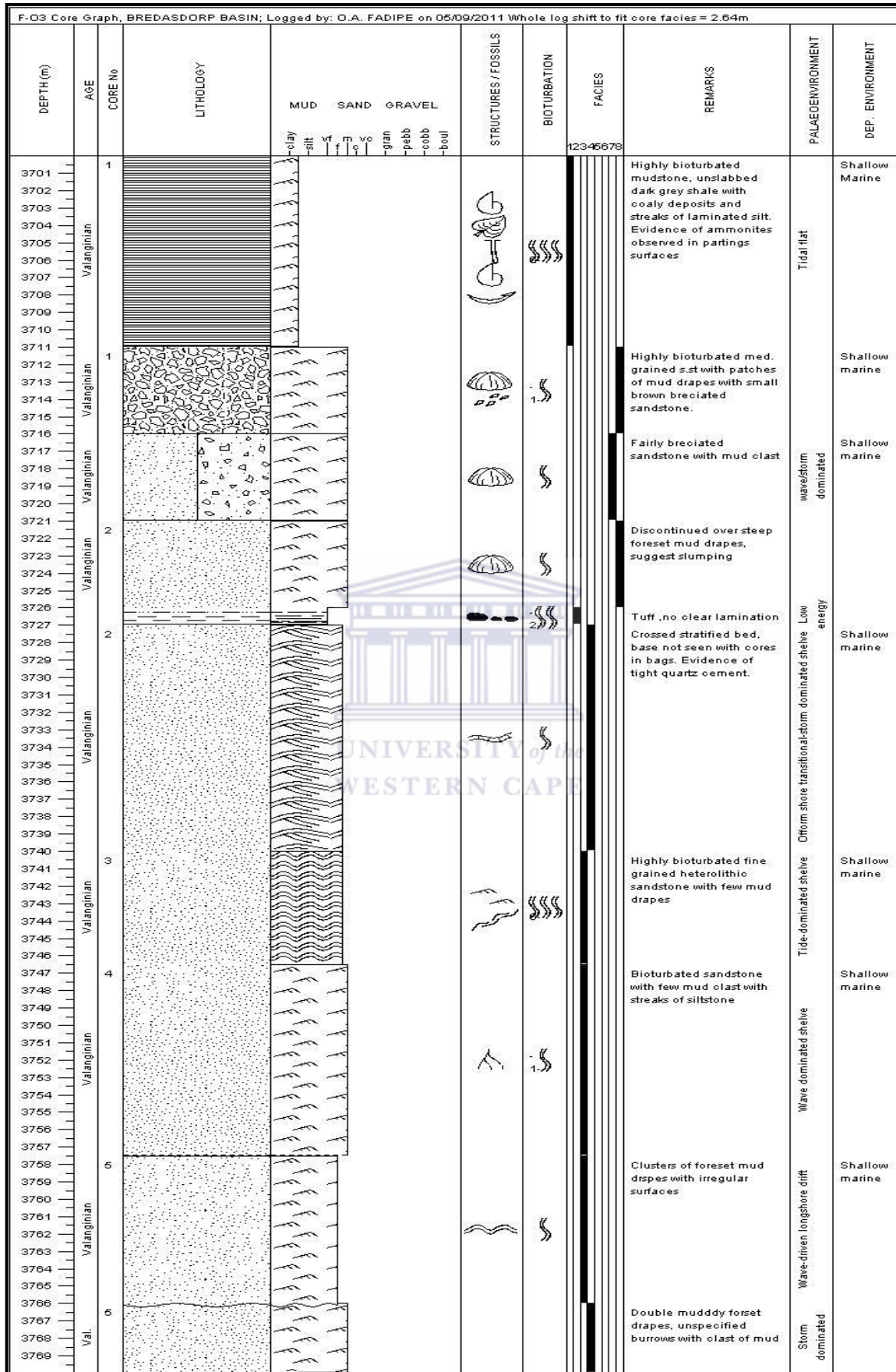


Figure 5.14: Facies log of F-O3 well Bredasdorp Basin, offshore South Africa.

5.1.5: Core interpretation and sedimentological analysis of F-O4 well

As shown in the core graph (Fig. 5.15), five facies were recognized from the F-O4 well (F3, F4, F5, F6 and F8) based on the same criteria used for the earlier discussed wells. The cored interval is predominated with sandstone, ranging from medium grained to fine and very fine grained sandstones. This cored section is highly bioturbated with imprint of micro-organism such as ophiomorpha, echinoids and bivalves coupled with patchy siderite cement. This ophiomorpha could be attributed to burrowing activities of animals penetrating down from the foreshore (Elliot, 1986). Facie 3 reveals the presence of a low-relief stylolites nucleated along mud drapes while cross stratification was observed along 3736 m with a vague presence of glauconite. Floating crystalline granules of quartz was also noticed at 3783m in facie 5 while same facie 5 at different depth range (3802 m – 3808 m) have some foreset mud drapes with calcarenite, few glauconitic sands and impure limestone (quartzose skeletal grainstone) was observed within core 3 with hummocky cross stratification in the F-O4 well (Fig. 5.15).

The presence of the glauconite mineral observed within some facie in F-O4 well might be attributed to bacterial activity which can promote its formation by producing micro-reducing conditions in the sediment. It forms from micaceous minerals or muds of high iron content where sedimentation rates are relatively low. Associated sediments are mainly calcareous (calcarenite; which was also observed) with high proportion of fecal pellets. Most clay mineralogist has regarded glauconite as being formed under marine conditions (Odom, 1984, Odin and Matter 1981). The hummocky cross stratification could be indicative of marine shoreface reworking of deltaic event beds.

The presence of siderite could be attributed to its formation in restricted chemical conditions, a reducing environment with high levels of bicarbonate, low dissolved sulphides and relatively high pH (Robert, 1998). Its presence is also buttressed with the presence of earlier mentioned glauconite is related early during diagenesis is subject to greater rate of sulphate reduction being more than rate of ferric iron reduction (Robert, 1998). The controlling factor for this reaction is how much oxidized glauconite is present.

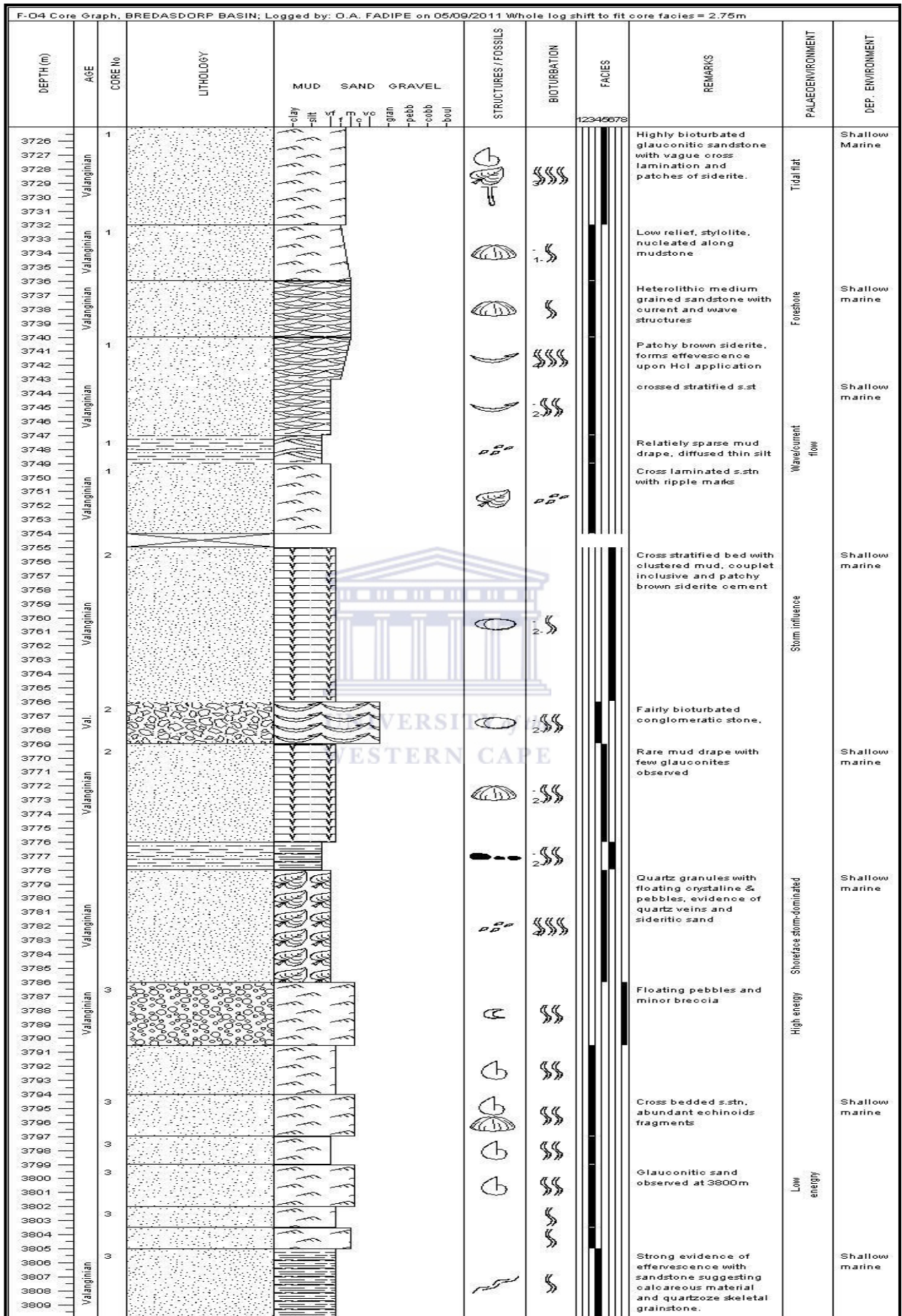


Figure 5.15: Facies log of F-O4 well Bredasdorp basin, offshore South Africa.

5.1.6: Core interpretation and sedimentological analysis of F-R1 well

F-R1 cored section has just two cores available for description (Figs. 5.16a, b). Three facies (F1, F4 and F6) were delineated from this core examination with core 1 having more of mudstone (F1) while core 2 has prevalence of massive sandstone, tight to slightly porous, clear to white to light-grey, argillaceous sandstone, containing lenticular inclusions and wavy bedding with foreset mud drapes (F4), and a siltstone with strong bioturbation (F6). The 10 m Core 1 (3825 m – 3835 m) reveals a fairly bioturbated dark grey muddy stone (Figs. 5.10F & Fig. 5.16a) with part of the core box having some shattered coaly rocks (Fig. 5.11I). Core 2 with huge distance separating it from core 1 (3835 m – 3950 m; ~ 115 m), shows some parallel laminations with pillow structures and are highly compacted sands (Fig. 5.16B). The presences of hummocky stratification coupled with syneresis cracks in some sandy intervals are noted. Lineated streaks of clayey sediment, evidence of bioturbation with braided stream structure were also observed.

The abundance of pyrite and carbonaceous materials and the fine grained nature of core 1 could be indicative of deep water marine, reducing environment of deposition for the recovered sediments (Fig. 5.16a). The hummocky stratification is diagnostic of marine shoreface while the syneresis cracks in within the sandy intervals could be indicative of fresh water event beds deposited in marine water (Cazier et al., 2011). Generally, the sedimentary structures present as well as the fine grained nature of the sandstones indicate a shallow marine environment of deposition, possibly muddy sand flats or lagoon seaward of coastal bars or distributary mouth bars.

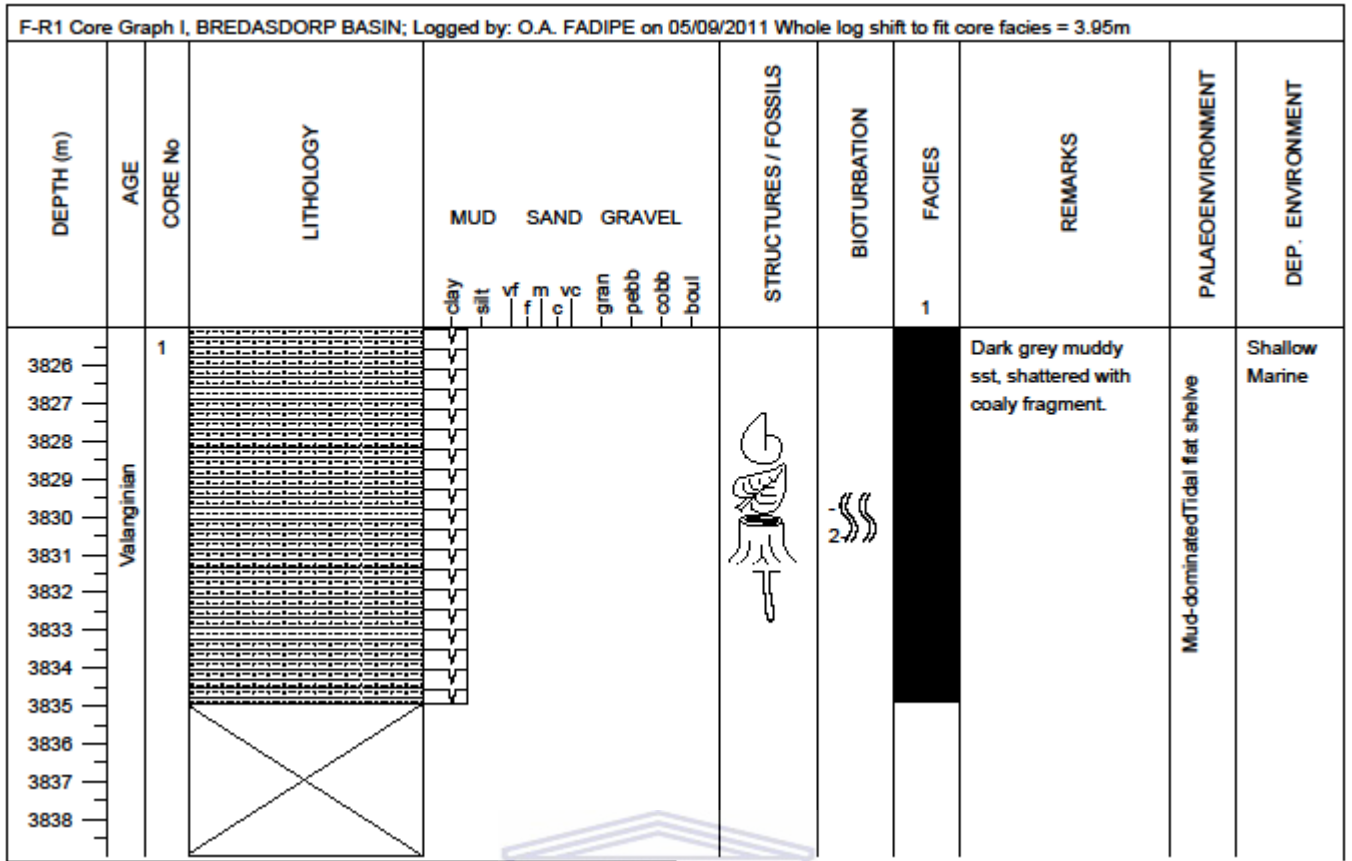


Figure 5.16a: Facies log of F-R1 well Bredasdorp basin, offshore South Africa.

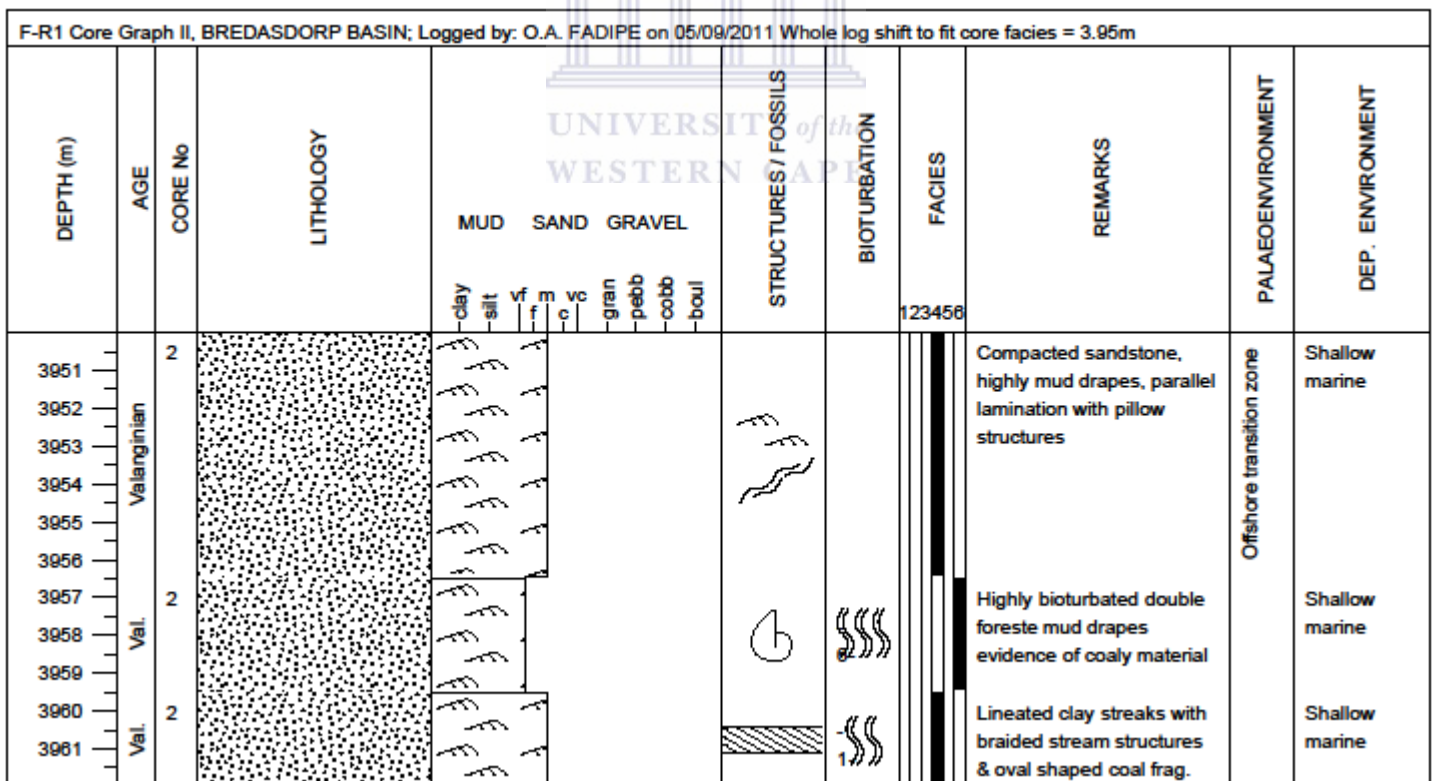


Figure 5.16b: Facies log of F-R1 well Bredasdorp basin, offshore South Africa.

5.1.7: Core interpretation and sedimentological analysis of F-S1 well

The F-S1 cored section examination reveals six different facies (F1, F3, F4, F5, F6 and F7) delineated from five cores with the sixth core (core two) missing (Fig. 5.17). The succession from the core graphs reveals intercalation of shale, silt and sandstones. Facie 4 (massive sandstone with foreset mud drapes) was the first one to be noticed in the course of carrying out core description of F-S1 well. Core 1 (3620 m – 3635 m) has pronounced bioturbation with few grey coloured siltstone and evidence of glauconitic sandstone. Internal bedding with flaser lenses was also observed within this core section. Core 3 and 4 (3660 m – 3725 m) seem to be more compacted having medium grained sandstone with foreset mud drapes and water flow imprint structure and less evidence of bioturbation with flaser lenses in facie 4. Facie 6 has a rough coarse face with extreme bioturbation. Core 5 and 6 (3725 m – 3760 m) reveals some clast of concretions (Fig. 5.10D) with evidence of oxidation, cross laminations, conjugate structure with low relief stylolite and nucleated mud drapes. Macro-faults were also evident with brecciated reddish brown sandstone. A wavy-seismic like (Fig. 5.10E) structure with a foreset mud drape was noted towards the bottom part of the core graph (Fig. 5.17).

The presence of a wavy formed structure indicates a marine origin. However the interlamination of clay-silt and sand with some cross lamination may have produced gradation between flaser and streaky lamination which could be to have formed in an anaerobic condition. The water imprint structure may have originated from local liquefaction and fluidization processes which are favoured by rapid sediment accumulation, presence of less permeable layers and immature sediment texture.

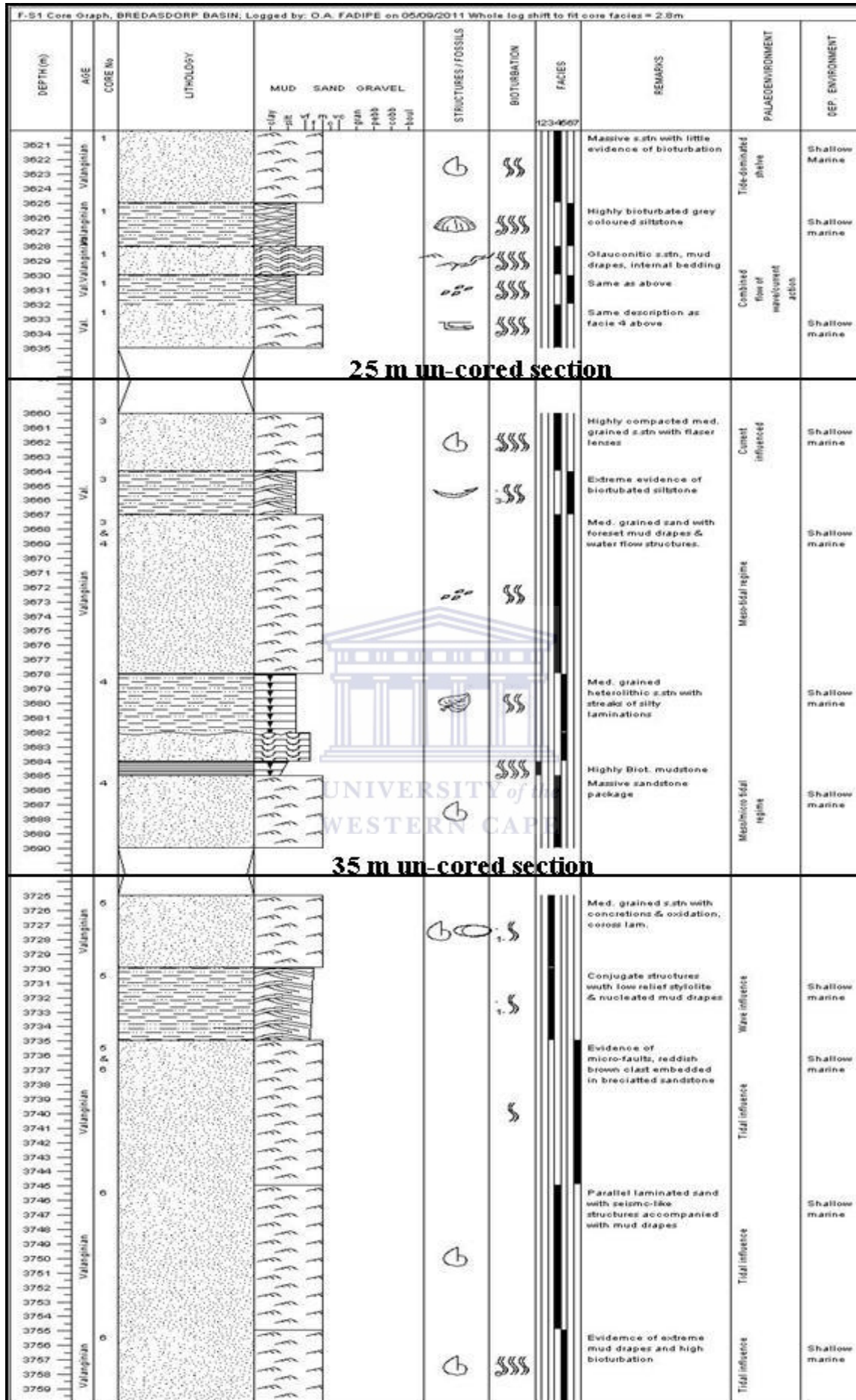


Figure 5.17: Facies log of F-S1 well Bredasdorp basin, offshore South Africa.

5.1.8: Summary of the depositional settings for the six wells in F-O field

Facies and depositional environment analyses indicate that the Valanginian reservoir section in the studied wells within the F-O gas field was deposited in the upper shallow marine settings with some strings of deltaic settings. These interpretations are limited to the reservoir intervals with interpreted core data. Distinct intervals record predominantly normal marine shoreface features, such as hummocky cross stratification in sandstones, diverse and robust bioturbation with normal marine traces, and glauconite. In contrast, few interbedded intervals display deltaic signatures. These include soft-sediment deformation often with synaeresis cracks, fluidized mudstones that could be products of both hyperpycnal and hypopycnal flows, restricted trace fossil assemblages, as well as terrigenous plant material (Cazier et al., 2011). The inter-fingering nature of the delta and shoreface depositional systems records the complicated interplay. Nonetheless, vertical stacking patterns suggest trend in delta activity within an overall marine shoreface setting.

The general upward increase in grain size, decrease in mudstone content and progressive change in style of sedimentary structures indicate progradation of sandstone body. The bioturbated nature of the silty-shales at the base of most cored sections, indicate that the sediment body prograded into a brackish water body below fair-weather wave base as evidence by the high density/low diversity opportunistic trace fossil suite. The increase in occurrence and thickness of sharp bases, parallel-laminated sandstone beds reflects the progressive increase in intensity of freshwater in composition as they would make environmental conditions often difficult, if not intolerable, even for most organisms (Mitchell et al., 2006). The presence of oscillatory ripples and cross stratified sands within most sandstone related facies indicates an influence of background wave dominated processes.

The lack of evidence for sub-aerial emergence (e.g roots paleosoils, desiccation cracks) indicates a permanently subaqueous environment. Fully marine salinity for the entire upper shallow marine is indicated by echinoids fragments. Foreset mud drapes reflect spring-neap tidal cyclicity and double mud drapes indicate sub-low tide settings.

5.2: Well log results and discussion of the F-O field

5.2.0: Introduction to well log analyses

Well log analysis is the most important task for any well after drilling to determine the petrophysical parameters of reservoir rocks. Such analysis depends on the output needed. Lithologic identification can be considered as the most important information desired prior to any computations, especially those concerning fluid saturations. This is due to the relationship between the contained rocks and the implicated water, oil and gas contents. The mixed lithology possesses a particular problem for the log analyst because the difficulties arise from the mineralogical complexity reflected from varying rock associations, facies and depositional environments. By this way, the demand for appropriate techniques to solve the lithologic problems is advisable.

In this work, logging applications are primarily directed for determining the lithologic components and reservoir zones through adequate combinations of logging data. At first, the rock types can be easily identified through the various crossplots. A number of crossplots (GR- RHOB and RHOB-NPHI) are established for recognizing the rock types. These crossplots assist in defining the different lithologies: sandstones, shales and limestones e.t.c (Schlumberger, 1972). The qualitative interpretation of these crossplots is based on the transformation of the encountered log responses into the lithologic components and mineral constituents (Serra, 1986). The quantitative interpretation of this type of crossplots revealed the rock type and amount in addition to the effect of shaliness, secondary porosity and gas (Schlumberger, 1974). Second, the effects of clay minerals (kaolinite, montmorillonite, illite, mixed clay layer, mica and glauconite) are determined by observing the geophysical log response to these clay minerals.

The qualitative and quantitative interpretation of this type of crossplots helped in determining the clay type and amount in the evaluated rock unit (Schlumberger, 1982). Moreover, the presence of clay minerals within any reservoir interval normally complicates the problem for the log analyst when evaluating the potentials of this reservoir (i.e. shale volume, effective and total porosities, permeability and water and hydrocarbon saturations e.t.c). As a result, it is very essential to define their effects on both effective porosity and hydrocarbon saturation by clay minerals-saturation crossplots and lithologic-geologic models. Thus, this study will give an insight on the

mineralogical and lithologic evaluation of the studied core units and the effects of both on the fluid contents in the later chapter.

The development of geologic pattern displaying stratigraphic units that are equivalent in time, age, or stratigraphic position through the use of electric wireline logs is generally referred to as log correlation (Rider, 1996). It is a product of basic geological principles, which include sound understanding of depositional processes and environment, concepts of logging tools and measurements, reservoir engineering fundamentals, and qualitative and quantitative log analyses. The shapes of well log curves have long been interpreted in terms of depositional facies because of their resemblance to grain size succession (Selly, 1978).

A number of published works used simplistic “pigeon-hole” approach to interpretation. An example is the classification of bell shaped gamma ray profile as fining upward meandering stream facie successions (Douglas, 1987). Although, there are problems associated with this approach which involved the most typical vertical patterns seen on gamma ray, SP and resistivity logs (Douglas, 1987). It is therefore emphasized that no pattern is unique to, or diagnostic of any particular depositional environment. It follows that interpretation based on log curves shape alone is a predictive method. In those particular wells where log-pattern has been calibrated to understand depositional environment succession in cores, the log pattern method can be applied successfully to the interpretation of correlative un-cored facies succession. The crossplots of different logs from each reservoir zone identified in each well will be used coupled with analysed core samples for a sound understanding regarding the diagenetic activities within the reservoir intervals.

5.2.1: F-O1 well log interpretation

The well section of the Valanginian age for the F-O1 well falls within the range of (3701 -3750) mRKB; however the cored section terminated at the depth of 3730m (Fig. 5.21). A quick look at the log section (Fig. 5.21) reveals a thick pack of sandstone interval using the gamma ray log while an interesting spike of deep resistivity log (LLD, 2000 Ω m) at depth range of 3730 m – 3733 m with a corresponding low neutron porosity (NPHI, 0.047 v/v) reading signifying a pay-flag based on petrophysical calculation which could be attributed to the presence of hydrocarbon within the interval (possibly gas).

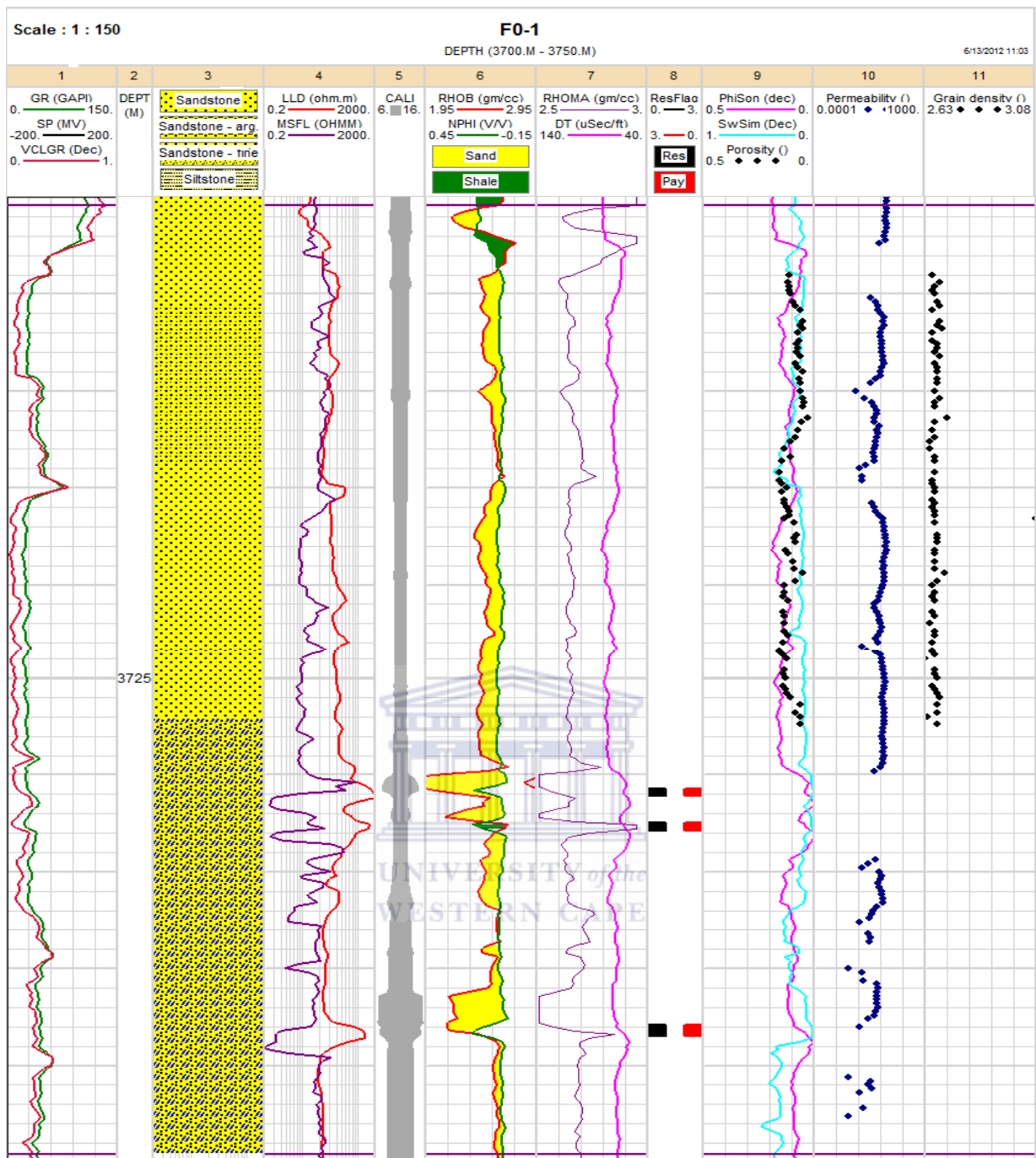


Figure 5.21: well section diagram of F-O1 well

5.2.2: F-O2 well log interpretation

The reservoir interval in the F-O2 core 1 well spans from 3650 m – 3683 m while core 2 ranges from 3720 m – 3750 m (Fig. 5.22). The gamma ray signature in both core 1 and 2 shows that the reservoir interval portrays a clean sandstone unit based on log signatures while the corresponding high deep resistivity log values (LLD), medium neutron porosity log values (NPHI) and pay flag signature (based on petrophysical calculations) all signals towards a possible presence of hydrocarbon within this interval (Fig. 5.22).

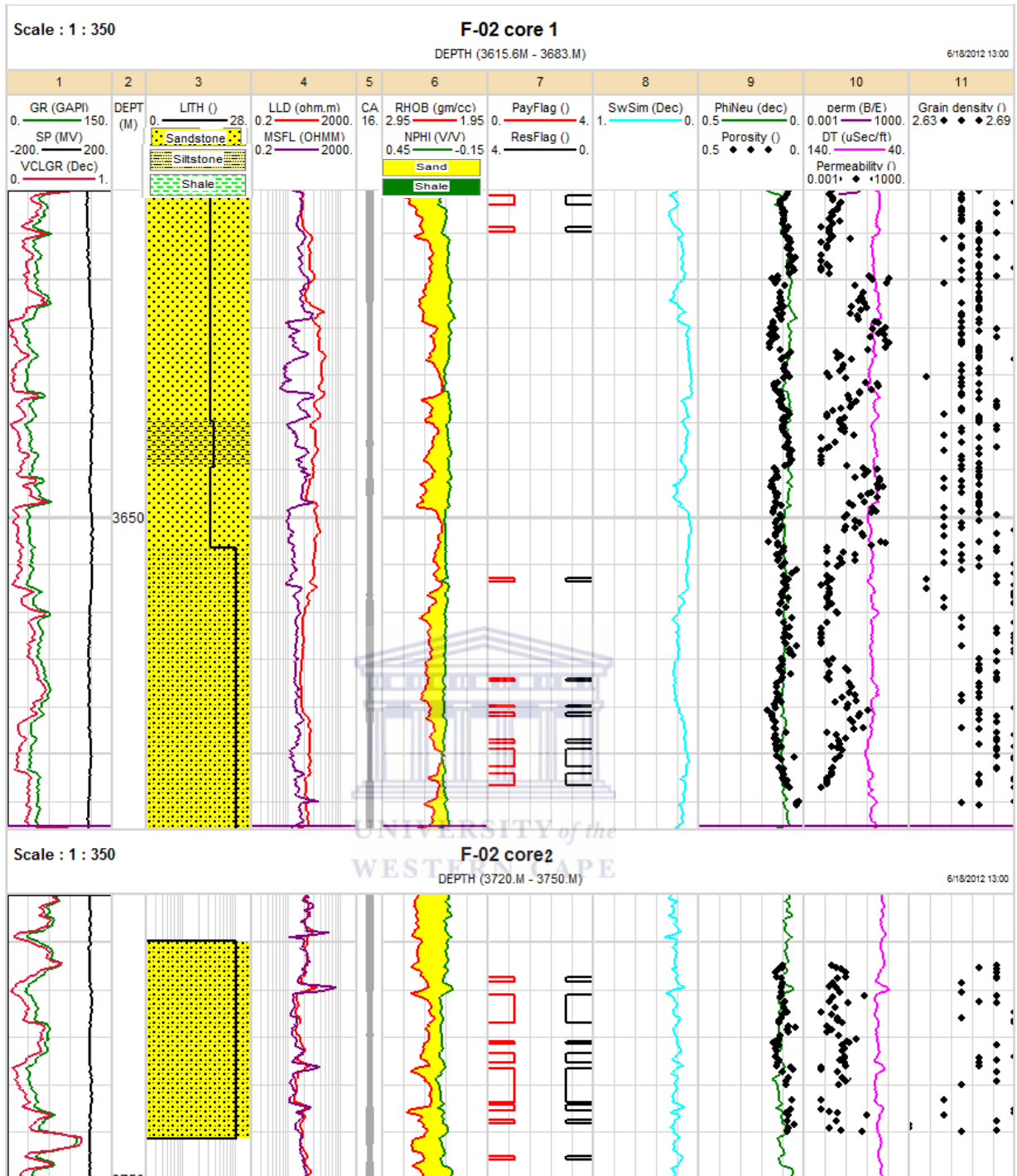


Figure 5.22: well section diagram of F-O2 well

5.2.3: F-O3 well log interpretation

The well section interval for F-O3 well ranges from 3700 m – 3770 m showing some clean sandstone unit with intercalation of sand and siltstone intervals as well. The volume of clay as revealed by its signature within the sandstone unit is 0.111 which is very low (Fig. 5.23). Limitations to some petrophysical parameters obstructed the opportunity of presenting the possible pay flags for hydrocarbon shows

within the well section. However, quick look at the well sections shows some high spike in both medium and deep resistivity log which is a sign for the presence of hydrocarbon within this zone.

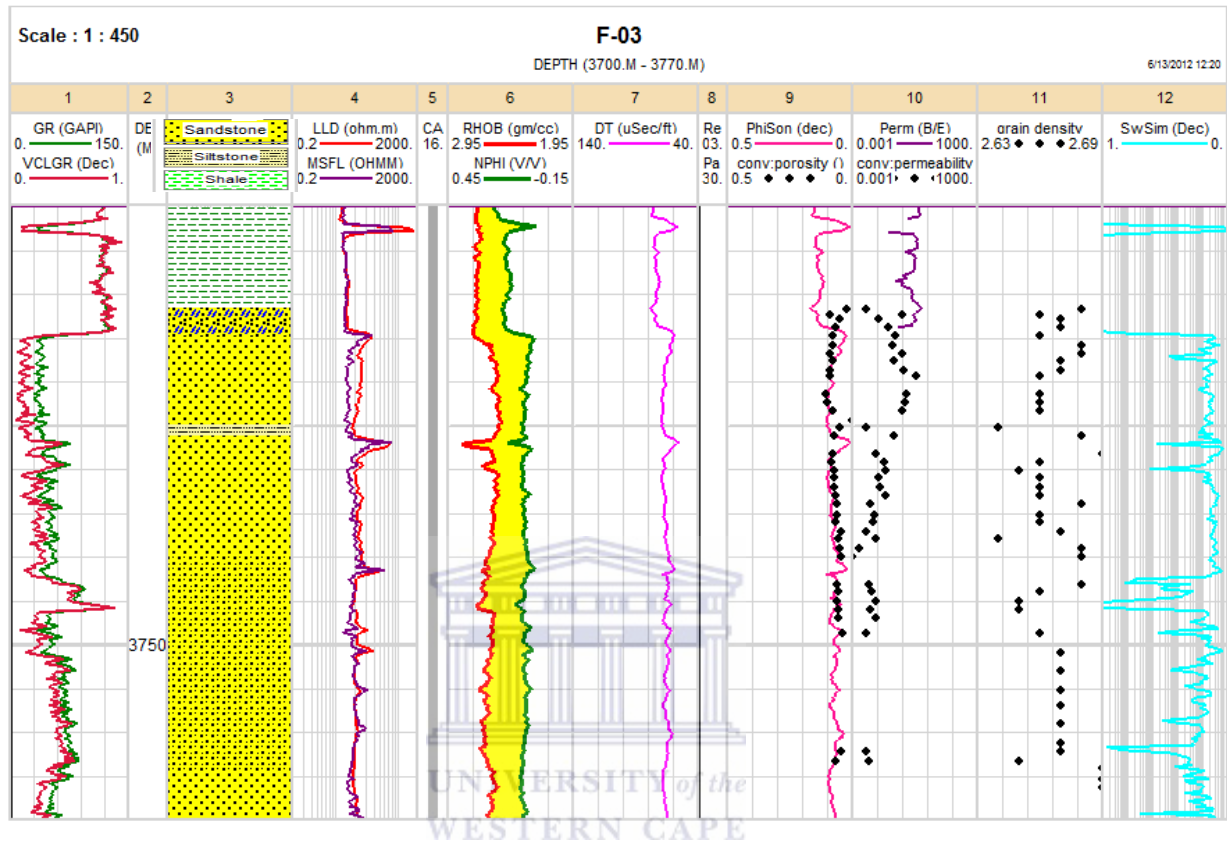


Figure 5.23: well section diagram of F-O3 well

5.2.4: F-O4 well log interpretation

F-O4 well sections has 5 cored sections with core 1 and 2 ranging from 3620 m – 3635 m, core 3 and 4 ranging from 3660 m – 3690 m, core 5 and 6 ranging from 3725 m – 3760 m (Fig. 5.14; core graph). Conventional core results (permeability and porosity data) are not available for this well hence limiting the interpretation of the reservoir sections. However, the use of wireline log has proved to be desirable in having more than a basic idea as regards where possible hydrocarbon could be. The log section for core 3 and 4 (Fig. 5.24) shows some interesting spike looking to the deep resistivity log and the corresponding depth for both neutron porosity and density log. The low gamma ray, high deep resistivity and low neutron log within this section could be attributed to the presence of hydrocarbon. Core 5 (Fig. 5.24) also shows a good trend in terms of the gamma ray and deep resistivity logs. Notable is the depth

range 3670 m – 3780 m revealing clean sandstone package with a corresponding high value of deep resistivity indicating presence of hydrocarbon within the interval.

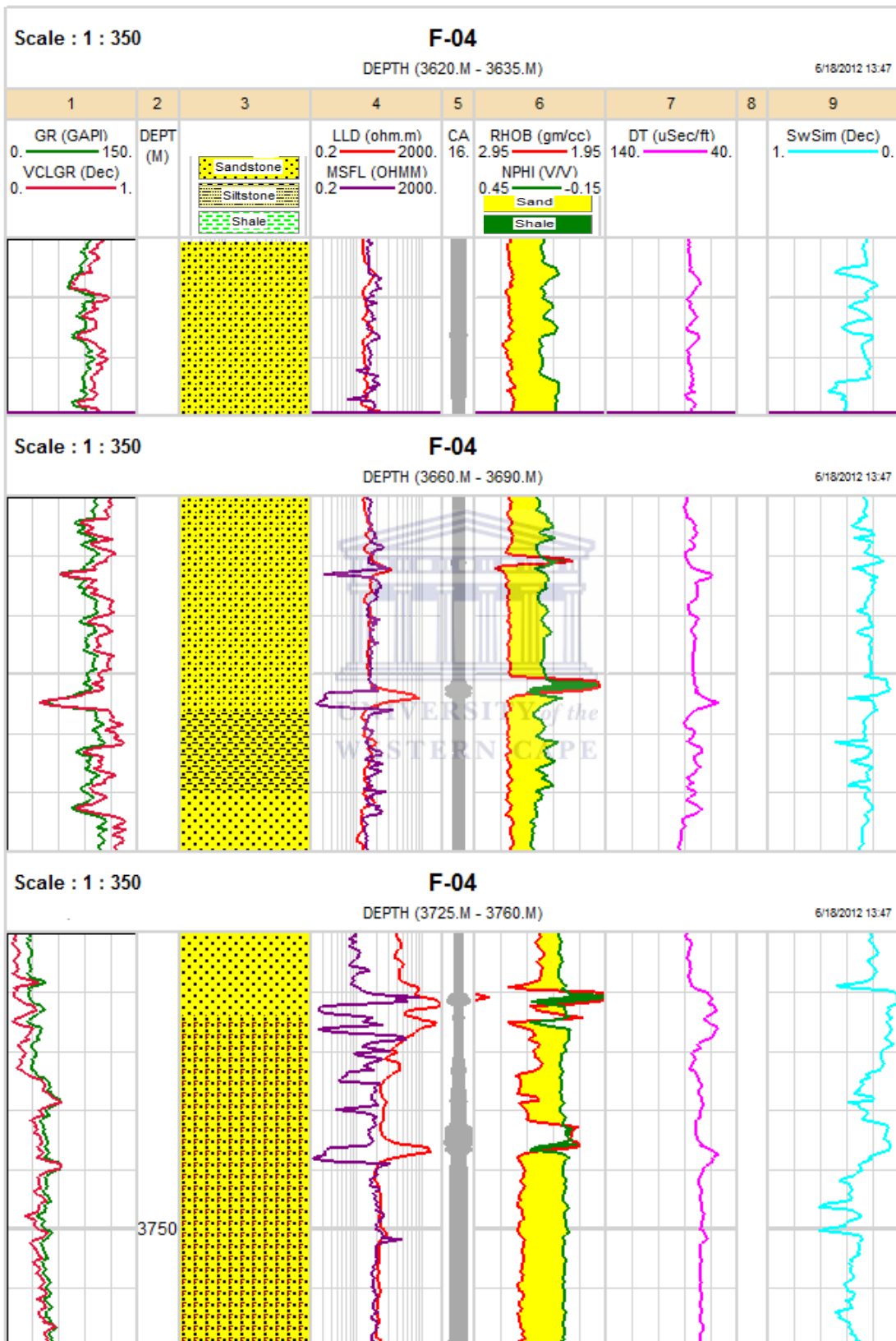


Figure 5.24: well section diagram of F-O4 well

5.2.5: F-R1 well log interpretation

This well consists of core 1 and core 2 with depth range of 3825 m – 3835 m and 3950 m – 3962 m, respectively. The well section displayed in figure 5.25 shows the log signature for both cores. Core 1 does not have conventional core data while core 2 has very few points for evaluation. Figure 5.25 reveals the predominance of shale within the well section of core 1 (3825 m – 3835 m) with a considerable signature (moderate values) from both resistivity and neutron logs (20.4 Ω m and 0.098 v/v). Core 2 shows the presence of sandstone units with streaks of intercalation observed within the sandstone unit (3950 – 3963) m. Data presented only reveals the availability of medium resistivity log which was use in predicting the presence of hydrocarbon coupled with its integration with neutron porosity log. However, the conventional core result available for cross plot could not be displayed on the cross plot window due to the minute points available.

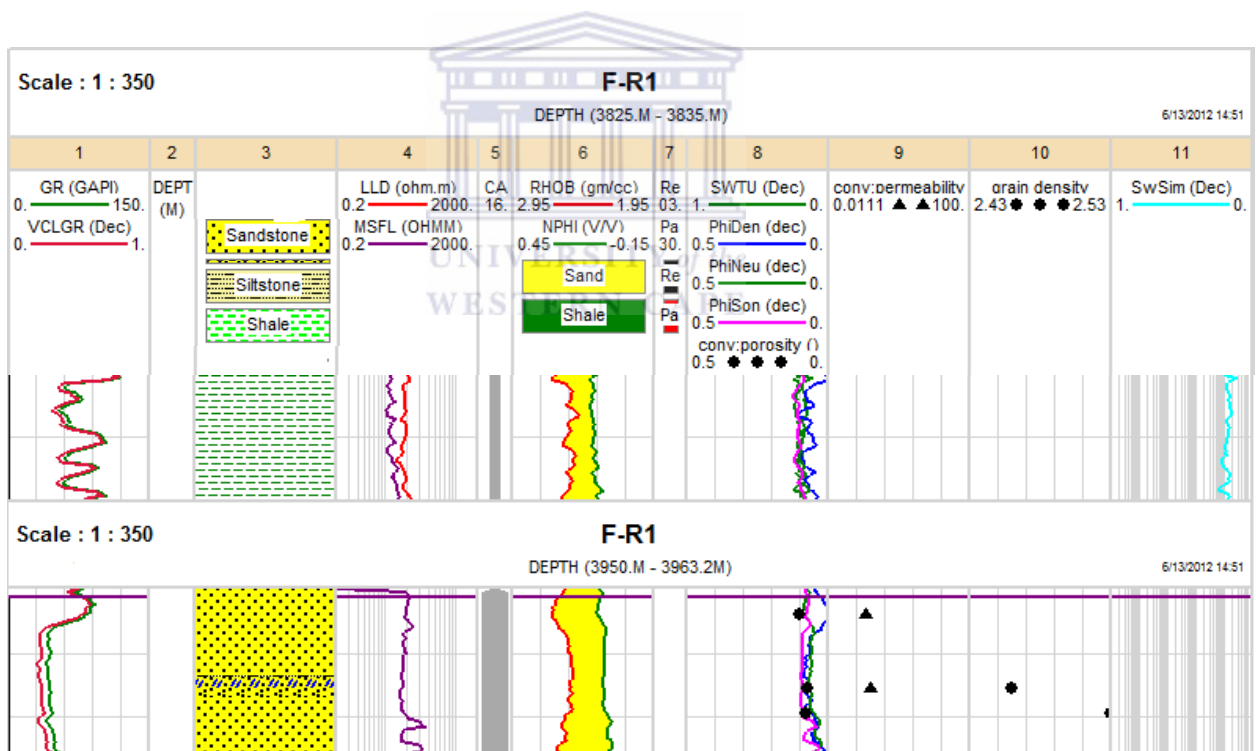


Figure 5.25: well section diagram of F-R1 well

5.2.6: F-S1 well log interpretation

F-S1 well has six different cores (core 1 – 6) displayed in the well section below (Fig. 5.26). The first well section interval ranging from 3620 m – 3635 m shows a cleaner sandstone package with few intercalation of silt within the sandstone unit. Resistivity and neutron log signature coupled with some petrophysical data input for

calculation gave rise to the presently displayed pay flags to give an idea of the possible zone(s) for hydrocarbon presence. The third section (Fig. 5.26) with intervals between 3725 m – 3760 m shows just very minute signature of pay flag revealing possibly a diminutive presence of hydrocarbon within that interval.

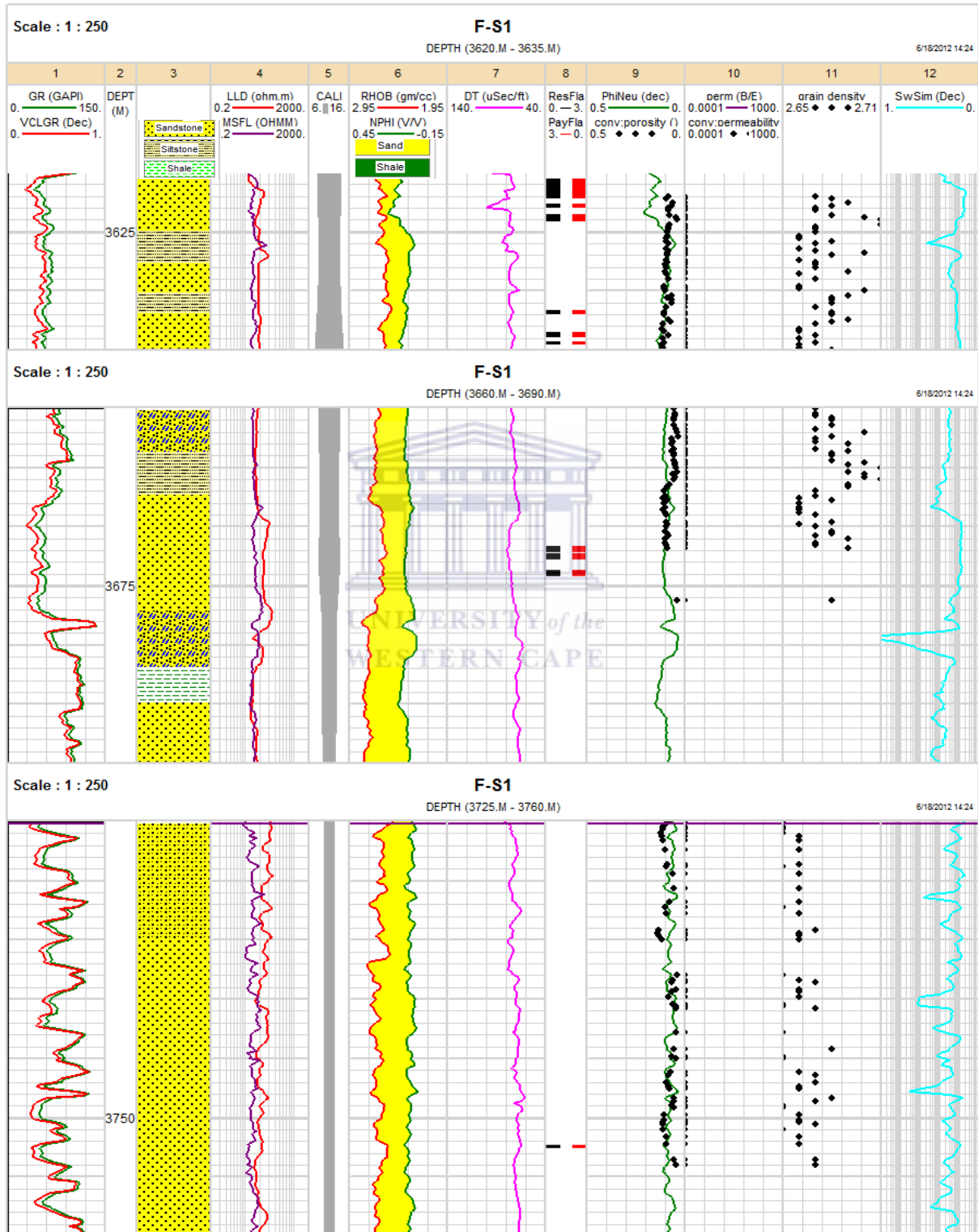


Figure 5.26: well section diagram of F-S1 well

5.3: Cross-plot results and discussion of the F-O gas field

5.3.0: Cross-plotting compatible logs

Both the neutron and density logs are difficult to use for gross lithology identification individually. However, once combined, they become probably the best available indicator (Rider, 1996). The cross-plot of neutron-density log can be used to identify pure matrix and/or the related porosity while the corresponding conventional core analysis results (core porosity and permeability) can be used to estimate the porosity and permeability within the interval of interest.

5.3.1: F-O1 cross-plots

The F-O1 cross-plot (Fig. 5.31A) reveal that (3700 – 3750) m, the lithology is more of clean sand formation and a notably sparse observation of limestone formation below the clean sandstone. The 3D surface projection of the conventional core porosity and permeability plot reveals that the corresponding interval (3700 – 3750) m has a low porosity with a fair permeability (Fig. 5.31B).

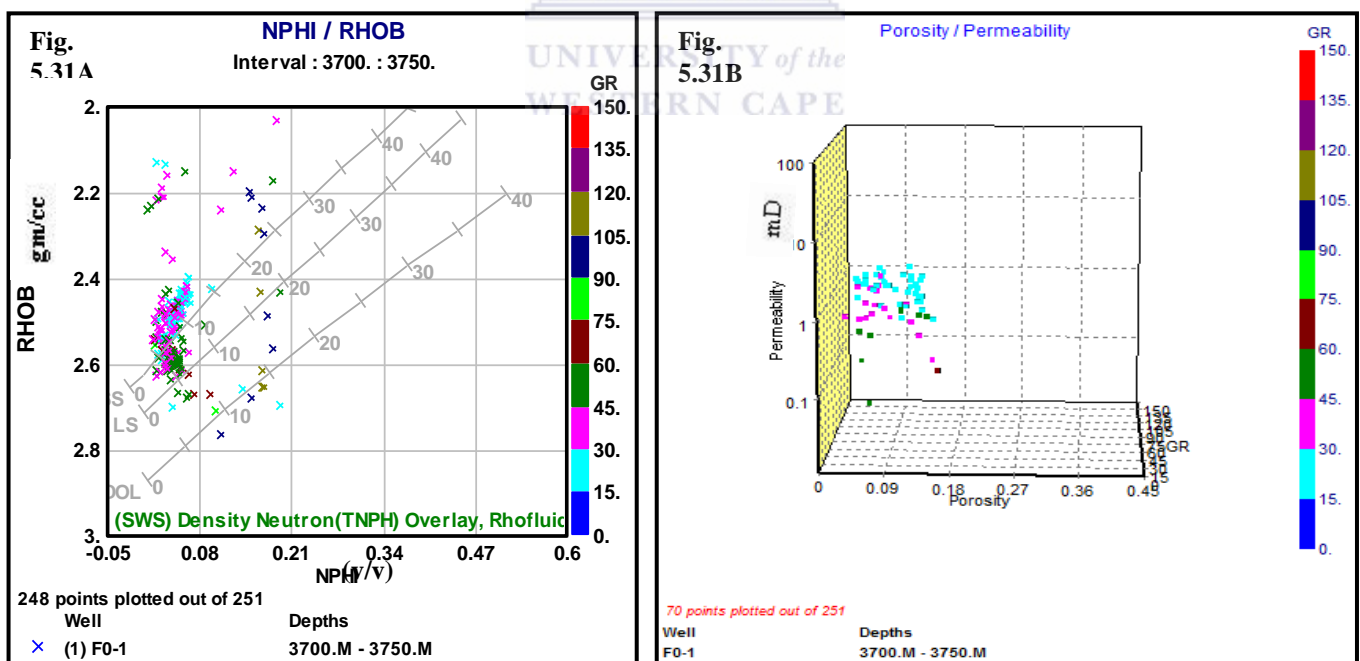


Figure 5.31: (A) Crossplots of neutron–density (B) Core porosity–permeability of the F-O1 gas field

5.3.2: F-O2 cross-plots

The neutron-density plot of F-O2 well reveals more of clean sand in core one (3615.6 - 682.4) m with little plot falling around the dolomitic formation (Fig. 5.32A). The plot of core two (3720 - 3750) m spans in-between the clean sandstone and limestone area. The 3D surface projection of core porosity and permeability plot (Fig. 5.32B) for core 1 shows a relatively fair porosity (ranging from 12 % - 25 %) and a corresponding increase in permeability while core two 3D surface projection plot reveals low – fair porosity and permeability interval (Figs. 5.32C and D).

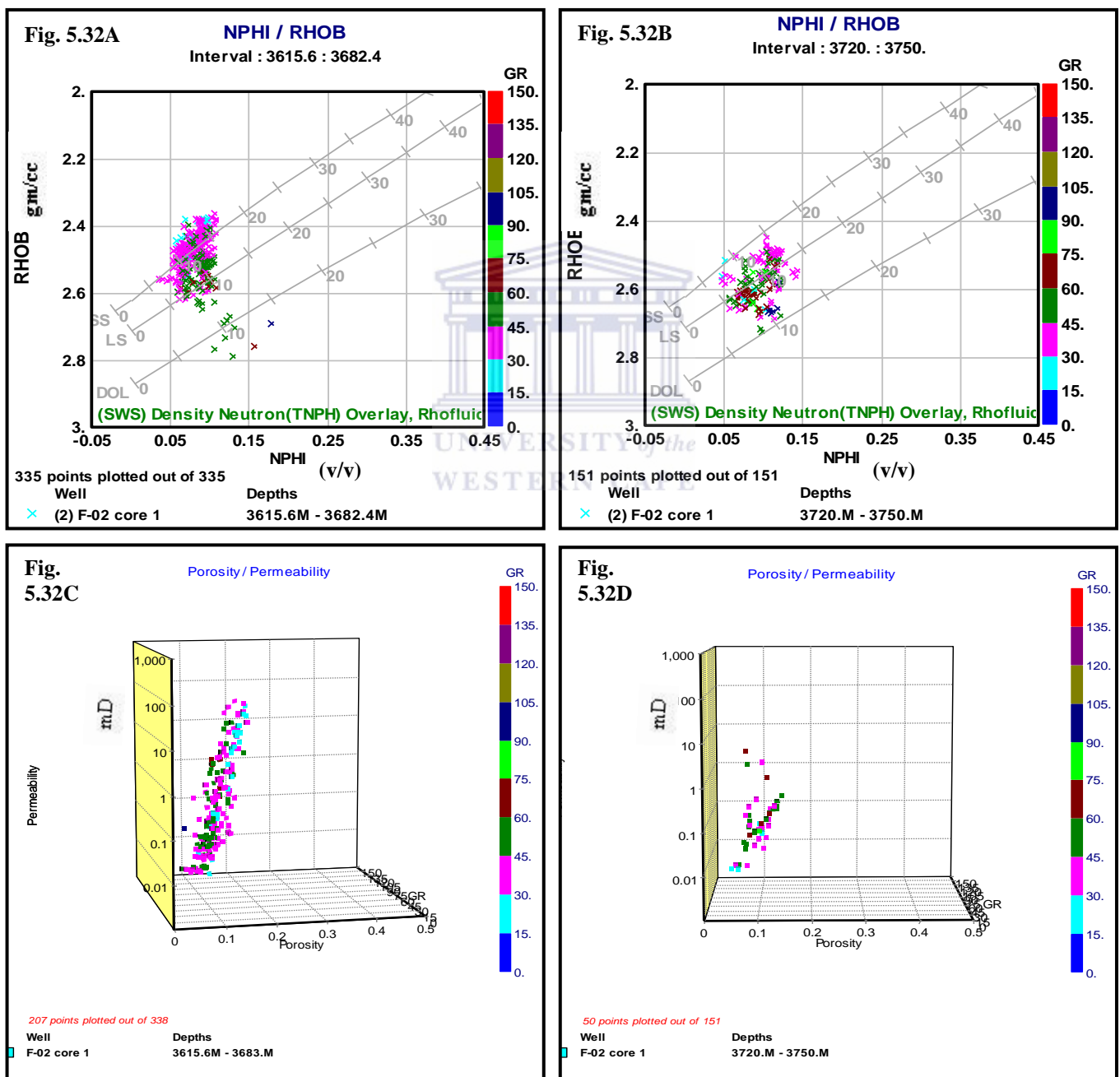


Figure 5.32: (A, B) Crossplots of neutron–density (C, D), core porosity-permeability of the F-O2 gas field

5.3.3: F-O3 cross-plots

This well interval (3700 - 3770) m reveals a range of formation from clean to limestone and dolomitic formations with more of clean-limestone formation (Fig. 5.33A). This could serve as a notable factor to check more for the calcitic minerals that might be present within this interval during multi-mineral analysis. The 3D surface projection for the earlier mentioned interval shows that the interval has low porosity and permeability (Fig. 5.33B).

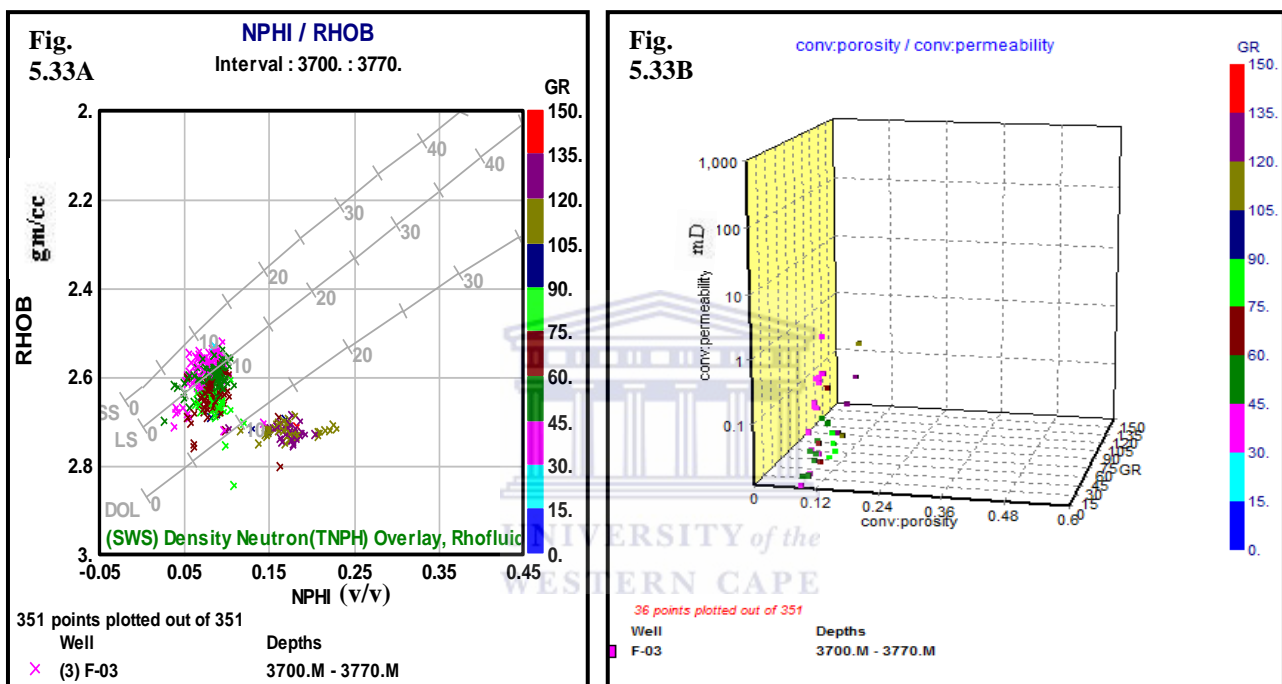


Figure 5.33: (A) Crossplots of neutron–density (B) Core porosity–permeability of the F-O3 gas field

5.3.4: F-O4 cross-plots

F-O4 well has three distinctive interval of interest with the first two intervals (3620 - 3635; 3660 - 3690) m having a plot that falls within the calcareous silty-shale sand i.e. between limestone and dolomitic nature rocks with a more dense sediment as revealed by the plot (Figs. 5.34A, B and C) while the third interval (3725 - 3760) m shows a considerable clean sandstone formation and less dense sediment. Conventional core analysis results were not available for this well in order to estimate the porosity and permeability measured from core samples (Fig. 5.34D).

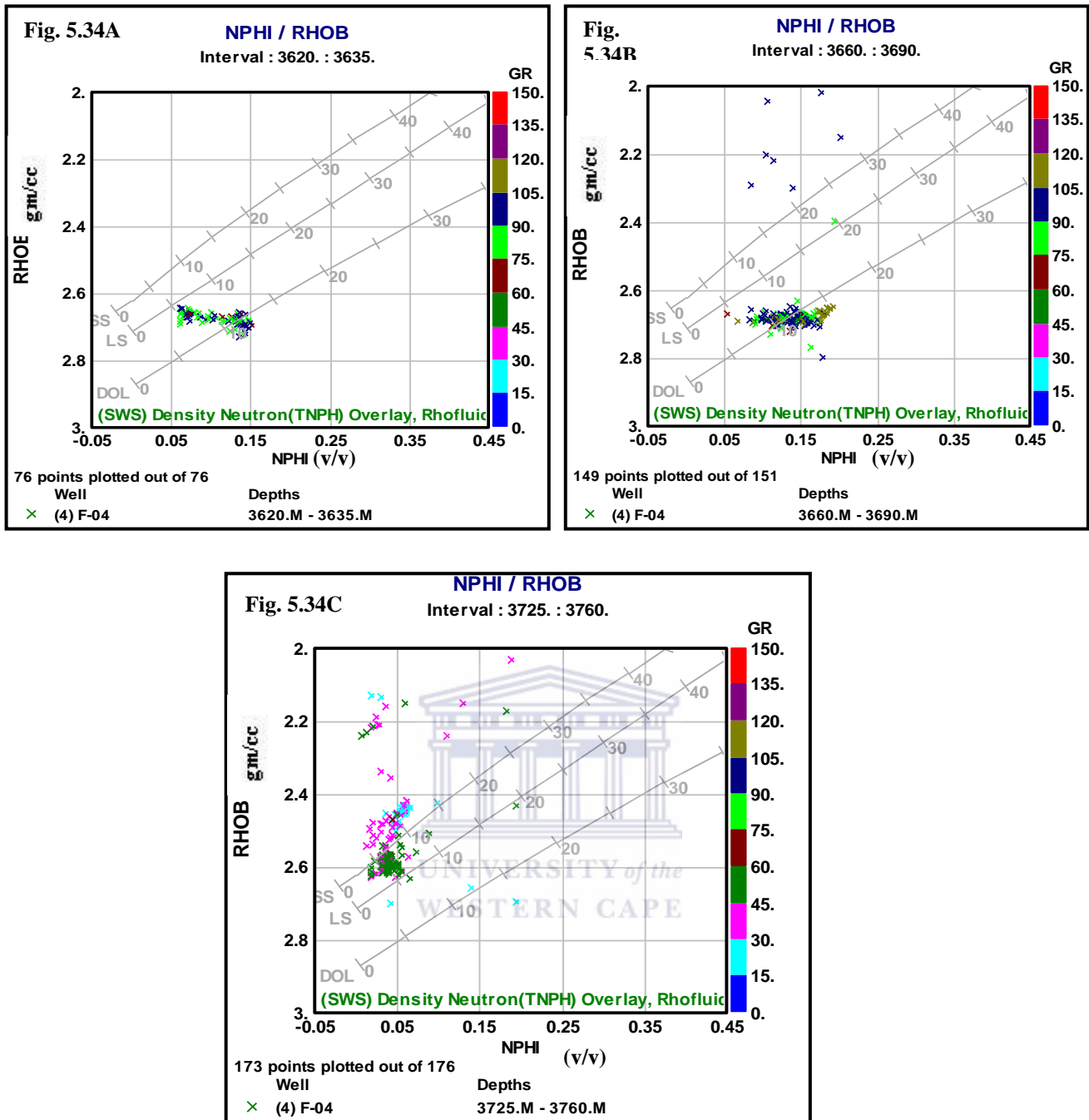


Figure 5.34: Crossplots of neutron–density F-O4 gas field

5.3.5: F-R1 cross-plots

F-R1 has two cores (core 1 & 2) with the first core (3825 - 3835) m showing a neutron-density plot around the clean sandstone and limestone sediment while the second core (core 2; 3950 m – 3963 m) reveals neutron-density plot falling around the clean sandstone formation with a relatively low neutron-porosity values (highest = 9 %). Conventional core analysis could not be projected using the Interactive petrophysics software due to the very small quantity of examined cores (just two core sampled results).

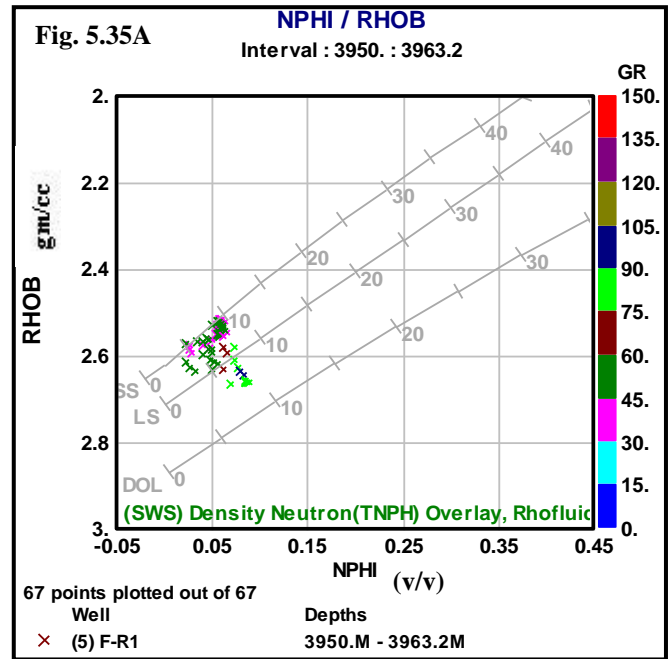
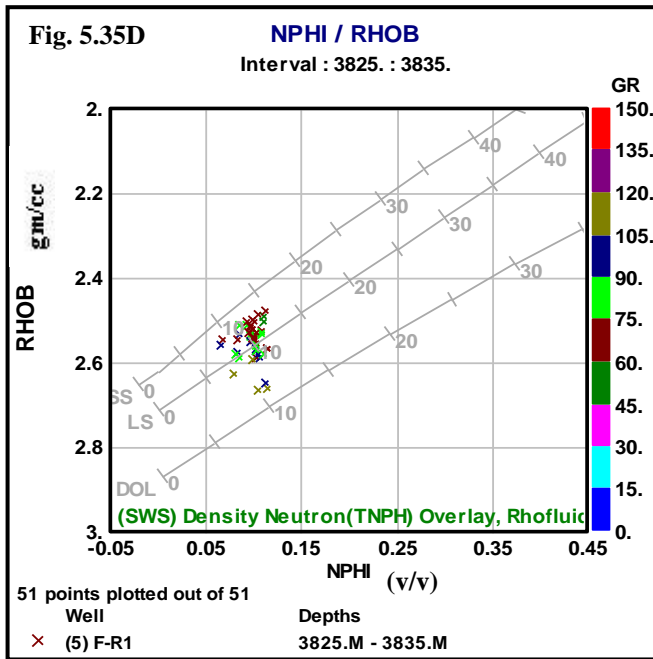
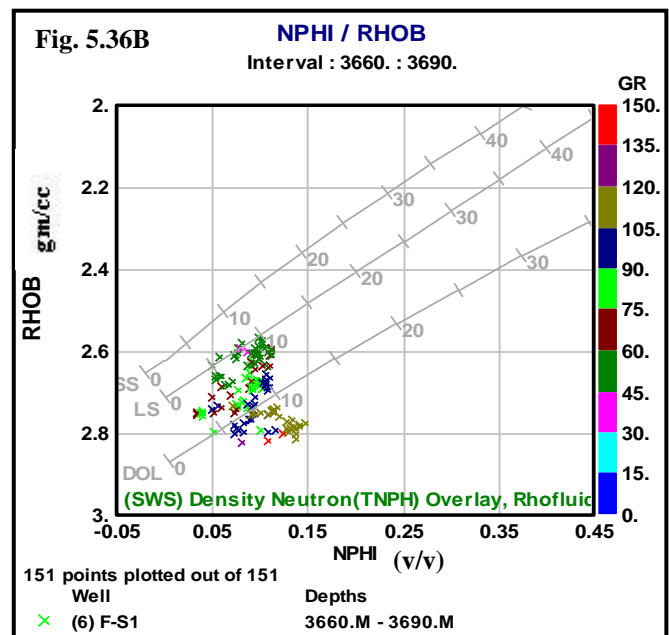
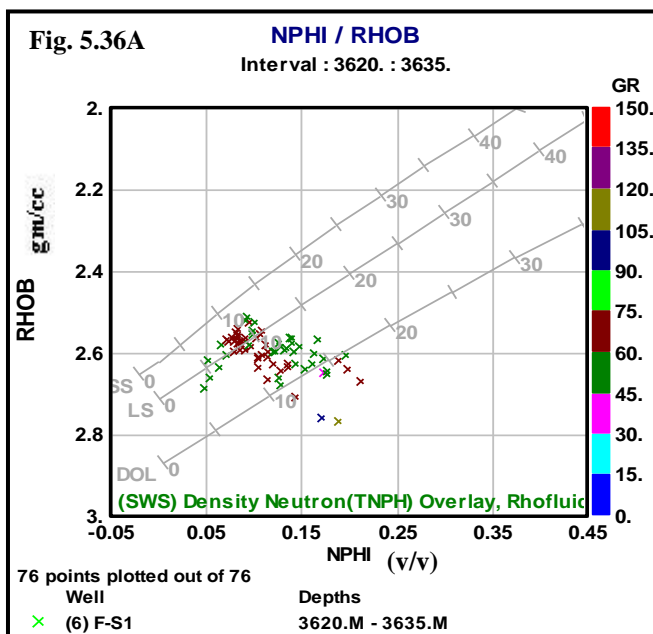


Figure 5.35: Crossplots of neutron–density F-R1 gas field

5.3.6: F-S1 cross-plots

Three cores were examined from the F-S1 well [core 1, (3620 – 3635) m; core 2, (3660 – 3690) m ; core 3, (3725 – 3760) m] and their plots reveals mostly a more dense sediments/rock types and also falls between the sandstone and limestone formation based on the neutron-density cross-plots (Figs. 5.36A, B, C). The 3D surface projection of the conventional core analysis plots (Figs. 5.36D, E, F.) also reveals a relatively low porosity and permeability (< 15 % and < 1 MD, respectively).



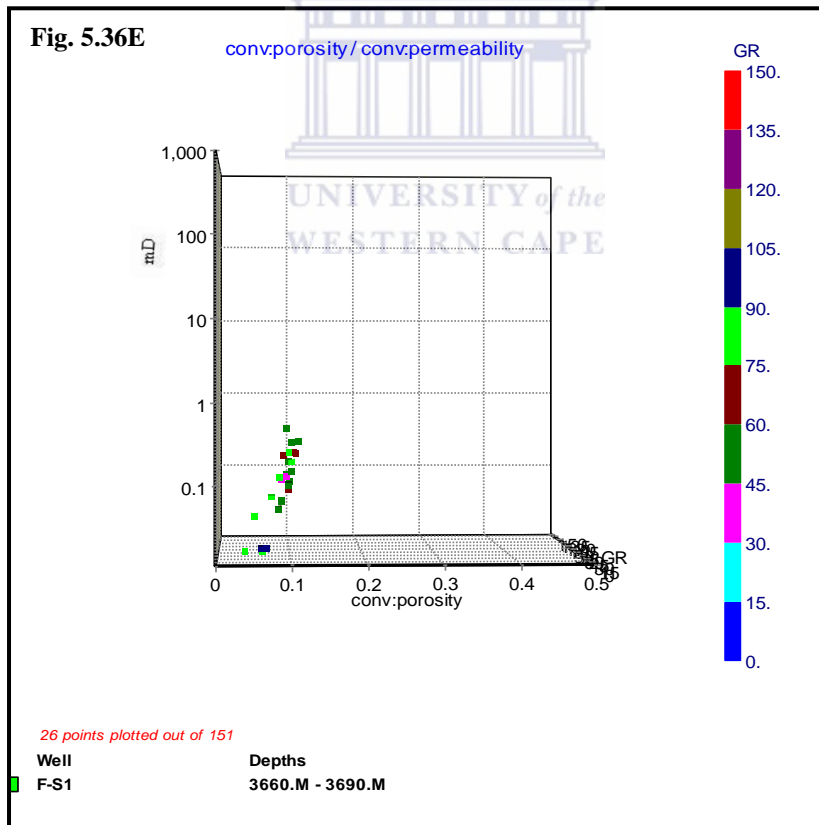
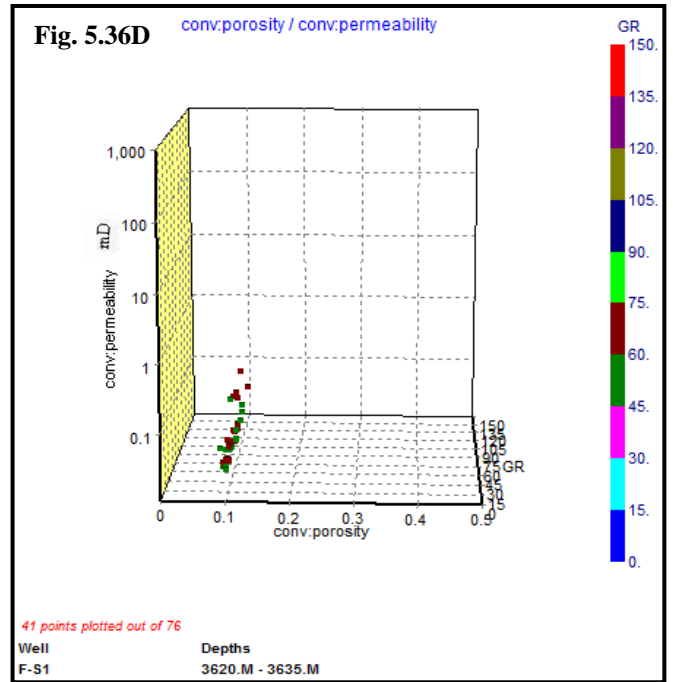
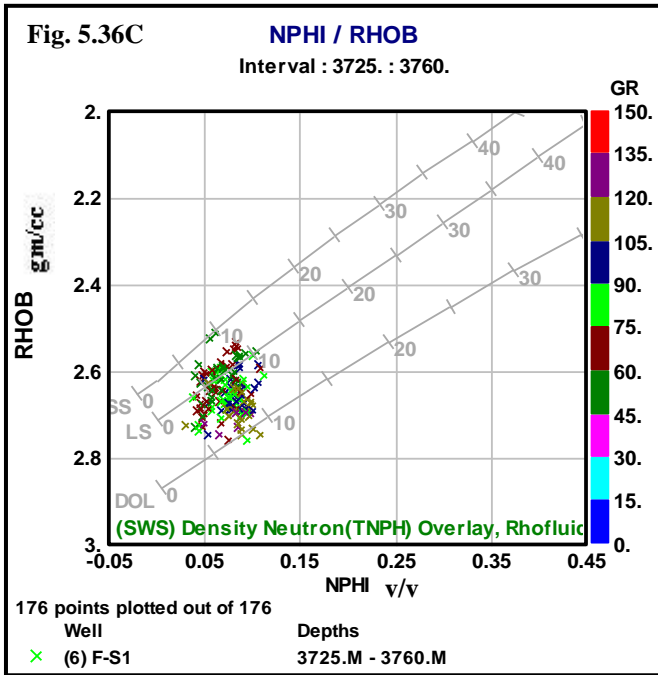


Figure 5.36: (A, B, C) Crossplots of neutron–density (D, E) Core porosity–permeability of the F-S1 gas field.

5.4.0: Seismic interpretation and discussion

5.4.1: Introduction and brief background of the F-O gas field

Conventional seismic interpretation implies picking and tracking laterally consistent seismic reflectors for the purpose of mapping geologic structures, stratigraphy and reservoir architecture (www.pangea.stanford.edu/~quany/QSI_chapter-4). Primary seismic reflections are generated in response to significant impedance changes along strata surfaces or unconformities. Detailed mapping of seismic profile for fault and horizon pick was carried out on dip section (cross lines) since faults are easily recognized on dip sections than on strike sections. However, the limitations attached to the use of a 2D seismic data did not allow a clearly defined and expected 3D seismic interpretation model to be generated. Hence, these lines were individually interpreted with reference to base map showing the lines and the studied well location on each line (Fig 5.41).

Sediment distribution and non-deposition or erosion is important in the depositional and tectonic history of the F-O structures in Bredasdorp Basin and its adjacent basins. The unconformities reflect tectonic events and, although they cannot be easily identified in the seismic profiles in the selected seismic lines due to poor imaging and structural complexities. The interpreted reference chart for seismic reflectors nomenclatures is also used to interpret the major events that happened during tectonic evolution within the Bredasdorp Basin (Fig. 5.42). The F-O structure was formed by rollover adjacent to a major east-west trending faults and consists of combined domal and fault-bounded closure. The proposed target for the studied environment is a shallow marine sequence, situated beneath horizon 1At1 at the crest of the F-O domal feature for F-R1 well. Pre-loaded formation tops were used as guide to map some horizons while newly assigned names (pre-1At1, base of unconformity) were given to newly created horizons based on their geological significance and strong seismic reflection across the seismic profiles. Figure 5.49 reveals a 3D geological view of the interpreted horizons showing the sequential alliance of the independently mapped seismic lines with a reasonable interconnectivity of the mapped horizons.

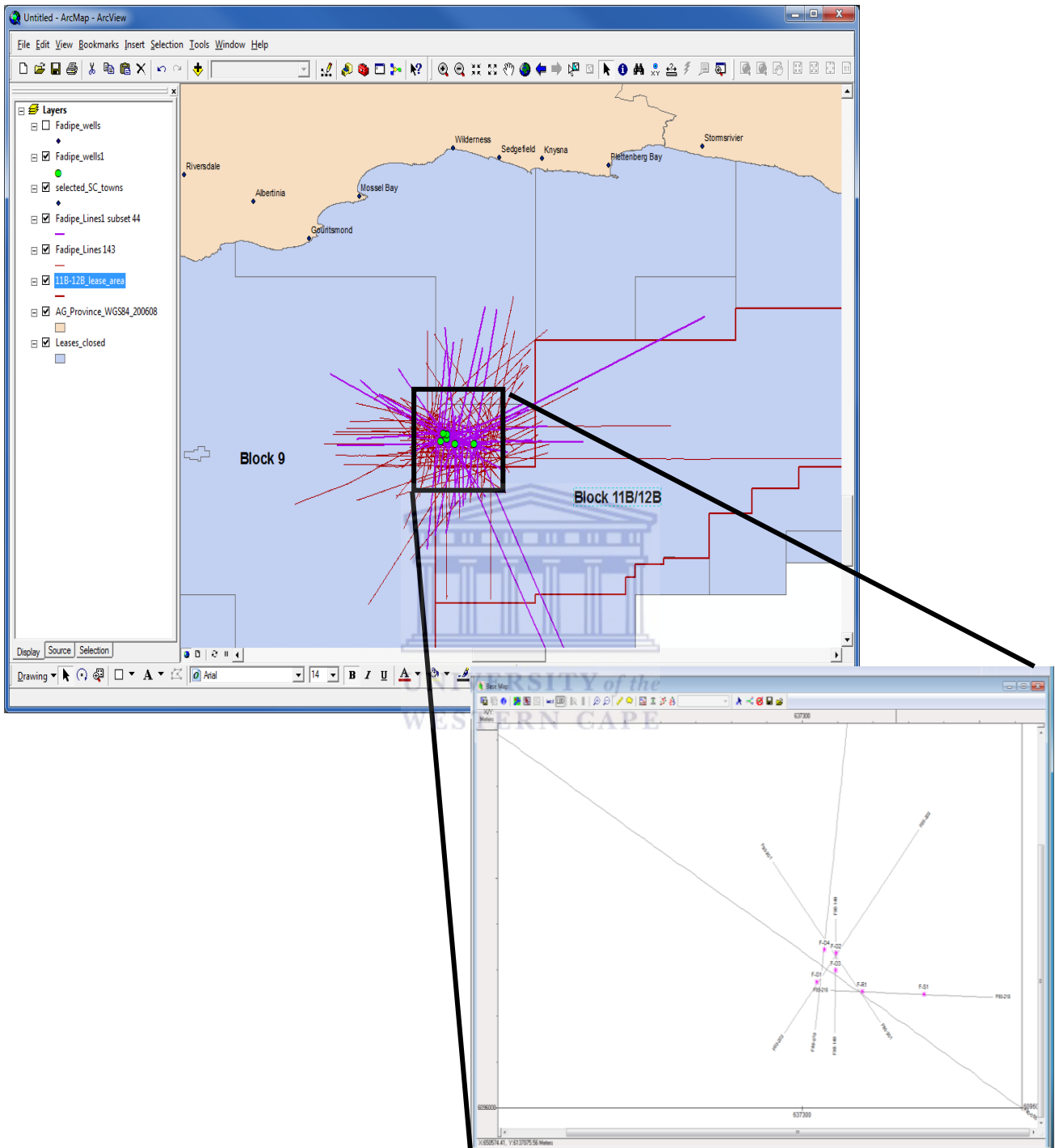


Figure 5.41: Purple lines are a subset of 143 2D seismic lines in the vicinity of the study area while black thin lines are subsets of 44 2D seismic lines in the nearest vicinity of the 6 wells

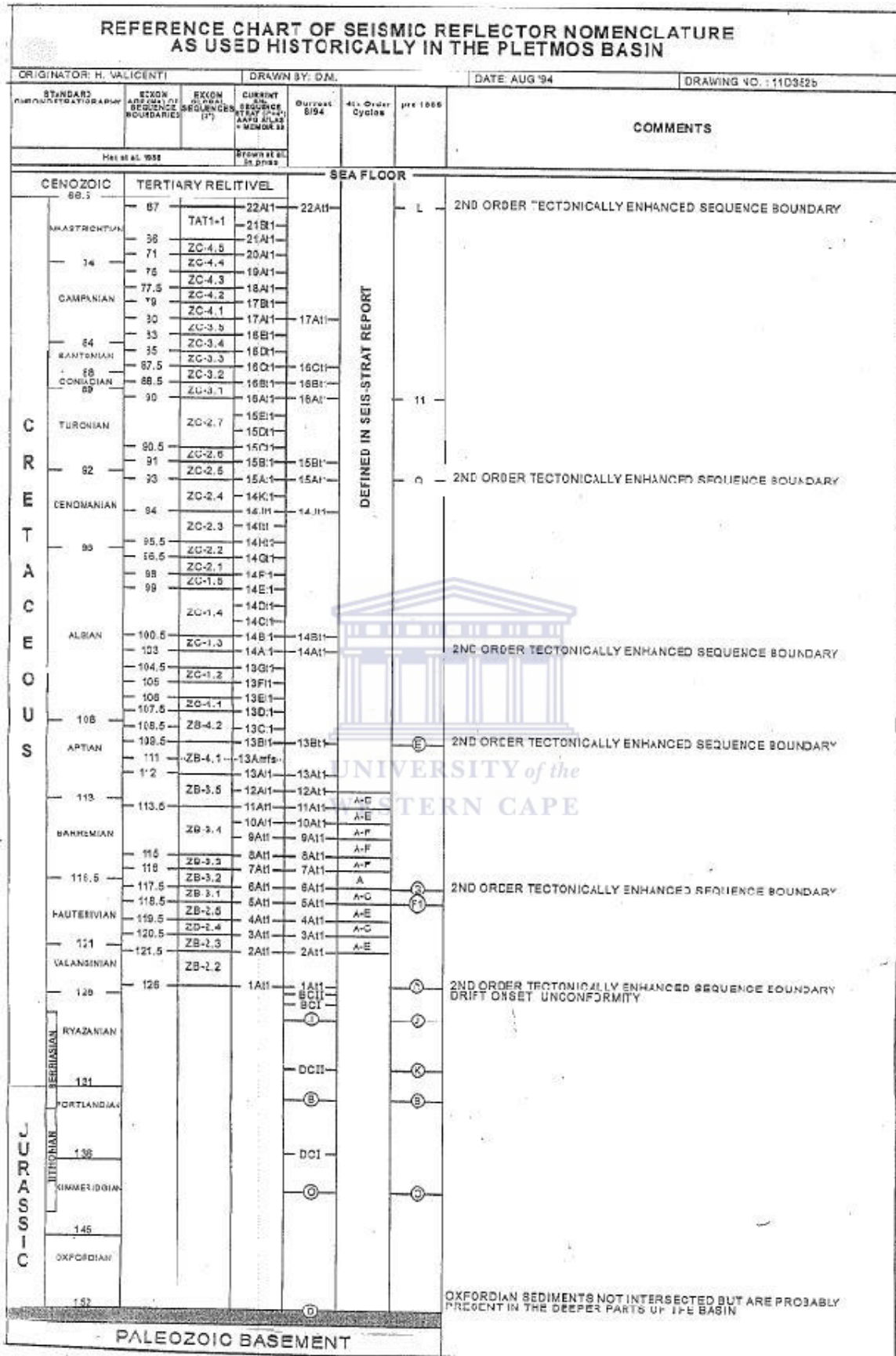


Figure 5.42: Seismic reference reflector nomenclature of Pletmos basin historically used for Bredasdorp basin (modified from PASA, 2004)

5.4.2: Seismic profile discussion and interpretation of F93-203 line

The interpreted seismic line spans SW - NE at close proximity to F-O1 and F-O2 wells with 4139 m apart. Hence, a total of 10 horizons were picked with reference to the loaded well tops including seafloor mapping. Major unconformity is denoted by black colour line (Fig. 5.43) below the “bottom log” formation top (yellow line) line where a pronounced fault was observed due to rifting of sediment as seen in Figure 5.43. Time-depth conversion data reveals the location of the Valanginian age (126 ma) and the predicted shallow marine reservoir sediments (core description) to be pre-1At1 horizon which is tagged as the drift-onset unconformity (Fig. 5.43). Major structures identified in the area include a normal fault close to the basement within the Lower Cretaceous sandy-shale package which cuts the south-west dipping layers of the Cretaceous and associated series of listric faults within 16At1 and 22At1 horizons (Fig. 5.43).

5.4.3: Seismic profile discussion and interpretation of F90-149 line

Seismic line F90-149 (Fig. 5.44) is a north-south representation of the structural seismic section across the study area. Two wells F-O2 and F-O3 of about 1888 m apart are situated directly on this line with F-O2 about 4km NE of F-O1. Eight different horizons were mapped based on pronounced seismic reflectors and formation tops including seafloor and basement of unconformity (Fig. 5.44). The predicted primary target reservoir of the two wells is situated beneath 1At1 horizon at the crest of the F-O structure. Some major structures in the area identified include growth faults and associated rollover anticline around F-O3 well with a step-wise pattern on the TLVS horizon (Fig. 5.44). The section shows more or less a symmetric sedimentary record immediately after the series of faults around 16At1 horizon except for the major fault seen around the 1At1 surface that could possibly be representing the structural trap for F-O3 well. Sequence boundaries were also noted towards the southern section of the seismic profile associated with listric faults (Fig. 5.44).

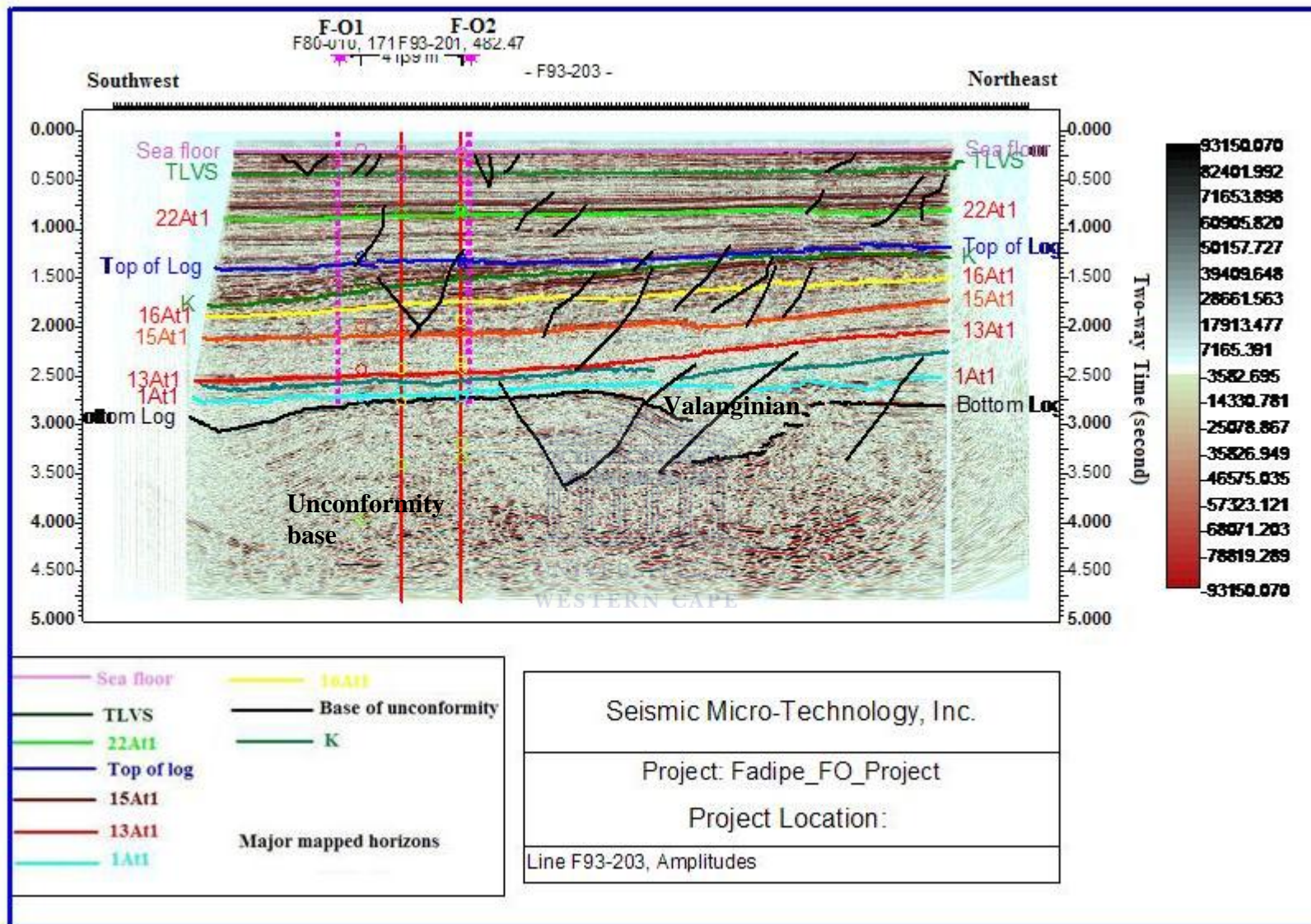


Figure 5.43: Interpreted seismic profile revealing a distinct normal fault directly on the mapped base of unconformity.

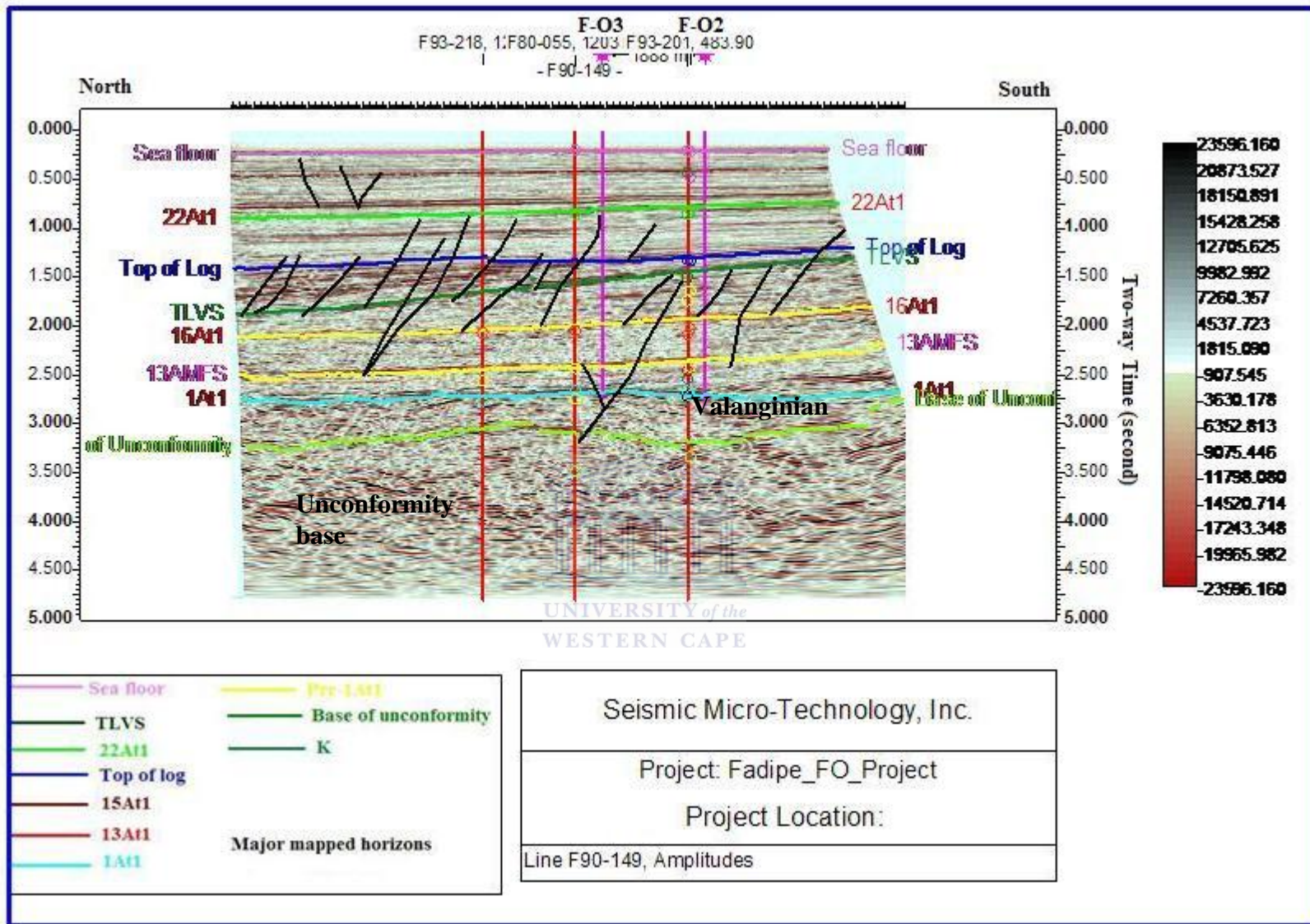


Figure 5.44: Interpreted seismic North-South revealing pronounced listric faults with a retrogradational sequence between TLVS and Top of log horizons.

5.4.4: Seismic profile discussion and interpretation of F80-010 line

The N-SW F80-010 line runs almost parallel to F90-148 line and continues further south. The seismic data clearly shows basin-bounding faults dipping westward. Nine horizons were mapped from this line including seafloor and basement unconformity with F-O4 situated directly on the seismic line. The absence of formation top and conventional data for F-O4 well has limited the extent of analysis for the well; hence the horizons were mapped based on strong seismic reflections with the mapped section showing an agreement between the other formation tops in relation to the mapped section within F80-010 line. Deep seated faults along F-O4 margin are pronounced and are situated along erosional seismic reflection surfaces between top of log and 'K' horizon (Fig. 5.45). A syn-rift sequence with a pronounced antithetic fault and asymmetric deformation was observed trending from 15At1 horizon down to 1At1 horizon hence, forming a possible trap for hydrocarbon accumulation within Valanginian F-O4 sandstone reservoir (Fig. 5.45). A retrogradational sequence associated with several listric faults towards the SE section was observed. The timing of hydrocarbon generation and migration in the Lower Cretaceous time would have been favourable for filling of the available traps (this assumption is based on the general tectonic knowledge of the area hence, more data will be needed in order to make it affirmative) Notable within this section is also a synclinal deformation with major normal faults observed pre-1At1 horizon causing a major displacement trending to the base of unconformity. The distorted nature of the sediments within this synclinal structure could be due to gravity gliding along the zone. The seismic reflections within the synclinal architecture are very clear contrary to the associated anticline (Fig. 5.45). This phenomenon could be attributed to diapirism (Duque-Caro, 1984).

5.4.5: Seismic profile discussion and interpretation of F93-201 line

The NW-SE trending seismic line F93-201 cut-crosses F90-149 and F93-218 seismic lines making it very close to F-O2 well and situated between F-R1 and F-S1 well (Fig. 5.46) therefore, the understanding of the different events that happened along the profile could give a clearer understanding regarding the sedimentation processes and possible orogenic history of F-O2, F-R1 and F-S1 in connection with there respective seismic profiles. Nine different horizons were mapped based on seismic reflections and the loaded formation tops of F-O2. Series of faults were seen trending from the seafloor down to 1At1 horizon. The seismic profile is continental

towards NW and oceanic to the SE, however series of faults are revealed between 22At1 and pre-K horizon with a progradational sequence with evidence of ramping observed towards SE with a significant lateral changes in thickness (Fig. 5.46). Several truncation events were also seen during the later thickness changes bounded by sequence boundaries between Top of log and 16At1 horizon.

5.4.6: Seismic profile discussion and interpretation of F93-218 line

Seismic line F93-218 trends W-E crossing the NW-SE F80-055 seismic profile. Eight horizons were mapped based on formation tops and strong seismic reflection observations. The section shows a Lower Cretaceous sequence (22At1 – K) characterized by series of listric fault trending westward possibly due to differential stress along depths. Series of strong reflector observed within this seismic profile might be attributed to the igneous intrusion observed within the F-R1 well. F-S1 shows a considerably developed thick sandstone unit below 1At1 horizon (3650 – 3660) m and (3720 – 3729) m. Below this, the sandstone becomes thinner, although the sand/shale ratio remains good. Erosional surfaces was noted pre-22At1 across the W – E trending erosional surface horizon, this could be attributed to a global oceanographic events forming strong reflectors on the seismic profile. Hydrocarbon fingerprints were observed above “K” horizon towards the western part of the seismic profile.

5.4.7: Seismic profile discussion and interpretation of F80-055 line

The seismic line trending NW – SE is situated offset of F-O3 and F-R1 but closer to F-R1. Seven horizons were mapped with some syn-deformational series of events observed. “Extrados graben” was observed NW (between 22At1 - 15At1) of the profile with accommodation rotation along shallow faults system (Fig. 5.48). This deformation could also be termed “ramp anticline” with a distorted normal fault. Movement along the listric normal fault is instrumental in formation of several traps (e.g. rollover anticline and up-thrown-fault-block closures) around 22At1 horizon towards the NW. This type of fault may occur where brittle rocks overlies ductile rocks in an extensional regime. This same up-thrown could be termed as “fault breccia”, creating a random array of non-systematic mesoscopic fractures that surrounds angular blocks of rock or “horsetail” (fault splitting into numerous splays near its end, thereby creating a fan of small fractures). Horst is noticed above 1At1 with differential distance between the two hanging walls (Fig. 5.48). This could be due to differential stress acting during subsidence. Anticlinal structure was also observed

with a close relationship between 1At1 and pre-1At1 bounded by fault. This could likely represent a prospect owing to the anticlinal structure bounded by faults and a possible 1At1 cap-rock (Fig. 5.48). The several listric normal faults form during rifting, drifting and evolution of passive continental margins with concomitant basinal development (Shelton, 1984).



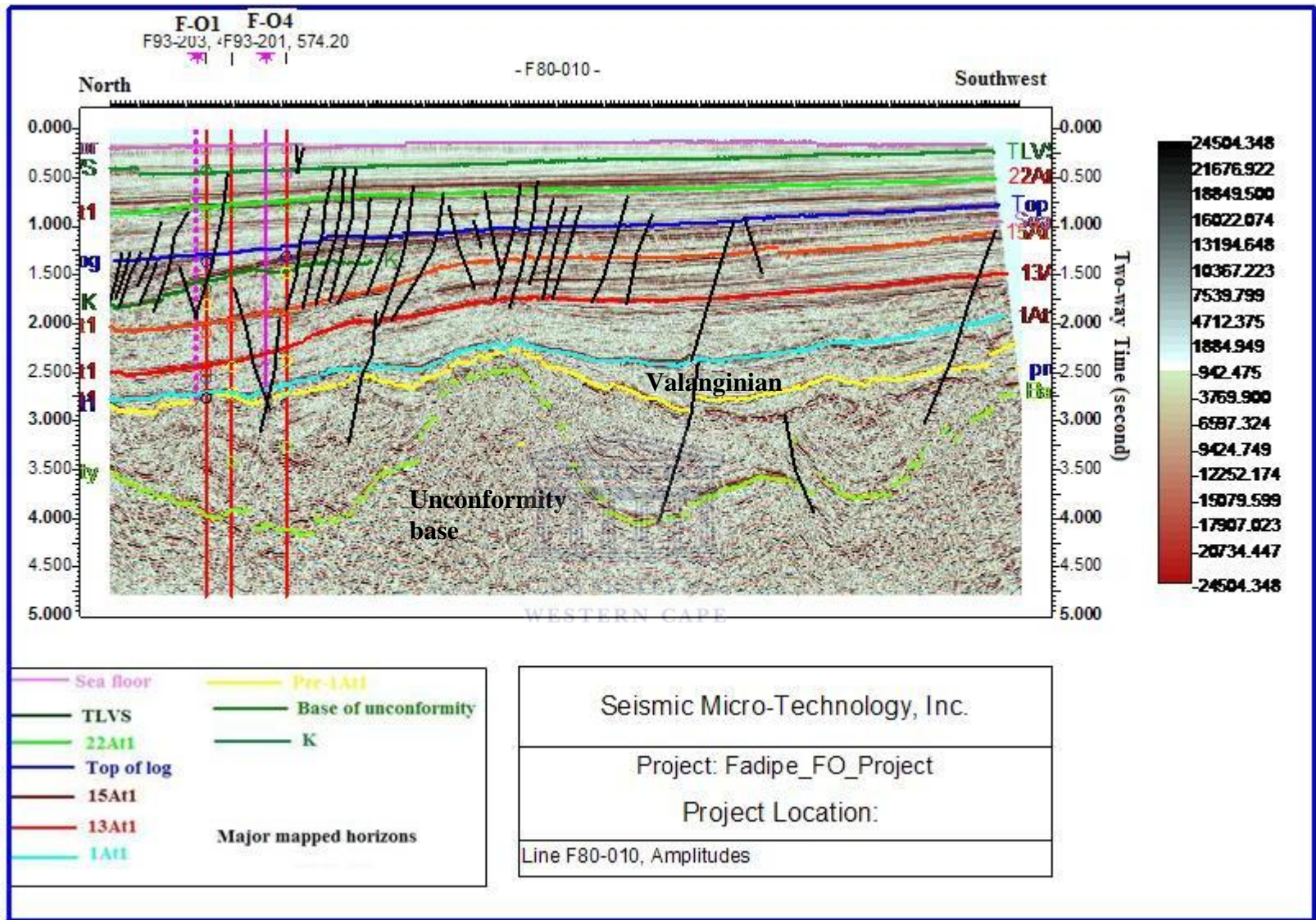


Figure 5.45: Interpreted seismic across North-Southwest showing pronounce faults with synclinal and anticlinal structures.

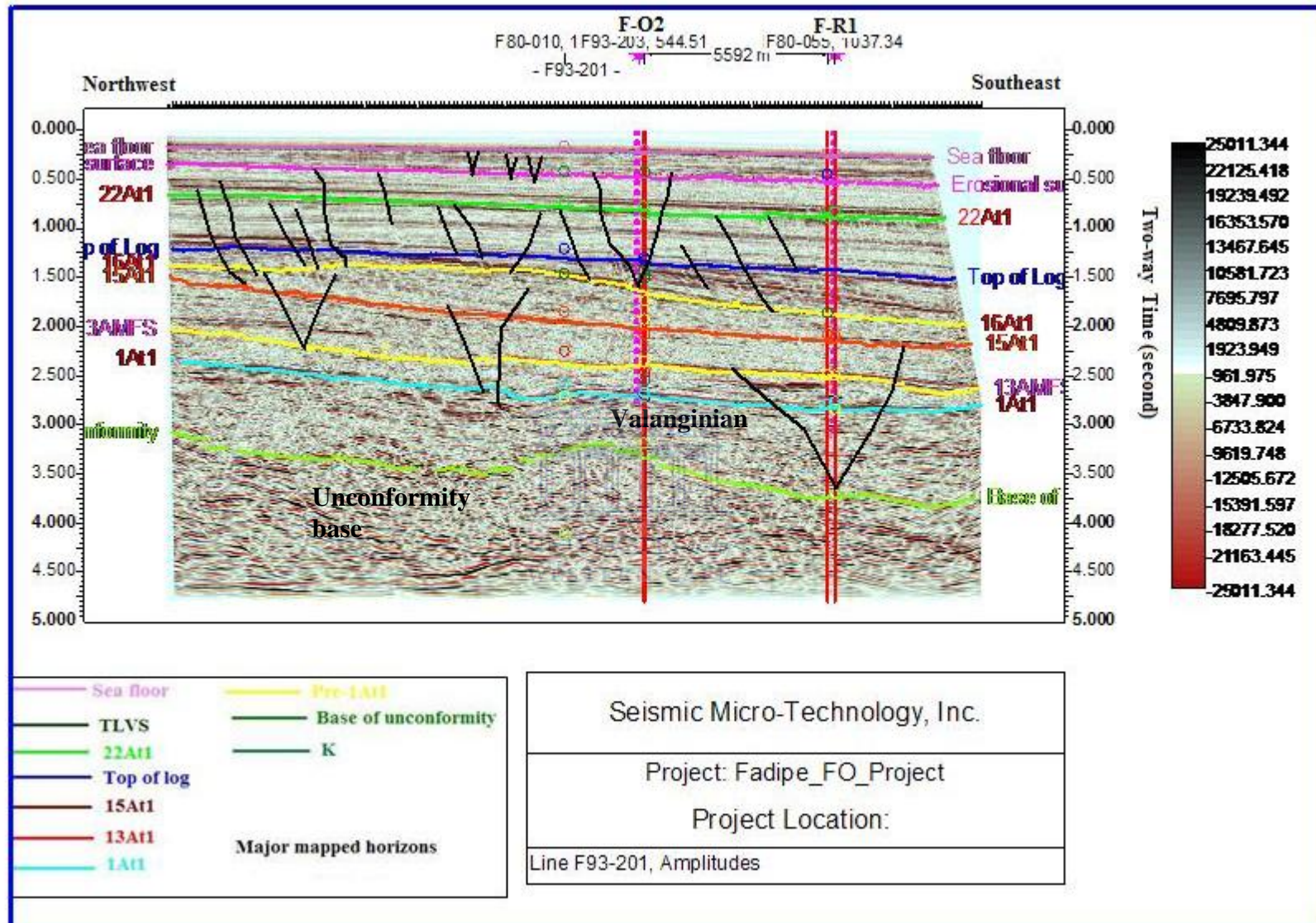


Figure 5.46: Interpreted seismic Northwest-Southeast showing pronounced erosional surface beneath the seafloor.

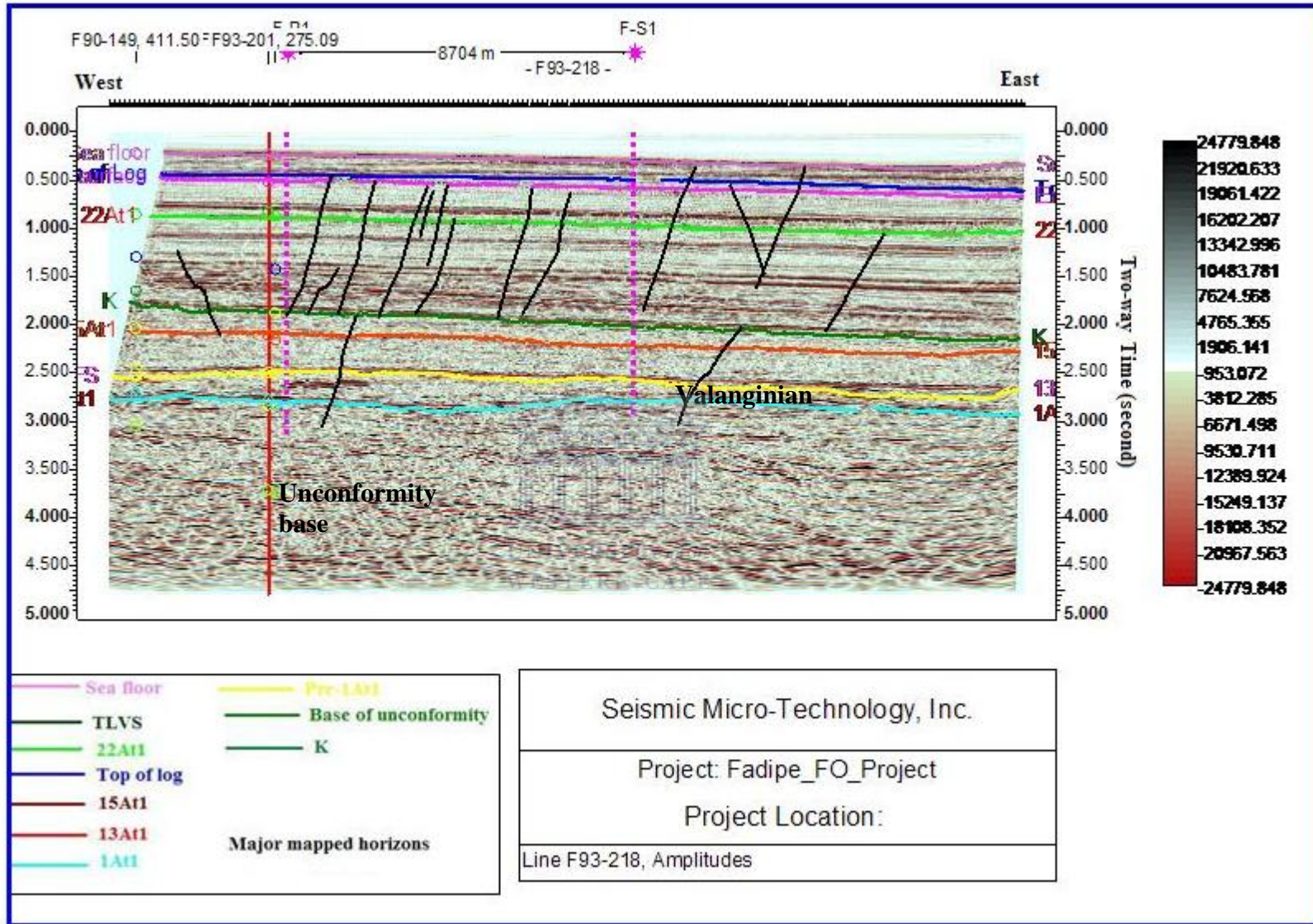


Figure 5.47: Interpreted seismic revealing breaks in surface layering between 22At1 and K horizon accompanied by listric faults.

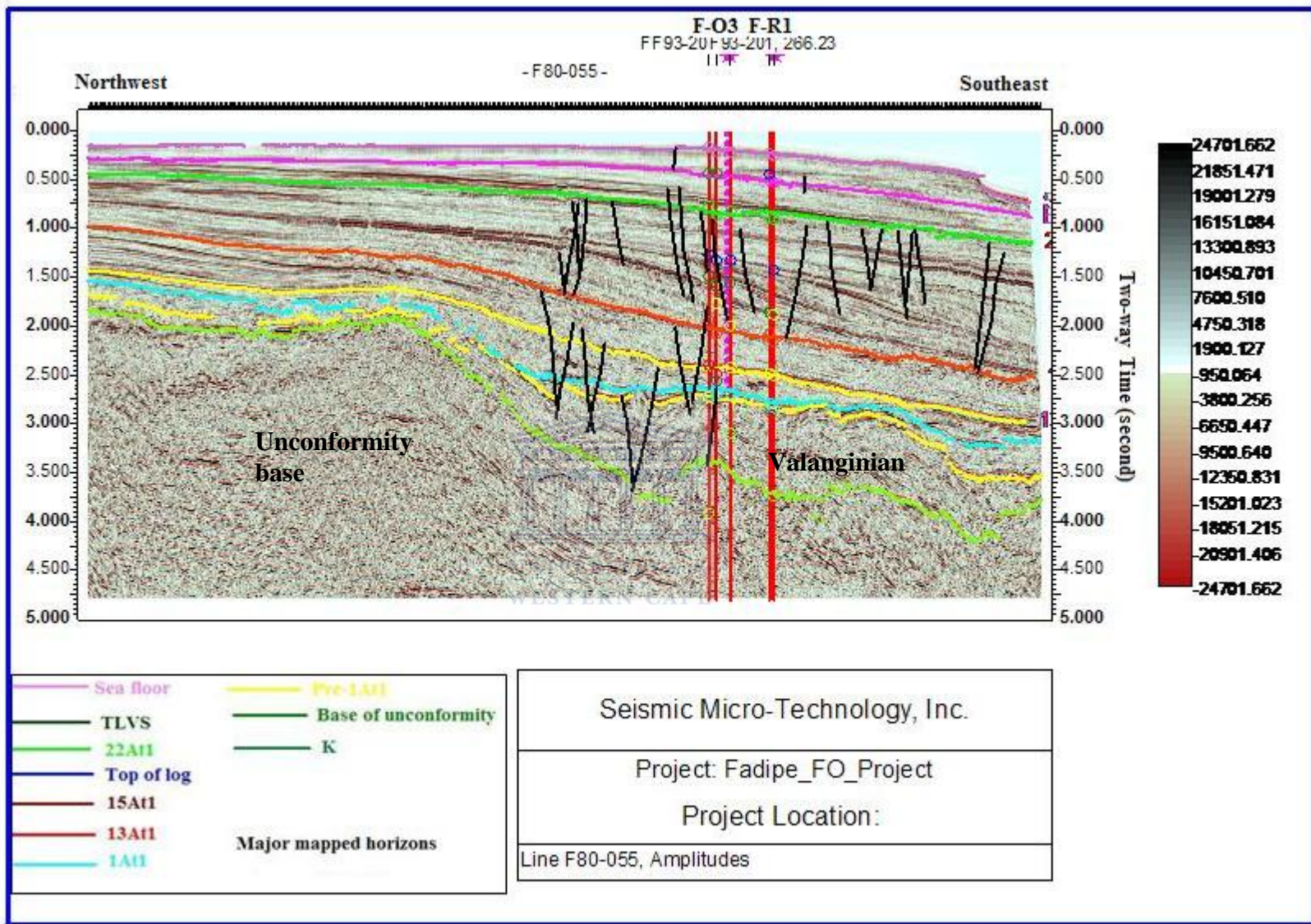


Figure 5.48: Interpreted seismic Northwest-Southeast showing progradational sequence towards Southeast section.

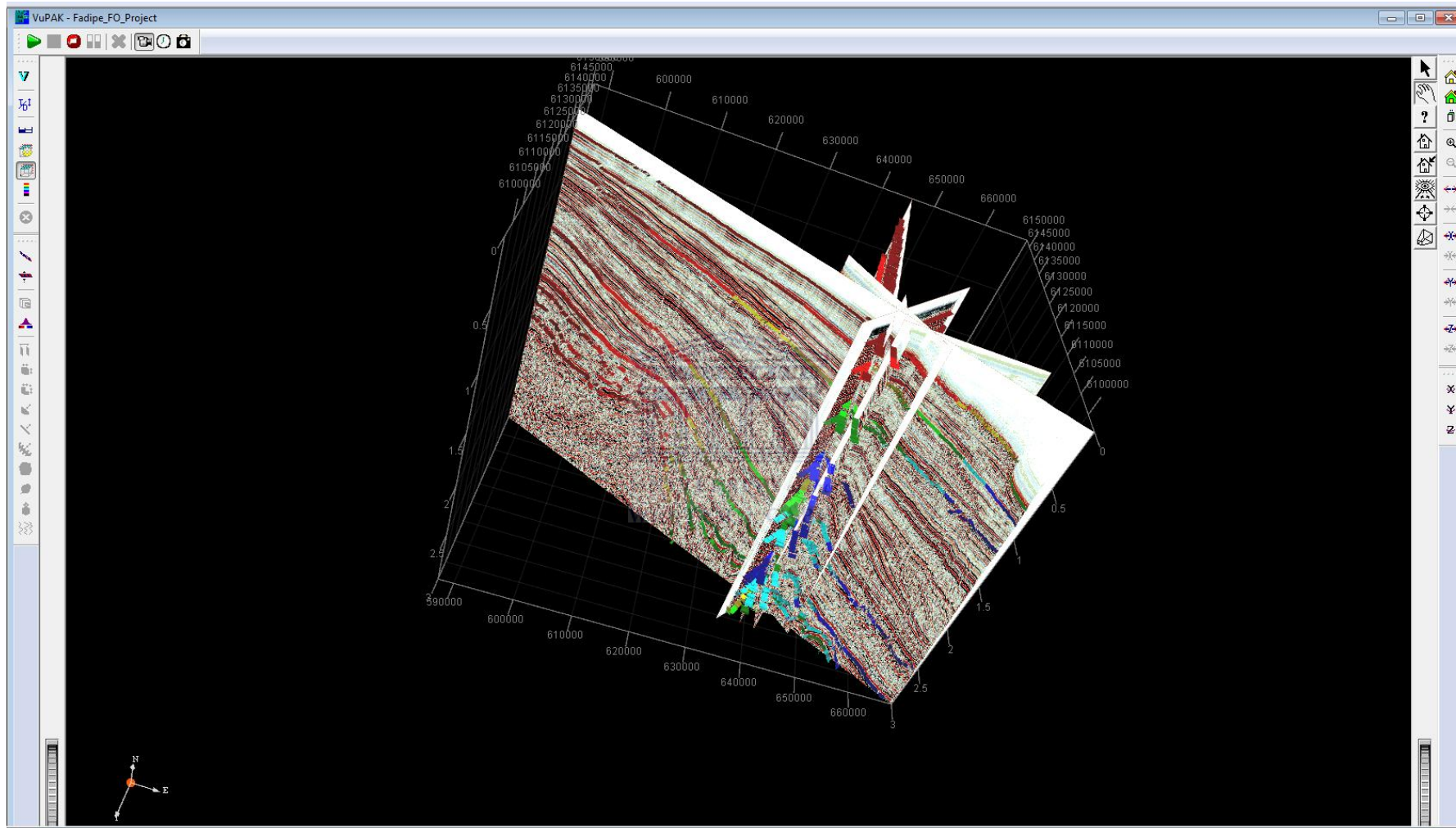


Figure 5.49: Interpreted 3D view of the combined seismic profiles showing the different mapped horizons and the interconnectivity of several mapped layers

CHAPTER SIX

6.0: Multi-mineral and geochemical analyses results and discussion

6.1: Introduction

The standard petrographic microscope was used to examine the mineralogy of the studied thin section plates so as to identify the various rock forming and possible authigenic minerals that are present in the Valanginian age sandstone in the Bredasdorp Basin. The studied sediments are siliciclastic in nature and they contain diversified group of rocks, ranging from fine-grained mudrocks, through siltstone to sandstones and breccias. The sediments are composed largely of grains (clast) derived from pre-existing igneous, metamorphic and sedimentary rocks. The mineralogy and textural maturity were predicted based on the content of the fine grained materials, sorting and roundness of grains coupled with the basic mineral compositions observed. Two important features of siliciclastic sediments are their sedimentary structures and textures; the former has been adequately described in the previous chapter (five) while this chapter will shed more light on the textural features and buttress the observed structures highlighted in chapter five.

6.1.1: Petrography of F-O1 well

The major rock forming minerals based on thin section observation in F-O1 well are quartz, feldspar (potassium and plagioclase) and mica (muscovite) while the diagenetic mineral includes quartz, stylolite and glauconite. The most common detrital mineral is quartz, mainly monocrystalline (Fig. 6.11A, C) with minor amounts of polycrystalline quartz visible (Fig. 6.11D). Both potassium-rich (K-feldspar) and plagioclase feldspars are visible with evidence of lustrous fibre-like mica (muscovite) observed at depth of 3722.40 m within the samples (Fig. 6.11C). Quartz grains exhibits some sub-angular to sub-rounded framework with grain size ranging from coarse to fine having normal extinction. Their degree of sorting ranges from moderately sorted to poorly sorted grains and occasionally well sorted ones are encountered. The sandstone exhibits some evidence of lithification, compaction and increased cementation with increase in depth towards the deeper part of the F-O1 well (Fig. 6.11).

The increase in compaction with increase in burial must have played a role in porosity reduction within the reservoir zone (Figs. 5.21 and 5.31) because compaction comprised of mechanical re-arrangement of grains as well as chemical alteration

which must have been responsible for the formation of stylolite (Fig. 6.11B) and could give rise to grain size reduction with respect to leaching (Ahmad and Blatt, 2005).

Mica being one of the members of group lamellar silicate minerals (feldspar, mica, quartz and olivine) are distinguished from each other mainly by their ratio and elasticity, their ductility as revealed in Figure 6.11C. This could be attributed to their high resistance as a result of mechanical stress. Detrital muscovite is common in clastic rock of North Sea and other prolific basins (Morad et al., 1990) as porosity impairing agent; this mineral was also observed in Bredasdorp Basin.

It is often difficult to distinguish between authigenic quartz and detrital ones by mere thin section observation. However, the close observation of dust rims and fluid inclusion trails could serve as a powerful tool in achieving this. Fluid inclusion petrography will be discussed in later chapter to elaborate more on this pending challenge. Notwithstanding, the observed variability in mineralogy of fringe cement observed across the samples could be an intrinsic explanation for hydrodynamic flow and involvement of sea water. This variability may point to different growth rate and degree of saturation of fluids reflecting locally changes in environmental conditions with respect to sediment textural changes (Rushdi et al., 2000). The common heterogeneity of early marine cementation as inferred in chapter five reflects the processes involved and the constrained factors on that process such as sedimentary textures, framework mineralogy and time. Having predicted in chapter five that the depositional environment could be of marine settings, early cementation when dependent on hydrodynamic flows and external supply is strongly constrained by permeability of sediments and the presence and force of supply mechanism (Harris et al., 1985). Possible mechanism to move sea water through the sediments is waves and tidal currents operating in shallow marine environment and at platform edges, the occurrence of glauconite (Fig. 6.11D) further emphasize on the predicted depositional environment as shallow marine.

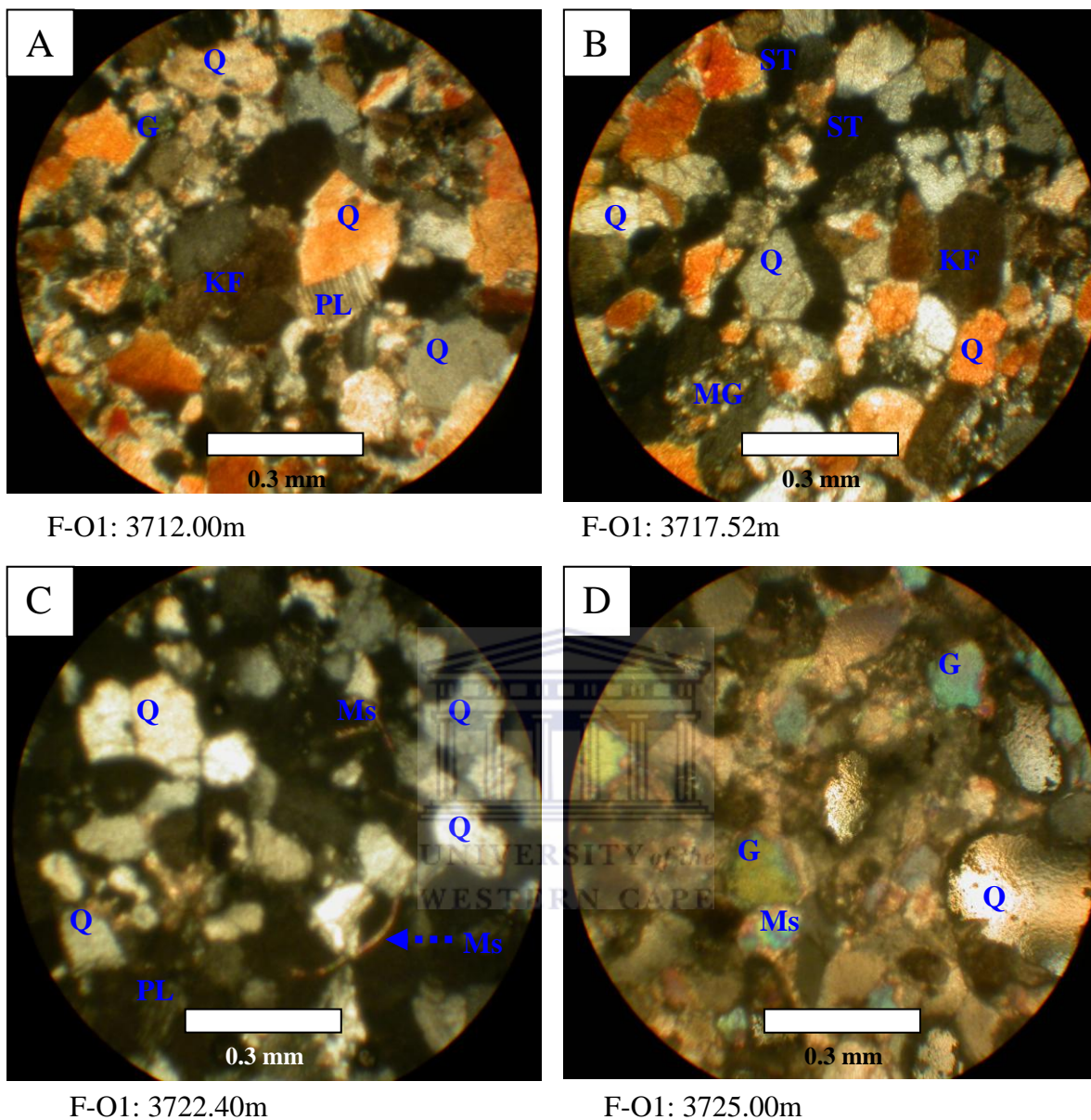


Figure 6.11: Photomicrograph revealing a generally subangular to subrounded grain shapes. MG = Micrographic granite, Q= Quartz, KF = K-feldspar, PL = Plagioclase Feldspar, ST = Stylolite, Fe = Iron rim (cement), Ms = Muscovite, G = Glauconite.

6.1.2: Petrography of F-O2 well

Diagenetic signatures observed in F-O2 sandstones include different stages of compaction, cementation, and change in crystal boundaries and neomorphism which evolved during the above mentioned stages. In addition to the main framework constituents, a suite of feldspar (plagioclase), stylolite, glauconite and mica (muscovite) forms the major part of these mineral assemblages (Figs. 6.12A, B, D). The quartz grains are generally non-luminescent without zonation suggesting few changes in the chemistry of pore fluid (Table 6.41) during quartz precipitation or single cement precipitation phase (Nicolaas et al., 2008). The cluster of crystalline grains of microcrystalline and polycrystalline quartz (Fig. 6.12D) are important constituent framework grains of these sandstones. Detrital quartz grains are evident across the reservoir interval with irregular shapes and few grain contacts coupled with high degree of cementation (Figs. 6.12B, C and D). The development of calcite rim cement occurs as micritic coating on grains (Fig. 6.12D) while some occurs as superficial pore filling between grains (Fig. 6.12C).

The key portion of the framework grains is subangular to sub-rounded in shape while the occurrence of narrow grain size range as evident in figure 6.12A & C could suggest either more or less uniform size of the sediments supplied to the well or the uniform hydrodynamic conditions prevailing during deposition of these sandstone units (Ahmad, 2006). The co-occurrence of moderately sorted and poorly sorted sediments (Figs. 6.12B, D) either reflects the change in water turbulence during deposition or pulses of sediment supply during episode of rifting and uplift (Ahmad, 2006). Plagioclase feldspar is also observed from the slides (Fig. 6.12B) with its twinning effect, its formation might be due to metasomatism which involves the reconstruction of partially degraded feldspar to form potash feldspar. The presence of mica in the studied sediments is deduced from their occurrence as highly stressed, deformed and mainly wrapped around detrital quartz (Fig. 6.12C). The occurrence of stylolite as revealed in Figure 6.12B and C is thought to have been formed as a result of pressure solution that normally reduces pore space under pressure during diagenesis.

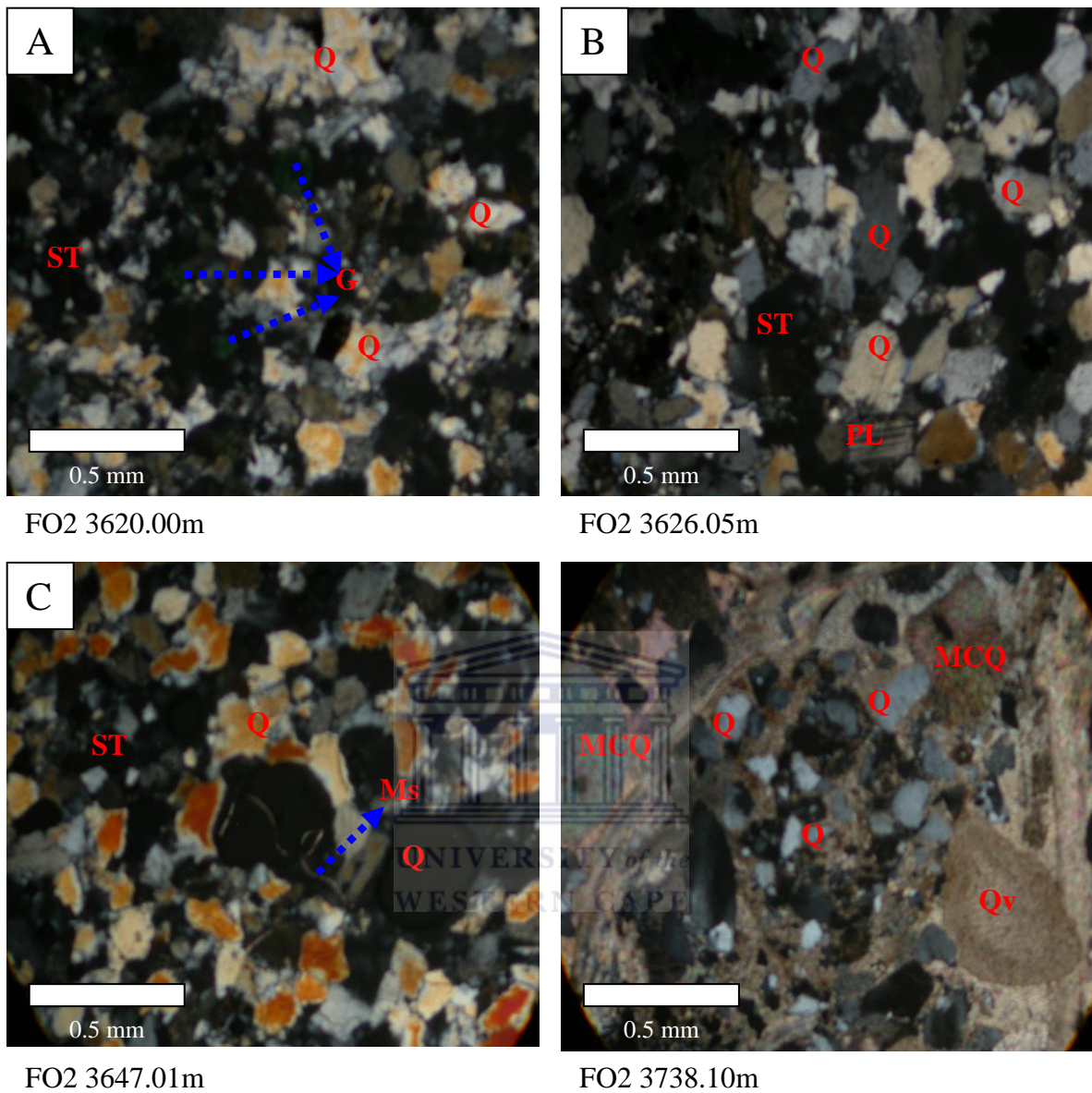


Figure 6.12: Photomicrograph deformed strings of mica and microcrystalline quartz. Q = Quartz, KF = K-feldspar, PL = Plagioclase feldspar, ST = Stylolite, Fe = Iron rim (cement), Ms= Muscovite, G = Glauconite, Qv = Quartz overgrowth, MCQ = Microcrystalline quartz.

6.1.3: Petrography of F-O3 well

Some sediments in the reservoir intervals of the F-O3 well are loosely indurated to hard (Fig. 6.13A & B) depending upon the composition of the cement. The presence of silty and clayey matrix in varying amounts in the upper depth of the reservoir zone (Fig. 6.13A) might have influenced the diagenetic processes by supplying Fe and reducing porosity and permeability by pore occlusion. The major observed minerals with regards to the thin section slides are quartz, K-feldspar, mica and glauconite while stylolite are also noted occurring across the stretched pore spaces (Fig. 6.13D). Pressure dissolution is also noticed (but minute) in the sandstone along discrete spaced surfaces, such as mica (muscovite formation; Fig. 6.13A) with a wiggled ring-like structure showing evidence of differential stress along traces of cleavage planes. Progressive burial of sediments and subsequent increase of diagenetic grade might also be responsible for the transformation of this micaceous mineral down the depths.

The nature of point contact and contact index are helpful in understanding the aggregate packing of the rocks. In F-O3 sands the closely packed sandstone exhibit a concavo-convex types of grain contacts (Fig. 6.13C) but this contacts are not very pronounced as such, it is suggestive of limited pressure solution activity in the sandstone (Kierkegaard, 1998). Some detrital grain have been dissolved and replaced by calcite cement, it has both quartz and feldspar grains being corroded along grain boundaries and cleavage planes with the grain shape generally ranging from subangular to sub-rounded suggestive of a poor degree of sorting. Stylolite on the other hand was observed in Figure 6.13D (zig-zaged green dotted line) showing sites of accumulation of insoluble residues (clays, iron oxides and others) as the rock closes up which is what makes the stylolite to be dark in colour. The generally smaller mineral grains with cementation between the grains coupled with the variation shapes of grains could be attributed to compression, rotation of grains and their mechanical breakage during burial which could in turn be responsible for reduction in the sandstone porosity.

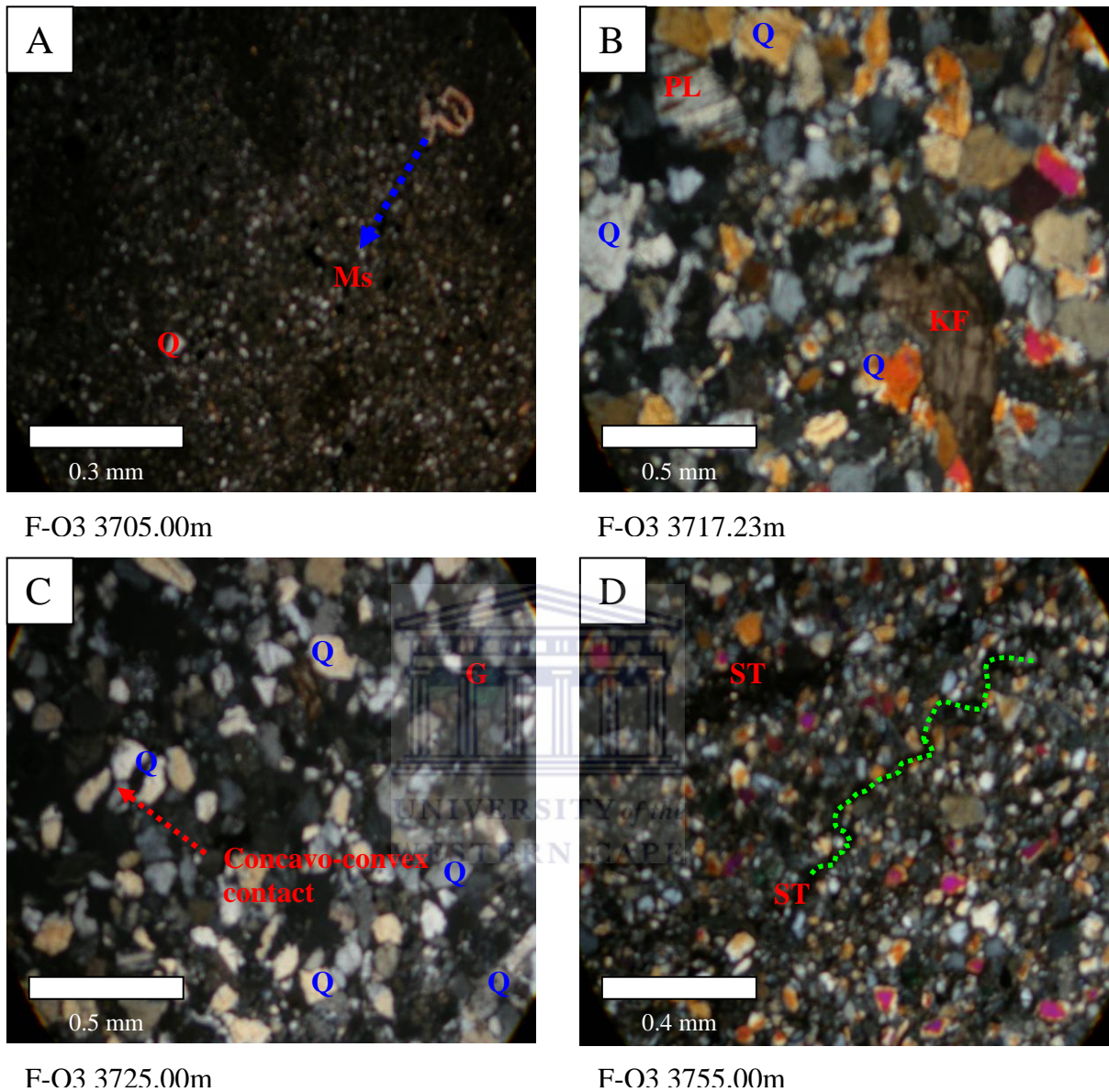


Figure 6.13: Photomicrograph showing variation in grain shape and contact, cementations and stylolitic veins. Q = Quartz, KF = K-feldspar, PL = Plagioclase feldspar, ST = Stylolite, Ms = Muscovite, G = Glaucanite,

6.1.4: Petrography of F-O4 well

The major minerals observed in F-O4 well thin sections are quartz, feldspar (plagioclase and potassium), micrographic granite and fragmented minerals are stylolite, concretions and micrographic granite. Grain contacts are dominated by long (Fig. 6.14C) and concavo-convex (Fig. 6.14A) surfaces that have likely resulted from compaction. The development of feldspar grains was also noted, it contains significant secondary porosity that must have developed during burial and diagenesis (Figs. 6.14B and C). In some cases, the secondary porosity has been occluded by mineral concretions (Fig. 6.4B) while in other cases have major carbonate cement growths within the pore spaces (Figs. 6.14C and D). Quartz cement is a main factor influencing reservoir quality in siliciclastic sandstone. The majority of the detrital quartz grains are monocrystalline while the detrital feldspar in these sandstone are mostly variably altered K-feldspars (Figs. 6.14B, C and D). Altered K-feldspars are associated with kaolin which is evident in the scanning electron microscopic studies as will be seen later.

Feldspar grains are derived from the same crystalline rocks as quartz (Tucker, 2001). These chiefly are granites and gneisses, where potash feldspar dominates over sodic plagioclase however; the presence of micrographic granite (Figs 6.14C and D) could be as a result of incomplete break-down of the granitic origin of the studied sandstone. Figures 6.14C and D shows a pronounced calcite cementation with fewer quartz grains embedded between the cements. The grains exhibit a subangular to subrounded and elongated shape. The calcite cement is probably responsible for the porosity reduction due to its pore-filling nature which replaces partly and/or totally detrital grains. The observed mineral concretion looks micritic in nature (Fig. 6.14B) and also could be a micro-crystalline calcite surrounded with iron rim within which scattered detrital grains are embedded (Fig. 6.14B), as local patches.

Stylolite seam is also observed in F-O4 sandstone (Fig. 6.14A) which may influence the rate of quartz dissolution and stylolite development (Baron and Parnell, 2006). The occurrence of the stylolite may be said to have been formed in response to compression as a result of progressive burial due to its parallel to bedding nature (Fig. 6.14A).

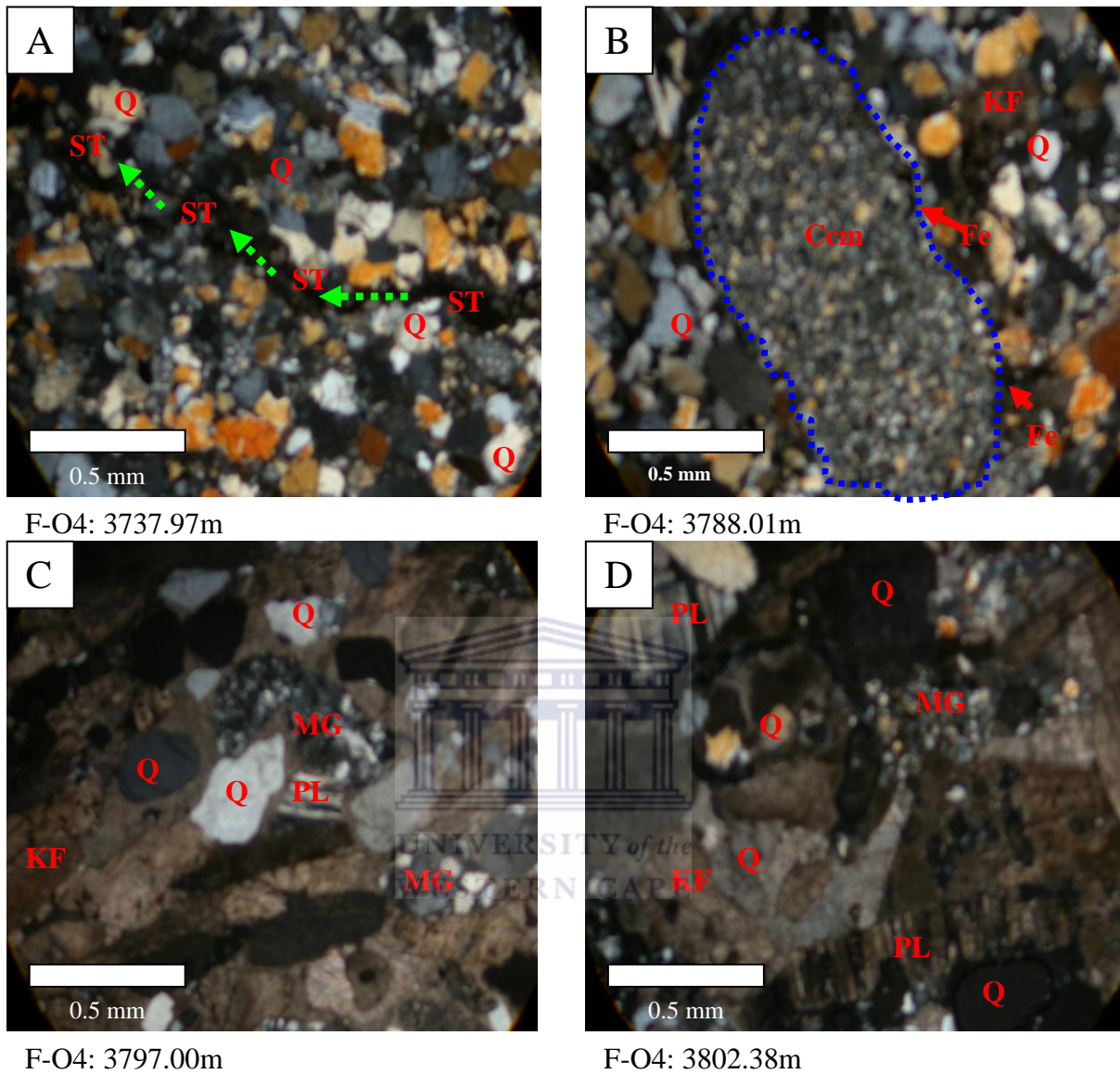


Figure 6.14: Photomicrograph showing lithified calcite cemented sandstone and pronounced elongated concretion. MG = Micrographic granite, Q = Quartz, KF = K-feldspar, PL = Plagioclase feldspar, ST = Stylolite, Fe = Iron rim (cement). Ccm = Mineral Concretions (with string cleavage displaying variable colours) or rhizocretionary structure (B).

6.1.5: Petrography of F-R1 well

The microphotograph for the F-R1 sandstones reveals the presence of quartz, mica, glauconite, K-feldspar and stylolite across the observed interval. The F-R1 sandstone ranges from very fine to coarse grained with predominance of fine to medium grain size. The degree of sorting also ranges from moderately sorted to well sorted with a well marked mixture of angular grain and subangular to rounded grains in these sandstones, indicating a blend of recycled and first cycle sediments (Lima and De Ros, 2002). The main cementing material in the F-R1 well reservoir is quartz, which occurs as syntaxial overgrowth near site of intergranular dissolution and around closely packed detrital quartz grain which could be attributed to a mesogenetic origin (McBride, 1989; Worden and Morad, 2000) in most of the studied samples. Heterolithic sandstones may lack quartz cement when they are matrix supported (Fig. 6.15A) due to bioturbation which was more evident at same depth in the core graph (Fig. 5.15). Quartz cement partially fills pore spaces and it could probably be one of the main causes of porosity loss within the Valanginian age sandstone reservoir in F-R1 well. Detrital quartz grains are evident across the sandstone sample (Fig. 6.15) with irregular shapes and few grain contacts.

The mechanical stability of feldspar in F-R1 sandstone seems lower than that of quartz because feldspar is softer and has a stronger cleavage. This leads to disintegration of feldspars crystals during transportation especially in turbulence environments. On a broader scale, fluvial sediments contain more feldspar than shallow marine and aeolian sandstone (Tucker, 2001) which is in line with the minor amount of visible feldspar observed in the F-R1 sediments (Fig. 6.15). The chemical stability is also lower to that of quartz owing to the ease at which they hydrolyse (Tucker, 2001). The greater resistance to chemical stability of K-feldspar to plagioclase feldspar must have been responsible for the absence of plagioclase in this sandstone which suggests that chemical activity must have been more pronounced in F-R1 than the neighbouring wells (F-O4).

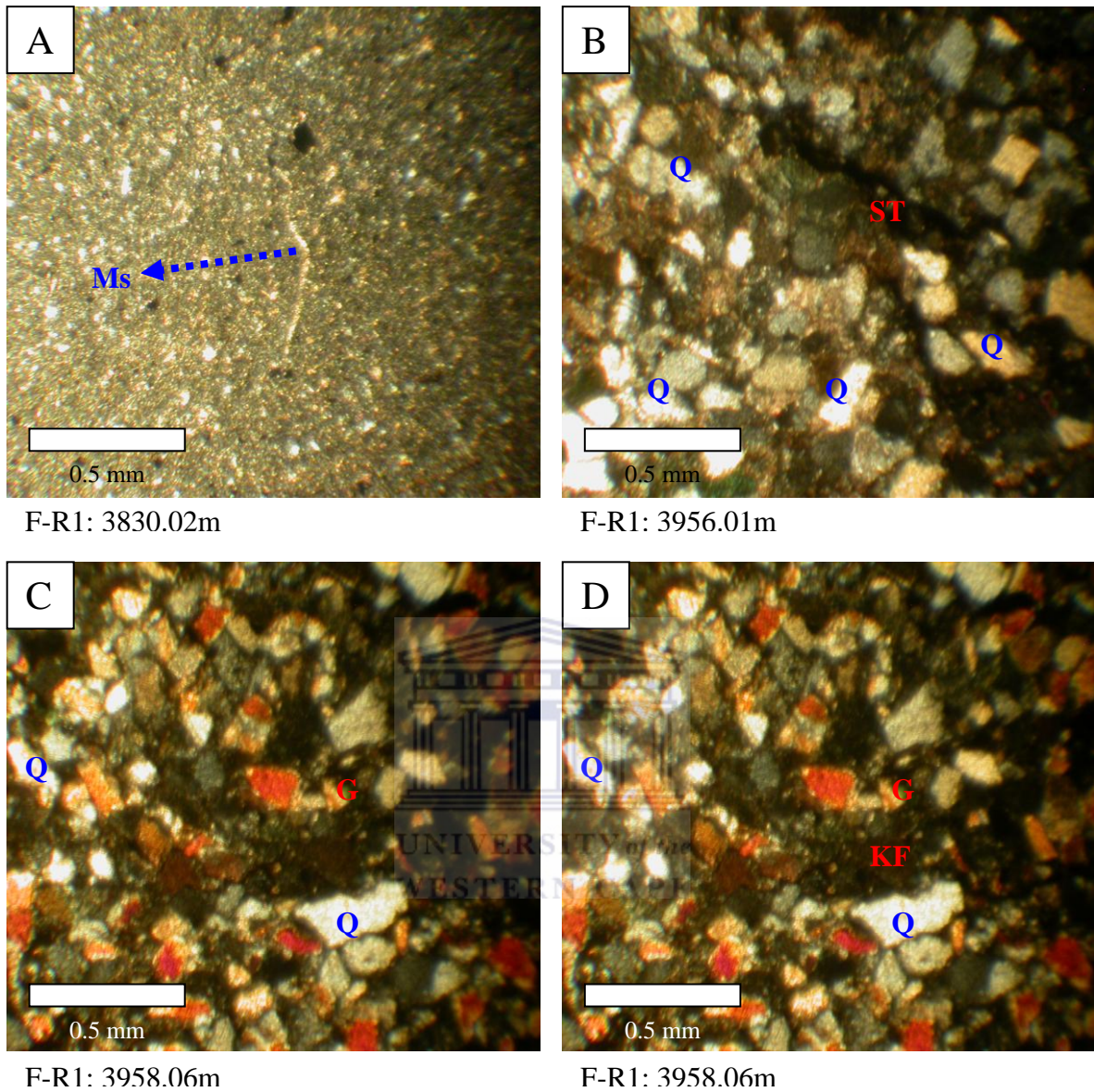
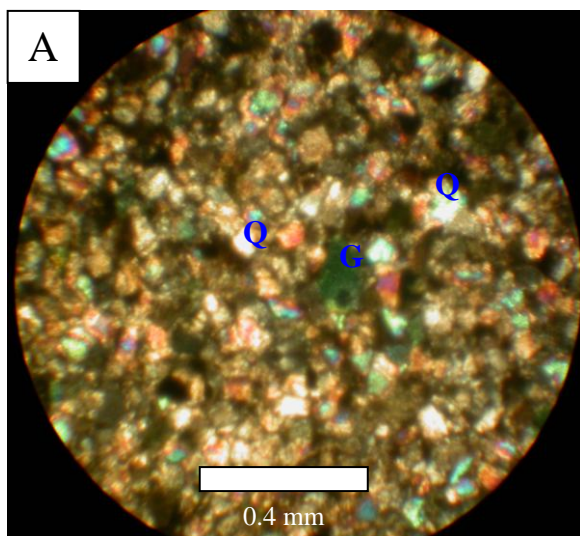


Figure 6.15: Photomicrograph showing elongated mica embedded in fine grained sandstone and some showing stylolitic vein with distinct quartz grains. Q = Quartz, KF = K-feldspar, ST = Stylolite, Ms = Muscovite, G = Glauconite.

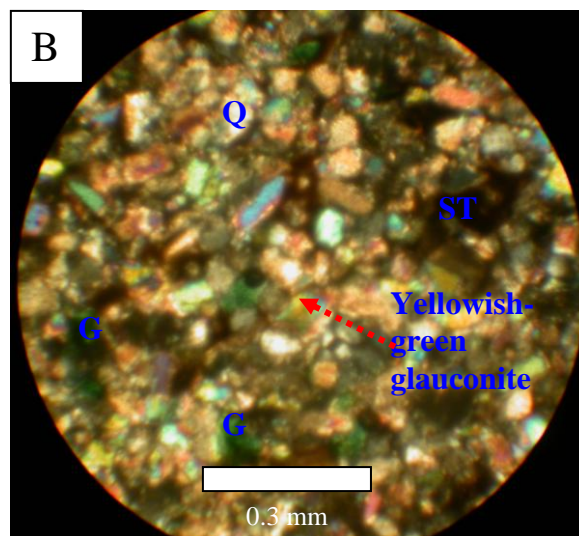
6.1.6: Petrography of F-S1 well

F-S1 well clearly reveals glauconitic sandstone however with more of quartz grains than the glauconite itself (Figs 6.16A, B). The quartz cementation like most diagenetic phenomena is a kinetically controlled process. There is a widespread controversy about whether quartz grows in short, fast burst (episodic) or in a long, continuous but inevitably slow manner (Worden and Morad, 2000). These well might probably shed more light to proffer some solutions to the above mentioned daisy occurrence of quartz once other results are integrated with thin section. Glauconite on the other hand broadly assumed to be an indicator of deposition in shallow marine sedimentary conditions (e.g. Odin and Matter, 1981), is present in nearly all the samples (Figs. 6.16A, B, D). Glauconite occurred as scattered elongated to subrounded and light green to dark green grains with microcrystalline textures (Figs. 6.16A, B). Grain contacts are dominated by concavo-convex surfaces that have likely resulted from compaction. Glauconite occurs also as mica-like flakes with obvious cleavage planes yellowish to green to relatively dark green colour (Fig. 6.16B). However, micaceous clay coats sits between some grain-grain surfaces suggesting the grain-coating clay developed before mechanical compaction started (Fig. 6.16A, B).

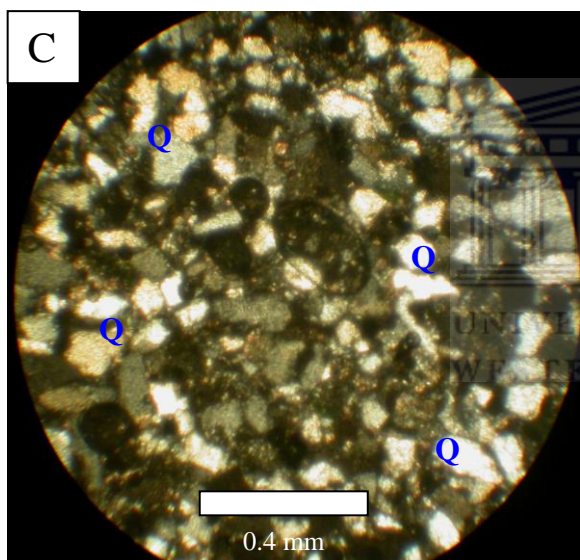
Several elements such as packing of the framework grains, fractures and dissolution seams within the F-S1 sandstones indicate the presence of mechanical compaction and chemical compaction in different stages of diagenesis. Compaction causes the reduction of the existing pore space in two forms: (1) the change of contacts between the framework grains in grainstones; (2) re-precipitation of dissolved cements involving certain physical and chemical conditions. Where early cementation was abundant and almost completely occluded primary porosity, later dissolution was compensated by re-precipitation of cement (Zhang et al., 2008).



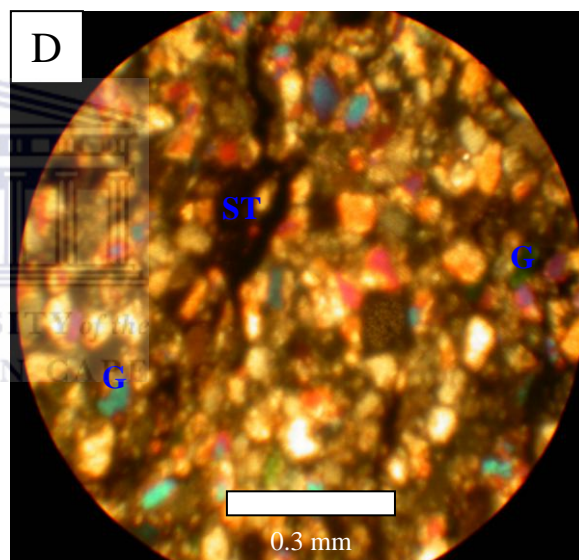
F-S1: 3623.00m



F-S1: 3635.02m



F-S1: 3664.00m



F-S1: 3671.00m

Figure 6.16: Photomicrograph showing glauconitic sandstone with some stylolitic veins. Q = Quartz, ST = Stylolite, Ms = Muscovite, G = Glauconite.

6.2: Morphology of F-O field sandstone samples

The need for accurate reservoir characterization is imperative in developing an understanding of geologic complexity that positively affects field development. Reservoir quality primarily determined by porosity and permeability of relevant formations is controlled by many parameters. These include the nature of the constituent minerals and cement, degree of cementation and distribution of pore size. Quartz as observed in F-O gas field is an important cementing material in siliciclastic sandstones that can reduce porosity and permeability severely while mica alteration can reveal the extent of material transfer in diagenetic systems and elucidate the role of mica cementation in sandstone.

6.2.1: SEM petrography for F-O1 well

The authigenesis of silica developed several habits in the Valanginian sandstones of the F-O1 reservoir interval which includes: (1) intergranular pore filling microquartz, (2) syntaxial quartz overgrowth, (3) prismatic quartz outgrowths and (4) Kaolinitic platelets. The two later habits are widespread across the F-O field. Kaolinite was observed across the whole analysed F-O1 reservoir sandstone with blocky platelets locally resting on quartz overgrowth (Fig 6.21). Extensive formation of kaolin must have occurred during burial diagenesis and is commonly associated with degraded feldspar (Fig. 6.21C) and mica (recognized petrographically in thin sections; Figs. 6.11C and D). Its occurrence across the reservoir interval might be due to meteoric flushing of the sandstones (Fadipe et al., 2011). The dissolution of potassium feldspar which partially covers detrital feldspar grain with a distinct stick-like outline (Fig. 6.21) is revealed in the mineral architecture. K-feldspar overgrowth is engulfed by pore filling calcite that precipitated during progressive sediment burial and quartz overgrowth (Fig. 6.21).

The volume of syntaxial quartz overgrowths do not increase with depth, but rather vary widely across the depths (visual observations). Quartz overgrowths are abundant both in the shallow-buried sandstones and deeply buried once. The occurrence of poorly developed and discontinuous syntaxial quartz overgrowths (Figs. 6.21A and B) in early silica/clay-cemented sandstones suggests that the overgrowth distribution is controlled by microquartz and authigenic clays (Lima and De Ros, 2002). Overgrowths are mostly post-compactional, as evidence by their absence along intergranular contacts. Quartz overgrowths occlude most of the remaining intergranular porosity in tightly compacted sandstones, and eventually engulfed of

diagenetic products of mica (kaolinite, illite etc). Prismatic macro quartz outgrowths occurs on quartz grains discontinuously coated by microquartz, extending into mouldic, intra- and inter- granular pores mostly in sandstones cemented by early clay (Fig. 6.21).

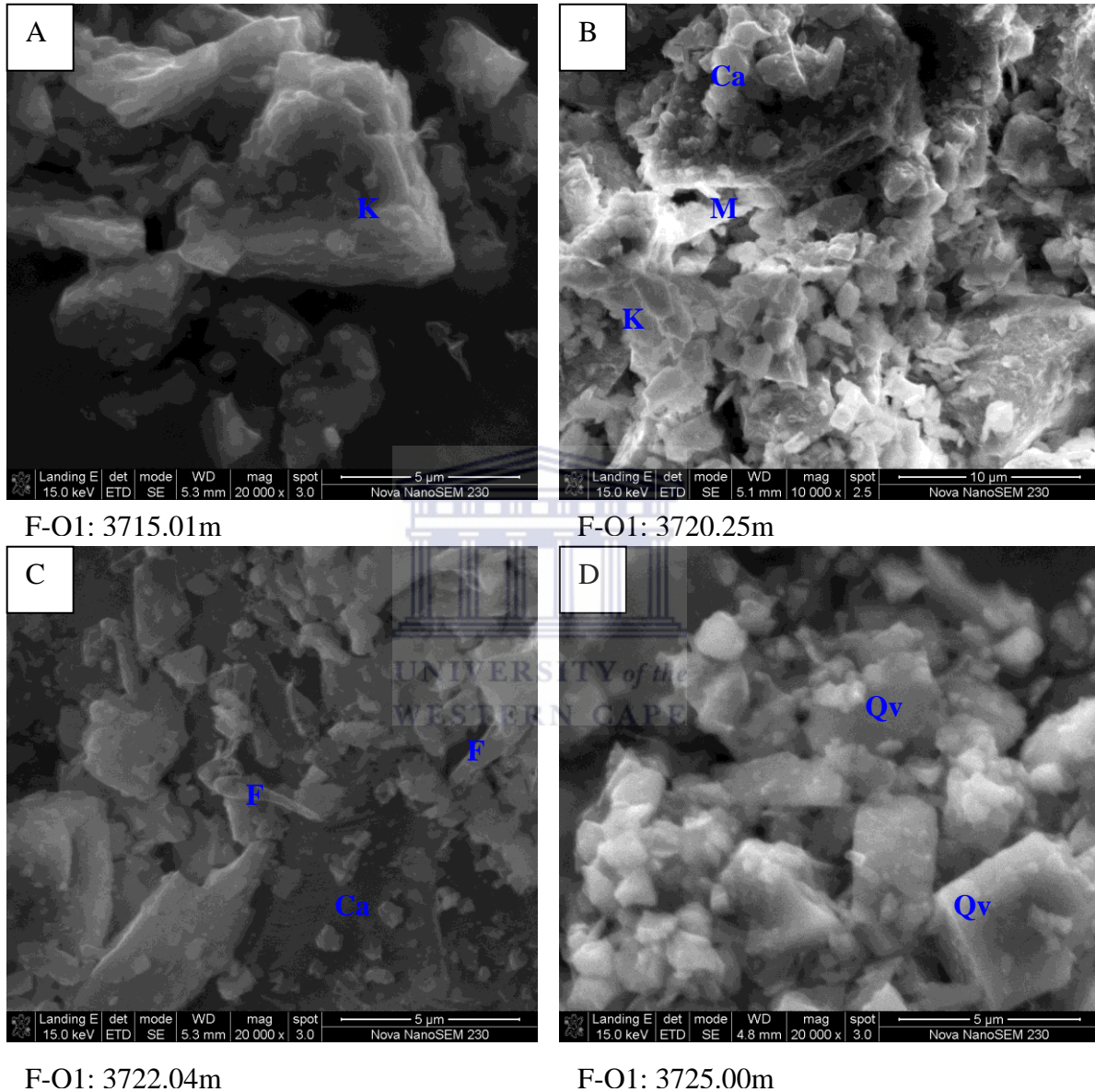


Figure 6.21: (A) Kaolinite booklet resting on each other. (B) Flakes of kaolinite with grains of calcite (C) Rod-like feldspar with shape edges showing evidence of alteration (D) Quartz overgrowth associated with calcite grain.

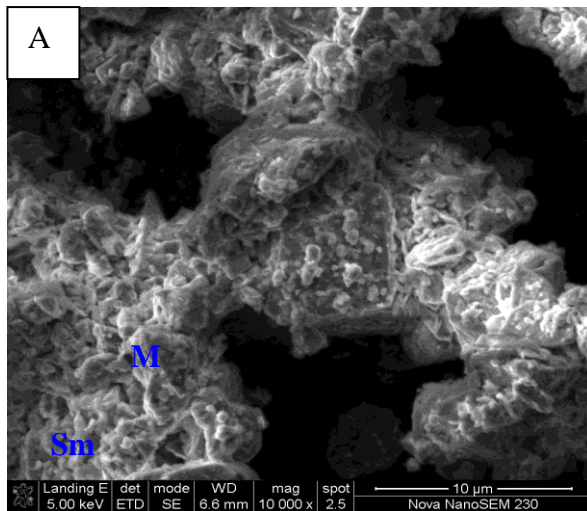
Note: F = leaching of feldspar grain, M = Mica, K = Kaolinite, Qv = Quartz overgrowth, Ca = Calcite.

6.2.2: SEM petrography for F-O2 well

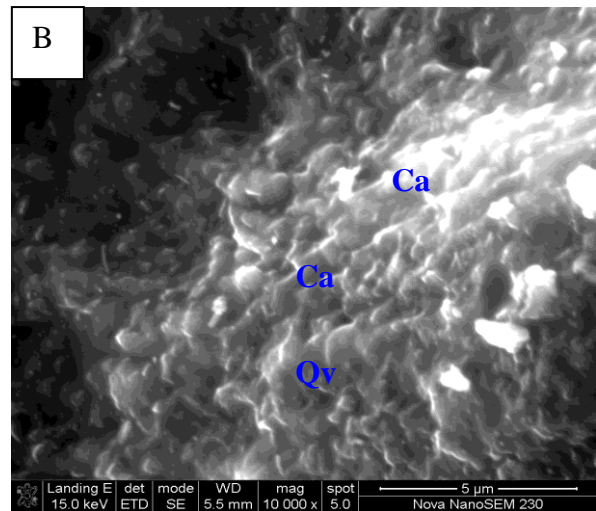
Calcite is one of the most common cement in sandstone, which was observed in F-O2 reservoir interval (Figs. 6.22A, B), but other carbonate cements of more local importance are dolomite and siderite which are easier to detect using X-ray diffractometry. The cement observed in the F-O2 sandstone exhibits an even-to-patchy distribution, to local segregations and concretions (Figs. 6.22B, E, F). The calcite could be classified as “drusy” calcite mosaics owing to the predicted equant crystals, which fill the pores between grains (Tucker, 2001). Calcite also fills fractures, either alone or as successor to earlier quartz cement in reactivated fractures (Fig. 6.22B). The primary cementing material of F-O2 Valanginian sandstone is calcite precipitated probably in the sub-aerial vadoze zone due to capillary action under wet and dry climatic conditions (Tandon and Varshney, 1991).

There is no visible observation of K-feldspar within the examined samples. This could be explained using the several authors’ work that suggested that alkali feldspar can undergo extensive dissolution during burial diagenesis of sandstone (Miliken, 1989; Harris, 1992; Wilkinson and Haszeldine, 1996). Dissolution of K-feldspar is probably as a result of interaction with weakly acidic pore fluid formed by decomposition of organic matter (Selly, 1985). The dissolution of K-feldspar could increase the percentage of K, Al, Fe and SiO₂ concentrations in the diagenetic fluid which can cause precipitation of quartz as observed in figure 6.22F. Chlorite flakes was vaguely observed in figure 6.22E, with an irregular shape suggesting subsequent dissolution by pore waters.

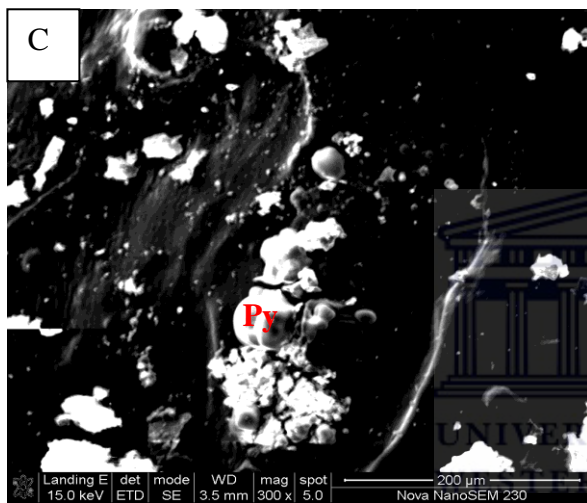
Pyrite is a minor but ubiquitous diagenetic component of F-O2 well, and takes a number of forms, occurring as disseminated sub-cubic crystals, pyrite framboid and spherulitic clusters (Fig. 6.22C, D). In some samples, pyrite framboids are clearly located against grain surfaces and, therefore those samples at least preceded chlorite cementation (Fig. 6.22C, D). Pyrite framboids are well known to form soon after burial (Cookenboo and Bustin, 1999) in response to low oxygen-high sulphate pore conditions characteristics of the sulphate reduction zone (Berner, 1984). Such conditions are usually restricted to upper few metres of organic rich sediments; this is supported by shaly nature of the sediment at depth 3657.13 m (Fig. 5.12; F-O2 core graph) which is known to be associated with organic matters. The presence of smectite must have reduced the porosity of the reservoir zone due to its ability to imbibe water hence swell to block pore spaces (Figs. 6.22A, F).



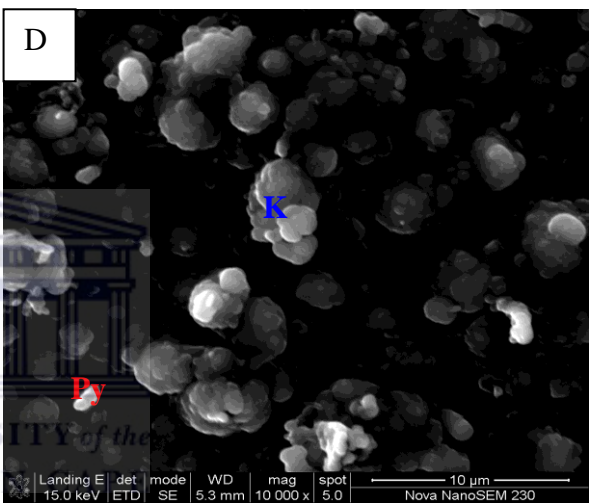
F-O2: 3620.00m



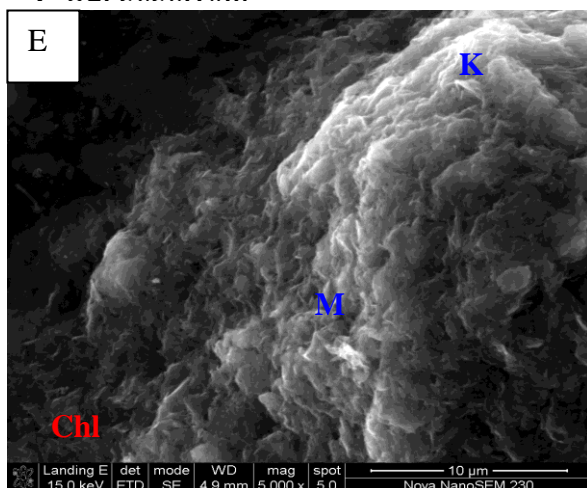
F-O2: 3626.05m



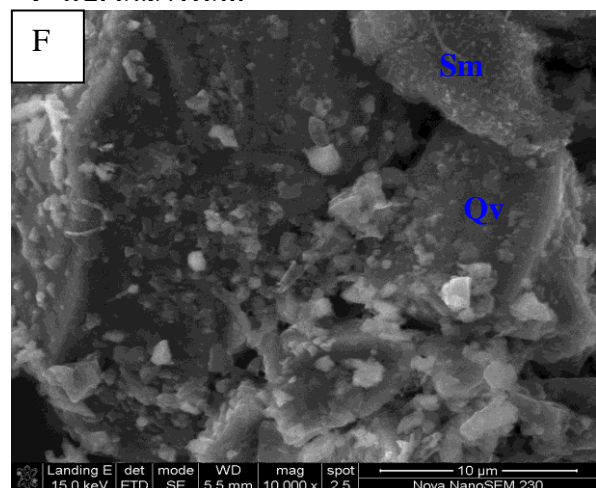
F-O2: 3638.10m



F-O2: 3657.13m



F-O2: 3665.01m



F-O2: 3717.52m

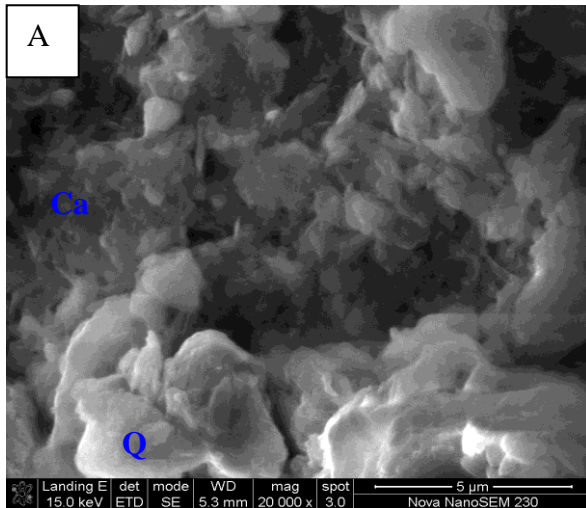
Figure 6.22: (A) Spine-like micaceous material (B) Clear surface texture in the calcite cement concretion (C) Framboidal pyrite resting on quartz grain (D) Rhombohedral flakes of kaolinite (E) Edgy steps of kaolinitic clay (F) Quartz over growth with evidence of smectization.

Note: F = leaching of feldspar grain, M = Mica, K = Kaolinite, Qv = Quartz overgrowth, Ca = Calcite, Sm = Smectite, Py = Pyrite, Chl = Chlorite.

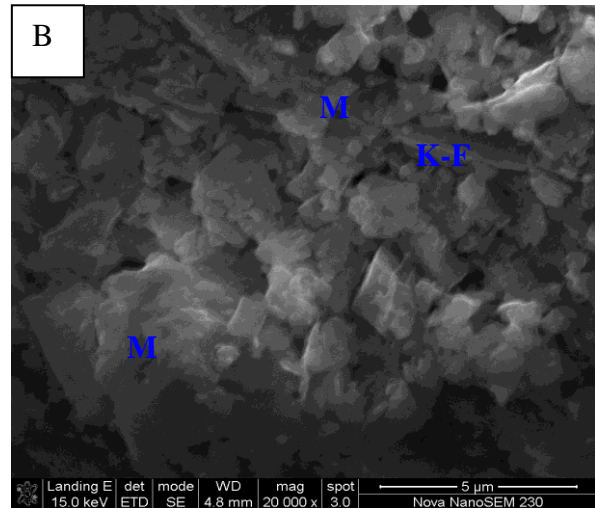
6.2.3: SEM petrography for F-O3 well

Quartz cement commonly occurs in this well as overgrowths on detrital grains where calcite and quartz cements co-exists, the edges of quartz cement are irregular or angular and overlain by calcite cement (Figs. 6.23A, C, D), indicating that calcite cements post dated quartz overgrowths. The euhedral growth shape of quartz (Fig. 6.23A) compromises its relationship with calcite cement suggesting that either the calcite or quartz was precipitated contemporaneously or calcite post dated precipitation.

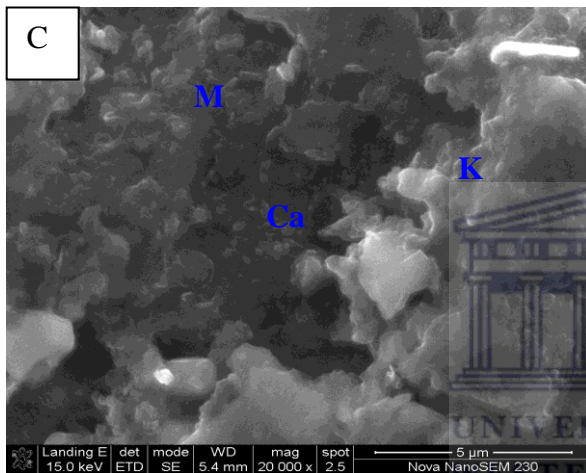
Kaolinitization of mica was noted in sandstones buried at depths 3717.23 m. At this depth, replacement was common in mica deformed between rigid quartz and feldspar grains (Fig. 6.23C). Variable amount of pyrite were noted in the immediate vicinity of or between the cleavage planes of kaolinitized micas (Figs. 6.23C, E). Authigenic K-feldspar was not observed between sheets of kaolinitized mica, but was noted as overgrowths on detrital K-feldspar (BjØlykke et al., 1986). Authigenic kaolinite sits in primary porosity and secondary (dissolution) pores in feldspar grains, as well as altered micas. Kaolinite is present as euhedral booklet filling primary porosity within the sandstones (Fig. 6.23C) with extensive kaolinite present at depth 3717.23 m. It is primarily and petrographically associated with degraded feldspar and mica (Fadipe, et al., 2011) and its occurrence as blocky platelets in sandstone locally adjacent to quartz overgrowths are illustrated in Figure 6.23D. This kaolinite formation could have occurred soon after deposition due to meteoric flushing of sand before burial (Knarud and Bergan, 1990) but a later paragenesis is indicated by its relationship with authigenic quartz (clearly post-dating this) and by the lack of kaolinite in some siltstone samples within the reservoir interval.



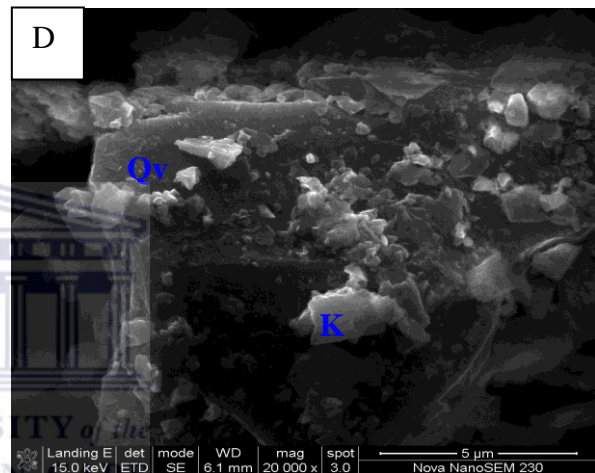
F-O3: 3705.02m



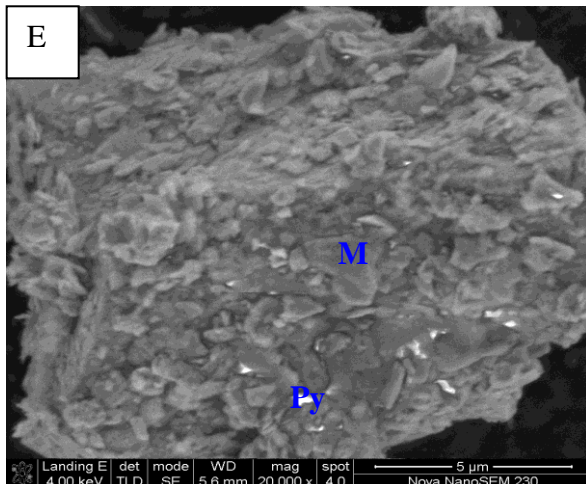
F-O3: 3713.08m



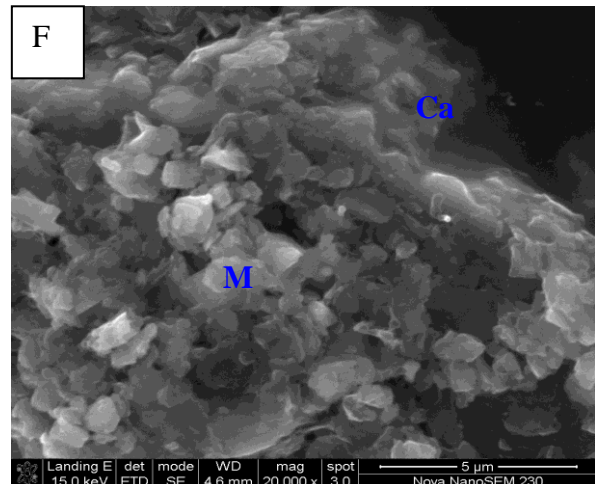
F-O3: 3717.23m



F-O3: 3725.00m



F-O3: 3741.00m



F-O3: 3755.00m

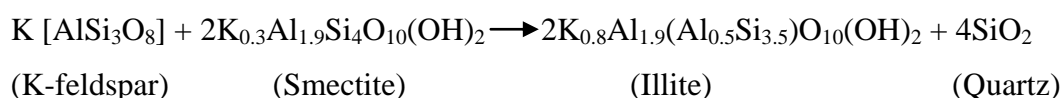
Figure 6.23: (A) images of calcite and quartz grain intergrowth (B) image of altered K-feldspar covered by micaceous crystals (C) Euhedral shaped kaolinite booklet particles (D) Image showing kaolinite particle locally resting on quartz overgrowth (E) SEM image of pyrite crystals filling micaceous matrix in sandstone (F) SEM image showing flakes of kaolinite sandstone particles.

Note: F = leaching of feldspar grain, M = Mica, K = Kaolinite, Qv = Quartz overgrowth, Ca = Calcite, Py = Pyrite, K=F = K-feldspar.

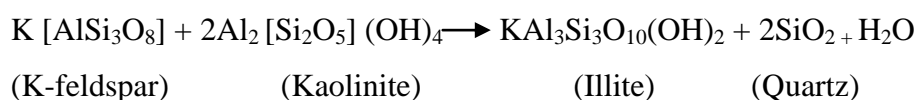
6.2.4: SEM petrography for F-O4 well

Diagenesis in the Valanginian age of F-O4 reservoir sandstone samples exerts a strong influence on the reservoir quality potential. The main diagenetic processes affecting the F-O4 sandstones are authigenesis of quartz and feldspar, mechanical and chemical compaction, and cementation of carbonate (calcite). Quartz overgrowth commonly occurs on detrital quartz grains; it appears that there is a positive relationship between the occurrence of quartz overgrowth and amount of detrital quartz grain (Fig. 6.24A and B). Actually, the precipitation of quartz cementation is largely temperature dependent and controlled by time-temperature history of the rock (Zhang et al., 2008). Jurassic sandstones research from Norwegian continental shelf by Walderhaug (1994) shows that the temperature required for quartz cementation to develop in sandstones is 75 - 165 °C and quartz cementation becomes intensive with increasing temperature.

Figures 6.24B, C and D reveals that the potential sources of silicon dioxide for quartz cement within sandstones are from intergranular pressure solution, dissolved and replaced feldspars and transformation of clay minerals. Mass balance calculations (Salem, 1995) show that abundant silicon dioxide was released during the dissolution of feldspars to provide the quartz cement in the lightly cemented sandstones as evident in Figures 6.24A and F with diminutive quartz cement and strong evidence of feldspar dissolution indicated with a rod-like architecture of feldspar leaching. Transformation between clay mineral also releases abundant silicon dioxide. The following reaction indicates that transformation of smectite into illite which releases silicon dioxide (Rodrigo and Luiz 2002).



Furthermore, illitization of kaolinite may supply silicon dioxide for mesogenetic quartz precipitation (Rodrigo and Luiz 2002).



Calcite is evident in F-O4 sandstone but as pore filling variety with a non-uniform distribution (Fig. 6.24A and F) indicating partial dissolution of crystals while kaolinite is also observed with vermicular booklet morphology (Fig. 6.24C).

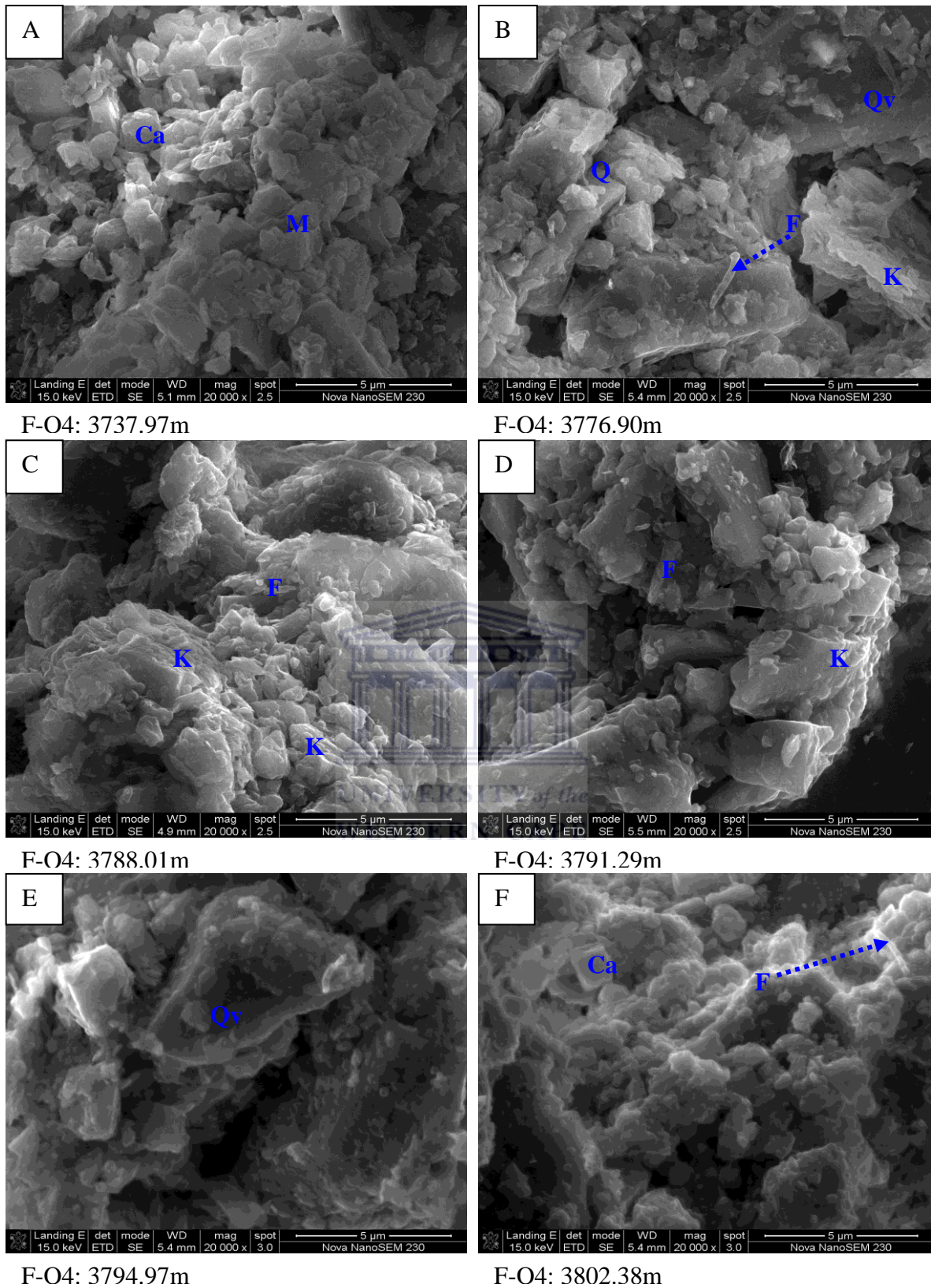


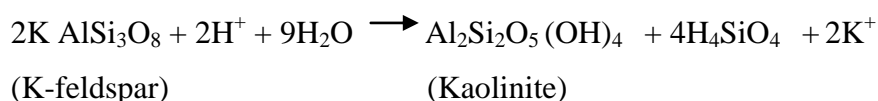
Figure 6.24: (A) Calcite grain in association with flakes of mica. (B) Booklets of kaolinite with rod-like feldspar showing evidence of leaching. (C) Kaolinite booklets formed by kaolinite euhedral particles in sandstones. (D) Plates of kaolinite minerals. (E) Image of quartz overgrowth. (F) Pore filling calcite associated rod-like crystals of K-feldspar.

Note: F = leaching of feldspar grain, M = Mica, K = Kaolinite, Qv = Quartz overgrowth, Ca = Calcite.

6.2.5: SEM petrography for F-R1 well

The F-R1 samples reveal a kaolinite-rich clay deposit of the Valanginian age developed during the early Cretaceous period. The large organic matter content as observed in the core description coupled with observed plasticity of the shaly unit indicate they could be ball clays. SEM reflects the occurrence of differential types of kaolinite within the reservoir unit.

Type 1: Kaolinite occurring as flakes filling pyritized plants. This mode has been observed only in some dark clay stones (Fig. 6.25A). Type 2: Kaolinite sandstone occurring as vermicular booklets (Fig. 6.25B) composed of pseudo-hexagonal plates in diameter. This architecture is attributed to twinning and pseudo-twinning intergrowths (Bauluz et al., 2008). Figure 6.25D shows the presence of kaolinite crystallization expanding at the expense of mica flakes; this has been supported by previous authors (MacAulay et al., 1993; Osborne et al., 1994; Arostegui et al., 2001). The vague presence of feldspar as revealed by SEM photograph could be attributed to the hypothesis reviewed from literatures suggesting that for the composition of fluid responsible for massive kaolin crystallization at the expense of plagioclase and K-feldspar. Kaolin crystallization is promoted at shallow burial by fluids of meteoric origin (Hancock, 1978; Hancock and Taylor, 1978; Sommer, 1978) that flush the formation either during early diagenesis or after structural inversion. As a consequence of feldspar dissolution, kaolin precipitates according to:



If meteoric fluids are responsible for the reaction, then the system must be open, with a constant supply of proton and removal of K cation in order to precipitate significant amount of kaolinite. Another hypothesis, CO₂-rich or organic acid rich fluid may be, together with meteoric fluid responsible for the feldspar alteration and subsequent precipitation of kaolinite in accordance with the above cited reaction (Rossel, 1992; Ehrenberg, 1991, Gaupp et al., 1993; Platt, 1993). These fluids result from the maturation of organic matter in shales or coal beds adjacent to the sandstones.

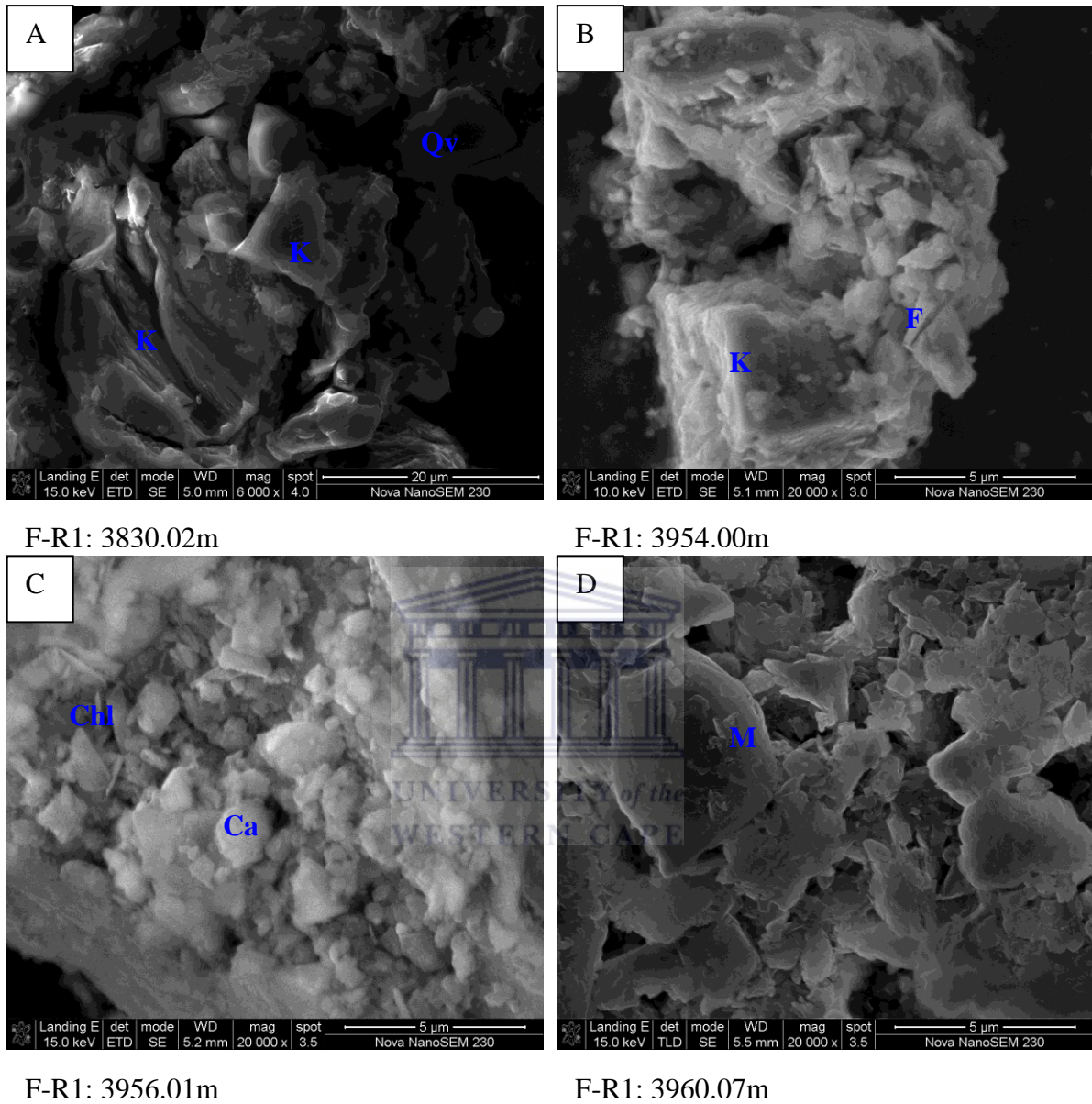
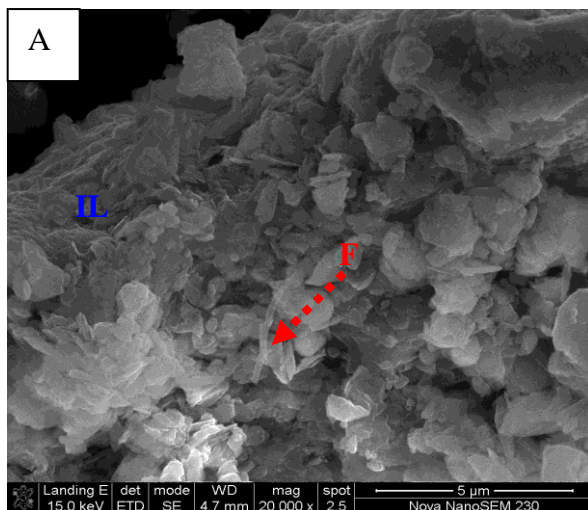


Figure 6.25: (A) Detrital pseudo-triangular plate of kaolinite and larger mica (B) Closely packed kaolinite plates with evidence of rod-like material showing feldspar leaching (C) Calcite grains and cements with small shows of chlorite flakes tangential to the calcite grain (D) Broken plate micaceous sandstone from Bredasdorp F-O gas field.
Note: F = leaching of feldspar grain, M = Mica, K = Kaolinite, Qv = Quartz overgrowth, Ca = Calcite, Chl = Chlorite

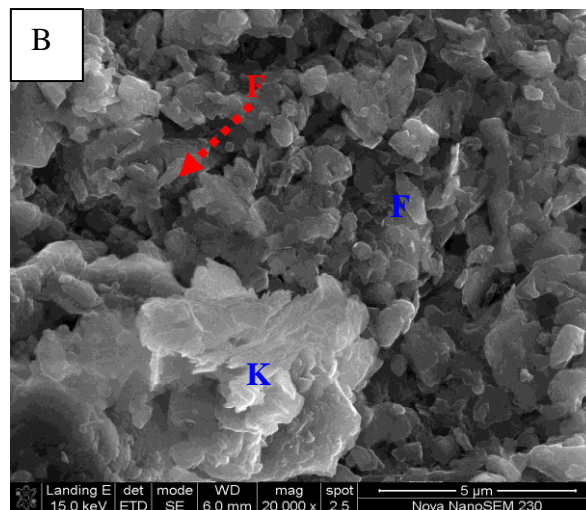
6.2.6: SEM petrography for F-S1 well

In F-S1 sandstone, the origin and petro-genetic significance of these kaolin minerals are not clearly understood and are still debated in petroleum exploration. However, the architecture and the understanding of the resultant reaction between K-feldspar and contained fluid coupled with temperature could give appreciable insight to the formation of kaolinite within the reservoir interval. Scanning electron microscopic study shows the occurrence of clay minerals like kaolinite, minor illite in the F-S1 well. In sandstone, diagenetic kaolins usually crystallize in two distinct sites (Beaufort et al., 1998). These kaolins are characterized by a range of size and morphologies which are described below. In diagenetic sandstones, the dissolution of feldspar increases with increasing burial depth leading to progressive replacement of feldspar by secondary pores (Beaufort et al., 1998).

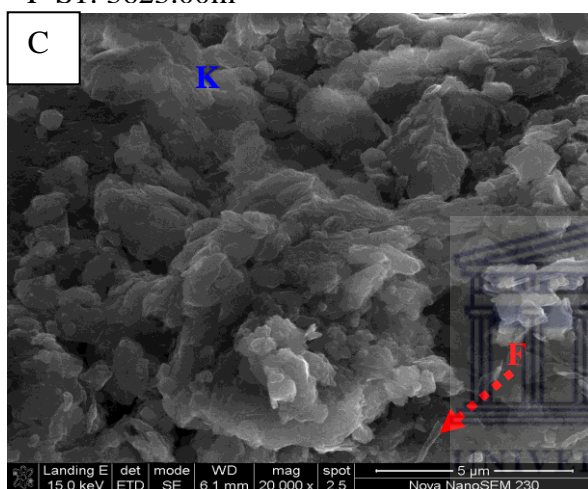
SEM images for F-S1 sandstones reveal the presence of feldspar in leaching form (rod-like shape) resulting in the formation of kaolinite within the sampled interval. The matrix comprises of a mixture of kaolinite with minor illite shows. The images (Fig. 6.26) also indicate that the matrix is formed mainly of kaolinite crystals that occur as subhedral and hexagonal plates. K-feldspar fragments with evidence of alteration (dissolution) are common, as are kaolinite crystals covering K-feldspar fragments. The suggested alteration of feldspar to kaolinite is buttressed by the feldspar relicts retaining their grain shape but with sharp edges (Figs. 6.26C, E) with the kaolinite showing irregular/uneven boundaries that skirt around and even fill the narrow gaps in between clastic grains. Such sharp grain boundaries are common in pseudomorphic replacement of feldspar. This type of kaolinite is mainly present in sandstones (Bauluz et al., 2008).



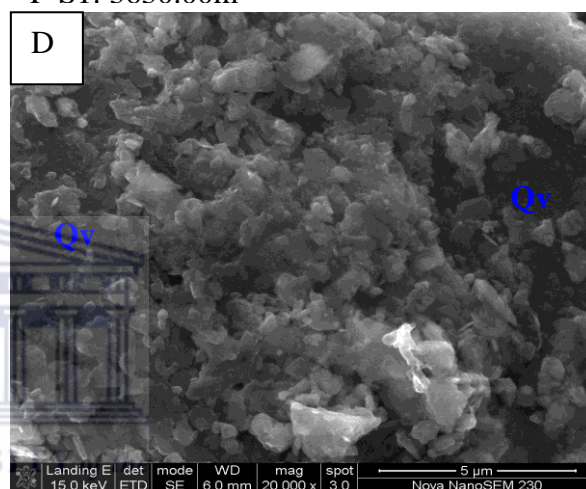
F-S1: 3623.00m



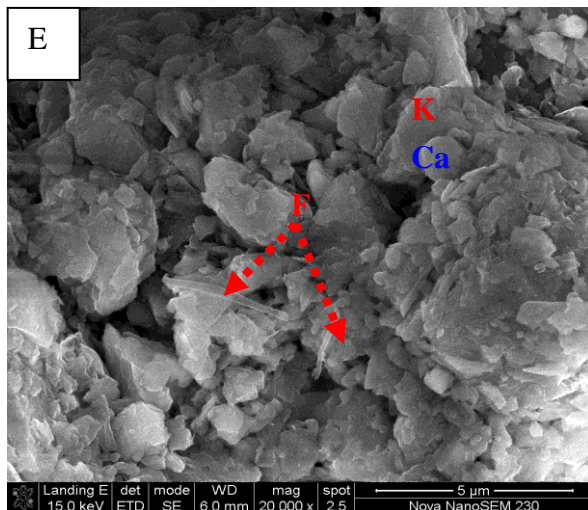
F-S1: 3630.00m



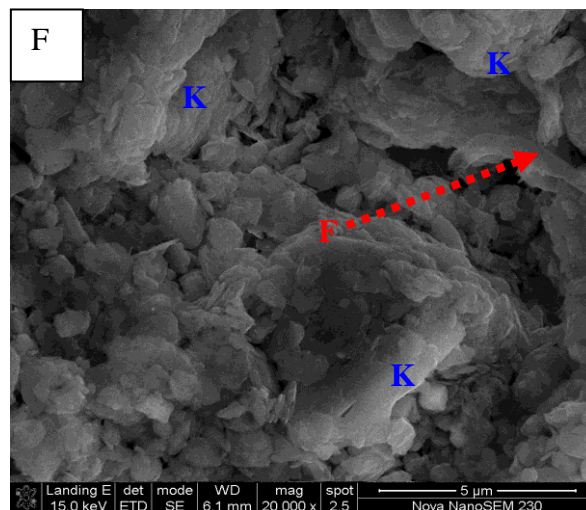
F-S1: 3660.02m



F-S1: 3664.00m



F-S1: 3668.00m



F-S1: 3684.10m

Figure 6.26: All SEM images except figure 6.26D shows the leaching of feldspar resulting to the formation of kaolinite due to potassium ion release. The process helps the development of secondary porosity. (D) Image of quartz overgrowth and some evidence of kaolinite flakes.

Note: F = leaching of feldspar grain, IL = Illite, K = Kaolinite, Qv = Quartz overgrowth, Ca = Calcite.

6.3: X-ray diffraction (XRD) results and discussion

The mineralogical analysis of the reservoir intervals from the studied Valanginian sandstones in the F-O gas field was carried out with X-ray diffraction techniques (XRD). A total of 52 pulverized core samples were analyzed both qualitatively and semi-quantitatively for whole-rock mineralogy. This is to understand the mineralogical changes across the study area better. The XRD patterns of the whole samples across the entire wells show that the rocks have relatively similar mineral associations (Appendix 4), while Table 6.31 reveals the average mineralogical composition (%) of the whole samples. They consist mainly of quartz, calcite (few wells), feldspar (microcline and plagioclase) and phyllosilicates, such as kaolinite and micaceous phases (illite and muscovite) and small proportions of chlorite. Occasionally, pyrite, rutile and ankerite were detected (Figs 6.31 – 6.36) but mostly as traces within the sandstones.

6.3.1: XRD results and discussion for F-O1 well

The XRD performed on the samples reveal that the rocks show (Fig. 6.31A) appreciable presence of quartz followed by albite with few peaks of calcite mineral while the quantification plot (Fig. 6.31B; Table 6.31) reveal high amount of quartz (84.64 %) followed by plagioclase (7.06 %) with minor traces of rutile (0.08 %) as the least abundant mineral. The major clay minerals present in this studied sandstone are muscovite (average of 2.25 %) and minor trace of chlorite (1.38 %). In addition, the sandstone also shows a minor amount of opaque mineral like pyrite with 0.13 %.

Albite seems to have a considerable presence within the F-O1 sandstone. Figure 6.31A shows occurrence of albite which is chemically similar to the plagioclase observed during the quantification process with an average of 7.06 % while microcline with 2.25 % could also represent K-feldspar chemically. Conditions with sufficient silica, potassium and reasonable pressure and temperature in pore fluid are conducive for the generation of albite. Diagenetic albite with typical pure end member composition is common ($K_{0.2}Na_{0.8}AlSi_3O_8$), occurring as replacement of feldspar and overgrowth on feldspar grains. Therefore, K-feldspar and plagioclase as observed in the thin section, SEM and now XRD can be deduced as being albitized with replacement occurring after partial grain dissolution as seen by variable amount of pore spaces within the grains (Figs. 6.11, 6.21, 6.31). The varying amount of the different clay minerals coupled with their transformation suggests the occurrence of porosity reduction in the reservoir.

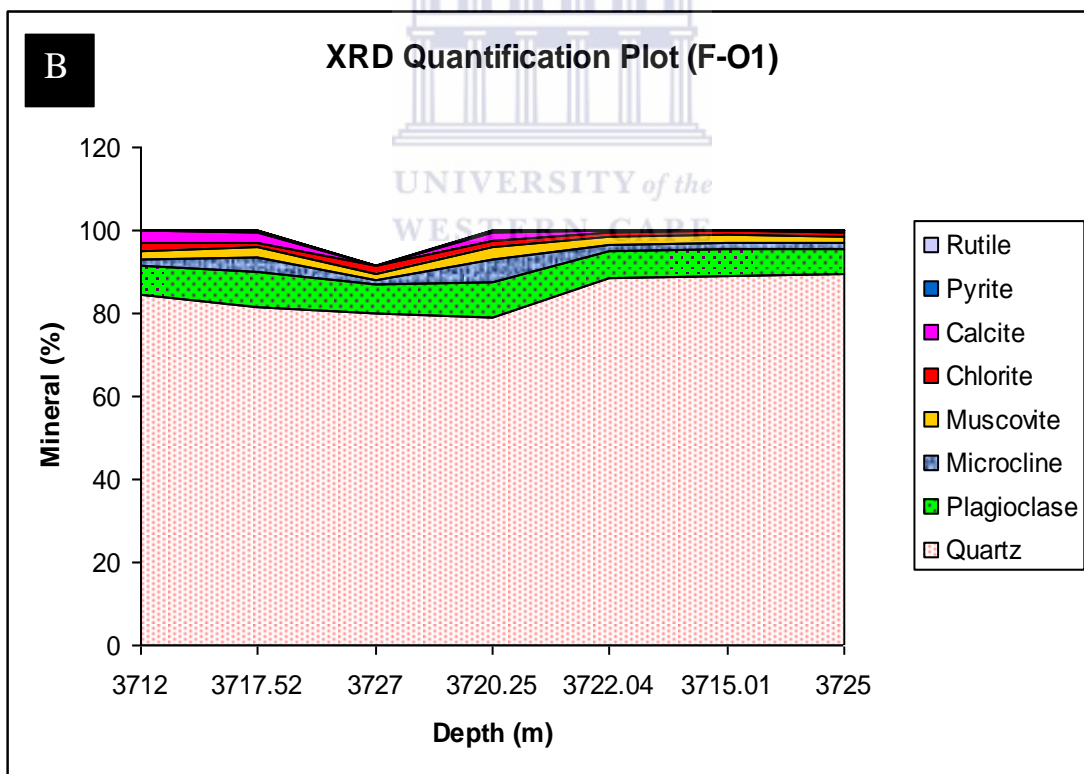
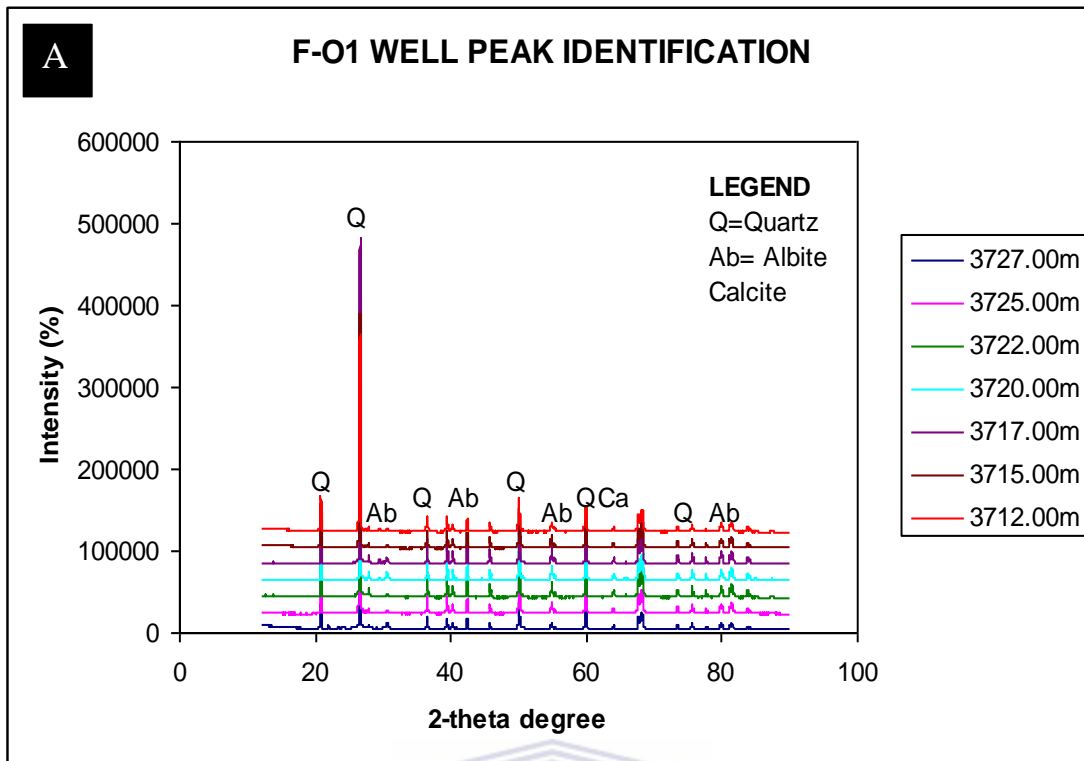


Figure 6.31: XRD qualitative and semi-quantitative plot of F-O1 well.

6.3.2: XRD results and discussion for F-O2 well

Quartz is the most dominant mineral also in F-O2 sandstone but lesser in quantity than the adjacent F-O1 sand. It was observed to be widespread across all sampled interval in the F-O2 reservoir sand. Spectra identification reveals the presence of montmorillonite as seen in Figure 6.32A. Montmorillonite is a very soft phyllosilicate group which belongs to smectite family. It typically forms a small platy micaceous crystal as revealed by thin section micrographs (Fig. 6.12). The reaction that formed this mineral is undoubtedly complex, but hydration and alteration of partially and completely devitrified lithic fragments in the original materials (feldspar) must have played an important role in its formation (Fadipe et al., 2011)

The presence of albite in F-O2 sandstone can also be due to albitization of feldspar and precipitation of albite overgrowths and minor ankerite (present at 3738.10 m). This can be interpreted to be deep mesogenetic phases that post-date the Cretaceous magmatism (Lima and De Ros, 2002). The origin and chemical composition of fluid from which albite precipitated cannot be unravelled from existing data however; pore water analysis will shed more light on these in the later chapter.

Calcite is also noted to be of high quantity (31.43 %) with an inverse relationship to quartz (30.93 %) relatively to other sampled intervals within the F-O2 sandstone where ankerite was only present within the studied samples (Appendix 1). The inverse relationship between calcite and quartz is attributed to the shaly nature of the sample as observed in the core graph (Fig. 5.12). Many authors have reported the co-existence of calcite-ankerite in both carbonate and clastic sandstones (Barron, 1974, Douglas et al., 1985; Hendry et al., 2000). This co-existence suggests that ankerite could have formed during deep burial after onset of overpressure but before hydrocarbon emplacement in the reservoirs (Hendry et al., 2000). This prediction could only be confirmed with stable isotopic data of oxygen and carbon which is not within the scope of this study.

Chlorite was observed during peak identification and quantification with an average value of 4.41 % across the sampled interval which is more than in F-O1 sand (1.38 %). The formation of this chlorite mineral could be related to the dioctahedral clay mineral (kaolinite and mica) reactions with carbonates. The growth of calcite, ankerite and chlorite all reduces the porosity of the reservoir interval.

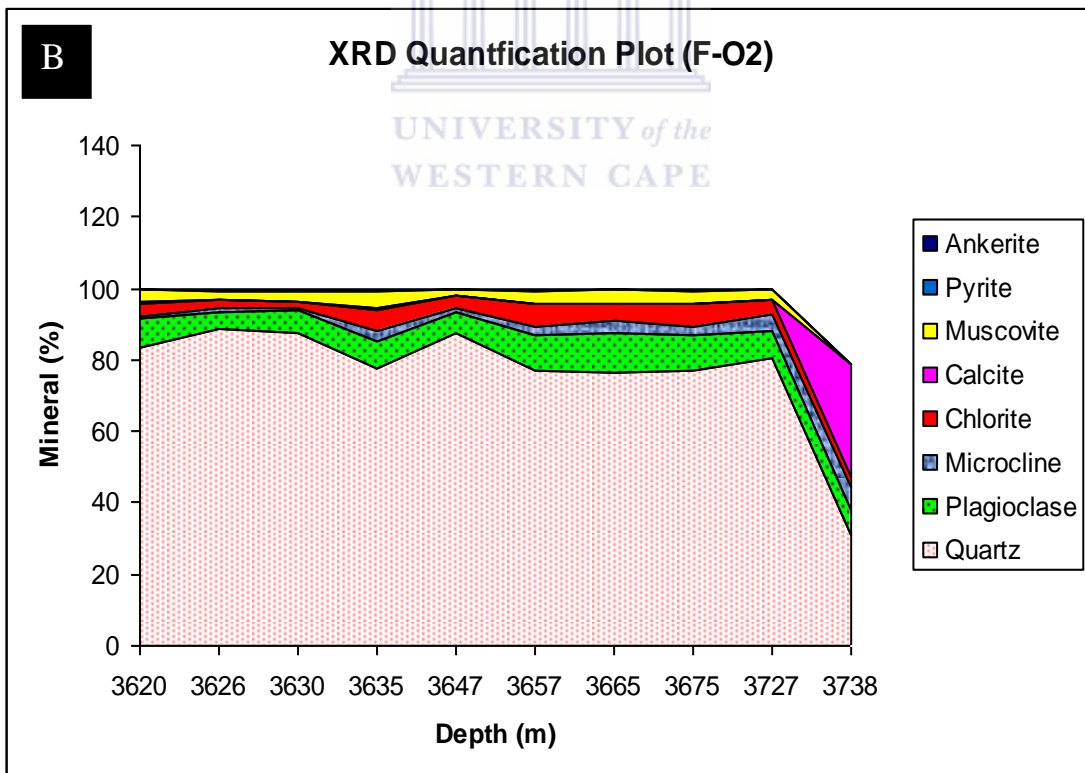
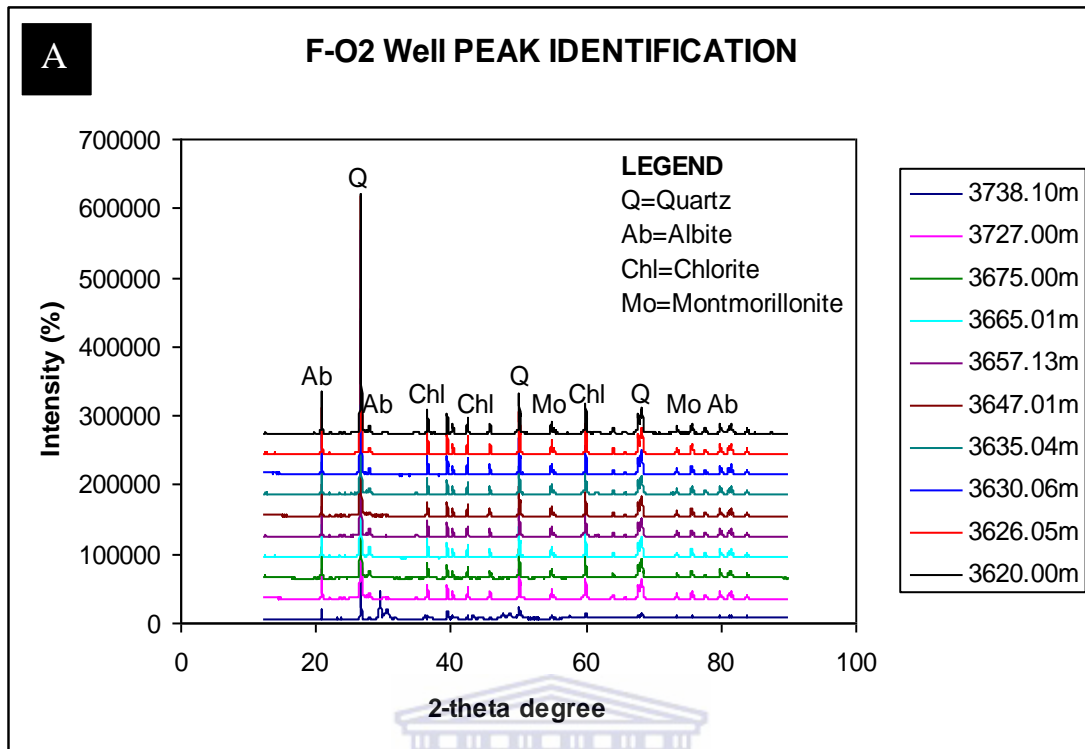


Figure 6.32: XRD qualitative and semi-quantitative plot of F-O2 well.

6.3.3: XRD results and discussion for F-O3 well

The results of XRD analysis for F-O3 reservoir intervals show that the rock samples is quartz dominated with 75.53 % average followed by plagioclase of 9.21 % and a considerable amount of chlorite (4.54 %). Calcite values seem insignificant which means F-O3 sand is more of silica rich rock than calcite. Figure 6.33A shows considerable peaks of albite and chlorite while quantitative plot reveals that plagioclase and chlorite (4.54 %) are also significant in the F-O3 well. Muscovite could sometimes be termed as having the presence of illite because the muscovite in this sandstone is like muscovite of very small crystallite size. The presence of muscovite could be attributed to the dissolution of feldspar and kaolinite releasing aluminium and hereby precipitating muscovite/illite, often replacing kaolinite and leaving secondary pore after K-feldspar. However, if the pore water is supersaturated with regards to albite, the reaction below may take place:



Albite as observed in Figure 6.33A is likely from pseudomorphic replacement of K-feldspar with a probable development of little secondary porosity. K-feldspar and albite is also extreme pure end member of alkali and plagioclase feldspar. They are frequent as early diagenetic mineral and predate tectonic deformation, their occurrence is not likely related to hydrothermal activity, and they form almost exclusively as overgrowth on detrital feldspar grains (Morse and Mackenzie, 1990).

Most of the present porosity in F-O3 is secondary originating from detrital feldspar grains. However, development of muscovite, kaolinite and albite all reduce this porosity. Formation of secondary porosity may not significantly have raised permeability owing to its low-fair permeability deduced from conventional core cross plot (Fig. 5.33B), since most feldspar dissolution porosity in F-O3 seems to be intergranular.

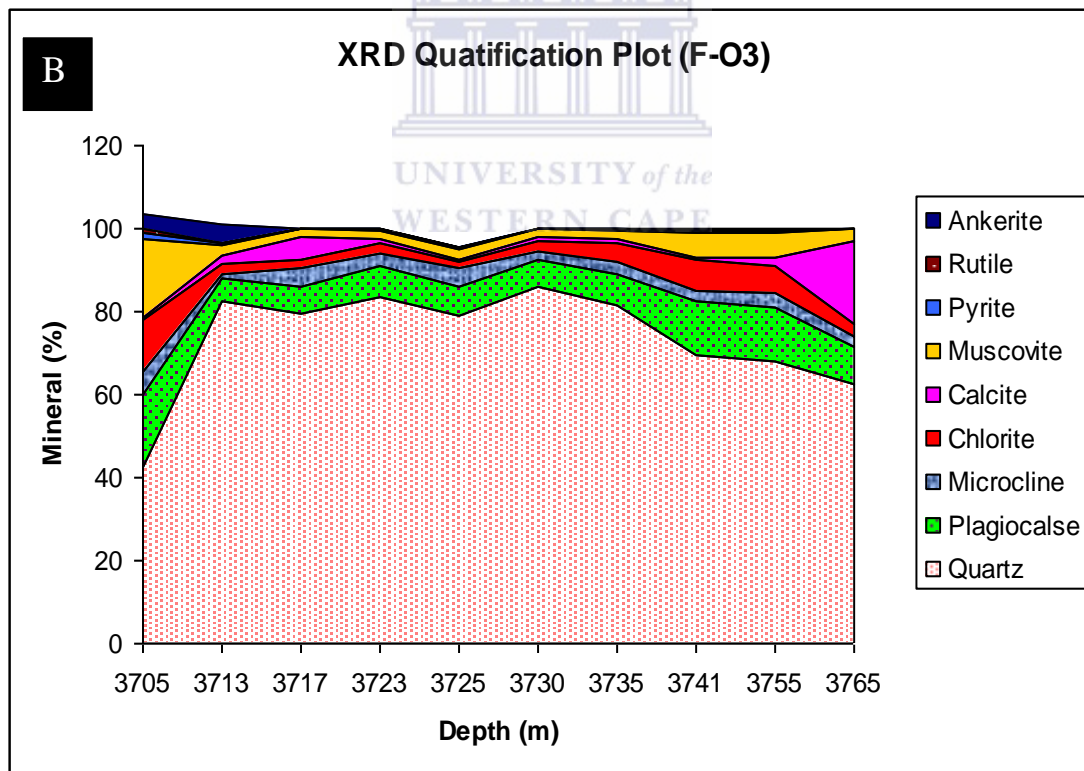
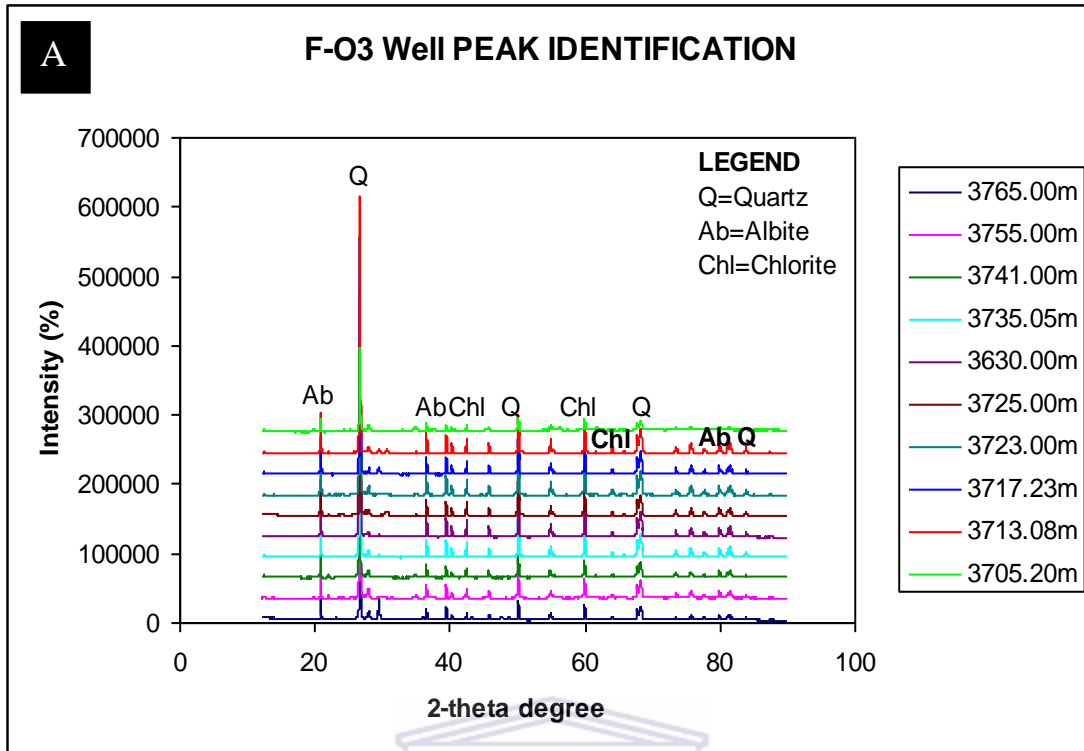


Figure 6.33: XRD qualitative and semi-quantitative plot of F-O3 well.

6.3.4: XRD results and discussion for F-O4 well

The dominant mineral in F-O4 sandstone is quartz (71.86 %) followed by calcite (12.47 %) and chlorite (3.66 %). Based on previously discussed petrographic studies (thin section, SEM) and the inverse relationship observed at depth 3802.38 m with calcite having 68.95 % and a significant corresponding depletion of silica (20.4 % from the whole rock (Appendix 1). These results buttress the predicted calcite cement present within the sampled sandstone. Figure 6.34B plot also shows the enrichment of calcite across the sampled intervals. The micritic, microcrystalline and coarse-crystalline texture of calcite cement as observed in Figure 6.14 (thin section), and its minerals abundance observed from XRD, suggest precipitation in various diagenetic regimes. Micritic and microcrystalline calcite in palaeosol have presumably formed in the vadose zone during near-surface diagenesis (Hall et al., 2004), as evidenced by dense micritic texture and rhizocretionary structure. There is also some minor evidence of dolomite observed at depth 3737.97 m (Appendix 1). The presence of dolomite at the top depth suggest its occurrence as local patches with microcrystalline textures and as small rhombs that fills large pores between loosely packed framework grains, precipitation is inferred to have occurred at near-surface during eodiagenesis. Dolomite precipitation could be attributed to an increase in the Mg^{2+}/Ca^{2+} ratio in pore waters due to evaporative ionic concentration (Made et al., 1994; Garcia et al., 1998). The 6.20 % occurrence of plagioclase feldspar from XRD quantification likely represents feldspar association with volcanic and metamorphic lithic fragments that was observed in thin section as micrographic granite (Fig. 6.14C, D).

The occurrence of chlorite in the F-O4 sandstones could have been during early diagenesis due to its inhibiting nature of the reservoir porosity thereby restricting subsequent quartz cementation during burial to higher temperature. This could also have explained the depletion in the quantity of quartz occurrence towards the deeper part of the sampled interval but chlorite comprises less than 4 % of the bulk rock components of the Valanginian sandstones, which is too low a volume to control quartz cementation and should not have significant influence on reservoir quality.

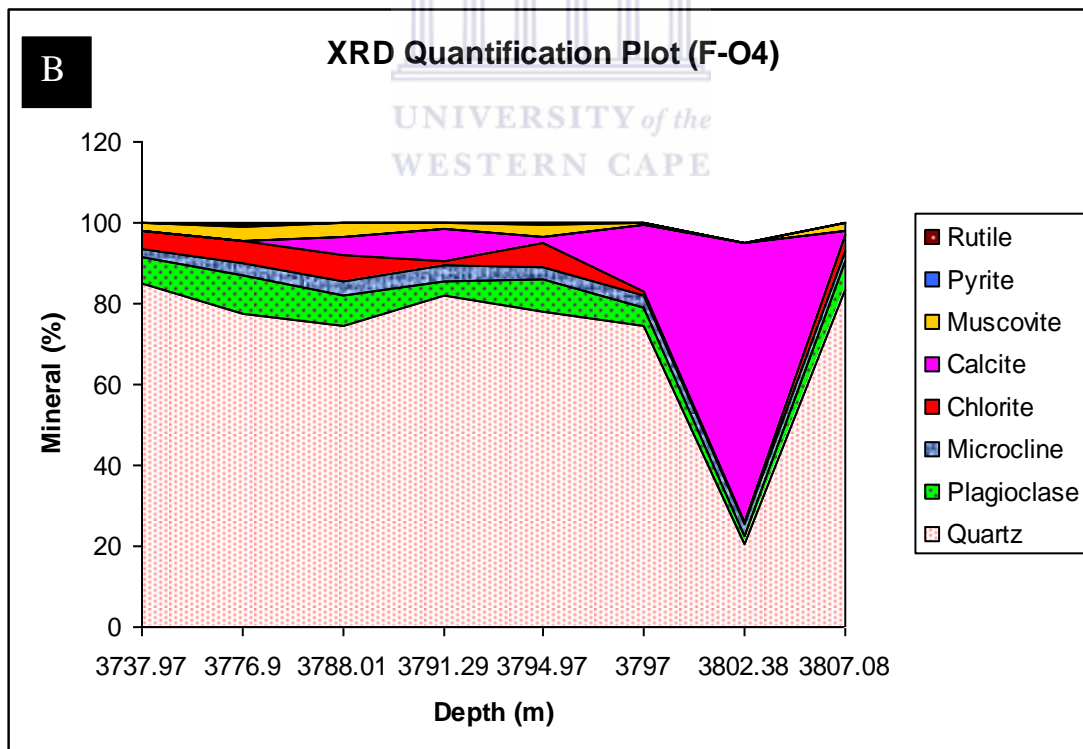
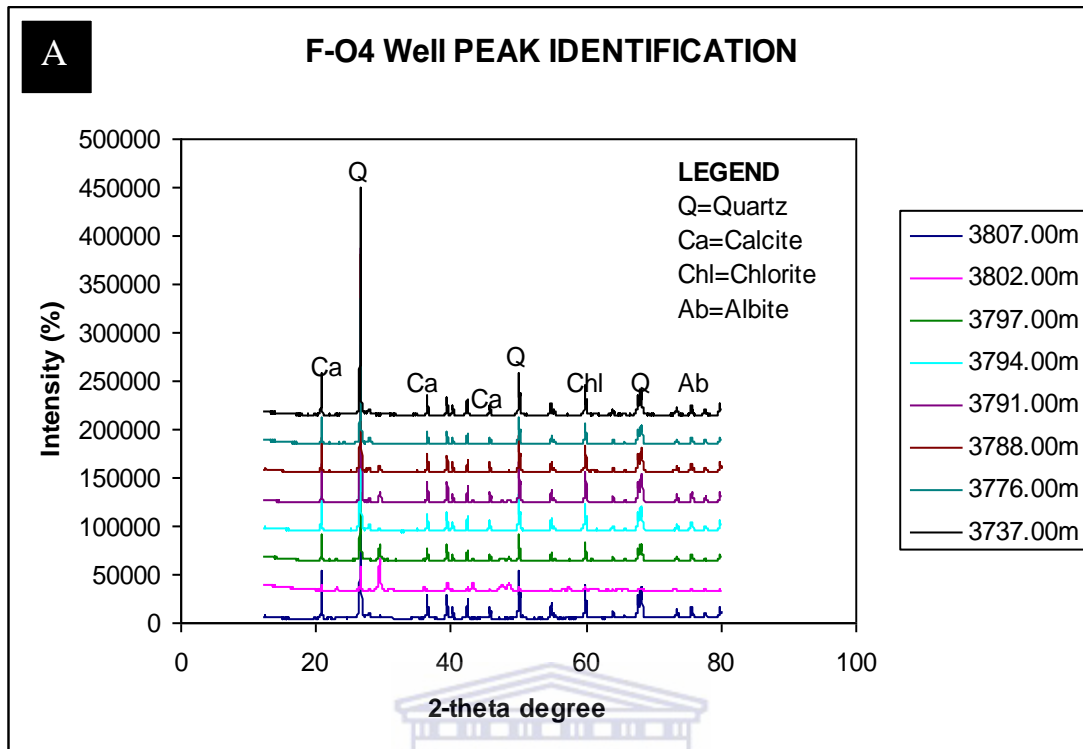


Figure 6.34: XRD qualitative and semi-quantitative plot of F-O4 well.

6.3.5: XRD results and discussion for F-R1 well

The sand/shale nature of the sampled interval in F-R1 sandstones has revealed more minerals than previously discussed wells. Quartz comprises of 60 % followed by a relatively significant enrichment of plagioclase and muscovite (13.39 % and 7.91 %, respectively). More distinctly observed is the 120 m interval between core 1 and 2 with variations in the occurrence of mineral in both cores. The occurrence of chlorite, haematite, albite and minor illite seem more prominent in core 1 while montmorillonite, calcite and quartz are more in abundance in core 2. The high percentage of quartz in core 2 (3952.04 m – 3960.07 m) is due to the more sandy nature of the sandstone while core 1 reveals a shaly nature as observed from core graphs (Fig. 5.15) and sample examination.

Feldspars occur as albitized plagioclase and trace amounts of microcline (detrital K-feldspar). Albite that has replaced detrital feldspar could have occurred as small prismatic crystals arranged along twinning planes of detrital feldspars. Generally, authigenic feldspar cement forms in mesodiagenesis occurring as overgrowth on feldspar grains and intergranular pore fill. The occurrence of feldspar grain is common in the F-R1 sandstones although it is not so wide spread as that of quartz grains. Conditions with sufficient silica, sodium, potassium and reasonable pressure and temperature in pore fluid are conducive for the generation of albite and K-feldspar.

The formation of hematite (Fig. 6.35A) could be during early diagenesis which includes processes that occur at or near the surface of sediments where the chemistry of the interstitial water is controlled mainly by depositional environment. This is the regime where the influence of original depositional pore water dominates; hematite might have been formed from oxidation of ferrous ion released by dissolution of unstable ferromagnesian minerals during early burial (Weibel and Friis, 2004). The little occurrence of illite could be attributed to the dissolution of feldspar and kaolinite releasing aluminium and hereby precipitating into illite, often replacing kaolinite and leaving secondary pore after K-feldspar.

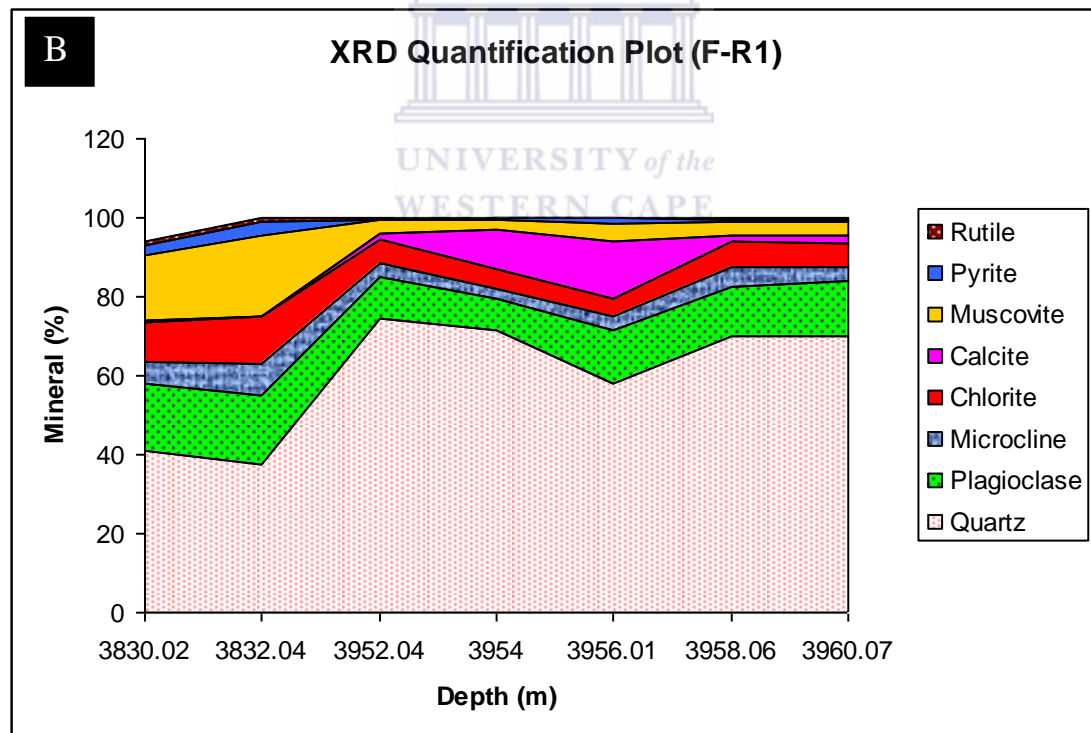
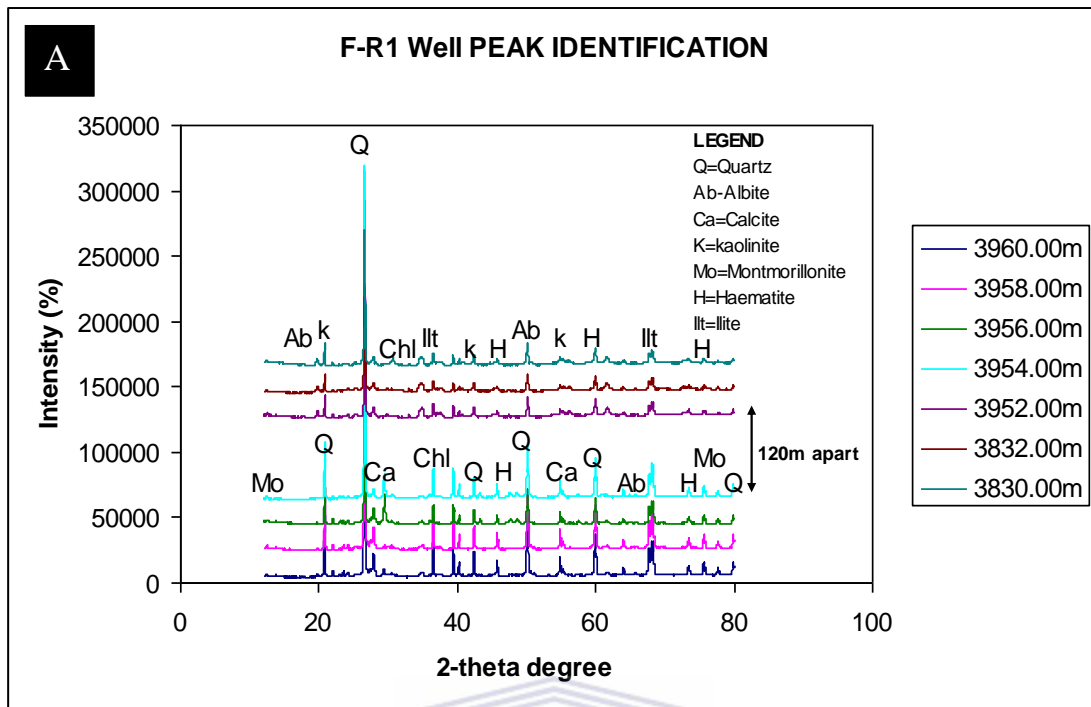


Figure 6.35: XRD qualitative and semi-quantitative plot of F-R1 well.

6.3.6: XRD results and discussion for F-S1 well

The XRD study of F-S1 sandstone reflects an average occurrence of quartz (70.03 %) as dominant mineral followed by plagioclase (12.11 %) and then chlorite (5 %). Microcline is also significant with 4.71 % while calcite exhibit low amount with 2.14 % (Fig. 6.36A, B). A decrease in the value of quartz was observed with an increase in burial at depth 3677 m with a corresponding increase but insignificant in the quantity of calcite cement (Appendix 1). This can be attributed to the textural changes observed down the core (changing from sandstone to finer sand). Ankerite occurs in some depths (3664 m and 3671 m with 5.2 % and 8.24 %, respectively) locally in the F-S1 sandstones probably in association with the observed stylolite from the thin section petrography (Fig. 6.16) along glauconite-rich laminae replacing considerable portion of these rocks.

Chlorite is also notable across the F-S1 sandstones, chlorite dissolution might have occurred prior to quartz and calcite cementation, because both quartz and calcite cements occurs in pores with all part of the earlier cement removed (Fig. 6.16). Kaolinite was not strongly observed during the analyses but after few test and I found that 7 angstrom peak collapsed, it was deduced that kaolinite could be present but sharing the same peak with chlorite. Simple observations of the abundance of plagioclase and the vague quantity of kaolinite/chlorite suggest that the dissolved plagioclase can easily have sourced the kaolinite and coincidentally facilitated the transformation of feldspar into glauconite/muscovite through the supply of potassium. There are no other obvious sources of Al for kaolinite cement although it is not impossible that some Al were derived from reaction of detrital clay minerals.

Table 6.31: Average mineralogical composition of the F-O field samples from XRD.

Well Name	Calcite	Chlorite	Microcline	Muscovite	Plagioclase	Pyrite	Quartz	Rutile	Ankerite
F-O1	1.24	1.38	2.25	2.04	7.06	0.13	84.64	0.08	0
F-O2	0.11	4.14	2.60	2.93	7.82	0.34	76.59	0.24	2.10
F-O3	3.33	4.54	3.21	4.72	9.21	0.38	73.53	0.28	0.80
F-O4	12.47	3.66	2.91	2.02	6.20	0.16	71.86	0.12	0
F-R1	4.31	7.12	4.37	7.91	13.39	1.18	60.35	0.48	0.88
F-S1	2.14	5.00	3.70	4.71	12.11	0.67	70.03	0.30	1.34

Note: XRD Measured in weight %

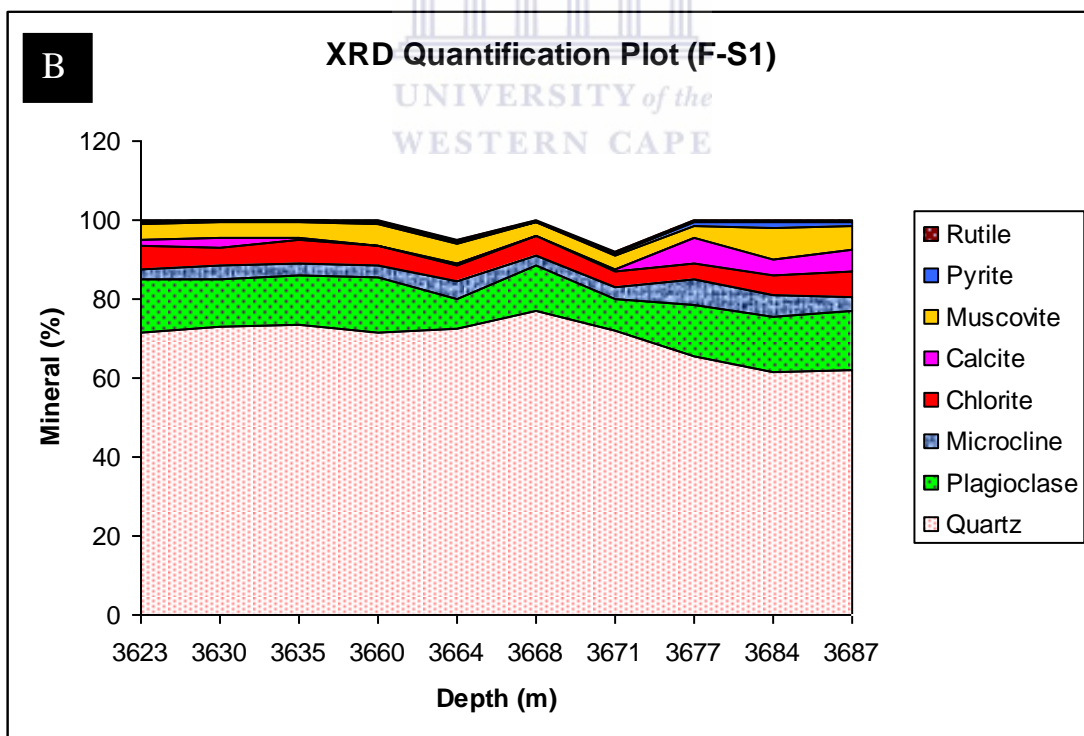
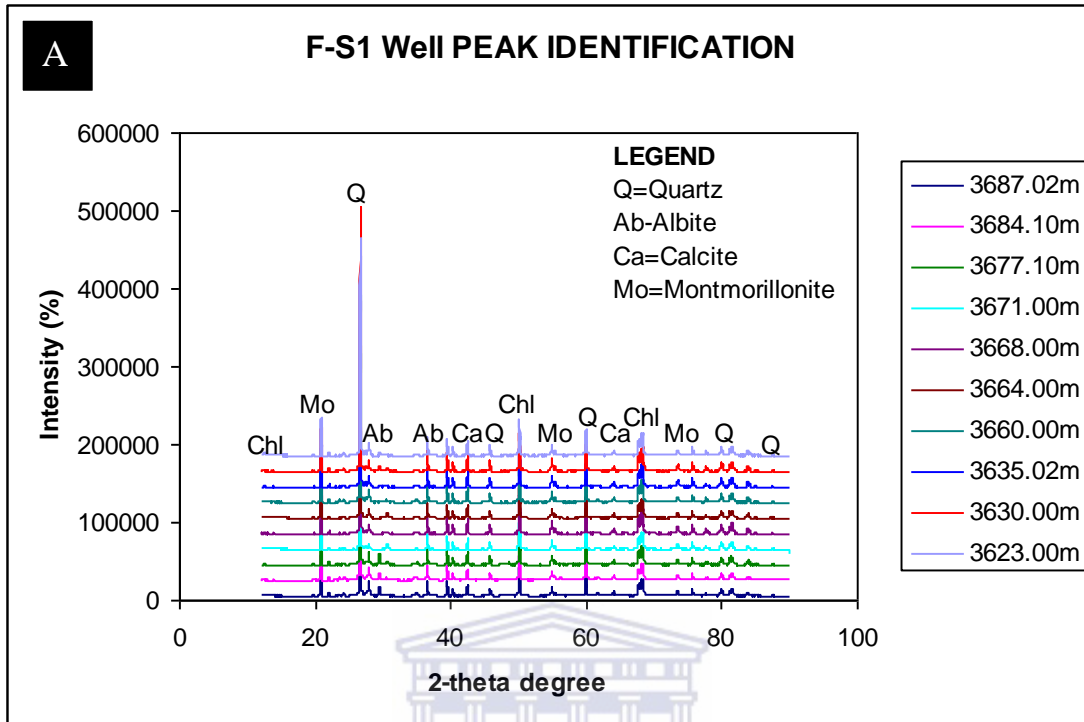


Figure 6.36: XRD qualitative and semi-quantitative plot of F-S1 well.

6.4: Geochemical analyses results and interpretation

6.4.1: Immobile fluid geochemistry results and discussion

In reservoir rocks, high immobile water saturations are generally associated with micro-porosity with high capillary pressures or heterogenous pore structure which allows bypassing of large quantities of water (Baldwin, 1993). Unlike in fine grained sediments, in sandstones the effect of physical compaction is subordinate to chemical cementation. Hence porosity loss with depth is often not as predictable as it is in the case of finer grained sediments. The diagenetic history of sandstone is controlled principally by the chemistry of pore fluid that has moved through its pore system and that of the adhered water that is usually held in minute pores by reason of capillary action. The main factors that determine mineral precipitation or solution includes: (1) the sediment chemistry (2) the Eh and pH composition of the pore fluids.

Chemical diagenesis involves dissolution and re-crystallization of primary minerals, as well as precipitation of cement in pore space while mechanical diagenesis caused by overburden of younger sediments and tectonic stresses expels pore water and leads to a rearrangement of sediment particles (Sanyal et al., 2005). The effect of these phenomena in various sediment types are quite complex but can be investigated using various proxies in which immobile water is one of them. pH is important as it can drastically change equilibrium state and speed of many reactions. It is well established through field observations, experiments, and chemical models that oxidation, redox state and pH exert a strong influence on the speciation of dissolved components and the solubility of minerals in hydrothermal fluids (Giordano, 2002).

This section presents the result and interpretation of the extracted immobile (pore) water geochemical analysis derived from the sampled cores based on squeezing experiment. The understanding of the behaviour of the types of subsurface water, redox reaction (Eh) and pH of the contained sediments in relation to mineral alterations is important for a reasonable interpretation and a constructive diagenetic trend within the study area. Details of compositional variation in pore fluid have been determined for the F-O gas field with summaries in table 6.41 and appendix 2.

6.4.2: Immobile fluid geochemistry of the studied well within the F-O gas field

Mineralogical analysis shows variation in the composition of the major rock forming and authigenic minerals within the reservoir intervals. Different mineralogical cement precipitates in response to changes in pore fluid, temperature

and pressure and their compositions. Three varieties of pore solution in-fill sediment pores: meteoric, connate and juvenile (MIT OCW, 2012). It is assumed that pore water composition represents meteoric water contained in sediments at deposition time, evolved until the present by diagenetic water-rock reactions and diffusive transport, and modified in terms of evaporation, as a consequence of storage and handling of samples (Turrero et al., 2006). Figures 6.41 and 6.42 present the result of pH analysis and Eh-pH plot for the F-O gas field, respectively. It was noted that most of the pH parameters spans within the alkaline medium (Figs. 6.41 and 6.42) with few samples of F-O2 reservoir sands been acidic. The pH results reveal that the reservoir zone fluid history forms under a slightly acidic to a more alkaline medium condition. Kaolinite was largely observed across the F-O field studied samples. This mineral is known as a product of feldspar dissolution forming booklet or pseudo hexagonal platy kaolinite, with both shapes being influenced by pore water composition, Eh and pH. Kaolinite is naturally known to form under an acidic medium however; mineralogical observations of the studied samples reveals that the illitization of kaolinite indicates increase in burial depths which was observed across the studied wells and most importantly the transformation of kaolinite to illite and/or chlorite. This could be responsible for the change in the pH of the pore water from slightly acidic to alkaline (Ahmed, 2008); (6.6 – 9.3) as observed in Figure 6.41, 6.42 and Table 6.41.

The plot of redox potential (Eh) against pH (Fig. 6.42) reveals that the pore water was largely formed around the water stability limit, sea water and fresh water zone modified from the Massachusetts Institute of Technology Open Course Ware (MIT OCW, 2012). Flushing by fresh water is widely believed to be an important process in kaolinization of sandstones (Blanche and Whitaker, 1978; Almon and Davies, 1979; BjØlykke et al., 1979), while experimental research carried out by Hurst and Irwin, (1982) shows that as sea water is approximately saturated with respect to muscovite and feldspar, kaolinite is likely to form as silicate equilibrate in pore water of marine sandstones. These could be likened to the present studies as predicted to be marine sandstone (chapter five) based on core interpretation. The most significant geochemical observation within marine sandstones is that the sandstones will not be invaded by large quantities of meteoric waters unless uplifted (Hurst & Irwin, 1982).

The solubility of calcite and silica are unaffected by Eh but strongly affected and in opposing ways by pH (Tucker, 2001). Silica solubility increases with pH,

whereas calcite solubility behaves otherwise (Fig. 6.43). Thus in alkaline pore fluids calcite cement precipitate and may even substitute for quartz. However, for a mildly alkaline fluid (pH 8 - 10) both quartz and calcite cements can form. This buttresses the mineralogical observations from the studied sandstones with calcite and quartz cements coexisting within the F-O field reservoir sand (siliciclastic sandstones).

Table 6.41: Physico-chemical results of immobile water extracts from the F-O field.

Well name	Depth (m)	pH	Eh(mV)	Eh(V)	Well name	Depth (m)	pH	Eh(mV)	Eh(V)
F-O1	3712	9.0	183	0.18	F-O4	3737.97	8.1	168	0.17
F-O1	3715.01	8.8	194	0.19	F-O4	3776.9	7.9	185	0.19
F-O1	3717.52	7.9	195	0.20	F-O4	3788.01	8.5	173	0.17
F-O1	3727	9.3	177	0.18	F-O4	3791.29	8.1	183	0.18
F-O1	3722.04	8.7	188	0.19	F-O4	3794.97	8.2	181	0.18
F-O1	3720.25	9.0	174	0.17	F-O4	3797	8.2	178	0.18
F-O1	3725	8.9	174	0.17	F-O4	3802.38	8.1	178	0.18
F-O2	3620	9.0	212	0.21	F-O4	3807.08	9.0	152	0.15
F-O2	3626.05	7.0	244	0.24	Well name	Depth (m)	pH	Eh(mV)	Eh(V)
F-O2	3727	7.9	216	0.22	F-R1	3830.02	9.3	124	0.12
F-O2	3635.04	6.6	214	0.21	F-R1	3832.04	8.0	167	0.17
F-O2	3647.01	7.8	203	0.20	F-R1	3960.07	8.7	153	0.15
F-O2	3657.13	7.5	187	0.19	F-R1	3956.01	8.5	159	0.16
F-O2	3675	8.1	182	0.18	F-R1	3954	8.6	153	0.15
F-O2	3630.03	6.6	213	0.21	F-R1	3952.04	8.2	159	0.16
F-O2	3665.01	8.5	167	0.17	F-R1	3958.06	7.7	150	0.15
F-O2	3738.1	8.0	180	0.18	Well name	Depth (m)	pH	Eh(mV)	Eh(V)
F-O3	3705.2	8.7	175	0.18	F-S1	3623	8.9	176	0.18
F-O3	3713.08	8.6	189	0.19	F-S1	3630	8.4	195	0.20
F-O3	3717.23	8.2	195	0.20	F-S1	3635.02	7.8	184	0.18
F-O3	3725	9.2	162	0.16	F-S1	3668	7.8	186	0.19
F-O3	3723	8.7	168	0.17	F-S1	3664	8.3	191	0.19
F-O3	3730	7.8	183	0.18	F-S1	3660	7.9	187	0.19
F-O3	3735.05	7.8	182	0.18	F-S1	3671	8.2	185	0.19
F-O3	3741	8.2	184	0.18	F-S1	3677.1	8.8	168	0.17
F-O3	3755	8.0	182	0.18	F-S1	3684.1	8.3	188	0.19
F-O3	3765	8.1	174	0.17	F-S1	3687.02	8.2	174	0.17

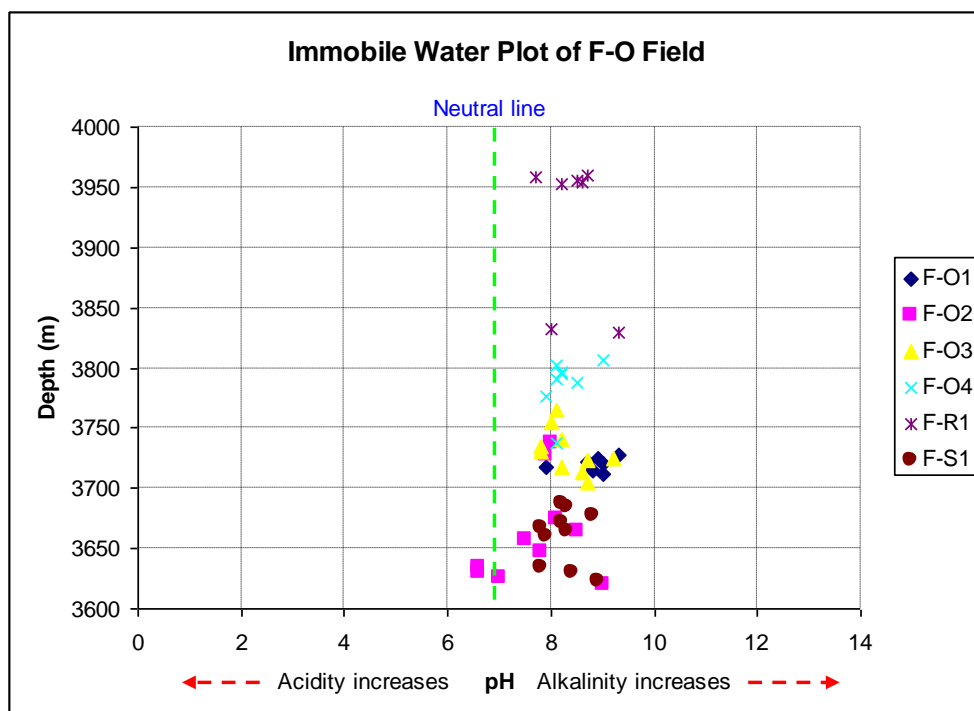


Figure 6.41: pH plot of the F-O gas field.

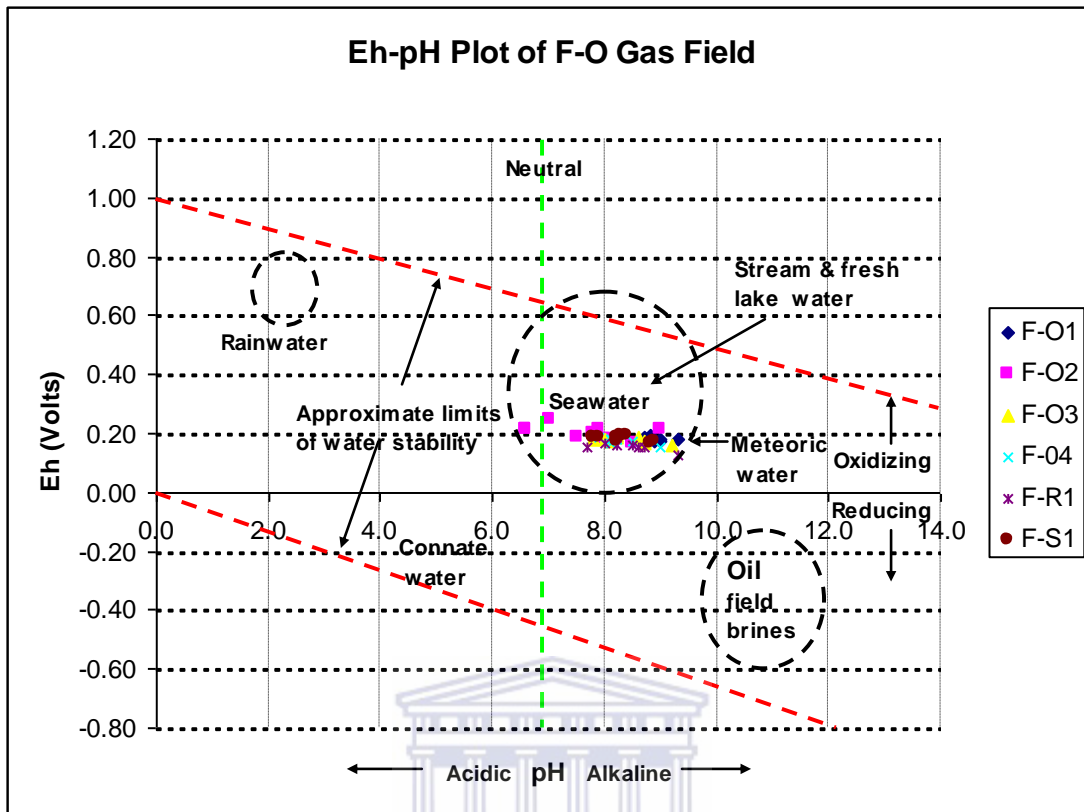


Figure 6.42: Eh-pH plot of the F-O field (modified from Tucker, 2001)

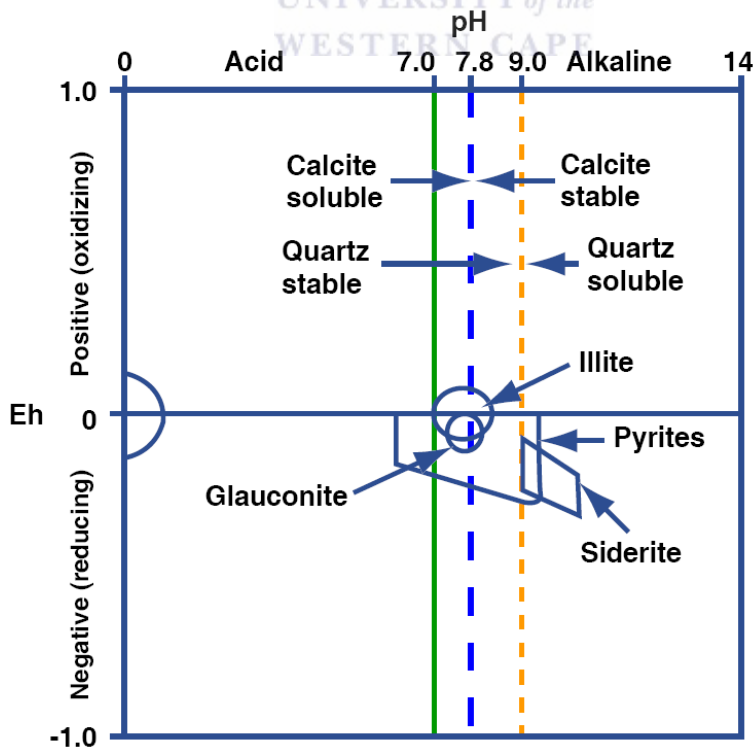


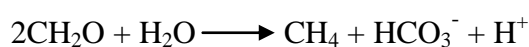
Figure 6.43: Stability curve of various diagenetic minerals in terms of pH and Eh (MIT OCW, 2012).

6.4.3: Immobile fluid ion ratios of the F-O gas field

Additional information on the processes that operate in the F-O gas field sediments can be derived from the ratios of major ions in the pore solutions. Sodium and potassium are two important abundant dissolved solutes in virtually all fresh water, brine and marine environments (Dove and Nix, 1997). It is well documented that dissolution rates of quartz increases with the introduction of low concentrations of these alkali cations to solution in low temperature as well as hydrothermal systems (Dove and Rimstidt, 1994). In the presence of sodium and potassium ions, dissolution rates become strongly pH-dependent (Dove and Elston, 1992). This section explores the ability to predict silica reactivity in the fluid of natural system by quantifying quartz dissolution rates in the presence of the alkaline earth cations, (Ca, Mg, Na and K. Both monovalent (Na^+ and K^+) and divalent (Ca^{2+} and Mg^{2+}) ions have distinctive significant difference as shown in Figures 6.44. Several studies have investigated quartz and amorphous silica rates in the presence of Ca^{2+} and Mg^{2+} bearing solutions (House, 1994; Barker et al., 1994; Dove and Nix, 1997) and findings has shown that rates are enhance more by monovalent ions, Na^+ and K^+ than Ca^{2+} and Mg^{2+} .

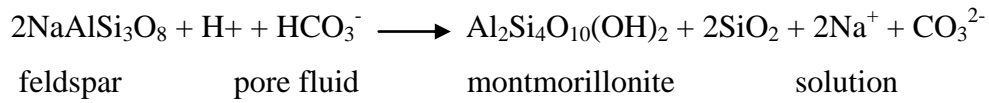
The vertical distribution of dissolved cations concentration plots within the F-O gas field generally reveals an increase in concentration following this sequence: $\text{Ca} < \text{Mg} < \text{Na} < \text{K}$ with the compositional variability more pronounced in Figures 6.44A, C, D and F than in Figures B and E with a corresponding increase in depth across the six studied wells. The rate of silica dissolution could be buttressed by the increase in the concentration of the monovalent ions as observed from the results. A significant zonation is observed in F-R1 cored intervals (Fig. 6.44E) with core 1 having a wide compositional variation in the cation concentrations while core 2 has the sequential increase in compositional variation in the analyzed cations similar to other wells. This can be attributed to the shaly nature (finer sediments) of core 1 as observed during core examination and notably the huge interval between the two cores (~115 m).

For alkaline conditions as observed in the F-O gas pore water results (Fig. 6.41; 6.42), a likely equation is:



From this reaction, higher $\text{Na}^+ / \text{Cl}^-$ ratios in organic rich sediments may be obtained by release of sodium, either by hydrogen-ion exchange with clays or through

dissolution of detrital silicates, such as feldspar, according to the reaction (Jones, et al., 1969):



This reaction provides for diagenetic formation of montmorilloid clays as observed during petrographic studies. If the above reactions were to balance each other, pH changes observation would be minimal, whereas if the organic matter were exhausted and the second reaction continued, utilizing H₂O as the supply of H⁺ ions, the pH would rise which supports the increasing alkalinity within the F-O field sediments.

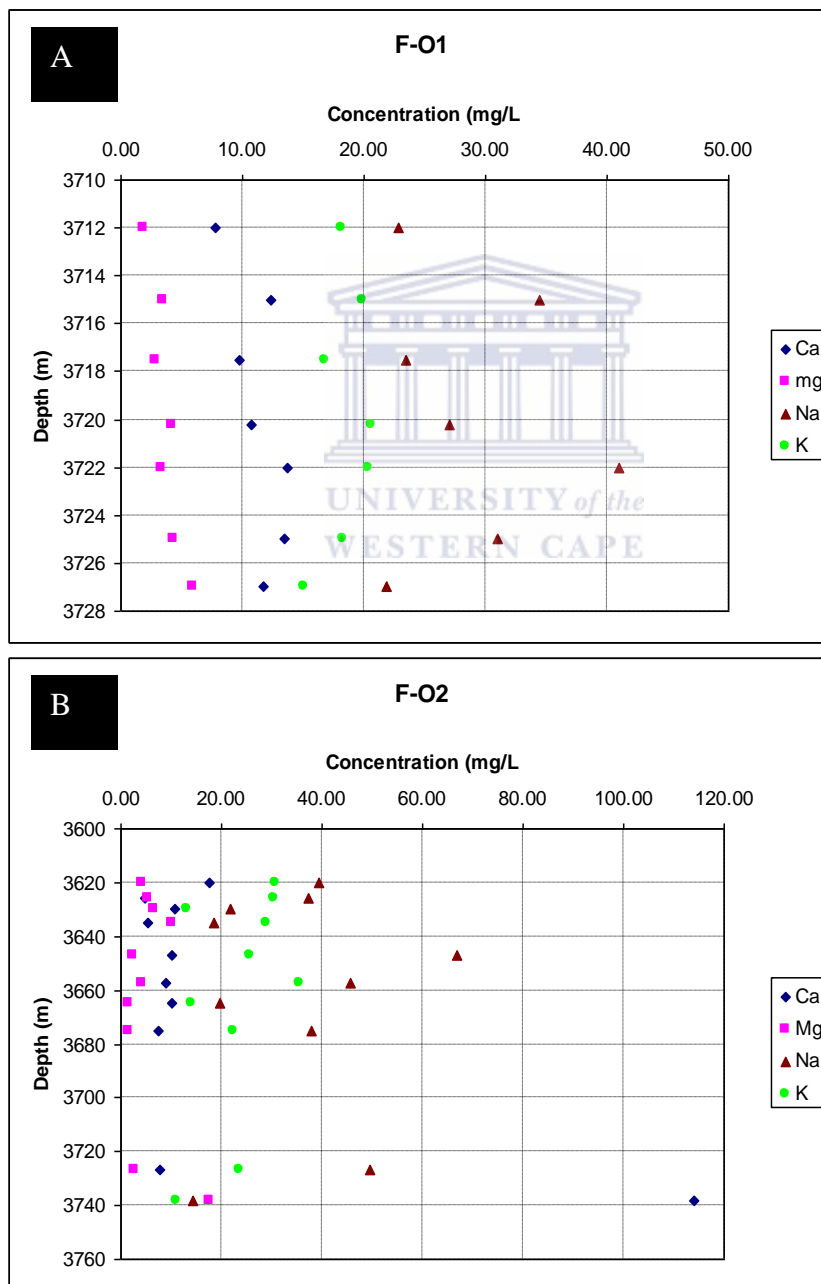


Figure 6.44a: Vertical distribution of dissolved-cations concentrations in pore water of F-O field

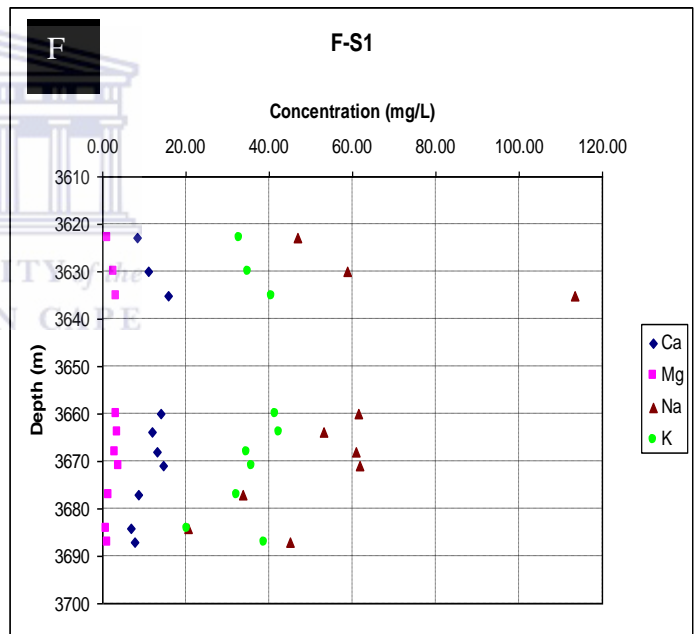
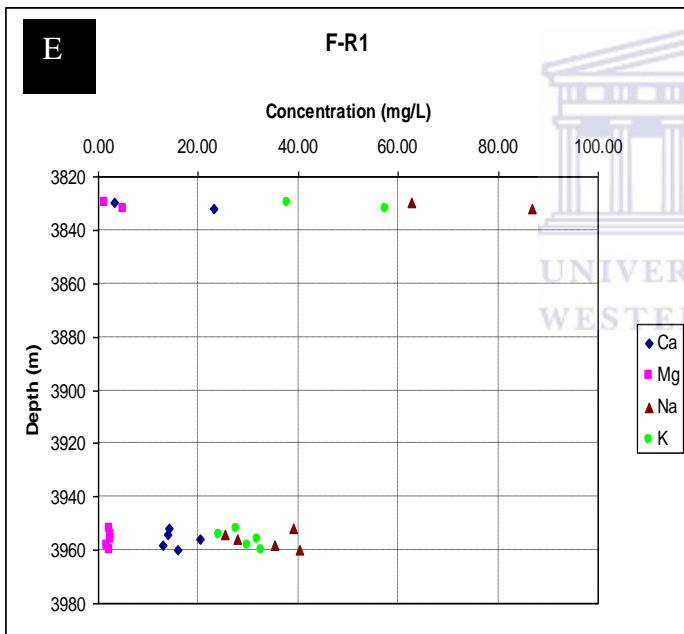
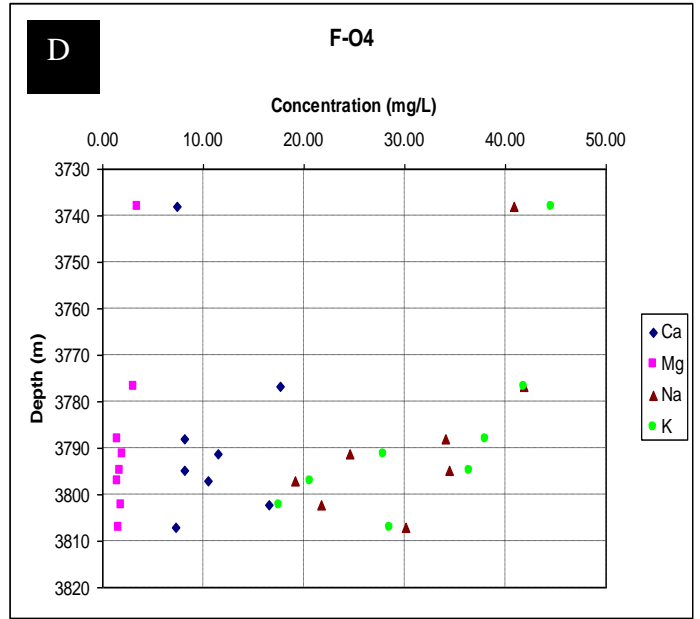
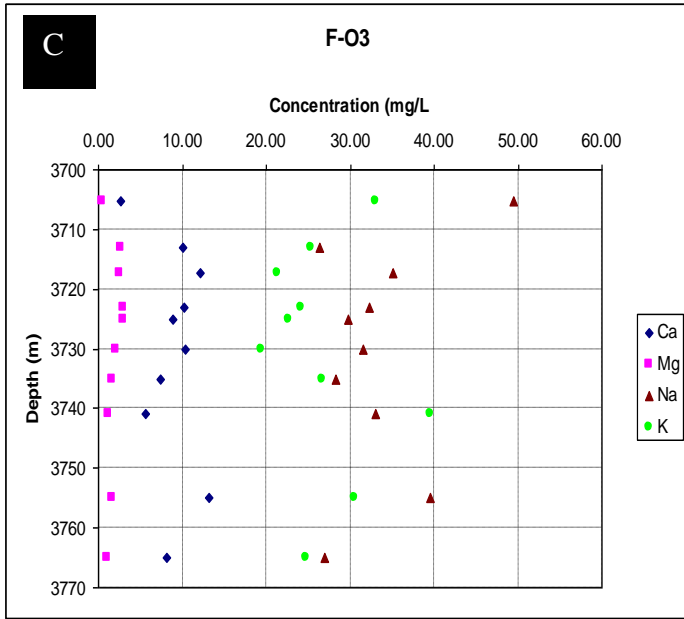


Figure 6.44b: Vertical distribution of dissolved-cations concentrations in pore water of F-O field.

6.5: Bulk rock geochemistry results and interpretation

6.5.1: X-ray fluorescence results and discussion

The bulk chemical composition of terrigenous sedimentary rocks are influenced by several factors such as sedimentary provenance, nature of sedimentary processes within depositional basin and the kind of dispersal paths that link provenance to depositional basin e.g. weathering, transportation, physical sorting and diagenesis (Roser and Korsch, 1986; McLennan et al., 1990; Weltje and Von Eynatten, 2004). The major and trace element compositions of sandstone, siltstone and shale have been important in determining provenance and tectonic setting in some cases (Culler, 2000; Cox et al., 1995; Bavinton and Taylor, 1980). For instance, index of mass percent (%) variability (ICV = $(\text{Fe}_2\text{O}_3 + \text{K}_2\text{O} + \text{Na}_2\text{O} + \text{CaO} + \text{MgO} + \text{TiO}_2) / \text{Al}_2\text{O}_3$) can be used to assess whether or not a given sequence of sandstones or siltstones represents first cycle sediment or if they were derived from recycling provided diagenesis does not alter the amount of K_2O , Na_2O , or CaO (Cullers and Podkovyrov, 2000). The geochemical investigation took into account samples from the Valanginian age of the six wells reported in this study.

Sandstone geochemistry varies systematically with the nature of the source rocks, weathering, diagenesis and metamorphism. In addition, tectonic settings have been identified as overall primary control on the composition of sedimentary rocks (Bhatia, 1983, Bhatia and Crook, 1986; Pettijohn et al., 1987). Various studies have shown that the chemical signature of some elements such as Mg, Cr, Ni, Co, Zr, Y, Nb, Sr, and Ba is generally preserved in sedimentary rocks through weathering and diagenesis (McLennan et al., 1983; Van de Kamp and Leake, 1985; Culler et al., 1988). Therefore, the geochemical investigation of abundance of these relative immobile elements usually provides information about the source material.

The major elemental compositions of the Valanginian age sandstone determined in this study are compared to the mean composition of principal sandstone classes (Pettijohn et al. 1987) and presented in table 6.51. Based on Pettijohn (1987) classification, the results of the wells in this study are therefore compared with the previous work of Pettijohn (1987) as presented in table 6.51. It was observed that F-O gas field wells predominantly falls within the lithic arenite sandstone classification with few samples falling within the arkosic and greywacke class.

The first well (F-O1) reveals the highest average value of SiO₂ (86.93 %) while F-R1 has the highest value of Al₂O₃ having 10.85 %. F-R1 generally reveals a relatively high compositional oxide values across the study wells (Table 6.51) except for the percentage of SiO₂ present within the sediments. This could be attributed to the nature of the sediment contained in the core 1 of the F-R1 reservoir sand (predominantly shaly in nature). The combination of varieties of major oxides points to a generally low Na₂O/K₂O with a corresponding high SiO₂/Al₂O₃ across the whole studied wells (Appendix 3).

Table 6.51: Mean composition of principal classes and average Valanginian age sandstone of the F-O gas field

Average sandstones (Pettijohn, 1987)					Average Valangian age sandstone						
Major oxides	Quartz arenite	Lithic arenite	Grey wacke	Arkose	Major oxides	F-O1	F-O2	F-O3	F-O4	F-R1	F-S1
SiO ₂	95.40	66.10	86.70	77.10	SiO ₂	86.93	80.27	80.73	86.81	69.08	78.02
Al ₂ O ₃	1.10	8.10	13.50	8.70	Al ₂ O ₃	2.74	4.81	6.04	4.23	10.85	7.54
Fe ₂ O ₃	0.40	3.80	1.60	1.50	Fe ₂ O ₃	1.87	2.98	2.76	2.77	4.36	2.98
MgO	0.10	2.40	2.10	0.50	MgO	0.52	0.58	0.61	0.62	1.09	0.81
CaO	1.60	6.20	2.50	2.70	CaO	2.44	3.19	2.62	8.48	3.23	2.33
Na ₂ O	0.10	0.90	2.90	1.50	Na ₂ O	0.54	0.77	0.85	0.5	1.12	1.27
K ₂ O	0.20	1.30	2.00	2.80	K ₂ O	0.79	1.33	1.63	1.03	2.88	1.93
TiO ₂	0.20	0.30	0.60	0.30	TiO ₂	0.15	0.28	0.33	0.23	0.51	0.39
P ₂ O ₅	-	0.10	0.20	0.10	P ₂ O ₅	0.10	0.1	3.73	0.15	0.11	0.11
MnO	-	0.10	0.10	0.20	MnO	0.15	0.66	0.13	0.68	0.11	0.12
Na ₂ O + K ₂ O	0.5	0.69	1.45	0.53	Na ₂ O + K ₂ O	1.33	2.10	2.48	1.54	4.00	3.19

Roser and Korsch, 1988 and Crook (1974) subdivided sandstones on the basis of SiO₂ content and the relative K₂O/Na₂O ratio into three classes and assigned each to plate tectonic settings and provenance. The quartz-poor variety, characterized by low SiO₂ content is typical of volcanic provenance. The quartz-rich (average 89 % SiO₂, K₂O/Na₂O > 1) content indicates a sedimentary provenance and the quartz-intermediate (average 68 - 74 % SiO₂; K₂O/Na₂O < 1) being of mixed provenance. The same techniques applied to the Valanginian sandstone suggest that the sediments may be derived from an “active continental margin” with few samples falling into the “passive margin zone” based on SiO₂ - K₂O/Na₂O ratio diagram (Fig. 6.51A) while Na₂O - K₂O diagram (Fig. 6.51B) reveals the intermediate quartz rich sandstone with K₂O/Na₂O ratio > 1 in all sampled intervals within the F-O gas field. This could be attributed to the mixed provenance in Figure 6.51A.

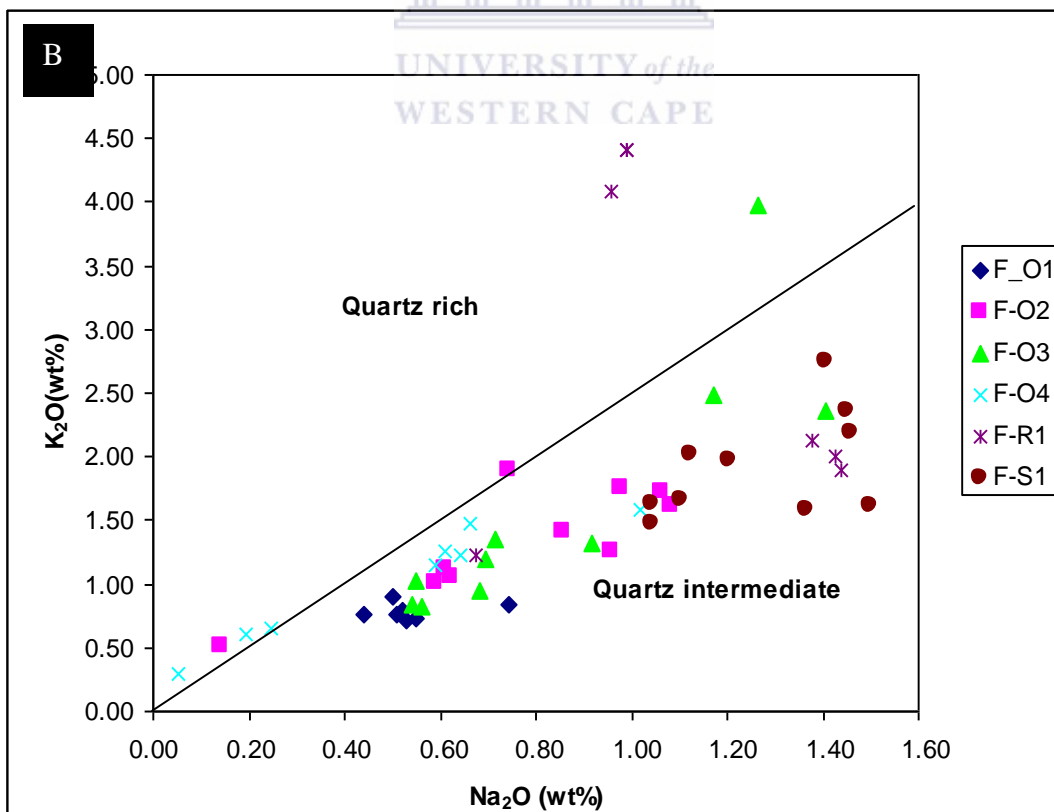
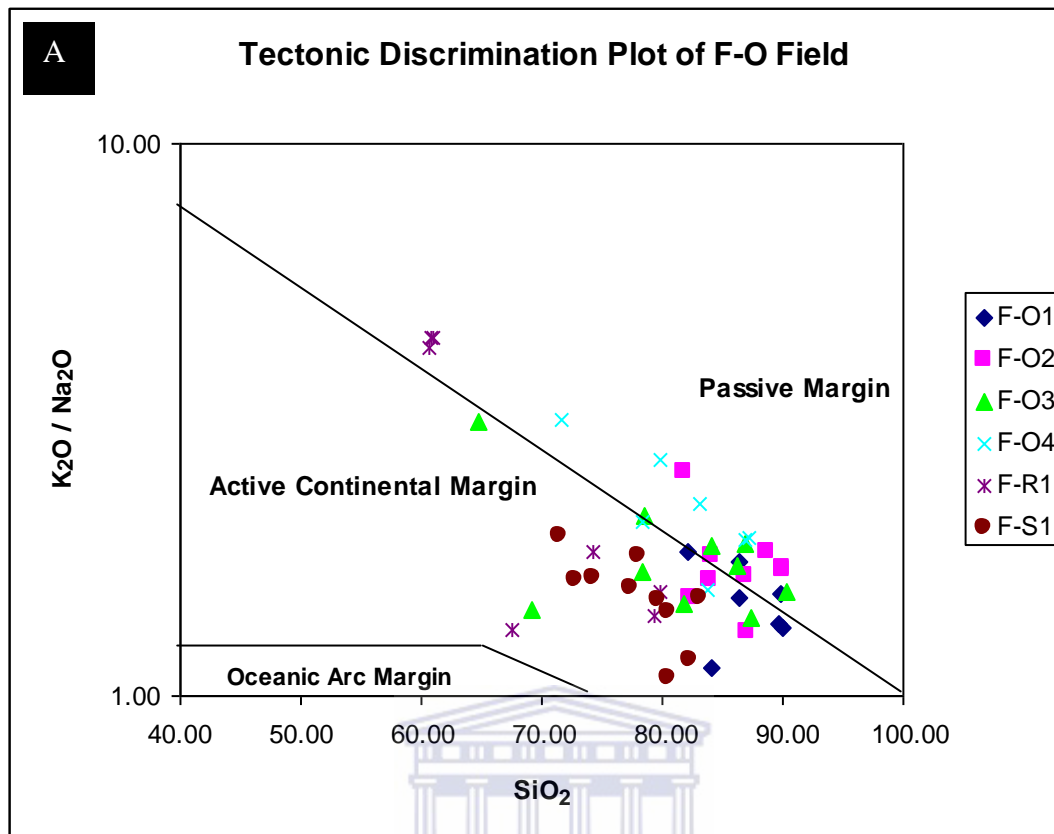


Figure 6.51: (A) Tectonic discrimination diagram (B) Alkali content of the F-O field gas sandstone (Following Roser and Korsch, 1988 and Crook, 1974 principles).

Table 6.52: Major oxide (wt %) compositions of the F-O field selected samples

Well name	Depth (m)	Al ₂ O ₃ (%)	CaO (%)	Cr ₂ O ₃ (%)	Fe ₂ O ₃ (%)	K ₂ O (%)	MgO (%)	MnO (%)	Na ₂ O (%)	P ₂ O ₅ (%)	SiO ₂ (%)	TiO ₂ (%)	LOI (%)	H ₂ O- (%)	Sum (%)
F-O1	3712.00	2.74	3.21	0.05	1.53	0.77	0.40	0.15	0.51	0.10	86.34	0.14	4.50	0.23	100.68
F-O1	3715.01	2.64	1.23	0.07	1.91	0.71	0.34	0.10	0.53	0.10	89.71	0.14	2.15	0.31	99.95
F-O1	3717.52	2.60	3.08	0.04	1.72	0.77	0.50	0.17	0.44	0.09	86.46	0.13	3.67	0.21	99.89
F-O1	3720.25	3.00	3.94	0.05	2.61	0.91	0.73	0.28	0.50	0.10	82.17	0.18	5.03	0.24	99.74
F-O1	3722.04	2.66	1.28	0.06	1.25	0.73	0.27	0.08	0.55	0.10	90.02	0.15	1.94	0.26	99.36
F-O1	3725.00	2.49	1.39	0.07	1.58	0.80	0.39	0.08	0.52	0.08	89.77	0.14	2.25	0.13	99.68
F-O1	3727.00	3.07	2.93	0.06	2.47	0.84	1.04	0.21	0.74	0.10	84.04	0.16	4.32	0.21	100.19
F-O2	3620.00	5.06	0.21	0.06	2.35	1.25	0.40	0.02	0.96	0.09	87.07	0.30	1.59	0.29	99.64
F-O2	3626.05	3.58	0.14	0.07	2.14	1.01	0.26	0.03	0.59	0.08	90.06	0.24	1.54	0.26	100.01
F-O2	3630.06	3.86	0.14	0.05	2.38	1.11	0.30	0.02	0.61	0.08	88.65	0.23	1.55	0.21	99.19
F-O2	3635.04	6.89	0.16	0.05	4.09	1.90	0.66	0.02	0.74	0.11	81.81	0.45	2.34	0.33	99.55
F-O2	3647.01	3.63	0.20	0.07	1.94	1.05	0.29	0.03	0.62	0.10	89.98	0.20	0.95	0.23	99.31
F-O2	3657.13	6.20	0.24	0.05	3.09	1.75	0.56	0.03	0.98	0.11	84.06	0.30	1.90	0.29	99.56
F-O2	3665.01	6.01	0.78	0.03	2.60	1.72	0.52	0.08	1.06	0.11	83.98	0.31	1.87	0.27	99.35
F-O2	3676.00	6.03	1.35	0.05	3.23	1.62	0.62	0.07	1.08	0.11	82.28	0.35	2.30	0.24	99.33
F-O2	3727.00	5.03	0.27	0.06	2.96	1.41	0.49	0.03	0.86	0.10	86.93	0.30	1.27	0.31	100.01
F-O2	3738.10	1.84	28.41	0.02	4.98	0.51	1.75	6.29	0.14	0.13	27.83	0.12	27.79	0.37	100.19
F-O3	3705.20	15.36	0.57	0.02	5.64	3.97	1.40	0.08	1.26	0.15	64.72	0.74	5.37	0.53	99.82
F-O3	3717.23	3.26	4.76	0.06	2.34	0.83	0.44	0.29	0.56	0.12	81.77	0.21	4.92	0.14	99.70
F-O3	3718.08	3.77	2.77	0.05	2.49	1.03	0.56	0.17	0.55	0.08	84.07	0.27	3.53	0.14	99.48
F-O3	3723.00	3.73	1.62	0.06	2.01	0.95	0.41	0.15	0.68	0.09	87.30	0.18	2.33	0.12	99.64
F-O3	3725.00	4.05	1.54	0.06	1.80	1.35	0.53	0.11	0.71	0.10	86.91	0.22	2.50	0.06	99.95
F-O3	3730.00	2.96	1.15	0.06	1.56	0.84	0.27	0.13	0.54	0.10	90.33	0.16	1.60	0.07	99.77
F-O3	3735.05	4.61	1.08	0.06	2.76	1.19	0.49	0.10	0.69	0.08	86.23	0.24	1.98	0.23	99.76
F-O3	3741.00	9.17	0.46	0.04	3.45	2.49	0.79	0.04	1.17	0.09	78.47	0.51	2.52	0.33	99.52
F-O3	3755.00	8.80	1.28	0.04	3.20	2.36	0.75	0.04	1.41	0.11	78.32	0.48	2.88	0.26	99.94
F-O3	3765.00	4.66	10.98	0.05	2.32	1.32	0.51	0.21	0.92	0.09	69.17	0.27	9.70	0.19	100.38
F-O4	3737.97	4.23	0.49	0.07	2.80	1.23	0.52	0.18	0.64	0.10	86.81	0.23	1.90	0.20	99.41
F-O4	3776.90	6.09	0.61	0.06	3.03	1.58	0.59	0.06	1.02	0.09	83.73	0.36	2.02	0.23	99.47
F-O4	3788.01	5.30	3.97	0.06	4.13	1.26	0.87	0.23	0.61	0.16	78.37	0.34	4.66	0.42	100.40
F-O4	3791.29	2.23	6.64	0.07	2.21	0.65	0.44	0.59	0.24	0.17	79.81	0.12	6.54	0.22	99.96
F-O4	3794.97	5.47	1.44	0.06	3.34	1.48	0.70	0.21	0.66	0.08	83.09	0.37	2.64	0.18	99.72
F-O4	3797.00	1.85	11.75	0.05	2.12	0.61	0.50	0.67	0.19	0.22	71.60	0.11	10.29	0.20	100.18
F-O4	3802.38	0.99	41.58	0.01	2.03	0.30	0.85	3.34	0.05	0.21	19.33	0.07	33.07	0.26	102.08
F-O4	3807.08	4.05	1.35	0.06	2.52	1.14	0.47	0.17	0.59	0.11	87.18	0.21	2.17	0.25	100.28
F-R1	3830.20	15.40	2.12	0.01	5.91	4.09	1.85	0.15	0.96	0.11	60.73	0.67	7.45	0.93	100.38
F-R1	3832.04	16.63	0.59	0.01	6.03	4.41	1.52	0.05	0.99	0.11	60.84	0.68	7.30	1.00	100.16
F-R1	3952.04	16.65	0.60	0.01	6.06	4.41	1.53	0.04	0.99	0.10	61.05	0.69	7.33	0.95	100.42
F-R1	3954.00	4.87	7.16	0.05	3.53	1.22	0.78	0.30	0.67	0.11	74.20	0.33	6.84	0.21	100.26
F-R1	3956.01	6.97	9.20	0.04	2.99	1.89	0.65	0.11	1.44	0.10	67.55	0.35	8.20	0.30	99.79
F-R1	3958.06	7.91	1.07	0.05	3.19	2.12	0.70	0.04	1.38	0.10	79.90	0.43	2.25	0.23	99.38
F-R1	3960.07	7.56	1.89	0.04	2.85	2.00	0.63	0.07	1.43	0.10	79.31	0.42	2.88	0.27	99.44
F-S1	3623.00	7.25	1.50	0.05	2.87	1.61	0.60	0.09	1.50	0.13	80.45	0.38	2.84	0.18	99.45
F-S1	3630.00	5.76	2.85	0.04	2.58	1.48	0.66	0.40	1.04	0.10	80.56	0.30	3.98	0.37	100.12
F-S1	3635.02	6.61	1.19	0.05	2.63	1.59	0.55	0.14	1.37	0.10	82.34	0.29	2.69	0.43	99.98
F-S1	3660.00	8.43	0.70	0.04	2.82	2.18	0.70	0.03	1.46	0.10	79.74	0.44	2.69	0.27	99.61
F-S1	3664.00	7.47	2.01	0.05	3.29	2.02	1.08	0.09	1.12	0.09	78.00	0.41	3.72	0.39	99.75
F-S1	3668.10	6.48	0.79	0.05	2.69	1.66	0.63	0.04	1.10	0.09	83.08	0.40	2.16	0.38	99.55
F-S1	3671.00	6.16	2.93	0.05	3.32	1.63	1.23	0.12	1.04	0.09	77.38	0.33	4.81	0.35	99.45
F-S1	3677.10	7.40	4.93	0.04	2.90	1.97	0.82	0.11	1.20	0.10	74.20	0.41	5.78	0.19	100.05
F-S1	3684.10	10.64	2.77	0.03	3.61	2.75	0.97	0.08	1.41	0.11	71.55	0.53	5.07	0.35	99.88
F-S1	3687.02	9.18	3.60	0.03	3.06	2.36	0.82	0.08	1.45	0.12	72.86	0.45	4.40	0.38	98.78

Weathering and paleo-environmental conditions during deposition.

6.5.2: Sediment maturity

Sediment maturity may be measured in terms of the SiO_2 content and the $\text{SiO}_2/\text{Al}_2\text{O}_3$ ratio (Potter, 1978), which reflects the relative abundance of quartz, feldspar and clay. Feldspar content can also be determined from whole rock chemistry using elemental content ($\text{Na}_2\text{O} + \text{K}_2\text{O}$). Using the index of chemical maturity $\text{SiO}_2/\text{Al}_2\text{O}_3$ and $\text{Na}_2\text{O}/\text{K}_2\text{O}$ ratio, Pettijohn et al., (1972) proposed a classification of terrigenous sands based on $\text{Log} (\text{Na}_2\text{O}/\text{K}_2\text{O})$ against $\text{Log} (\text{SiO}_2/\text{Al}_2\text{O}_3)$ plot. This classification diagram which has been modified from Herron (1988) shows the relationship between elemental composition, mineralogy and rock type. This was applied to the Valanginian age reservoir sandstones since there has been no major loss of K^+ and Na^+ species during diagenesis except transformation and cations exchange.

Generally, the F-O field studied wells show higher $\text{SiO}_2/\text{Al}_2\text{O}_3$ ratios with a corresponding lower $\text{Na}_2\text{O} + \text{K}_2\text{O}$ contents supporting the earlier plot of K_2O against Na_2O as intermediate quartz-rich sandstones (Fig. 6.51B). On the average the $\text{SiO}_2/\text{Al}_2\text{O}_3$ ratio of F-O1, F-O2, F-O3, F-O4, F-R1 and F-S1 are 31.90, 17.56, 17.79, 22.47, 8.12 and 10.75 respectively with a corresponding $\text{Na}_2\text{O} + \text{K}_2\text{O}$ content of the above mentioned wells being 1.33, 2.10, 2.48, 1.54, 4.00 and 3.19 respectively. An inverse relationship was observed with respect to $\text{SiO}_2/\text{Al}_2\text{O}_3$ and $\text{Na}_2\text{O} + \text{K}_2\text{O}$ contents in F-R1 and F-S1 in comparison to other wells (Appendix 3). Their $\text{SiO}_2/\text{Al}_2\text{O}_3$ contents are low with a corresponding higher $\text{Na}_2\text{O} + \text{K}_2\text{O}$ (Appendix 3) which is contrary to other wells, this could be attributed to the finer nature of the contained sediments within the reservoir intervals. Pettijohn et al., 1972 and Herron, (1988) modified classification diagram of the Valanginian age sandstones reveals that most sandstone samples fall between the litharenite and sublitharenite class with few subarkose sandstone samples (Figs. 6.52; 6.53). Litharenite sandstones are known to be mostly immature sandstones which suggest a minimum amount of weathering during erosion and deposition with limited transportation.

Herron (1988) modified the diagram of Pettijohn et al. (1972) by substituting $\text{Log} (\text{SiO}_2/\text{Al}_2\text{O}_3)$ with $\text{Log} (\text{Fe}_2\text{O}_3/\text{K}_2\text{O})$ on the Y-axis. The plot buttresses the earlier discussed plot (Fig. 6.52) with most of the analyzed sandstone samples falling within the litharenitic and sublitharenitic class (Fig. 6.53) and further explains the low iron content observed within the reservoir sands as observed during petrographic analysis.

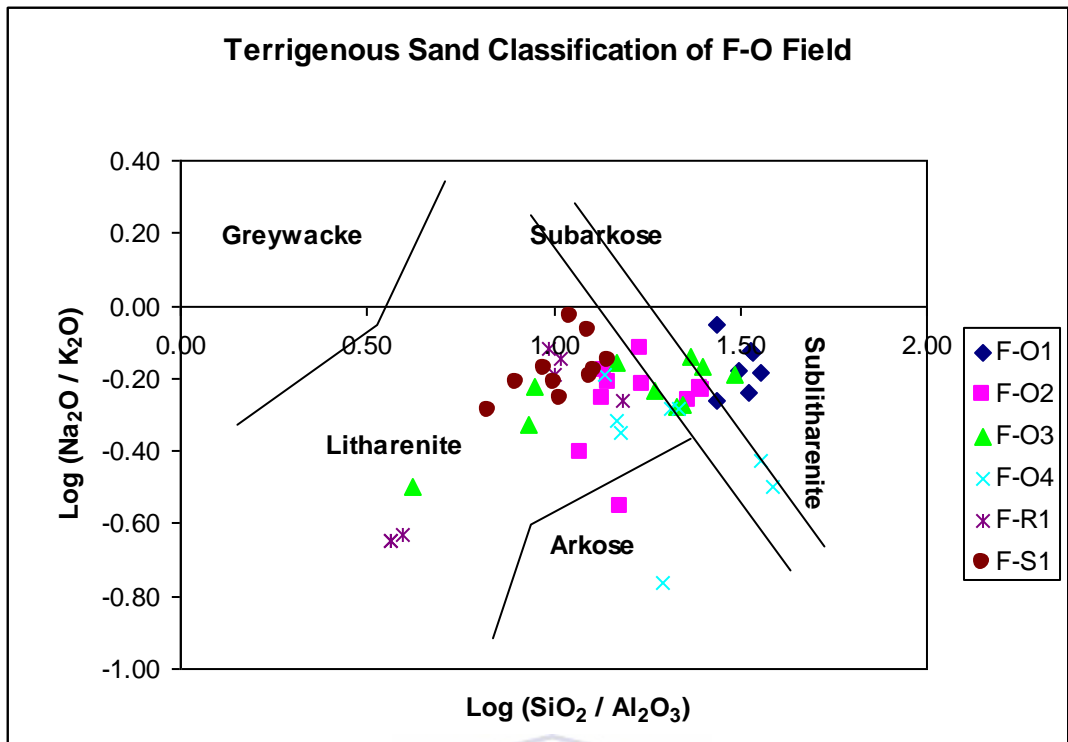


Figure 6.52: Classification of terrigenous sandstone using $\text{Log (Na}_2\text{O/K}_2\text{O)}$ versus $\text{Log (SiO}_2\text{/Al}_2\text{O}_3)$ from Pettijohn et al., (1972), following Herron (1988) principle.

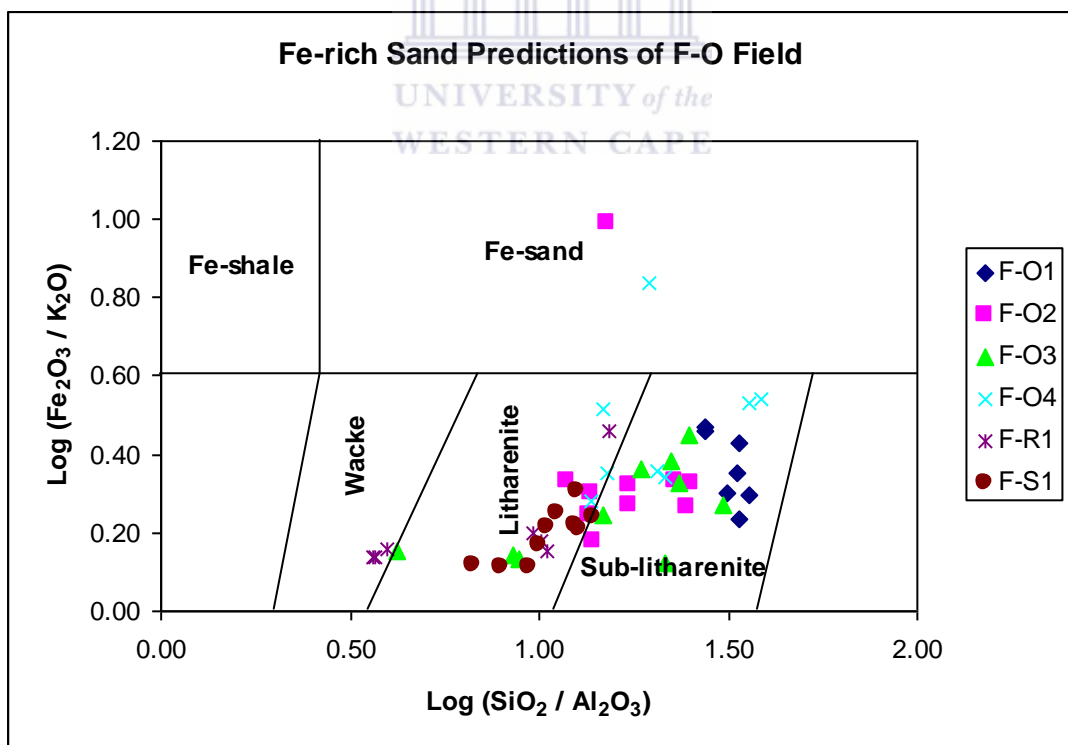


Figure 6.53: Geochemical classification of F-O field sandstone diagram (Following Herron, 1988 principle).

6.5.3: Weathering in source area

Petrographic data shows that plagioclase dominates over K-feldspar (Appendix 1), which may result from intense weathering in the source area or from diagenetic alterations. The earlier can be ruled out by the presence of abundant carbonate cement in some wells that developed probably during early diagenesis (Armstrong-Altrin et al., 2004). The intensity and duration of weathering in sedimentary rocks can be evaluated by examining the relationships between alkali and alkaline earth elements (Nesbitt and Young 1982; 1996). Feldspars are the most abundant of the reactive minerals with the dominant process during chemical weathering being the alteration of feldspars and neoformation of clay minerals. Calcium, sodium and potassium are largely removed during weathering of feldspars. The amount of these elements surviving in the sediment profile is a quantitative index of the intensity of weathering. A good measure of the degree of chemical weathering can be obtained by calculation of the chemical index of alteration (CIA); Nesbitt and Young 1982) using the formula of molecular proportions:

$$CIA = [Al_2O_3 / (Al_2O_3 + CaO^* + Na_2O + K_2O)] \times 100$$

Where CaO* is the amount of CaO incorporated in the silicate fraction of the rock.

The CIA mean values of the Valanginian age of the F-O gas field sandstone vary from ~ 41.55 – 60.18 with a significantly low values (5.94 and 2.31) at depths 3738 m of F-O2 well and 3802 m of F-O4 well respectively. High values (i.e. 76 – 100) indicate intensive chemical weathering in the source areas where as low values (i.e. ≤ 50) signifies un-weathered source areas. Therefore comparing these with the average calculated alteration values of area (F-O1 = 43.24 %; F-O2 = 60.18 %; F-O3 = 53.34 %; F-O4 = 41.35 %; F-R1 = 58.20 % and F-S1 = 58.01 %), the chemical data of the studied area suggest a relatively slightly low - moderate - high degree of chemical weathering with Figure 6.54 indicating the fine nature of the siliciclastic sandstone in the study area. Petrographic observations within the F-O field generally shows a considerable degree of diagenesis which in-turns could be attributed to some chemical weathering activities taken place, however the low CIA values as observed in F-O1 and F-O4 which does not really support the observed chemical alteration could be attributed to the sedimentary sorting effect that probably led to the concentration of quartz and feldspar that was observed during the core description and mineralogical observations of these two wells.

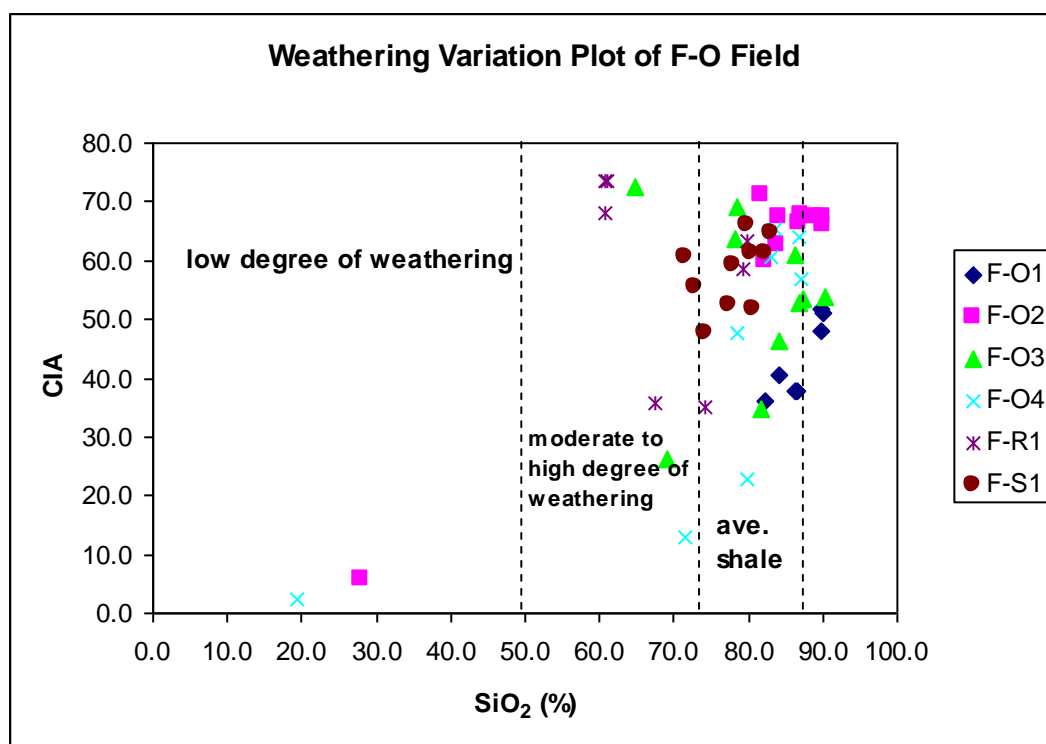


Figure 6.54: Diagram showing weathering variations (Chemical index of alteration of the F-O gas field.

6.5.4: ICV relation to recycling and weathering

The index of compositional variability (ICV) may be used to assess the original composition of sandstones and siltstones (Cox et al., 1995). The non-clay minerals in the original rocks have higher values of ICVs than the clay minerals. The ICVs of constituent minerals increase, for instance, in the order of kaolinite (~0.03 – 0.05), montmorillonite (~0.15 – 0.3), muscovite-illite (~0.3), plagioclase (~0.6), alkali feldspar (~0.8 – 1), biotite (~8), and amphibole-pyroxene (~10 – 100) (Cox et al., 1995). Therefore, in relatively unaltered sandstones and siltstones composed mostly of feldspar, pyroxene, amphibole, or biotite with less abundant clay minerals, ICVs should tend to be greater than one. Such sandstones and siltstones are usually deposited as first cycle deposits in tectonically active areas (Pettijohn et al., 1987; Van de Kamp and Leake, 1985).

Sandstones and siltstones with abundant clay minerals tend to have ICVs < 1 and form in areas of minimal uplift and are associated with extensive chemical weathering (Cox et al., 1995). Sands deposited in such areas approach a quartz arenite in composition. First cycle terrigenous sediment formed during intense chemical weathering or with long residence times in soils, however, may also become intensely weathered (Johnsson, 2000, 1993; Johnsson et al., 1988; Barshad, 1966) and thus

form ICVs < 1. Thus, sandstones and siltstones with ICVs > 1 are most likely first cycle sediments, and those with ICVs < 1 may be recycled or intensely weathered first cycle sediment.

The ICVs of sandstones from The F-O field have been calculated using the equation below:

$$\text{ICV} = (\text{Fe}_2\text{O}_3 + \text{K}_2\text{O} + \text{Na}_2\text{O} + \text{CaO} + \text{MgO} + \text{TiO}_2) / \text{Al}_2\text{O}_3$$

Most of the calculated samples reveal ICV value > 1 (1.12 – 8.28) except for a notable depth of 3802.38 m in F-O4 well with a significantly high ICV value of 45.35 (Appendix 3). This suggests that the F-O field sandstones are likely of first cycle materials. The relatively high CIA values and percentage of quartz relative to other minerals (Appendix 3) in all sandstones suggest relatively moderate- intense weathering of the sandstones.

6.5.5: Provenance composition: Trace elements

Trace elements concentration of the F-O field sandstones are reported in table 6.53. There is also a notable variation in the concentrations of most trace elements, generally having high (V, Cr and Zr) and low (Sc, Co, La and Th) as shown in table 6.53 below. The average relative concentration ratio lies between 0.25 – 0.97, except for Zr/Sc with consistently much higher average relative concentration values (~ 5.56 – 23.21). Figure 6.55 showing the plot of Th/Sc against Zr/Sc reveals Zr/Sc ratio enrichment across the study wells with F-S1 reservoir sandstone having the highest ratio (Average of 28.30). The V/Cr ratio has been used as an indicator of paleo-oxygenation conditions (Nagarajan et al., 2007). V/Cr ratio above 2 indicates anoxic conditions whereas values < 2 suggest oxidizing conditions. The V/Cr average ratio of the F-O gas field sandstones generally ranges from 0.15 – 0.71 signifying an oxidizing condition (Table 6.53).

There is an elevated abundance of Cr across the analyzed sandstone (Table 6.53). Chromium's occurrence maybe as result of its association with primary detrital phase while its behaviour could be likened to that of Al³⁺ leading to widespread accumulation in secondary oxides and clays. Chromium is a low mobility element under moderately oxidizing and reducing conditions and near-neutral pH values. High Cr and Ni abundances are clearly suggestive of mafic and/or ultramafic provenance (Armstrong-Altrin et al., 2004). Figure 6.56 plot reveals the silicic nature of the sandstone based on the plot of Th/Co against La/Sc. This agrees with siliciclastic sandstone interpreted from the petrographic results (Thin section, SEM and XRD).

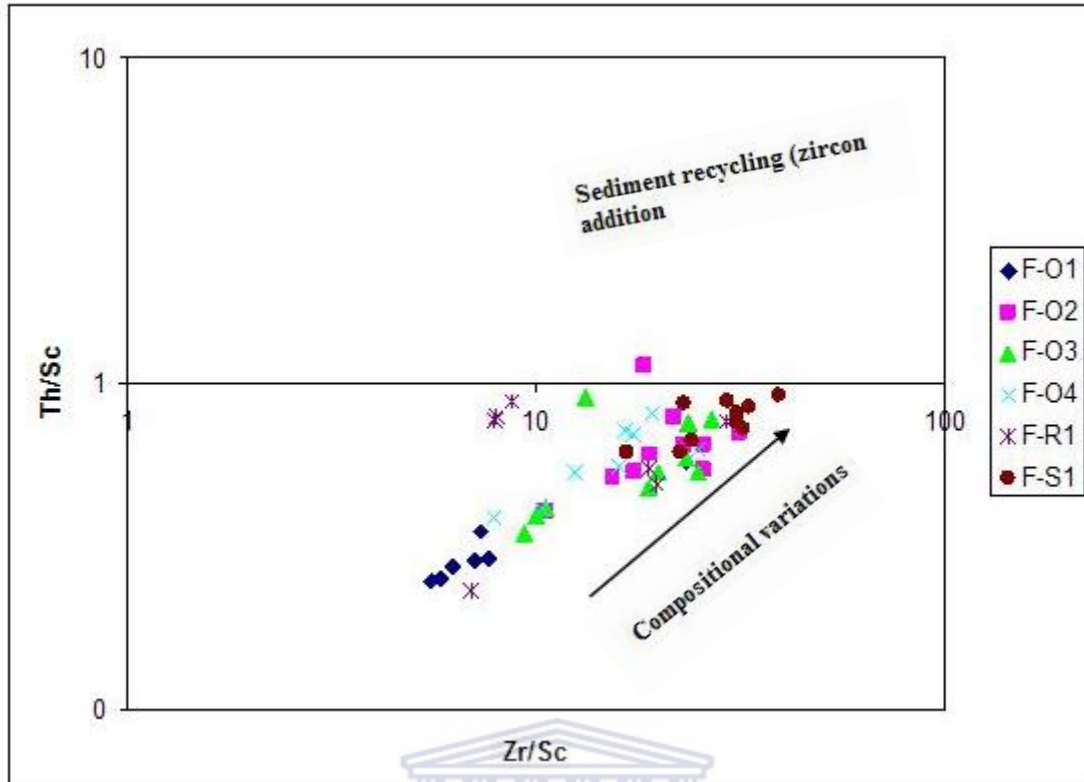


Figure 6.55: Plot of Th/Sc against Zr/Sc for sandstones from F-O gas field (Following McLennan et al., 1993 principle).

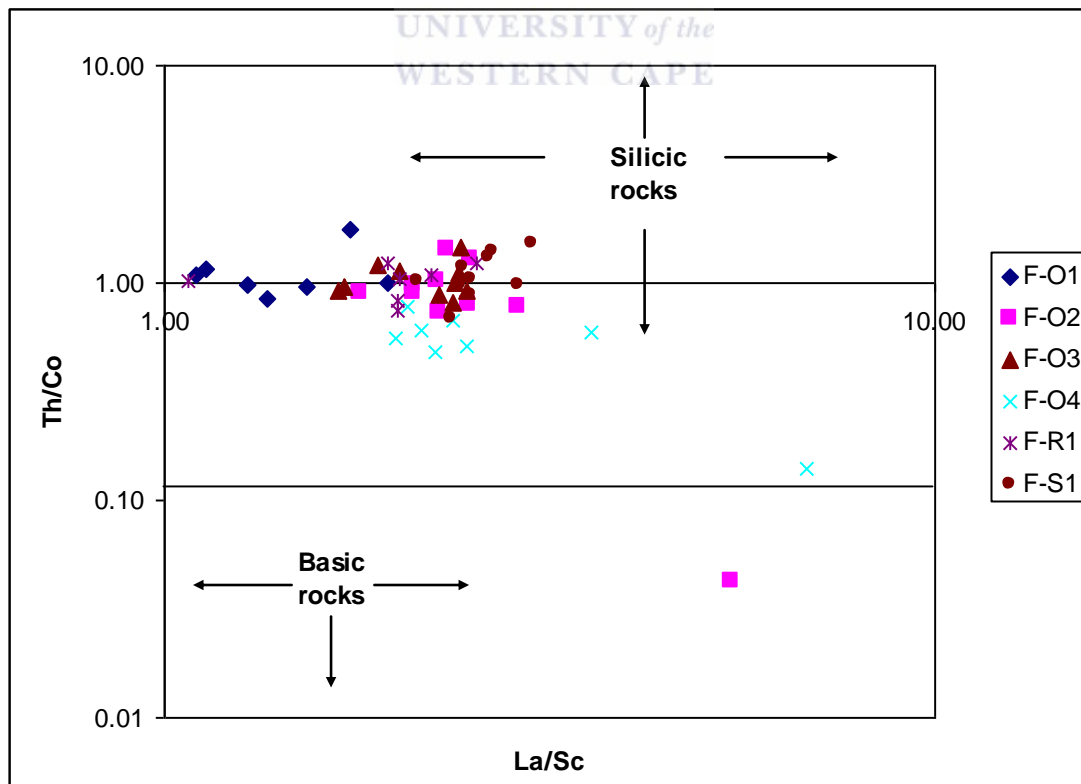


Figure 6.56: Th/Co against La/Sc diagram for sandstone samples from F-O gas field (Following Culler, 2002 in Nagaragan et al., 2007 principle).

Table 6.53: Trace element concentration of the F-O gas field

Well name	Depth (m)	Sc	V	Cr	Co	Ni	La	Th	Zr	La/Sc	Th/Sc	La/Th	V/Cr	Th/Co	Zr/Sc
F-01	3712.00	11.82	46.17	305.41	2.73	13.34	13.01	2.98	69.61	1.10	0.25	4.37	0.15	1.09	5.89
F-01	3715.01	10.36	61.99	513.22	2.93	16.94	13.30	2.85	64.71	1.28	0.28	4.67	0.12	0.97	6.24
F-01	3717.52	14.38	74.02	346.93	8.15	23.62	28.06	8.21	333.70	1.95	0.57	3.42	0.21	1.01	23.21
F-01	3720.25	11.46	56.09	368.46	4.15	17.78	17.54	4.01	84.40	1.53	0.35	4.38	0.15	0.97	7.36
F-01	3722.04	10.72	51.58	392.22	1.75	12.99	18.66	3.05	75.94	1.74	0.28	6.11	0.13	1.74	7.08
F-01	3725.00	11.86	56.98	462.37	2.55	17.16	13.41	2.93	66.00	1.13	0.25	4.57	0.12	1.15	5.56
F-01	3727.00	11.64	56.95	418.51	3.96	17.73	15.79	3.36	88.84	1.36	0.29	4.70	0.14	0.85	7.63
Average		11.75	57.68	401.02	3.75	17.08	17.11	3.91	111.88	1.44	0.32	4.60	0.15	1.11	9.00
F-02	3620.00	9.83	69.55	435.36	5.49	19.63	20.66	5.34	251.71	2.10	0.54	3.87	0.16	0.97	25.61
F-02	3626.05	8.72	67.35	472.24	6.20	20.60	19.75	4.48	135.23	2.27	0.51	4.41	0.14	0.72	15.52
F-02	3630.06	8.89	63.91	392.87	5.93	17.70	22.13	4.75	155.63	2.49	0.53	4.66	0.16	0.80	17.51
F-02	3635.04	10.63	75.77	322.03	10.85	26.63	30.52	8.43	231.88	2.87	0.79	3.62	0.24	0.78	21.82
F-02	3647.01	9.52	70.80	499.51	4.31	19.21	17.06	3.86	100.10	1.79	0.41	4.43	0.14	0.90	10.52
F-02	3657.13	9.85	73.48	342.36	6.71	21.47	20.78	5.99	187.37	2.11	0.61	3.47	0.21	0.89	19.02
F-02	3665.01	9.16	63.01	300.00	5.81	17.26	20.73	5.96	234.58	2.26	0.65	3.48	0.21	1.02	25.62
F-02	3676.00	9.31	69.46	358.14	5.05	19.75	23.19	6.53	291.03	2.49	0.70	3.55	0.19	1.29	31.28
F-02	3727.00	9.15	73.31	463.83	4.12	18.43	21.24	5.93	209.82	2.32	0.65	3.58	0.16	1.44	22.94
F-02	3738.10	4.87	48.51	125.98	131.39	46.83	26.56	5.52	89.74	5.46	1.13	4.81	0.39	0.04	18.45
Average		8.99	67.51	371.23	18.58	22.75	22.26	5.68	188.71	2.62	0.65	3.99	0.20	0.89	20.83
F-03	3705.20	16.17	115.18	133.75	16.68	41.22	36.72	14.58	213.30	2.27	0.90	2.52	0.86	0.87	13.20
F-03	3717.23	8.52	62.20	395.08	5.00	16.99	20.20	4.09	161.07	2.37	0.48	4.94	0.16	0.82	18.92
F-03	3718.08	9.02	63.97	411.18	5.25	19.42	22.30	4.80	224.32	2.47	0.53	4.65	0.16	0.91	24.88
F-03	3723.00	8.79	69.15	466.41	3.77	17.52	14.79	3.47	87.57	1.68	0.39	4.27	0.15	0.92	9.96
F-03	3725.00	9.05	64.93	398.39	3.10	16.90	17.07	3.76	95.93	1.89	0.42	4.54	0.16	1.21	10.61
F-03	3730.00	8.49	60.69	432.89	3.10	17.95	14.55	2.95	79.49	1.71	0.35	4.94	0.14	0.95	9.36
F-03	3735.05	9.23	66.83	429.56	4.35	16.10	18.63	4.91	183.65	2.02	0.53	3.80	0.16	1.13	19.91
F-03	3741.00	11.16	83.57	308.30	8.43	23.74	26.58	8.46	263.60	2.38	0.76	3.14	0.27	1.00	23.62
F-03	3755.00	10.78	73.41	278.02	7.59	24.39	25.96	8.42	291.04	2.41	0.78	3.08	0.26	1.11	27.00
F-03	3765.00	8.41	57.08	322.06	3.38	16.28	20.33	4.94	195.49	2.42	0.59	4.12	0.18	1.46	23.26
Average		9.96	71.70	357.56	6.06	21.05	21.71	6.03	179.54	2.16	0.57	4.00	0.25	1.04	18.07
F-04	3737.97	9.26	72.36	521.34	6.41	21.00	19.14	4.94	115.01	2.07	0.53	3.87	0.14	0.77	12.43
F-04	3776.90	9.84	75.16	406.97	9.19	22.36	23.33	6.22	243.98	2.37	0.63	3.75	0.18	0.68	24.79
F-04	3788.01	8.80	83.49	407.06	10.37	24.77	31.41	6.09	152.24	3.57	0.69	5.16	0.21	0.59	17.30
F-04	3791.29	7.60	64.58	476.47	5.56	19.69	15.16	3.10	78.57	2.00	0.41	4.89	0.14	0.56	10.34
F-04	3794.97	9.40	78.26	407.51	12.99	28.20	23.13	6.68	154.76	2.46	0.71	3.46	0.19	0.51	16.46
F-04	3797.00	6.60	55.75	356.15	5.36	17.59	14.78	2.57	52.06	2.24	0.39	5.75	0.16	0.48	7.89
F-04	3802.38	2.15	36.46	85.40	12.62	23.87	14.65	1.76	41.49	6.81	0.82	8.34	0.43	0.14	19.30
F-04	3807.08	7.97	73.86	484.49	7.27	24.23	17.22	4.41	127.74	2.16	0.55	3.90	0.15	0.61	16.03
Average		7.70	67.49	393.17	8.72	22.71	19.85	4.47	120.73	2.96	0.59	4.89	0.20	0.54	15.57
F-R1	3830.20	8.97	51.28	277.25	5.90	15.14	18.03	4.43	176.18	2.01	0.49	4.07	0.18	0.75	19.64
F-R1	3832.04	19.07	171.00	114.47	14.36	43.31	38.57	15.11	152.13	2.02	0.79	2.55	1.49	1.05	7.98
F-R1	3952.04	18.38	181.25	128.30	15.10	44.93	40.73	16.26	160.55	2.22	0.88	2.51	1.41	1.08	8.74
F-R1	3954.00	13.23	72.34	328.93	8.80	23.05	26.56	7.22	248.84	2.01	0.55	3.68	0.22	0.82	18.80
F-R1	3956.01	9.76	40.52	296.84	2.23	11.40	10.49	2.25	67.31	1.07	0.23	4.65	0.14	1.01	6.89
F-R1	3958.06	10.99	75.51	314.08	6.76	22.45	27.87	8.42	318.74	2.54	0.77	3.31	0.24	1.25	29.02
F-R1	3960.07	25.97	174.70	134.59	16.15	41.58	50.68	19.95	205.05	1.95	0.77	2.54	1.30	1.24	7.89
Average		15.20	109.51	227.78	9.90	28.84	30.42	10.52	189.83	1.97	0.64	3.33	0.71	1.03	14.14
F-S1	3623.00	10.18	69.47	310.61	10.87	25.97	24.00	7.39	328.32	2.36	0.73	3.25	0.22	0.68	32.27
F-S1	3630.00	9.79	67.78	279.27	6.08	18.79	23.70	5.97	219.34	2.42	0.61	3.97	0.24	0.98	22.42
F-S1	3635.02	10.21	73.28	343.10	6.04	24.44	21.79	6.23	170.36	2.13	0.61	3.50	0.21	1.03	16.69
F-S1	3660.00	11.19	75.60	323.24	6.78	21.45	29.73	9.46	372.63	2.66	0.85	3.14	0.23	1.40	33.32
F-S1	3664.00	10.52	75.01	341.10	7.62	26.22	26.30	8.00	328.85	2.50	0.76	3.29	0.22	1.05	31.26
F-S1	3668.10	9.28	71.58	355.13	7.59	20.15	26.69	7.48	287.46	2.88	0.81	3.57	0.20	0.99	30.99
F-S1	3671.00	9.93	69.75	331.29	7.57	20.54	24.75	6.67	239.21	2.49	0.67	3.71	0.21	0.88	24.09
F-S1	3677.10	9.82	67.43	280.59	6.00	21.79	29.43	9.04	387.29	3.00	0.92	3.26	0.24	1.51	39.46
F-S1	3684.10	11.54	80.55	231.27	8.44	22.62	28.19	10.01	265.74	2.44	0.87	2.82	0.35	1.19	23.04
F-S1	3687.02	10.84	77.35	237.96	7.28	20.62	28.56	9.57	319.39	2.64	0.88	2.99	0.33	1.31	29.48
Average		10.33	72.78	303.35	7.42	22.26	26.31	7.98	291.86	2.55	0.77	3.35	0.25	1.10	28.30

CHAPTER SEVEN

7.0: Fluid inclusion stratigraphy/petrography results and discussion

7.1: Introduction

Fluid inclusion studies used to be rather time consuming and therefore costly until the development of the analytical method “fluid inclusion stratigraphy” (FIS). This method chemically characterizes pore fluid trapped as inclusions in drill cuttings and core materials (Barclay et al., 2000). FIS could be further explained as a rapid analytical technique that involves the automated analysis of volatile compounds trapped within micron-sized cavities in rock materials taken from well cuttings, core or outcrop samples. These ‘fluid inclusions’ are representative samples of subsurface fluids, and are not subject to fractionation during sampling or evaporative loss during sample storage for any length of time. The procedure has major impact in the areas of both petroleum production and exploration applications providing information unattainable via more traditional methods and, has been instrumental in the discovery of significant petroleum reserves, influenced exploration, petroleum production and enhanced oil recovery operations.

The use of fluid inclusion techniques has become an increasingly important part of studies of diagenesis and petroleum generation and migration in sedimentary basins (e.g Burruss 1981; Roedder 1984; Rankin 1990; Emery and Robinson 1993). The presence of fluid inclusions in diagenetic phases allows constraints to be placed on the pressure-temperature conditions of mineral growth, the composition of pore fluids and the relative timing and nature of petroleum migration. However, despite the wealth of information which can be gleaned from fluid inclusions, there has been relatively very scarce literature on Bredasdorp Basin (especially F-O field) regarding fluid inclusion. This is possibly due, at least in part, to potential uncertainties in the validity of the method (Burrus 1981; Roedder 1984; Rankin 1990; Emery and Robinson 1993 Osborne and Haszeldine 1993), plus the practical difficulties in studying the extremely small inclusions generally occurring in authigenic phases.

This study looks at a total of number of 40 samples; which were subjected to analyses for trapped volatiles via the fluid inclusion stratigraphic technique while 13 samples were selected of out of the 40 samples for fluid inclusion petrographic studies due to the high cost of analysis. The samples were examined in both plane light and under UV illuminations for petrographic examination is also necessary to verify that

petroleum-bearing fluid inclusions present (if any) in the samples and responsible for the observed mass spectra are not relict features (i.e. that they were not already present in the mineral grains prior to deposition). The main objective was to evaluate samples for presence, distribution and character of hydrocarbon inclusions.

7.1.1: Fluid inclusion petrography of the F-O1 reservoir

Using conventional transmitted plane light microscopy, fluid inclusions were not clearly seen but few blebs of tar were observed adhered to grain surfaces of detrital quartz and quartz overgrowths in open porosity (Fig.7. 11A) at 3712 m and 3717.52 m (Fig. 7.11B). Grain shapes here reveals the angular to sub-rounded nature with a visible increase in porosity with corresponding increase in depth based on closeness between grain edges (Fig. 7.11). Stylolite was observed at depth 3727 m concentrating around quartz grain (Fig. 7.11C); this could probably be in conjunction with pressure solution as one of the major source of silica for the sandstone cementation in F-O1 sandstones which in-turn will have an adverse effect on reservoir quality.

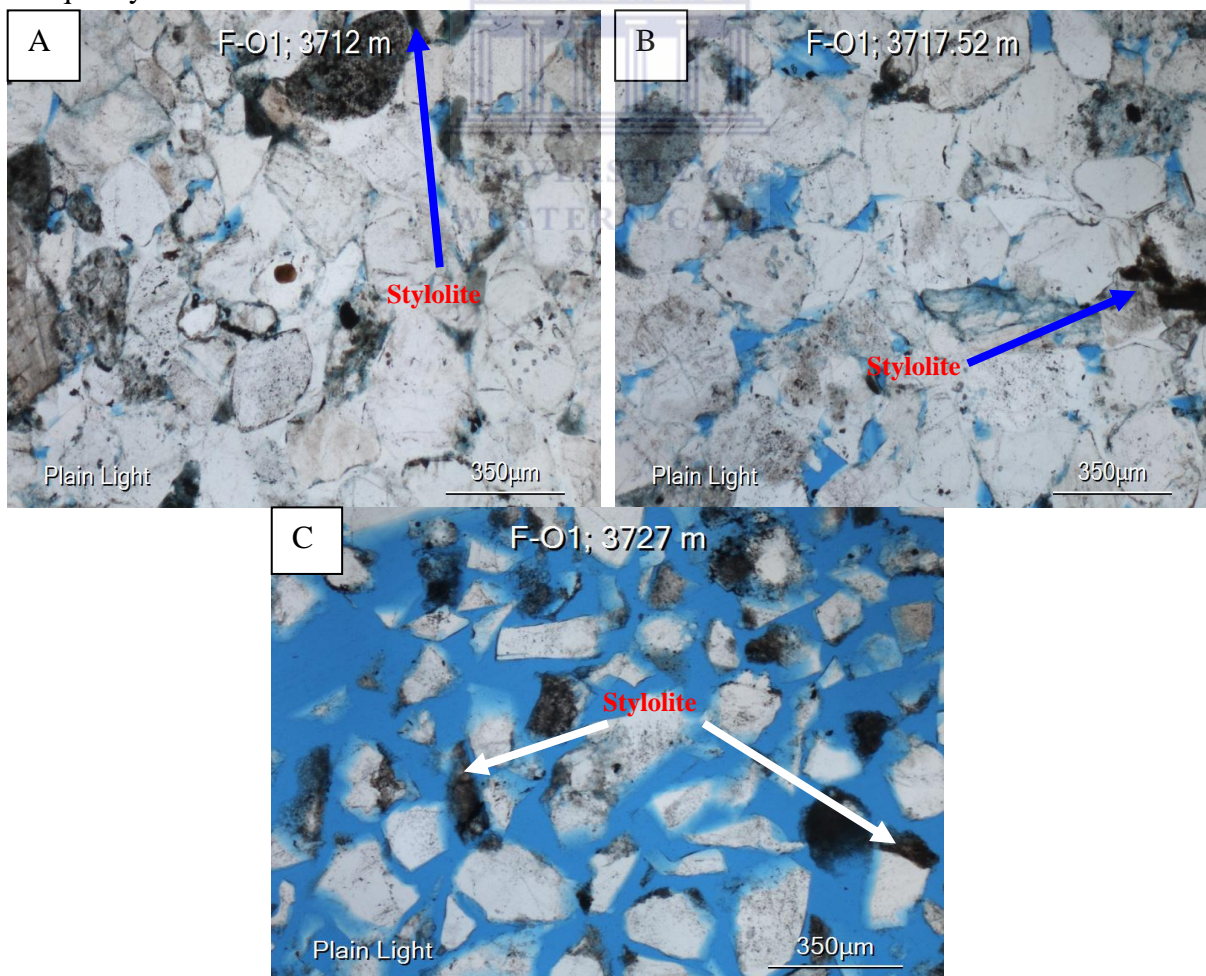


Figure 7.11: Fluid inclusion photomicrograph of F-O1 reservoir sandstone

7.1.2: Fluid inclusion petrography of the F-O2 reservoir

Fluid inclusion petrographic micrographs in F-O2 reveal an irregular grain shape ranging from angular to sub-angular to sub-rounded (Fig. 7.12). Pronounced stylolitization of the sandstone was observed at depth 3620 m with minor dead stain of oil seen at depths 3665.01 m and 3675 m (Figs. 7.12B, C). The observed stylolite might have probably truncated fluid inclusion decorated micro-fractures as no fluid inclusions were seen. Evidence of cementation is seen in F-O2 sandstone which is probably quartz cementation owing to the integration of the previously discussed petrography and geochemical results signalling high percentage of silica within the sandstone. This cement is regarded as a major porosity destroyer and also a critical control of reservoir quality in many types of sandstone.

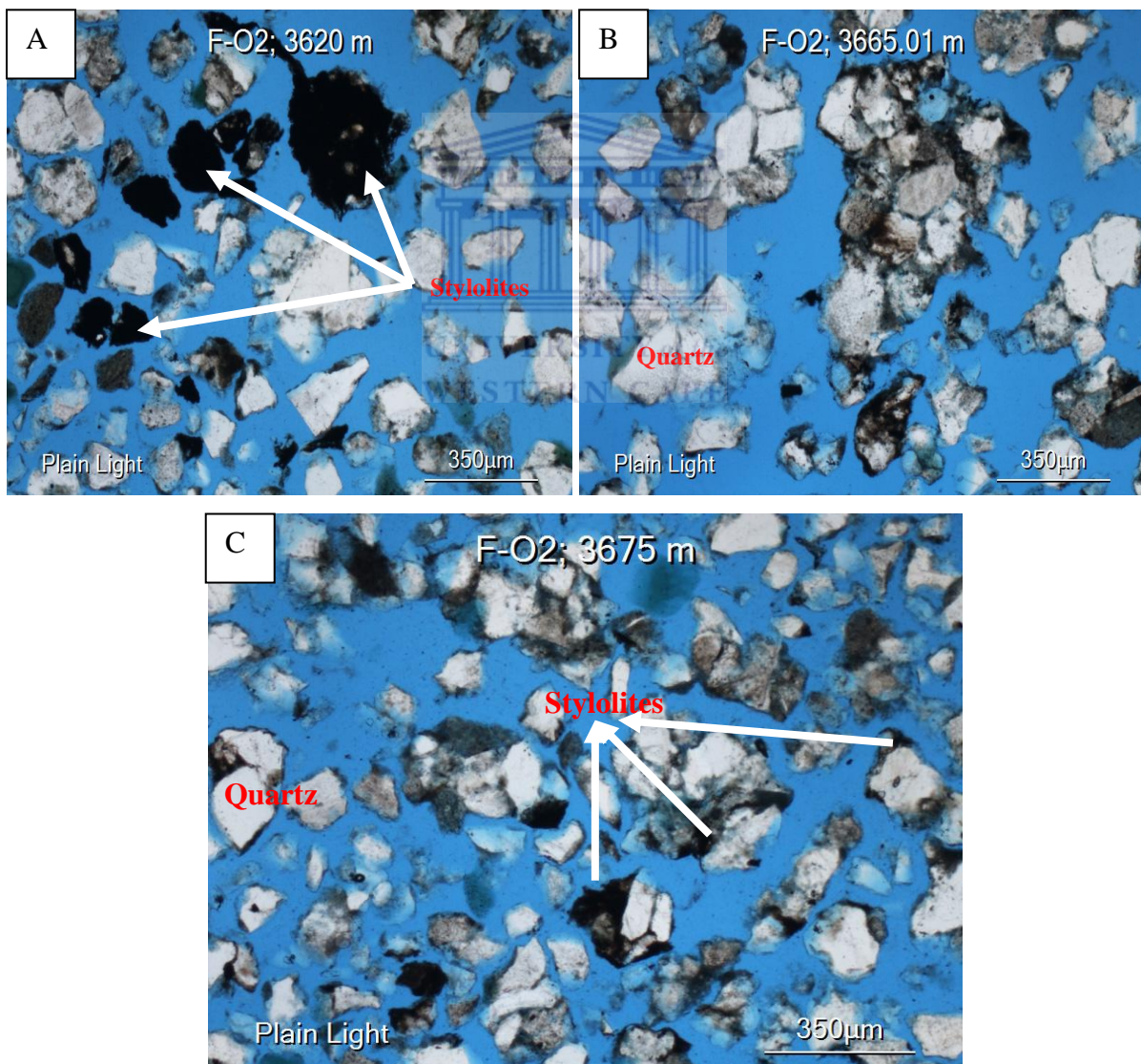


Figure 7.12: Fluid inclusion photomicrograph of F-O2 reservoir sandstone.

7.1.3: Fluid inclusion petrography of the F-O3 reservoir

Petrography result of F-O3 sandstone reveals a finer nature of the sediment as compared to the previously discussed wells. Stylolite was also observed across the analyzed samples which confirmed its presence as revealed in Figure 6.13 (Thin section petrography) comprising of muscovite and stylolite trace. This stylolite according to Figure 7.13B (Depth 3741 m) is probably acting as part of the cement blocking the intergranular space between each grain hereby reducing the reservoir quality. Stylolites are generally composed of illite often with muscovite and traces of iron oxide and pyrite (Baron and Parnell, 2006).

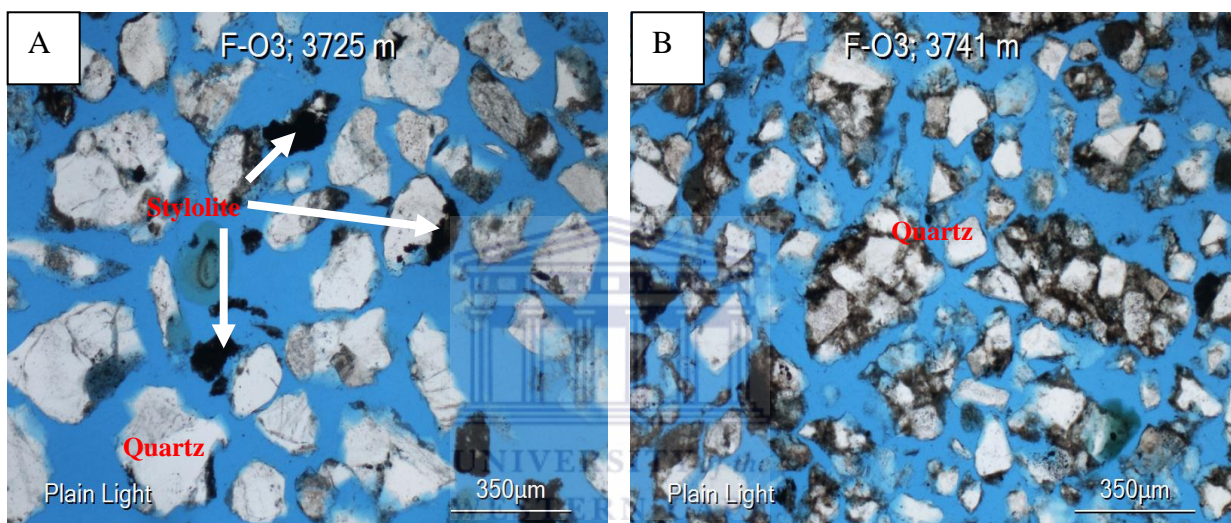


Figure 7.13: Fluid inclusion photomicrograph of F-O3 reservoir sandstone.

7.1.4: Fluid inclusion petrography of the F-O4 reservoir

Fluid inclusion petrography result of F-O4 sandstone shows sub-rounded to rounded grain shapes with some larger grain sizes having brownish particles filling (plant debris) the surface of some of the quartz grain especially at 3802.08 m (Fig. 7.14B). Stylolite is also seen on some grain surfaces and partly as rim rapped around the edges of some quartz grain (Fig. 7.14A). The photomicrograph reveals that there could be initially good porosity based on the pronounced intergranular space observed from the micrographs however, previous petrographic results shows the extent of diagenetic activities that has occurred during burial which must have played a significant role in reducing the porosity of the sandstone.

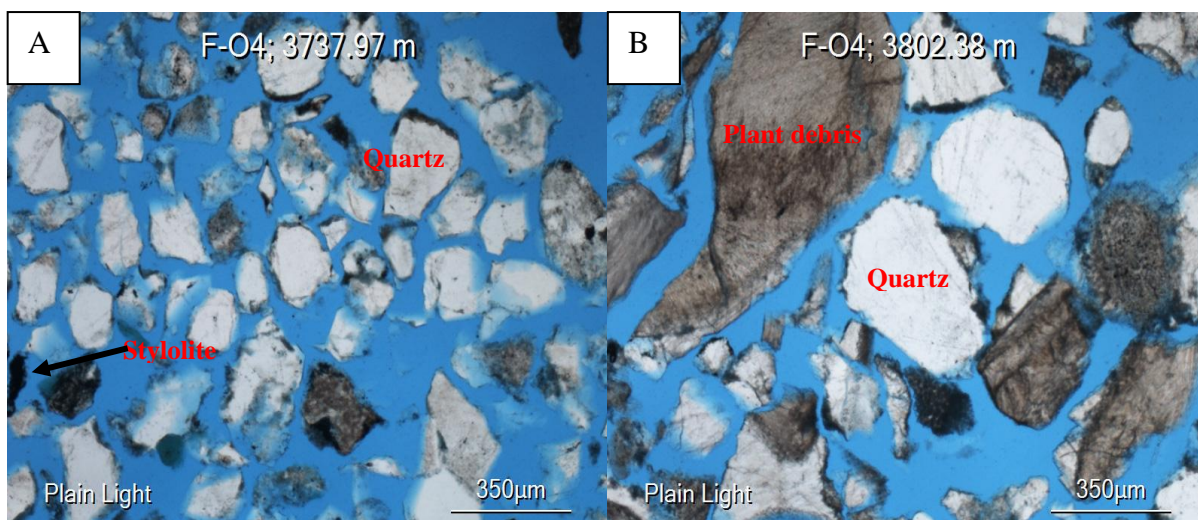


Figure 7.14: Fluid inclusion photomicrograph of F-O4 reservoir sandstone.

7.1.5: Fluid inclusion petrography of the F-R1 reservoir

The result obtained from the fluid inclusion petrography of F-R1 sandstone reveals a micro-fault with finer sediments (Fig. 7.15A). This could probably be attributed to grain comminution which could have a significant impact on fluid flow characteristics of the very fine sediment. Examples of such was cited in Terra Nova well of Jeanne d'Arc Formation in Newfoundland by Parnell et al., (2001). This finer sediment (Fig. 7.15A) also contains stylolite overlapping the small observed quartz grains. Figure 7.15B (3952.04 m) shows a sub-rounded to rounded grain shape with evidence of grain compaction and lithification with vague presence of stylolite cements filling the intergranular pore spaces. Rocks within core 1 are more shaly in nature than core 2 samples (Figs. 7.15A, B).

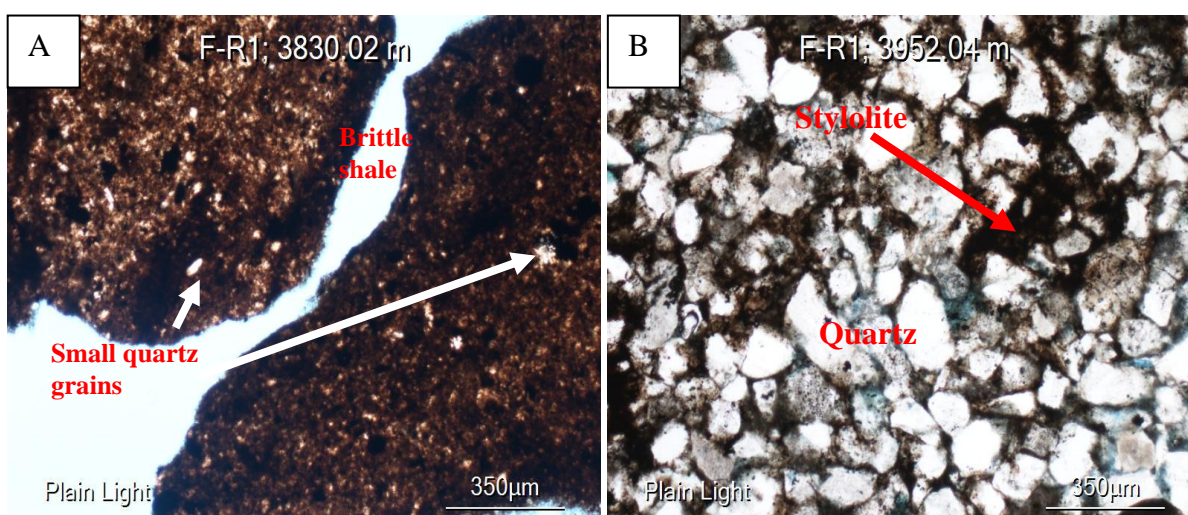


Figure 7.15: Fluid inclusion photomicrograph of F-R1 reservoir sandstone.

7.1.6: Fluid inclusion petrography of the F-S1 reservoir

Fluid inclusion petrographic study was performed only on one sample of the F-S1 reservoir sandstone as a representative sample. This sample reveals a sub-angular to sub-rounded grain shapes with stylolite (Fig. 7.16) occurring on some surfaces of the quartz grain. The sandstone shows the presence of some rare dead stain.

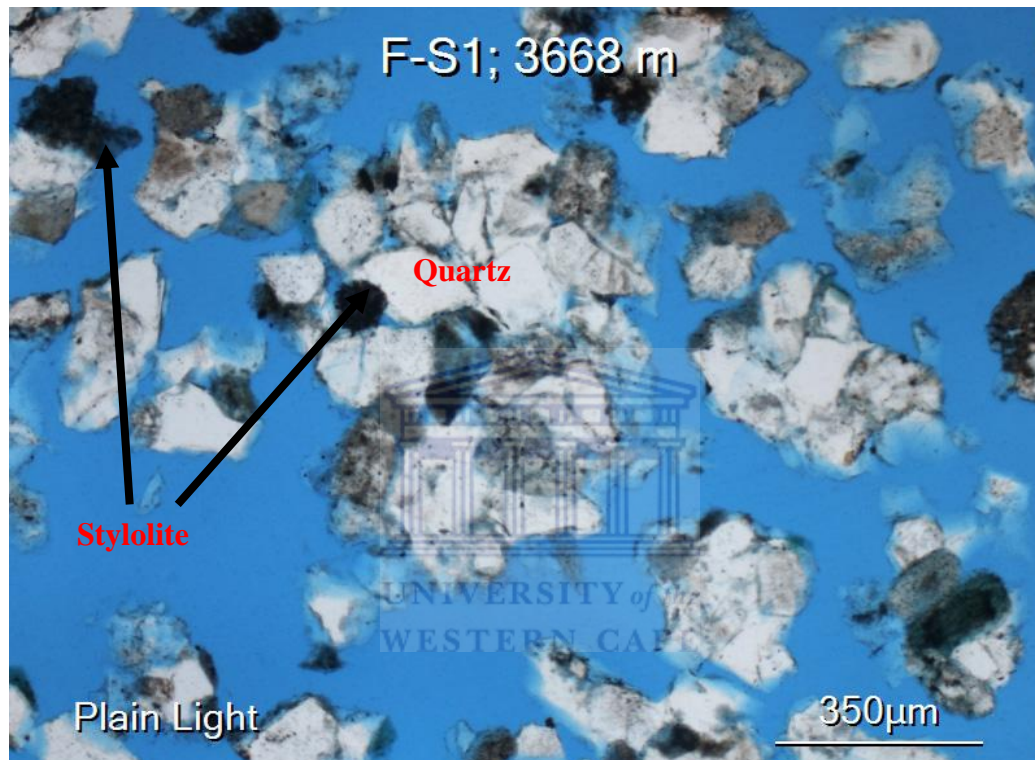


Figure 7.16: Fluid inclusion photomicrograph of F-S1 reservoir sandstone.

7.2: Fluid inclusion stratigraphy results and discussion

Fluid inclusion stratigraphic analysis was carried out on forty samples, which are representatives (typical) of the samples studied in research project. They were able to proffer solutions to challenges to proffer solution to the challenges regarding the hydrocarbon content of the field. Several important issues can be addressed in the F-O gas field by bulk volatile chemistry such as:

- ✚ Type of hydrocarbon present within the studied wells.
- ✚ Character of the observed hydrocarbon.
- ✚ Proximity to pay delineation.
- ✚ Better measurement of organic and sulphur species.

Tables 7.2 and 7.3 below show the summary of results obtained from fluid inclusion stratigraphic analysis. Generally the FIS data indicate the presence of dry gas to possible gas-condensate.

Table 7.2: FIS results showing the summary of results of the F-O gas field

Well Name	Depth	Rock Type		Petroleum Fluid Inclusion Populations	Kerogen (Possible source rock)			Bitumen	
		Dominant	Subordinate		Host Rock	Type	OP Flour Color	GP Abundance	Type
F-O1	3712.00	SS			-	-	-	-	ds sv
F-O1	3717.52	SS			-	-	-	-	ds r
F-O1	3727.00	SS			-	-	-	-	-
F-O2	3620.00	SS	Sh		sh	gp	-	c	-
F-O2	3665.01	SS			-	-	-	-	ds r
F-O2	3675.00	SS			-	-	-	-	ds r
F-O3	3725.00	SS			-	-	-	-	-
F-O3	3741.00	SS			-	-	-	-	-
F-O4	3737.97	SS			-	-	-	-	ds r
F-O4	3802.38	Cb	SS		-	-	-	-	-
F-R1	3830.02	Sh			sh	gp	-	c	-
F-R1	3952.04	Shly	SS		Sh	gp	-	sv	-
F-S1	3668.00	SS			-	-	-	-	ds r

ss: sandstone mt: metamorphic rk m: moderate r: rare ds: dead petroleum stain
 si: siltstone dr: quartz dust rim sv: several a: abundant po: pore-occluding bitumen
 sh: shale br: brown h: high c: common pb: pyro-bitumen
 cb: carbonate or: orange l: low gp: gas prone ls: live petroleum stain
 sa: salt an: anhydrite wt: white ch: chert go: oil & gas prone
 df: frac detrital feldspar co: coal qc: quartz cement cc: carbonate cement
 op: oil prone cm: matrix carbonate bl: blue xa: very abundant dq: frac in detrital quartz

7.2.1: Fluid inclusion stratigraphy results and discussion of F-O1 well

Aromatic enriched gas-condensate – light oil is noted from the FIS data with most samples having a maximum carbon of 10 (C₁₀) and methane (C₁) having a significant peak at depth 3715.01 m (Fig. 7.21 and Table 7.3). Table 7.3 shows a significant concentration of benzene (C₆H₆) noted across the reservoir intervals which could indicate similar zone in communication with gas proximal to pay gas (PTPG; in-house-unpublished report, 2011). Migration could also be inferred from the methane signature due to its significantly low response (www.fittulsa.com: accessed on 10-07-2012) in comparison to other studied wells except for F-O4 well which shows a lower response compared to F-O1 and most importantly due to the rare presence of visual petroleum inclusion abundances from fluid inclusion petrographic observations.

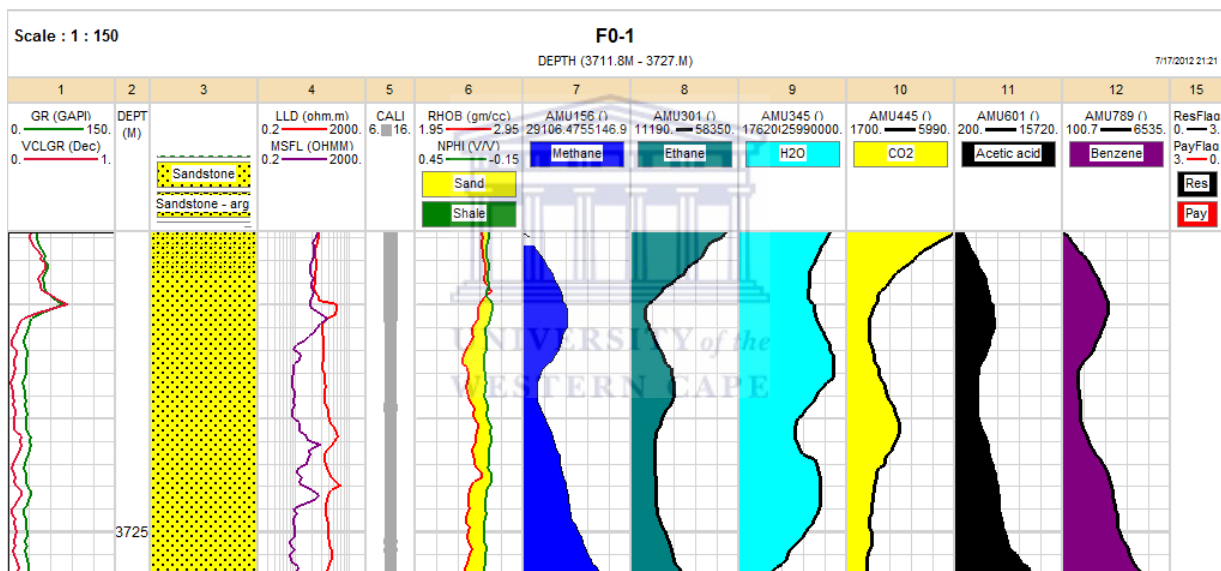


Figure 7.21: Bulk volatile analysis (FIS) of samples from F-O1 reservoir sand.

7.2.2: Fluid inclusion stratigraphy results and discussion of F-O2 well

Similar aromatic enriched wet gas to gas-condensate log and fingerprints of gas-oil logs are noted in the FIS data with stronger responses in samples from 3620 m – 3675 m, and the highest responses above 3650 m (Fig. 7.22 and Table 7.3). The significantly high peaks of the different tracks (Fig. 7.22) correlative closely with drilling shows and main pay calculated from integration of different petrophysical parameters (Resistivity / pay flag in Fig. 7.22). Specifically, with intervals at around 3635 m – 3659 m and analyzed intervals at 3738.10 m – 3757 m are anomalous of benzene. Deeper samples are more gaseous, and contain sulfur species, including S₂ or SO₂, suggestive of high Sw (water saturation) which is evidence at depth 3738.10 m (Table 7.3).

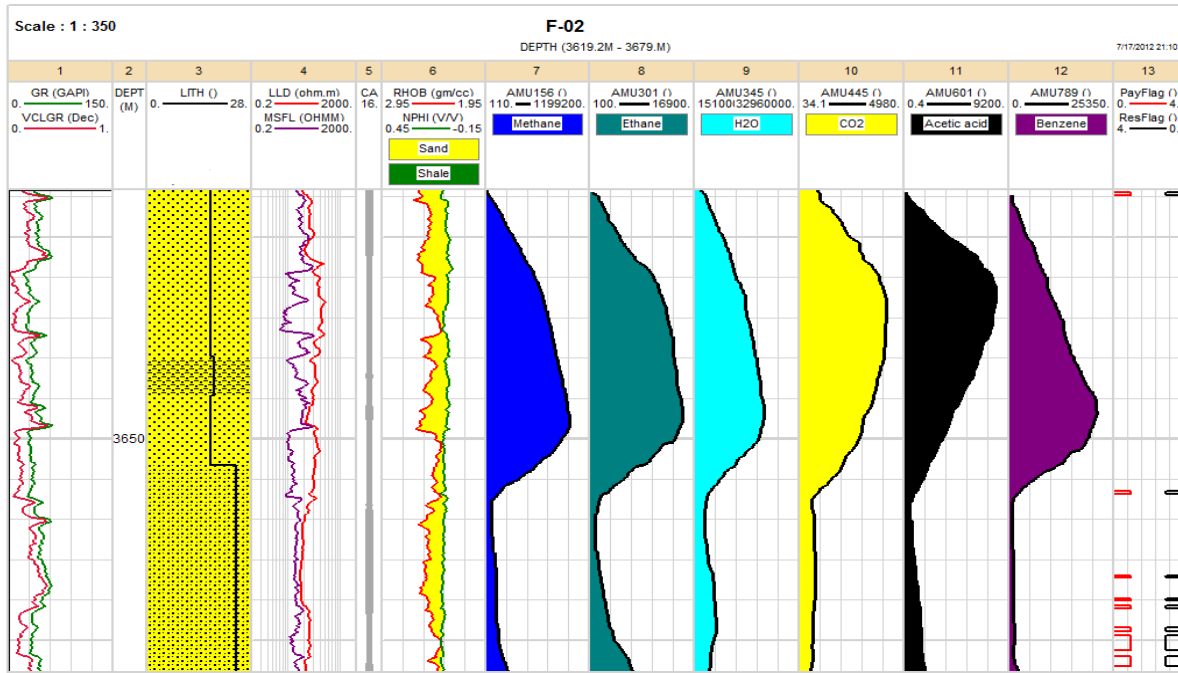


Figure 7.22: Bulk volatile analysis (FIS) of samples from F-O2 reservoir sand.

7.2.3: Fluid inclusion stratigraphy results and discussion of F-O3 well

Bulk volatile chemistry profiles indicate dominant wet gas across the sampled zone (Figs. 7.23 and Table 7.3) except for depth 3717.23 m having a significantly high C_1 indicative of dry gas with anomalous benzene observed in most sampled depths suggestive of nearby gas charge. Highest responses occur above 3735 m. Acetic acid (along some water-soluble aromatics such as benzene, CO_2 and toluene) acts as proximity-to-pay indicator due to diffusion away from petroleum accumulations through aqueous-dominated pore networks (Parnell et al., 1999; Fig. 7.23). Sulphur species are present, as above, and presence of S_2 or SO_2 suggests high S_w (water saturation) porous rock (Table 7.3) and a probably biodegradation in addition to the present petroleum species. The ratio of paraffins to naphthenes is low which indicates that metabolism of alkanes by bacteria to other classes of petroleum compounds must have taken place (www.fittulsa.com: accessed on 15-08-2012).

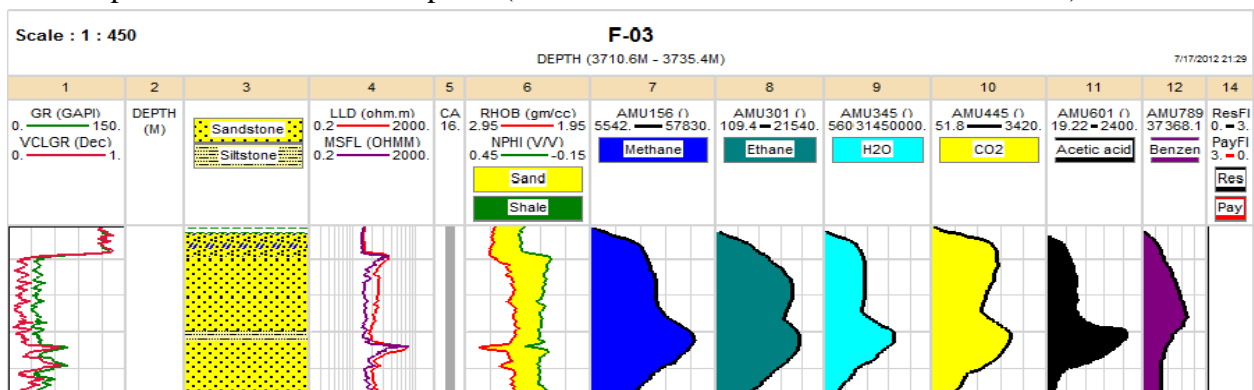


Figure 7.23: Bulk volatile analysis (FIS) of samples from F-O3 reservoir sand.

7.2.4: Fluid inclusion stratigraphy results and discussion of F-O4 well

FIS data indicate a wet gas – gas condensate responses with significant concentrations of benzene (possibly sensing nearby gas charge) and sulfur of probably thermal origin (FIT#FI020073a - Middleton - www.fittulsa.com: accessed on 10-07-2012). The log signatures (Table 7.24) indicate a decrease in methane (CH₄) with a corresponding increase in ethane (C₂H₆) and other carbon atoms ranging between C₂ to a maximum of C₁₀ within the reservoir zone (Table 7.3). This confirms the presence of wet gas – gas condensate as itemized in summary of findings (Table 7.3). Organic acids are considered to be in anomalous concentration when a distinct peak occurs at m/z 60 (acetic acids) (FIT#FI050810a - 721991 - www.fittulsa.com: accessed on 20-09-2012), this explains the anomalous concentration observed within certain depths in F-O4 well (Table 7.3; 3791.29 m for acetic acid and 3737.97 m – 3791.29 m for benzene). Acetic acid (along with some water soluble aromatics such as benzene and toluene) acts as proximity-to-pay indicator possibly due to diffusion away from petroleum accumulations through aqueous-dominated pore networks (Parnell et al., 2001). Ongoing research into source and sinks of organic acids and water-soluble aromatics indicate that the signal must be actively fed: so, it is unlikely that such signals would be reserved for periods of geological time. Hence, where such compounds are present they are thought to be encapsulated instantly as fluid inclusion due to thermal and mechanical processes acting on clay-rich lithologies in proximity to the drill bit. As such, acetic acid records proximity to present day rather than past petroleum accumulations (Parnell et al., 2001).

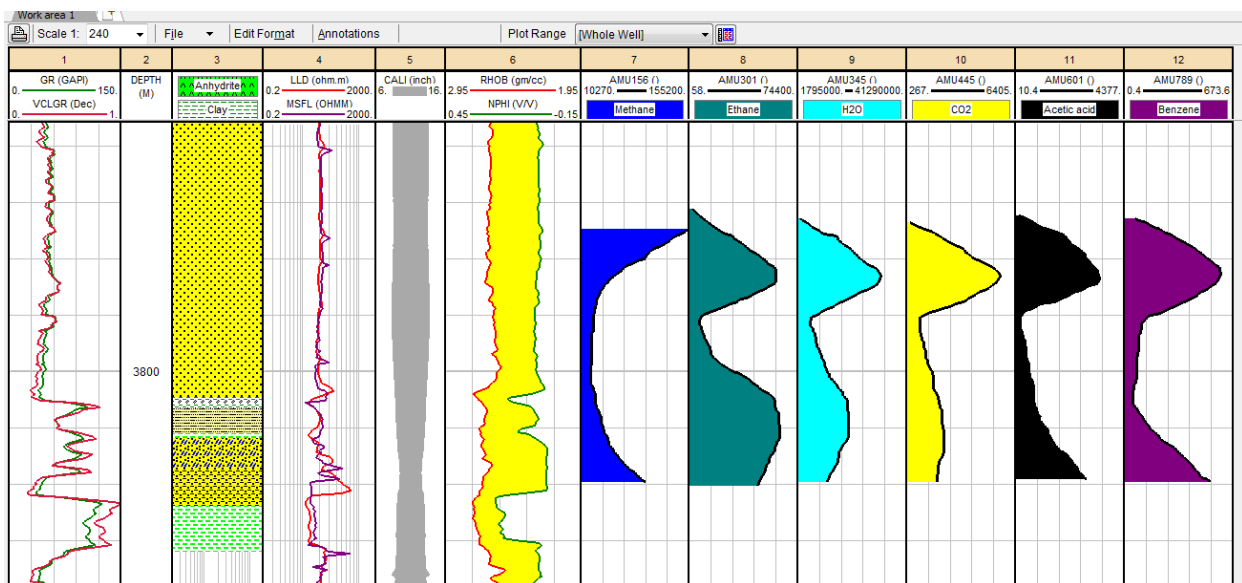


Figure 7.24: Bulk volatile analysis (FIS) of samples from F-O4 reservoir sand.

7.2.5: Fluid inclusion stratigraphy results and discussion of F-R1 well

Bulk volatile chemistry profiles indicate dry gas – wet gas with a considerable amount of benzene across the sampled zone (Fig. 7.25; Table 7.3). Acetic acid records proximity to present day rather than past petroleum accumulations. Acetic acid values remain generally low in F-R1 with the exception of a kick at 3956 m Fig. 7.25) which overlies a prominent silty-shale layer that may have high water saturation (Sw) in which water-soluble species like acetic acids will be concentrated within the major Valanginian reservoir sand, this could be the only indication of bypassed/proximal pay. This could be attributed to a generally poor lateral fluid connectivity between reservoir intervals in the present day (Parnell et al., 2001), probably owing to reservoir compartmentation by the observed faults from the previously interpreted seismic line that passed through pre1At1 F-R1 well (Fig. 5.46).

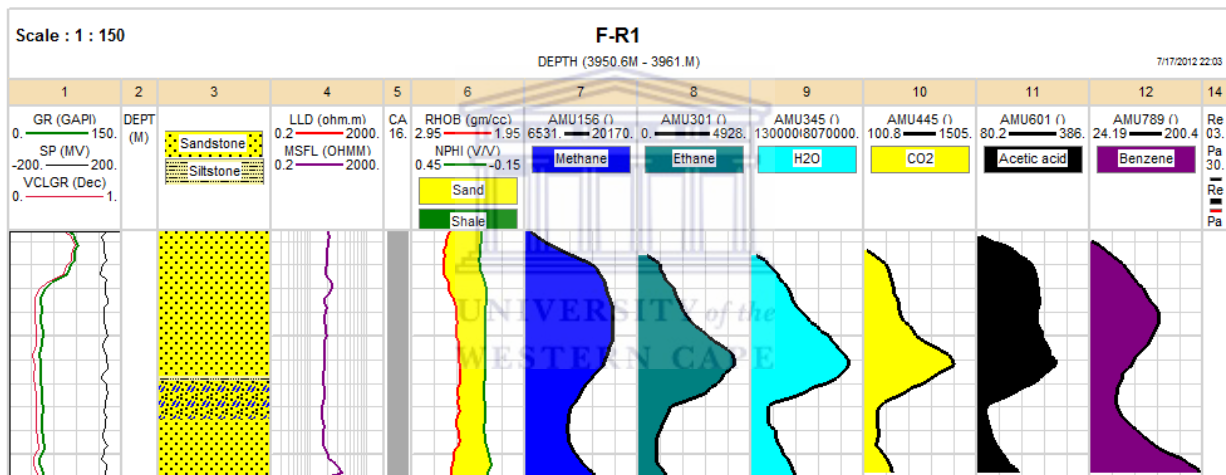


Figure 7.25: Bulk volatile analysis (FIS) of samples from F-R1 reservoir sand.

7.2.6: Fluid inclusion stratigraphy results and discussion of F-S1 well

The fluid inclusion geochemical profile of F-S1 sandstone is characterized by strong responses on C₄ – C₈ hydrocarbons with dwindling responses in C₁ at 3668 m, and essentially no response in the C₉₊ range (Table 7.3). This same depth (3668 m) shows an anomalous benzene value with a considerable peak for sulfur and a corresponding proximal to pay gas (Fig. 7.26). These indicate condensate responses (A. Akinlua pers. comm., September, 10 2012) with a significant concentration of benzene (possibly sensing nearby gas charge) and sulfur species of probably thermal origin (FIT#FI020073a - Middleton - www.fittulsa.com: accessed on 10-07-2012).

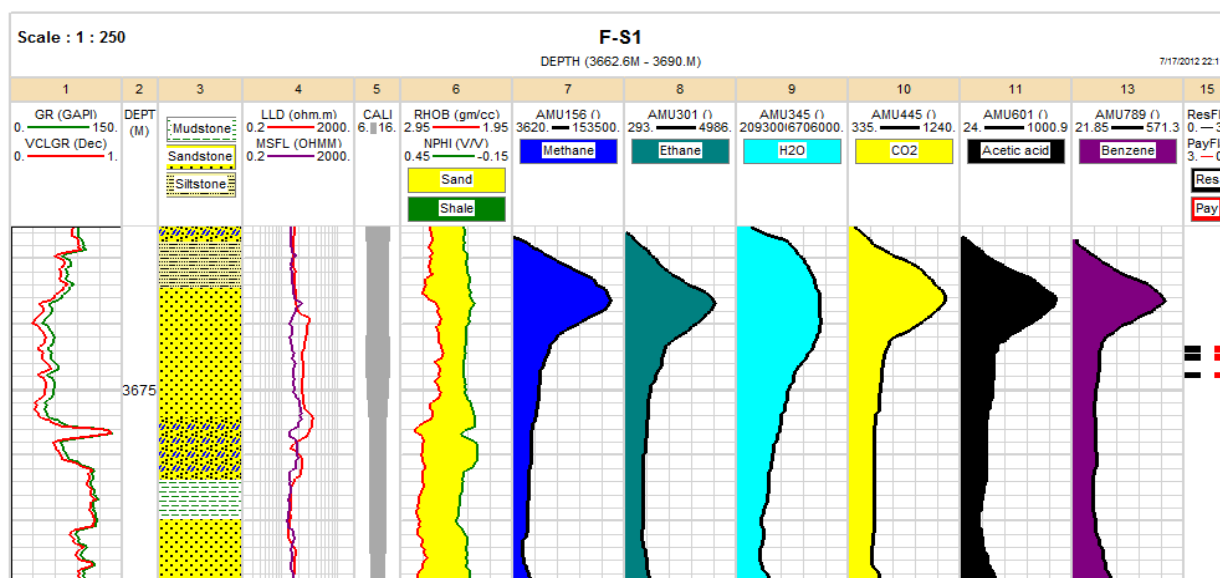


Figure 7.26: Bulk volatile analysis (FIS) of samples from F-S1 reservoir sand.

Table 7.3: Summary of classification of fluid inclusion mass spectra of F-O gas field

Well Name	Depth (m)	HC Type	CMax	C1 High	C7 High	PTP	Acetic/COS	Benzene	CS2	H ₂ S	S ₂ -SO ₂	Petrography
F-O1	3712.00	GC	10	---	---	PTPL	ANOMALOUS	ANOMALOUS	---	H ₂ S	---	x
F-O1	3715.01	GC	10	BIGGER	---	PTPG	---	ANOMALOUS	---	---	---	
F-O1	3717.52	GC	10	---	---	PTPG	---	ANOMALOUS	---	H ₂ S	---	x
F-O1	3720.25	GC	10	---	---	PTPG	---	ANOMALOUS	---	---	---	
F-O1	3722.04	GC-OIL	11	---	---	PTPG	---	ANOMALOUS	---	---	---	
F-O1	3725.00	GC-OIL	11	---	---	PTPG	---	ANOMALOUS	---	---	---	
F-O1	3727.00	GC-OIL	11	---	BIGGER	PTPG	---	ANOMALOUS	---	---	---	x
F-O2	3620.00	GC	8	---	---	---	---	---	---	---	---	x
F-O2	3630.06	GC-OIL	11	BIGGER	---	PTPG	---	ANOMALOUS	---	---	---	
F-O2	3647.01	GC-OIL	12	---	BIGGER	PTPG	---	ANOMALOUS	---	---	---	
F-O2	3657.13	WG-GC	8	---	---	---	---	---	---	---	---	
F-O2	3665.01	WG-GC	10	---	---	---	---	---	---	---	---	x
F-O2	3675.00	WG-GC	10	---	---	---	---	---	---	---	---	x
F-O2	3738.10	WG	4	---	---	PTPL	ANOMALOUS	ANOMALOUS	---	H ₂ S	S ₂ -SO ₂	
F-O2	3757.00	WG-GC	8	---	---	PTPG	---	ANOMALOUS	---	---	---	
F-O3	3713.08	WG-GC	2	---	---	---	---	---	---	---	---	
F-O3	3717.23	WG	4	BIGGER	---	PTPG	---	ANOMALOUS	---	---	S ₂ -SO ₂	
F-O3	3723.00	WG-GC	4	---	BIGGER	PTPG	---	ANOMALOUS	---	---	S ₂ -SO ₂	
F-O3	3725.00	WG-GC	4	---	---	PTPL	ANOMALOUS	ANOMALOUS	---	---	S ₂ -SO ₂	x
F-O3	3730.00	WG-GC	4	---	---	PTPG	---	ANOMALOUS	---	---	S ₂ -SO ₂	
F-O3	3735.05	WG-GC	2	---	---	---	---	---	---	---	---	
F-O3	3741.00	WG-GC	2	---	---	---	---	---	---	---	---	x
F-O3	3755.00	WG-GC	2	---	---	---	---	---	---	---	---	
F-O4	3737.97	WG-GC	10	BIGGER	BIGGER	PTPG	---	ANOMALOUS	---	---	---	x
F-O4	3788.01	WG	6	---	---	PTPG	---	ANOMALOUS	---	H ₂ S	S ₂ -SO ₂	
F-O4	3791.29	WG-GC	10	---	---	PTPL	ANOMALOUS	ANOMALOUS	---	H ₂ S	S ₂ -SO ₂	
F-O4	3794.97	WG-GC	4	---	---	---	---	---	---	---	---	
F-O4	3802.38	DG	2	---	---	PTPG	---	ANOMALOUS	---	H ₂ S	S ₂ -SO ₂	x
F-O4	3807.08	WG-GC	8	---	---	PTPG	---	ANOMALOUS	---	H ₂ S	S ₂ -SO ₂	
F-S1	3630.00	WG	7	---	---	---	---	---	---	---	---	Limited sample
F-S1	3664.00	WG	4	---	---	---	---	---	---	---	---	
F-S1	3668.00	GC	8	BIGGER	BIGGER	PTPG	---	ANOMALOUS	---	---	S ₂ -SO ₂	x
F-S1	3671.00	WG	4	---	---	---	---	---	---	---	---	
F-S1	3687.02	WG	4	---	---	---	---	---	---	---	---	
F-R1	3830.02	DG-WG	2	---	---	---	---	---	---	---	---	x
F-R1	3952.04	DG-WG	2	---	---	---	---	---	---	---	---	x
F-R1	3954.00	WG	4	---	---	---	---	---	---	---	---	
F-R1	3956.01	DG-WG	2	BIGGER	---	---	---	---	---	---	---	
F-R1	3958.06	WG	4	---	---	---	---	---	---	---	---	
F-R1	3960.07	DG-WG	2	---	BIGGER	---	---	---	---	---	---	

Note: See next page for table 7.3 abbreviations interpretation.

7.2.7: Fluid inclusions stratigraphy abbreviations

Hydrocarbon type (HC)

This track interprets the bulk hydrocarbon response in terms of hydrocarbon type

NH = hydrocarbon response is below a global threshold and generally may be considered background.

DG = dry gas (species at least to C1 above a minimum value).

WG = wet gas (species at least to C5).

WG-GC = wet gas to gas condensate to oil (species at least to C9).

GC-Oil = gas-condensate to oil (species to at least C11).

It is emphasized that the actual trapped fluid may not correspond to the designated phase, due to the potential for multiple trapped fluids, and analytical limitations. However, in general, zones that are oily have liquids potential and those that are gassy are more likely to be gas dominated.

Carbon maximum (C-Max)

This track documents the maximum hydrocarbon number in the bulk extracts, using a combination of absolute response and a peak counting algorithm.

There will be a general correspondence between this track and the HC track, but it is included to provide more detail for a given hydrocarbon type.

PTP

This track documents the so called “proximity-to-pay” anomalies.

Anomalous concentrations of acetic acid +/- benzene are often associated with high Sw zones proximal to static oil or condensate accumulations (PTP Liquid).

Benzene anomalies can indicate similar zones in communication with gas (PTP Gas).

Anomalies typically indicate accumulations within a few kilometres distance.

Sulfur

This track indicates the presence of sulfur species, generally produced by bacteria sulphate reduction low temperature or thermo-chemical sulphate reduction at high temperature. Species include H₂S, COS, CS₂, SO₂ and/or SO₂+/-S₂ is distinguished with a unique colour, as it can be associated with porous, high Sw reservoir intervals.

7.3: General diagenetic sequence of the F-O gas field

Diagenesis in sedimentary environment involves the growth of cements in crystals in the pore space of rocks (McLimans, 1987). The process of diagenesis commonly controls the quality of petroleum reservoirs as in the case of Bredasdorp Basin. The diagenetic sequence of F-O gas field was developed based on the integration of various petrographic and geochemical analysis carried out on the core samples coupled with inputs from the geophysical log responses. The diagenetic features that occurred prior to deep burial stage(s) may no longer exist in these samples due to dissolution and replacement.

Detrital clay, authigenic quartz overgrowth and kaolinite are the main cause of porosity-permeability reduction. Pseudomatrix is also commonly developed by compaction of glauconite and clay clast with the growth of minor amount of locally developed carbonate cements. Figure 7.3 below represents the diagenetic model of the studied well within the F-O field. Mechanical infiltration of clay and compaction especially in the associated mudstone and siltstone expelled large volume of mineralized water, which migrated in the sandstone-rich section of the wells. This water has a significant role in the trend of sandstone diagenesis. Meteoric water also plays a significant role in the transport of dissolved ions which eventually cause dissolution of unstable grains in the diagenetic environment. In rift-related basin like the F-O field, gravity-driven meteoric water flow must have penetrated several kilometres into sedimentary basin. This water plays a considerable role in the leaching and circulation of ions (Si^{4+} , Al^{3+} , K^+ , Ca^{2+} , Mg^{2+} , Fe^{2+} , Fe^{3+}) down the basin, for the precipitation of different authigenic minerals.

Grain and cement dissolution started at the early diagenetic stage and it was observed across all the wells (Fig. 7.3) while feldspar disintegration started between early and mid-diagenetic stage. Increase in depth of burial, temperature and compacted towards the distal period of the early stage gave rise to mica formation from feldspar reaction followed by kaolinite precipitation post mica formation towards the end of the mid-diagenetic stage. Mineral concretions were noted in F-O4 reservoir sandstone possibly due to grain dissolution and its reaction with the transported pore/meteoric water towards the end of early-middle diagenetic stage. Syn-formation of glauconite with mica was evident in F-S1 reservoir interval while stylolite was evident across the study wells as compaction features that concentrated around quartz grains (Fig. 7.3).











DIAGENETIC EVENTS	EARLY DIAGENESIS	MIDDLE DIAGENESIS	LATE DIAGENESIS
Mechanical infiltration of detrital clays			
Mechanical compaction			
Grain/cement dissolution			
Quartz overgrowth			
Feldspar disintegration			
Mica formation			
Kaolinite precipitation			
Mineral concretions			
Glaucconite formation			
Stylolite formation			

Figure 7.3: Generalized diagenetic model of F-O gas field studied wells

CHAPTER EIGHT

8.0: Conclusions and recommendations

8.1: Introduction

The Valanginian age sandstone reservoir was delineated from six wells within the F-O field using an integrated approach involving geology, sedimentology, and geophysics with petrophysics. The geophysical log signatures in all six wells indicate good quality due to borehole conditions. Interpretation of the Valanginian age sandstones are based on detailed core descriptions which have been integrated with well logs and 2D seismic data to further understand the evolution of the study area. On the basis of core description, an average of six facies was delineated from the cored sections.

8.2: Conclusions

Facies and depositional environment analysis indicates that the Valanginian reservoir section in the studied wells was deposited in the upper shallow marine settings with some strings of deltaic settings. Distinct intervals record predominantly normal marine shoreface features, such as hummocky cross stratification in sandstones, diverse and robust bioturbation with normal marine traces, and glauconite. The lack of evidence for sub-aerial emergence (e.g roots paleosoils, desiccation cracks) indicates a permanently subaqueous environment. Fully marine salinity for the entire upper shallow marine is indicated by echinoids fragments. Foreset mud drapes reflect spring-neap tidal cyclicity and double mud drapes indicate sub-low tide settings.

Wireline log interpretation based on gamma ray, resistivity, density and neutron-porosity spikes and shapes with an input from conventional core analysis (poro-perm data) gives a clear indication of the reservoir zone within the shallow marine sandstones. The result generally shows tight heterogenous reservoir sandstones with low – fair porosity and permeability. The 2D seismic reflection profile interpretation reveals highly faulted Valanginian shallow marine sandstones beneath the drift-onset 1At1 unconformity. The evolution of the F-O field was controlled by extensional events owing to series of interpreted listric normal faults and rifting or graben generated possibly by the opening of the Atlantic. The F-O field stratigraphic sequence shares some characteristics with volcanic arc sequence. This includes in situ hemipelagic clastic sediments supplied from the continent and sediments carried

along the channel by turbidity current. The field is on a well defined structural high at the level of the regional drift-onset unconformity 1At1 with a structural trap classification for most of the interpreted profiles.

Multi-mineral analysis reveals the presence of quartz and kaolinite as the major porosity and permeability constraint respectively along with micaceous phases within the upper shallow marine sandstone. Three types of kaolinite have been recognized in the sandstone, (1) kaolinite growing in between expanded mica flakes; (2) vermiform kaolinite; and (3) euhedral kaolinite crystals forming matrix. An increase in temperature must have favoured the formation of kaolinite thermodynamically coupled with their in situ growth as a response to incipient diagenesis by K-feldspar dissolution. Furthermore, the presence of illite can be attributed to tectonically active periods inducing increased heat flows, severe fracturing and faulting, and possible cross-formational fluid flow. The distribution of quartz and feldspar overgrowth and crystals varied from formation to formation, beds to beds, within the same bed, and also within the same thin section. The increase in temperature leading to kaolinite formation must have caused the low-porosity observed, because low-porosity sandstone is found where the exposure to high temperature over time was above average. This can be attributed to permeability distribution and pore water saturation with regards to silicon, potassium and aluminium ions. Authigenic quartz and feldspar occurred in decreasing abundance from sandstone to siltstone to mudstones. Glauconite was pronouncedly observed within F-S1 upper shallow marine sandstone and it could be related to the diagenetic product of the observed micaceous phase during transformation due to increase in temperature. Stylolite was also observed concentrating around quartz grains serving as compactional features. The presence of illite, muscovite, and pyrite traces in stylolite materials must have enhanced the low quality of the reservoir sandstone observed. The upper shallow marine sandstones are geochemically classified as majorly litharenite having few F-O2 samples as subarkose with all F-O1 samples classified as sub-litharenite sandstone. However, the combination of different geochemical parameters reveals the immature nature of the contained sediments with minimum amount of weathering during erosion and deposition.

Fluid inclusion stratigraphic data reveals the presence of dry gas – wet gas – gas condensate with oil shows in F-O1. Most of the studied wells are more of wet gas, characterized by strong response of C₂ – C₅ with F-O1 well showing more of gas

condensate with oil shows (C₇ – C₁₁) based on the number of carbon atom present. In some cases sulfur species (characterized by the presence of H₂S, COS, CS₂ and SO₂) of probably thermal origin are identified while some log signatures reveal aromatic enriched sandstones possibly sensing nearby gas charges.

8.3: Main scientific contributions of the dissertation

Information about the reservoir quality, structural architecture and type of hydrocarbon present in the Bredasdorp basin is relatively scarce. Where available, they remain restricted for public benefit. The thesis has demonstrated the high potential for hydrocarbon production in the study area if necessary attention is given to the highlighted points in this dissertation. The thesis has revealed the cause for the poor quality of reservoirs in the study wells and has been able to ascertain the hydrocarbon type in the study wells. This will help the concerned oil and gas companies to be able to design proper production platform/methods for optimum oil and gas recovery to enhance the economic growth of the region and globally.

8.4: Recommendations

I strongly recommend that image log be run in future wells not only to enhance the depositional environment interpretation but also for studying orientation distributions (fractures) which are essential for modelling production behaviour. A dip-meter study is also recommended also to enhance facies model with a detailed net-sand mapping for all reservoirs. A possible investigation of poro-perm differences between bioturbated and non-bioturbated sands should also be considered.

A 3D seismic acquisition will be desirable in the F-O field to further enhance the clarity and understanding of the complexities and different structures apparent during 2D seismic interpretation.

8.5: Conference contributions

Fadipe, O.A, Donker, J.V.B., Carey, P.F., (2012). The application of fluid inclusion studies to decipher diagenesis and hydrocarbon type: insights from the Bredasdorp Basin, offshore South Africa. *Geofuture workshop Potsdam, Germany, Nov., 2012.*

Fadipe, O.A, P.F Carey, Donker, J.V.B, (2012). Facies, provenance and reservoir quality of the Valanginian age sandstone of the Bredasdorp Basin, South Africa. *AAPG International conference and exhibition, Singapore, 2012.*

REFERENCES

Adekola, S.A, Akinlua, A., Fadipe, O.A., (2009) Sequence stratigraphy and diagenetic alterations within the siliciclastic reservoir deposits of Orange Basin, Southwestern Africa margin. *11th SAGA Biennial Technical Meeting Exhibition*, Swaziland, pp. 552 - 557.

Ahmad, A.H.M., and Bhat, G.M., (2005) Petrofacies, provenance and diagenesis of the Dhosa sandstone member (Chari Formation) at Ler, Kachchh sub-basin, Western India. *Journal of Asian Earth Sciences*, **27**, 857 - 879.

Ahmed, W., (2008) Contrast in clay mineralogy and their effect on reservoir properties in sandstone formations. *Bulletin of Chemical Society of Ethiopia*, **1**, 41 - 65.

Akinyemi, S.A., Akinlua, A., Gitari, W.M., and Petrik, L.F., (2011) Mineralogy and mobility patterns of chemical species in weathered coal fly ash. *Energy Sources, Part A*, **33**, 768 – 784.

Al-Ramadan, K., Morad, S., Proust, J.N., and Al-Asam, I., (2005) Distribution of diagenetic alterations in siliciclastic shoreface deposits within a sequence stratigraphic framework: evidence from the Upper Jurassic, Boulonnais, NW France. *Journal of Sedimentary Research*, **75**, 943 - 959.

Armstrong-Altrin, J.S., Yong I.L., Lee., Surendra, Verma, P., and Ramasamy, S., (2004) Geochemistry of sandstones from the upper Miocene Kudankulam formation, Southern India: Implication for provenance, weathering and tectonic setting. *Journal of Sedimentary Research*, **74**, 285 – 297.

Arostegui, J., Irabien, M.J., Nieto, F., Sanguesa, J., and Zuluaga, M.C., (2001) Microtextures and origin of the muscovite-kaolinite intergrowths in sandstones of the Utrillas Formation, Basque Cantabrian Basin, Spain. *Clays and Clay Minerals*, **49**, 529 - 539.

Barker, P., Fontes, J.C., Gasse, F., and Druart, J.C. (1994) Experiment dissolution of diatom silica in concentrated salt solutions and implications for paleoenvironmental reconstruction. *Limnology Oceanography*, **39**, 99 - 110.

Baker, J. C., P. J. Havord, K. R. Martin, and A. R. Ghori, (2002) Diagenesis and petrophysics of the Early Permian Moogooloo sandstone, Southern Carnarvon Basin, Western Australia: *AAPG Bulletin*, **84**, pp. 250-265.

Baldwin, B.A., (1993) Immobile water determination in shaly sandstone. SCA Conference paper no: 9314.

Barclay, S. A. Worden, R. H Parnell, J. Hall, D. L. and Sterner, S. M. (2000) Assessment of fluid ontacts and compartmentalization in sandstone reservoirs Using Fluid Inclusions: An Example from the Magnus Oil Field, North Sea. *AAPG Bulletin*, **84**, No. 4 P. 489-504.

Baron, M., and Parnell, J., (2006) Relationships between stylolites and cementation in sandstone reservoirs: Examples from the North Sea, U.K. and East Greenland. *Sedimentary Geology*, **194**, 17 - 35.

Barron, B.J., (1974) The use of coexisting calcite-ankerite solid solutions as geothermometer. *Contribution to Mineralogy and Petrology*, **47**, 77-80, © by Springer-Verlag

Barshad, I., (1966) The effect of a variation in precipitation on the nature of clay mineral formation in soils from acid and basic igneous rocks. In: *Proceedings of the International Clay Conference*, **2**, 167-173.

Basan, P.B., (ed.) (1978) Trace Fossils Concepts. *Society of Sedimentary Geology (SEPM) Short Course No. 5*, 142 - 143.

Basan, P.B., (ed.) 1(978) Trace Fossils Concepts, SEPM Short Course No. 5. pp. 142 – 143.

Bassoioni, Z., (1994). Theory, measurement, and interpretation of well logs. *SPE Text book series 4*, pp. 92 – 339.

Bateman, R. (1985) Open hole log analysis and formation evaluation: Boston International Human Resources Development Corporation pp. 647.

Bauluz, B., Mayayo, M.J., Yuste, A., and Gonzalez Lopez, J.M., (2008). Genesis of kaolinite from Albian sedimentary deposits of the Iberian Range (NE Spain): analysis by XRD, SEM and TEM. *Clay Minerals*, **43**, 459 - 475.

Bavinton, O.A., Taylor, S.R., (1980) Rare-earth element geochemistry of Archean meta-sedimentary rocks from Kambalda, Western Australia. *Geochimica et Cosmochimica Acta*, **44**, 639 - 648.

Beauchemin, D. (2008) Inductively Coupled Plasma Mass Spectrometry. *Analytical Chemistry*, **80**, 4455 - 4486.

Beaufort D., Cassagnabère A., Petit S., Lanson B., Berger G., Lacharpagne J.C. and Johansen H. (1998) Kaolinite-to-dickite conversion series in sandstone reservoirs. *Clay Minerals*, **33**, 297 - 316.

Berner, R.A. (1984) Sedimentary pyrite formation: an update. *Geochimica et Cosmochimica Acta*, **47**, pp. 605 – 615.

Bhatia, M.R., (1983) Plate tectonics and geochemical composition of sandstones. *Journal of Geology*, **91**, 611 - 627.

Bhatia, M.R., Crook, K.A.W., (1986) Trace element characteristics of graywackes and tectonic setting discrimination of Sedimentary Basins. *Contributions to Mineralogy and Petrology*, **92**, 181 - 193.

BjØlykke, K., Aagaard, P., Dypvik, H., Hasting, D.S., and Harper, A.S. (1986) Diagenesis and reservoir properties of Jurassic sandstones from Haltenbanken, offshore mid Norway: in Mica alteration reactions in Jurassic reservoir sandstones from the Haltenbanken area, Offshore Norway. *Clay and Clay Minerals*, **38**, 584 - 590.

BjØlykke, K., Elverhoi, A., and Malm, O., (1979) Diagenesis in mesozoic sandstones from Spitzbergen and the North Sea: a comparison. *Geologische Rundschau*, **68**, 1152 - 1171.

Blanc, E. J.-P. (1998) Soft-sediment deformation structures interpreted as seismites in the uppermost Aptian to lowermost Albian-transgressive deposits of the Chihuahua basin (Mexico). *International Journal of Earth Science/ Geologische Rundschau* **86**, 875 - 883.

Blanche, J.B., and Whitaker, J.H.MCD., (1978) Diagenesis of part of the Brent sand formation (Middle Jurassic) of the northern North Sea Basin. *Journal of Geological Society of London*, **135**, 73 - 82.

Bloch, S., (1994) Secondary porosity in sandstones: significance, origin, relationship to subaerial unconformities, and effect on predrill reservoir quality prediction. In Wilson, M.D. ed., reservoir quality assessment and prediction in clastic rocks: *Society of Sedimentary Geology (SEPM) short course* **30**, 137 - 159.

Bloch, S., and Frank, S.G., (1993) Preservation of shallow plagioclase dissolution porosity during burial and aluminium mass balance: *American Association of Petroleum Geologist (AAPG) Bulletin*, **77**, 1488 - 501.

Broad, D., (2004) South Africa activities and opportunities, an unpublished Power Point Presentation to PetroChina.

Broad, D.S. (2000) Petroleum exploration offshore South Africa: *Journal of African Earth Science*, **31(1)**, pp. 50 - 51.

Brown, L.F. Jr., Benson, J.M., Brink, G.J., Doherty, S., Jollands, A., Jungslager, E.H.A., Keenan, J.H.G., Muntingh, A. and Van Wyk, N.J.S (1996) Sequence stratigraphy in offshore South Africa divergent basins. An atlas on exploration for Cretaceous Lowstand traps by Soekor (Pty) Ltd *American Association of Petroleum Geologist Studies in Geology*, **41**, 184.

Burruss, R.C., (1981) Hydrocarbon fluid inclusions in studies of sedimentary diagenesis, in Hollister, L. S., and Crawford, M. L., eds., MAC short course in fluid

inclusions: Applications to petrology: Toronto, *Mineralogical Association of Canada*, 138 - 156.

Cannon, D. E., and G. R. Coates, (1990) Applying Mineral Knowledge to Standard Log Clastic Reservoirs: *The Log Analyst*, **22**, pp. 3-16.

Catuneanu, O., (2002) Sequence stratigraphy of clastic systems: concepts, merits, and pitfalls, *Journal of African Earth Sciences*, **35**, 1 - 43.

Cazier, C.E., Hein, M., and Pemberton, G., (2011) Sedimentology of early Aptian reservoir, Dunga field, Kazakhstan. *American Association of Petroleum Geologist Search and Discovery article # 50394*.

Cody, J., Youn, S., Riddy, A. and Gittins, S. (2001) Implication of Reservoir “Compartments” on the design and execution of Christina Lake Thermal Recovery Project. *PanCanadian Resources*, 150 - 9th Avenue, Calgary AB.

Cookenboo H.O. and Bustin R.M (1999) Pore water evolution in sandstones of the Groundhog Coalfield, northern Bowser Basin, British Columbia. *Sedimentary Geology*, **123**, 129 – 146.

Cox, R., Lowe, D.R., Cullers, R. L., (1995) The influence of sediment recycling and basement composition on evolution of mudrock chemistry in South-western United States. *Geochimica et Cosmochimica Acta*, **59**, 2919 - 2940.

Crain, E.R. (2004) Crain’s Petrophysical Handbook: Canada, Spectrum 2000 Mindware, 3rd Millennium Edition. URL: <http://www.spec2000.net/lcmain.htm>
Accessed on the 24th September 2010.

Crook, K.A.W., (1974) Lithogenesis and geotectonics: the significance of compositional variation in flysch arenites (greywackes). *Soc. Econ. Paleont. Mineral Spec. Publ. No. 19*, 304 - 310.

Cullers, R.L., (2000) The Geochemistry of Shales, Siltstones, and Sandstones of Pennsylvanian–Permian Age, Colorado, USA: Implications for Provenance and Metamorphic Studies. *Lithos*, **51**, 181 - 203.

Culler, R.L., Basu, A., and Stuttner, L.J., (1988) Geochemical signature of provenance in sand-size material in soils and stream sediments near the Tobacco root batholith, Montana, USA: *Chemical Geology*, **70**, 335 - 348.

Cullers, R.L., Podkovyrov, V.N., (2000) Geochemistry of the Mesoproterozoic Lakhanda sandstones in South-eastern Yakutia, Russia: Implications for Mineralogical and Provenance Control, and Recycling. *Precambrian Research*, **104**, 77 - 93.

Dingle, R.V, Siesser, W.G & Newton, A.R (1983) Mesozoic and Tertiary Geology of Southern African. A.A. Balkema/Rotterdam. pp. 99 - 106.

Dionex, (1998) Application notes on conductivity detection. Dionex DX-120 Ion Chromatography Operator's Manual, Dionex. Overview of principles behind conductivity and concentration relation of ionic solutions, as well as description of auto self-regenerating suppression module, and eluent composition for anion analysis.

Duque-Caro, H., (1984) Structural style, diapirism and accretionary episodes of Sinú-San Jacinto Terrane, South Western Caribbean border: *Geological Society of America, Memoir* **162**, 303 - 316.

Douglas, J.C. (1987) Subsurface facies analysis. Geological Survey of Canada, 3303 – 33rd St. N.W. Calgary, Alberta T2L 2A7.

Douglas, S., McDowell & Paces, J.B., (1985) Carbonate alteration minerals in the Salton Sea geothermal system, California, USA. *Mineralogical Magazine*, Vol. 49, pp. 469 - 479.

Dove, P.M., and Nix, C.J., (1997) The influence of the alkaline earth cations, magnesium, calcium and barium on the dissolution kinetics of quartz. *Geochimica et Cosmochimica Acta*, **61**, 3329 - 3340.

Dove, P.M. and Elston, S.F., (1992) Dissolution kinetics of quartz in sodium chloride solutions: Analysis of existing data and rate model for 25 °C. *Geochimica et Cosmochimica. Acta*, **56**, 4147 - 4156.

Dove, P.M., and Rimstidt, J.D., (1994) Silica-water interactions. In Dove, P.M., and Christopher, J.N., The influence of the alkaline earth cations, magnesium, calcium and barium on the dissolution kinetics of quartz. *Geochimica et Cosmochimica Acta*, **61**, 3329 - 3340.

Ehrenberg S.N. (1991) Kaolinized, potassium-leached zones at the contacts of the Garn formation, Haltenbanken, mid-Norwegian continental shelf. *Marine Petroleum Geology*, **8**, 250 - 269.

Ehrenberg, S. N., Aaraard, P., Wilson, M. J., Fraser, A. R. and Duthie, D.M.L., (1993) Depth-dependent transition of kaolinite to Dickite in sandstones of the Norwegian Continental Shelf. *Clay Minerals*, **28**, 325 - 352.

Elliott, T., (1986) Siliciclastic shorelines. In Reading, H.G. (ed.): *Sedimentary Environments and Facies*. 2nd edn. *Blackwell Scientific Publications*, Oxford. pp. 158 - 188.

Embry, A.F., Johannessen, E.P., (1992) T-R sequence stratigraphy, facies analysis and reservoir distribution in the uppermost Triassic- Lower Jurassic succession, western Sverdrup Basin, Arctic Canada. In: Vorren, T.O., Bergsager, E., Dahl-Stamnes, O.A., Holter, E., Johansen, B., Lie, E., Lund, T.B. (Eds.), *Arctic Geology and Petroleum Potential*, (Spec. Publication). *Norwegian Petroleum Society (NPF)*, **2**, 121 - 146.

Emery, D., and Robinson, A.G., eds., (1993) Inorganic geochemistry: applications to petroleum geology: *London Blackwell Scientific Publications*, p. 254.

Emery, D., Myers, K.J., and Young, R., (1990) Ancient subaerial exposure and freshwater leaching in sandstones: *Geology* **18**, 1178 - 1181.

Fadipe, O.A., Carey, P.F., Akinlua, A., Adekola, S.A., (2011) Provenance, diagenesis and reservoir quality of the Lower Cretaceous sandstones of the Orange Basin, South Africa. *South African Journal of Geology*, **114**, 433 - 88.

Frewin, J., Grobber, N., & Feddersen, J. (2000) The Oribi and Oryx oil fields: geological characterisation of a deep-marine channel-lobe system, Block 9,

Bredasdorp Basin, offshore South Africa. *Journal of African Earth Sciences*, **31(1)**, 22.

Fritz, J. S. (2005) Factors affecting selectivity in ion chromatography. *Journal of Chromatography A*, **1085**, 8 - 17.

Frost, E. J., and W. H. Fertl, (1981) Integrated core and log analysis concepts in shaly clastic reservoirs: *The Log Analyst*, **22**, pp. 3-16.

Garcia, A.J.V., Morad, S., De Ros, L.F., Al-Aasm, I.S., (1998) Palaeogeographical, palaeoclimatic and burial history control on the diagenetic evolution of Reservoir sandstones: evidence from Lower Cretaceous Serraria sandstones in Sergip-Alagoas Basin, NE Brazil. In Morad, S. (Ed.), carbonate cementation in sandstones. *International Association of Sedimentologists*, Special Publication, **26**, 107 - 140.

Gaupp R., Matter A., Platt J., Ramseyer K. & Walzebuck J. (1993) Diagenesis and fluid evolution of a deeply buried Permian (Rotliegende) gas reservoir, Northwest Germany. *American Association of Petroleum Geologists Bulletin*, **77**, 1111 - 1128.

Gerhard, E., (2000). Sedimentary Basins - Evolution, facies and sediment budget. Springer-Verlag, New York.

Geiger, W. M. and Raynor, M. W. (2009): ICP-MS: A Universally Sensitive GC Detection Method for Specialty and Electronic Gas Analysis. ICP-MS: Available at <http://spectroscopyonline.findanalytichem.com/spectroscopy/ICP-MS/ICP-MS-AUniversally-Sensitive-GC-Detection-Method/ArticleStandard/Article/detail>.

Accessed on 18th, November 2010.

Giles, M.R., and Marshall, J.D., (1986) Constraints on the development of secondary porosity in the sub-surface: re-evaluation of process: *Marine and Petroleum Geology*, **7**, 378 - 397.

Giordano, T.H., (2002) Transport of Pb and Zn by carboxylate complexes in basinal ore fluids and related petroleum-field brines at 100 °C: the influence of pH and oxygen fugacity. *Geochemical Transactions*. **8**, 56 - 72.

Glasmann, J.R., Clark, R.A., Larter, S., Briedis, N.A., and Lundegard, P.D., (1989) Diagenesis and hydrocarbon accumulation, Brent Sandstone (Jurassic), Bergen area, North Sea: *American Association of Petroleum Geologists Bulletin*, **73**, 1341 – 1360.

Gluyas, J.G., Robinson, A.G., and Primmer, T.P., (1997) Rotliegend sandstone diagenesis: a tale of two waters: In Hendry, J., Carey, P., Parnell, J., Ruffel, A., and Worden, R., eds., *Geofluids II 1997*: Belfast, the Queen's University of Belfast, pp. 291 – 294.

Granberry, R.J., Jenkins, R.E., and Bush, D.C., (1968) Grain density values of cores from some Gulf coast formations and their importance in formation evaluation, *Society of Professional Well Log Analyst (SPWLA) 9th annual logging symposium*, pp. 1 - 18.

Guest, K., (1990) The Use of Core-derived Quantitative Mineralogical Data to improve Formation Evaluation: European Core Analysis Symposium, pp. 29 -187.

Gunther, D., Audetat, A., Frischknecht, R., and Heinrich, C.A., (1998) Quantitative analysis of major, minor and trace elements in fluid inclusions using laser ablation-inductively coupled plasma mass spectrometry. *Journal of Analytical Atomic Spectrometry*, **13**, 263 - 270.

Haddad, P. R. (2004) Ion chromatography. *Analytical and Bioanalytical Chemistry*, **379**, 341 – 343.

Haddad, P. R., Nesterenko, P. N., Buchberger, W. (2008) Recent developments and emerging directions in ion chromatography. *Journal of Chromatography A*, **1184**, 456 - 473.

Hadley, S., Hall, D., Sterner, M., and Wells, S., (1997) Hydrocarbon pay delineation and product characterization with fluid inclusions: examples from East Coast Canada and Western Canada Sedimentary Basin. In *Site* (Canadian Well Logging Society) (**1**), 2 - 4.

Hall, J.S., Mozley, P., Davis, J.M., Roy, N.D., (2004) Environments of formation and controls on spatial distribution of calcite cementation in Plio-Pleistocene fluvial deposits, New Mexico, USA. *Journal of Sedimentary Research*, **74**, 643 - 653.

Hancock, N.J. (1978) Possible causes of Rotliegend sandstone diagenesis in northern West Germany. *Journal of the Geological Society*, London, **135**, 35 - 40.

Hancock, N.J. and Taylor, A.M., (1978) Clay mineral diagenesis and oil migration in the Middle Jurassic Brent sand formation. *Journal of the Geological Society*, London, **135**, pp. 69 - 72.

Haq, B.U., Hardenbol, J. and Vail, P.R., (1988) Mesozoic and Cenozoic chronostratigraphy and eustatic cycles of sea-level change. In: The geology of South Africa edited by M.R Johnson, C.R Anhaesser and R.J Thomas. 2006.

Harris, N.B., (1992) Burial diagenesis of Brent sandstone: a study of statford, hutton and Lyell fields. In: Morton, A.C., Haszeldine, R.S., Giles, M.R., Brown, S. (Eds.), Geology of the Brent Group, *Geological Society, London*. Special Publications, **61**, 351 - 376.

Harris, P.M., Kendall, C.G.S.C. and Lerche, I., (1985) Carbonate cementation: a brief review. In: Molenaar, N. Zijlstra, J.J.P. Differential early diagenetic low-Mg calcite cementation and rhythmic hardground development in Campanian-Maastichtian chalk. *Sedimentary Geology*, **109**, 261 - 281.

Harwood, G., (1988) Microscopic Techniques II: Principles of Sedimentary Petrography, in M. Tucker, ed., *Techniques in Sedimentology*: Oxford, Blackwell, pp. 108 - 173.

Hald, M.T., and Larese, R.E., (1973) The significance of the solution of feldspar in porosity development. *Journal of Sedimentary Petrology*, **43**, 458 - 460.

Hean C.L., Ebanks W. J., Tye R.S. & Ranganathan V., (1984) Geological factors influencing reservoir performance of the Hartzog Draw Field, Wyoming. *Journal of Petroleum Technology*, 1335 - 344.

Hearn, C.L., Ebanks, W.J., Tye, R.S. and Ranganathan, V., (1984) Geological factors influencing reservoir performance of the Hartzog Draw Field, Wyoming. *Journal of Petroleum Technology*, August, pp. 1335 - 1344.

Hendry, J.P., Wilkinson, M., Fallick, A.E., Haszeldine, S.R., (2000) Ankerite cementation in deeply buried Jurassic sandstone reservoirs of the Central North Sea. *Journal of Sedimentary Research*, **70**, 227 - 239.

Helland-Hansen, W., Martinsen, O.J., (1996) Shoreline trajectories and sequences: description of variable depositional-dip scenarios. *Journal of Sedimentary Research*, **66** (4), pp. 670 - 688.

Herron, M.M., (1988) Geochemical classification of terrigenous sands and shales from core or log data. *Journal of Sedimentary Petrology*, **58**, 820–829.

Herron, S.L., and Herron, M.M., (2000) Application of nuclear spectroscopy logs to the derivation of formation matrix density,” 41st Annual logging symposium of the *Society of Professional Well Log Analyst* held in Dallas, Texas, June 4 - 7.

Hogg, A.J.C., Hamilton, P.J., and Macintyre, R.M., (1993) Mapping diagenetic fluid flow within a reservoir: K-Ar dating in the Alwyn area (UK North Sea): *Marine and Petroleum Geology*, **10**, 279 – 294.

House, W.A., (1994) The role of surface complexation in the dissolution kinetics of silica: Effects of monovalent and divalent ions at 25 °C. *Journal of Colloid Interface Science*, **163**, 379 - 390.

Howard, J.J., (1992) Influence of authigenic clay minerals on permeability. In: Hunt, D., and Tucker, M.E., (1992). Stranded parasequence and the forced regressive wedge systems tract: deposition during base-level fall, *Sedimentary Geology*, **81**, 1 - 9.

Hudson, M.R., (1997) Structural geology of French peak accommodation zone, Nevada test site, Southwestern Nevada: U.S. Department of Interior, U.S. Geological Survey Open-file report.

Interpretation: *SPWLA 31st Annual Logging Symposium*, pp. 6-24.

Hudson, M.R., (1998) Structural geology of French peak accommodation zone, Nevada: *Geological Society of America Bulletin*, **104**, 581 - 594.

Hunt, D., and Tucker, M.E. (1995) Stranded parasequence and the forced regressive wedge systems tract: deposition during base-level fall-reply, *Sedimentary Geology*, **95**, 147 - 160.

Hurst, A., (1987) problems of reservoir characterisation in some North Sea sandstone reservoirs solved by the application of microscale geological data, North Sea oil and gas reservoirs, *Graham and Trotman*, 153 - 167.

Hurst A., (1984) The role of sedimentary facies in the control of clay mineral diagenesis in sandstones: examples from the North Sea. *Clay Minerals Society. Annual Meeting, Baton Rouge*, abstracts, 64.

Hurst, A., and Irwin, H., (1982) Geologic modelling of clay diagenesis in sandstones, *Clay minerals*, **17**, 5 - 22.

Hurst, A., and Nadeau, P.H., (1995) Clay microporosity in reservoir sandstones: an application of quantitative electron microscopy in petrophysical evaluation. *American Association of Petroleum Geologists*, **79**, 563 - 573.

Illife, J.E., Robertson, A.G., Ward, G.H.F., Wynn, C., Pead, S.D.M., & Cameron, N., (1999) The importance of fluid pressure and migration to hydrocarbon prospectivity of the Faero-Shetland White Zone. In The use of integrated fluid inclusion studies in constraining oil charges history and reservoir compartmentation: examples from the Jeanne d'Arc Basin, Offshore Newfoundland. *Marine and Petroleum Geology*, **18**, (2001), 535 - 549.

Jahasz, I., (1990) Core Analysis – Opportunity and Challenges in the 1990's: *Europe Core Analysis Symposium*, pp. 1 - 15.

Jeon, Y.M., and Sohn, Y.K., (2003) Sedimentary characteristics and stratigraphic implications of the Kusandong Tuff, Cretaceous Gyeonsang Basin, Korea. *Geoscience Journal*, **7**, 53 - 64.

Jikelo, N.A. (2000) The natural gas resources of southern Africa: *Journal of African Earth Sciences*, **31(1)**, 34.

Johnsson, M. J., (1993) The system controlling the composition of clastic sediments. In: Johnsson, M. J., Basu, A., eds., processes controlling the composition of clastic Sediments. *Special Paper—Geological Society of American*, **284**, pp. 1 - 19.

Johnson, H.D. and Baldwin, C.T. (1996) Shallow clastic seas. In: H.G. Reading (ed.), *Sedimentary Environments: Processes, Facies and Stratigraphy*, 3rd edition, Blackwell Science, Oxford, pp. 232 - 280.

Johnsson, M.J., (2000) Tectonic assembly of East-Central Alaska: Evidence from Cretaceous-Tertiary sandstones of Kandik river terrane. *Geological Society of American Bulletin*, **112**, 1023 - 1042.

Johnsson, M.J., Stallard, R.F., Meade, R.H., (1988) First-cycle quartz arenites in the Orinoco river Basin, Venezuela and Colombia. *Journal of Geology*, **96**, 263 - 277.

Jone, B.F., Vandenburg, A.S., Truesdell, A.H., Rettig, S.L., (1969) Interstitial brine playa sediment. *Chemical Society*, **4**, 253 - 262.

Ketzer, J.M.M. (2002) Diagenesis and sequence stratigraphy: An integrated Approach and Constrain Evolution of Reservoir Quality in Sandstone. Dissertation for the Doctor of Philosophy in Mineral Chemistry, Petrology and Tectonics at the Department of Earth Sciences, Uppsala University Sweden.

Knarud, R. and Bergan, M., (1990) Diagenetic history of Upper Triassic-Lower Jurassic alluvial sandstones and mudstones of the Lunde and Staffjord Formations, Snorre Field, Norwegian North Sea [abstract]. In: 13th International Sedimentological Congress, Nottingham, UK, 276 - 277.

Kierkegaard, T., (1998) Diagenesis and reservoir properties of Campanian–Paleocene sandstones in the GANT#1 well, western Nuussuaq, central West Greenland. *Geology of Green Land Survey Bulletin*. **31**, 31 - 34.

King, G. E., (1992) Formation clays: Are they really a problem in production. In: Houseknecht, D. W. and Pittman, E. D., eds., Origin, diagenesis and petrophysics of clay minerals in sandstones, Oklahoma, *Society of Sedimentary Geology (SEPM)* special publication no. **47**, 264 – 272.

Kupecz, J.A., and Land, L.S., (1994) Progressive recrystallization and stabilization of early-stage dolomite: Lower Ordovician Ellenburger Group, West Texas, in Purser, B., Tucker, M., and Zenger, D., eds., Dolomite, a volume in honour of Dolomieu: *International Association of Sedimentologists (IAS)* Special Publication, **21**, 255 - 279.

Kupecz, J.A., Gluyas, J., and Bloch, S., (1997) Reservoir quality prediction in sandstones and carbonates. *American Association of Petroleum Geologists (AAPG)* *Memoir* **69**, vii – xiii.

Lambert-Aikhiobare, D.O., and Shaw, H.F., (1982) Significance of clays in the petroleum geology of the Niger Delta. *Clay Minerals*, **17**, 91 - 103.

Lewis, D.W., and McConchie, D., (1994). Analytical sedimentology: New York, Chapman Hall, pp. 197.

Li, S., Du, Y., Zhang, Z., and Wu, J., (2008) Earthquake-related sot-sediment deformation structures in Palaeogene on the continental shelf of the East China Sea. *Frontiers of Earth Science China*, **2 (2)**, 177 - 186.

Lima, R.D., and De Ros, L.F., (2002) The role of depositional setting and diagenesis on the Reservoir quality of Devonian sandstones from the Solimoes Basin, Brazilian Amazonia. *Marine and Petroleum Geology*, **19**, 1053 - 055.

Liu, C. W., Lin, K. H., Y. M., and Kuo, Y. M. (2003) Application of factor analysis in the assessment of ground water quality in the Blackfoot disease area in *Taiwan*. *Sci. Total Environ*, **313**, 77 - 89.

MacAulay, G.E., Burley, S.D. and Johnes, L.H., (1993) Silicate mineral authigenesis in the Hutton and NW Hutton fields: implications for sub-surface

porosity development. Pp. 1377 - 1393 in: Petroleum Geology of Northwest Europe (J.R. Parker, editor). *The Geological Society, London*.

Made, B., Ben Baccar, M., and Fritz, B., (1994) Geomechanical modeling of diagenetic reactions: a thermodynamic and kinetic approach. *Mineralogy Magazine*, **58A**, 549 - 50.

Massart, D. L., Vandeginste, B. G. M., Deming, S. N., Michotte, Y., and Kaufman, L. (1988) Chemometrics, A Textbook. Amsterdam: Elsevier.

McAloon, W., Barton, K., Egan, J., and Frewin, J. (2000) Pre-development characterisation of a marginal deep-marine channel/lobe-system reservoir: block 9, the Bredasdorp Basin, offshore South Africa. *Journal of African Earth Sciences*, **31**, 47.

McBride, E.F., (1989) Quartz cementation in sandstones – a review. Earth Science reviews. In El-Ghali, M.A.K., Morad, S., Mansurbeg, H., Ajdanlijsky, A.A.C., Ogle, N., Al-Aasm, I., and Sirat, M.: Distribution of diagenetic alterations within depositional facies and sequence stratigraphic framework of fluvial sandstones: evidence from the Petrohan terrigenous group, lower Triassic, NW Bulgaria. *Marine and Petroleum Geology*, **xxx**, 10.

McHardy W.J., Wilson M.J. and Tart J.M., (1982) Electron microscope and X-ray diffraction studies of filamentous illite clay from sandstones of the Magnus Field. *Clay Mineralogy*, **17**, 23 - 29.

McLennan, S.M., Hemming, S., McDaniel, D.K., and Hanson, G.N., (1993) Geochemical approaches to sedimentation, provenance, and tectonics. In: Johnson, M.J., Basu, A., (Eds.), processes controlling the composition of clastic sediments. *Geological Society of America Special Paper*. **284**, 21 - 40.

McLennan, S.M., Taylor, S.R., Eriksson, K.A., (1983). Geochemistry of Archean shales from the Pilbara Supergroup, Western Australia. *Geochimica et Cosmochimica Acta*, Vol. 47, pp. 1211 – 1222.

McLennan, S. M., Taylor, S.R., McCulloch, M.T., (1990) Geochemistry and Nd-Sr isotopic composition of deep-sea turbidites: Crustal evolution and plate tectonic associations. *Geochimica et Cosmochimica Acta*, **54**, 2014 - 050.

McLimans, R.K., (1987) The application of fluid inclusions to migration of oil and diagenesis in petroleum reservoirs. *Applied Geochemistry*, **2**, 585 - 603.

Meadows N.S., Trueblood, S.P., Hardman, M., and Cowan, G., (1997) Petroleum Geology of the Irish Sea and Adjacent Areas. *Geological Society Special Publication No 24*, 447.

Milliken, K.L., (1989) Petrography and composition of authigenic feldspars, Oligocene Frio formation, South Texas. *Journal of Sedimentary Petrology*, **59**, 361 - 374.

Milliken, K.L., (1992) Chemical behaviour of detrital feldspar in mudrocks versus sandstones, Frio Formation (Oligocene), South Texas: *Journal of Sedimentary Petrology*, **62**, 790 - 801.

Milliken, K.L., McBride and Land, L.S., (1989) Numerical assessment of dissolution versus replacement in the subsurface destruction of detrital feldspar, Oligocene Fri Formation, South Texas; *Journal of Sedimentary Petrology*, **59**, pp. 740 - 757.

Mitchell, S.F, James, S.A., and Brown, I.C., (2006) A late Pleistocene progradational clastic shoreface succession in Jamaica: Implications for the preservation potential of the echinoid *Lethaia*. *Lethaia*, **39**, 321 - 327.

Moody, G.B (1961) Petroleum Exploration Handbook, A practical Manual Summarizing the application of Earth Sciences to Petroleum Exploration. 1st edition, McGraw-Hill Book Company, Inc.

Moore, D.M. and Reynolds, R. C. (1989) X-ray diffraction and the identification and analysis of Clay Minerals, Oxford University Press, New York.

Morad, S., Bergan, M., Knarud, R., Nystuen, J.P., (1990) Albitization of detrital plagioclase in Triassic reservoir sandstones from the Snorre Field, Norwegian North Sea. *Journal of Sedimentary Petrology*, **60**, 411 – 425.

Morris, K.A. and Shepperd, (1982) The role of clay minerals in influencing porosity and permeability characteristics in the Bridport sands of Wytch farm, Dorset: *Clay Minerals*, **17**, 41 - 54.

Morse, J.W., and Mackenzie, F.T., (1990) Geochemistry of sedimentary carbonates. Elsevier science publisher B.V. Amsterdam, Netherlands.

Mudaly, K., Turner, J., Escorcía, F., and Higgs, R., (2009) F-O gas field, Offshore South Africa - From Integrated approach to field development. *American Association of Petroleum Geologist (AAPG) Search and Discovery article # 20070*.

Nagarajan, R., Madhavaraju, J., Negenda, R., Armstrong-Altrin, J.S., and Moutte, J., (2007) Geochemistry of Neoproterozoic shales of the Rabanpalli Formation, Bhima Basin, Northern Karnataka, southern India: implication for provenance and palaeoecological conditions. *Revista Mexicana de Ciencias Geológicas*, **24**, 150 - 160.

Nesbitt, H.W., and Young, G.M., (1982) Early Proterozoic climate and plate motions inferred from major element chemistry of lutites: *Nature*, **299**, 715–717.

Nesbitt, H.W., and Young, G.M., (1996) Petrogenesis of sediments in the absence of chemical weathering effects abrasion and sorting on bulk composition and mineralogy. *Sedimentology*, **105**, 173 - 191.

Nicolaas, M., Jolanta, C., Salulius, S., and John, C., (2008) Lack of inhibiting effect of oil emplacement on quartz cementation: Evidence from Cambrian reservoir sandstones, Paleozoic Baltic Basin. *The Geological Society of America Bulletin*.

Odin, G.S., Matter, A., (1981) De glauconiarum origine. *Sedimentology*, **28**, 611 - 641.

Odom, I.E., (1984) Glauconite and celadonite minerals. In Evolution patterns of glaucony maturity: A mineralogical and geochemical approach. *Deep-sea Research II*, **54**, 1364 - 1374.

Olajide, O., (2005) The Petrophysical Analysis and Evaluation of Hydrocarbon Potential of Sandstone Units in the Bredasdorp Central Basin. (Unpublished Thesis, University of the Western Cape, South Africa.

Osborne, M., Haszeldine, R.S. and Fallick, A.E., (1994) Variation in kaolinite morphology with growth temperature in isotopically mixed pore-fluids, Brent group, UK North Sea. *Clay Minerals*, **29**, 591 - 608.

Osborne, M. and Haszeldine, R.S. (1993) Evidence for resetting of fluid inclusion temperatures from quartz cements in oilfields. *Marine and Petroleum Geology*, **10**, 271 - 278.

Pallat, N., Wilson, M.J., and McHardy, W.J., (1984) The relationship between permeability and the morphology of diagenetic illite in reservoir rocks: *Journal of Petroleum Technology*, **14**, 2225 - 2227, France.

Parnell, J., Middleton, D., Houghan, C., Hall, D., (2001) The use of integrated fluid inclusion studies in constraining oil charge history and reservoir compartmentation: examples from the Jeanne d'Arc Basin, offshore Newfoundland. *Marine and Petroleum Geology* **18**, 535 - 549.

Parnell, J., Carey, P.F., Green, P., & Duncan, W., (1999) Hydrocarbon migration history West of Shetland: integrated fluid inclusion and fission track studies. In A.J. Fleet and Boldy, Petroleum geology of Northwest Europe: Proceedings of the fifth conference. *Geological Society of London*, 613 - 625

Parnell, J., Carey, P.E., & Duncan, W., (1998) History of hydrocarbon charge on the Atlantic Margin: evidence from fluid migration in the Timor Sea: A key control on thermal and diagenetic histories. *Australian Petroleum Production and Exploration Journal (APPEA Journal)*, **36**, 399 - 426.

Penney, R.K., and Looi, S.Y., (1996) Understanding effective and total porosity: the key to optimising Mineralogical evaluations: *Australian Petroleum Production and Exploration Journal (APPEA Journal)*, 36, 284 - 292.

Petroleum Agency SA (2003/2004/2005/2006/2007) Petroleum exploration information and opportunities: Petroleum Agency Brochure.

Pettijohn, F.J., Potter, P.E., Siever, R., (1987) Sand and sandstone. Springer, New York.

Pettijohn, F.J., Edwin, P., Siever, R., (1972) Sand and Sandstone diagenesis: recent and ancient- Google Book pp. 462. Available Online at <http://books.google.co.za/books>

Pittman, E.D., Larese, R.E., & Heald, M.T., (1992) Clay coats: Occurrence and relevance to preservation of porosity in sandstones. In D. W. Houseknecht, & E. D. Pittman (Eds.), Origin, diagenesis, and petrophysics of clay minerals in sandstones Society of Economic Paleontologists and Mineralogists. *Society of Sedimentary Geology (SEPM) Special Publication* **47**, 241 - 264.

Platt J.D. (1993) Controls on clay mineral distribution and chemistry in the early Permian Rotliegend of Germany. *Clay Minerals*, **28**, 393 - 416.

Potter, P. E. (1978) Petrology and chemistry of modern big river sands. *Journal of Geology*, **86**, 423 - 449.

Primmer, T.J., Cade, J., Evans, J., Guyas, J.G., Hopkins, M.S., Oxtoby, N.H., Smalley, P.C., Warren, E.A., Worden, R.H., (1997) Global patterns in sandstone diagenesis: their application to reservoir quality prediction for petroleum exploration, in Kupecz, J.A., Gluyas, J. and Bloch, S., eds., Reservoir quality prediction in sandstones and carbonates. *American Association of Petroleum Geologists (AAPG) Memoir*, **69**, 61 - 77.

Radojević M. and Vladimir, B. N. (1999) “Practical environmental analysis”. The *Royal Society of Chemistry*, 353 - 355.

Ramm, M., (2000). Reservoir quality and its relationship to facies and provenance in Middle to upper Jurassic sequence, Northeastern North Sea: *Clay Minerals*, **35**, pp. 77-95.

Ramm, M., and BjØlykke, (1994). Porosity/ Depth trends in reservoir sandstones: Assessing the quantitative effect of varying pore-pressure, temperature history and mineralogy, Norwegian Shelf Data *Clay Minerals*, **29**, pp. 475-490.

Rankin, A.H. (1990) Fluid inclusions associated with oil and ore in sediments. In: Ala, M., Hatamian, H., Hobson, G.D., King, M.S. and Williamson, I. (eds) Seventy-five Years of Progress in Oil Field Science and Technology. Balkema, Rotterdam, 113 - 124.

Reading, H.G., (1996) Sedimentary environments: processes, facies and stratigraphy. 3rd edition, 688 - 1996.

Rider, M.H., (1996) The geological interpretation of well logs. Petroleum Exploration consultant Rider-French consultant Ltd Cambridge and Sutherland. Halsted press, a division of John Wiley and Sons, New York. pp. 147 - 167.

Robert, B., (1998) The origin and distribution of siderite layers within the Wandoo Field, Dampier Sub-Basin, Australia. Honours thesis, University of Adelaide.

Robison, A.C and Gluyas, (1992) The duration of quartz cementation in sandstones, North Sea and Haltenbanken Basins: *Marine and Petroleum Geology* **9**, pp. 324 – 327.

Rodrigo, D.L., Luiz, F.D.R., (2002) The role of depositional setting and diagenesis on the Reservoir quality of Devonian sandstones from the Solimo~es Basin, Brazilian Amazonian. *Marine and Petroleum Geology*, **19**, 1047 - 1071.

Roedder, E. (1984) Fluid Inclusions: Reviews in Mineralogy, *Mineralogical Society of America*. **12**, 644.

Roedder, E. (1984) Fluid Inclusions: Reviews in Mineralogy, *Mineralogical Society of America*. **12**.

Roedder, E. (1986) The origin of fluid inclusions in gemstones. In Photoatlas of inclusions in Gemstones, E. Gubelin and J. Koivula, eds., ABC Edition, Zurich, 62 - 87.

Roser, B.P., Korsch, R.J., (1986) Determination of tectonic setting of sandstone-mudstone suites using SiO₂ content and K₂O/Na₂O ratio. *Journal of Geology* **94**, 635 - 650.

Roser, B.P., Korsch, R.J., (1988) Provenance signatures of sandstone-mudstone suites determined using discriminant function analysis of major-element data. *Chemical Geology*, **67**, 119 - 139.

Rossel N.C. (1992) Clay mineral diagenesis in Roetliegend aeolian sandstones of the southern North Sea. *Clay Minerals*, **17**, 69 - 77.

Rushdi, A.L., McManus, J., and Collier, R.W., (2000) Marine barite and celestite saturation in seawater. *Marine Chemistry*, **69**, 19 - 31.

Saigal, G.C., BjØrlykke, K. and Larter, S.R. (1992) The effects of oil emplacements on diagenetic processes - Examples from the Fulmar Reservoir sandstones, Central North Sea. *American Association of Petroleum Geologists, Bulletin*, **76**, 024 – 1033.

Salem, A.M., (1995) Diagenesis and isotopic study of Paleozoic clastic sequence (Cambrian and Carboniferous), South-west Sinai. Unpublished PhD thesis Tanta University, p. 246.

Sanyal, P., Bhattacharya, S.K., Prasad, M., (2005) Chemical diagenesis of Siwalik sandstone: Isotopic and mineralogical proxies from Surai Khola section, Nepal. *Sedimentary Geology*. **180**, 57 – 74.

Schalkwyk, H.J., (2005) Assessment controls on reservoir performance and the effect of granulation seam mechanics in the Bredasdorp Basin, South Africa (M.Sc thesis in University of the Western Cape, Cape Town South Africa. Available online.

Scholz, H. & Obst, K. (2004) Einführung in die Geologie Skandinaviens. In: Skandinavien, Sedlacek, P. (ed.), *Geographische Rundschau*, Vol. **46**, 43 - 49.

Schlumberger, (1972) The essentials of log interpretation, practice, Schlumberger Ltd, Paris, France.

Schlumberger, (1982) Essentials of NGS, introduction, Schlumberger Ltd., Paris.

Selley, R.C. (1978) Concepts and methods of subsurface facies analysis: American Association of Petroleum Geologists, Continuing Education Course Notes Series 9, p. 82.

Selley, R.C., (1988) Ancient sedimentary environment and their sub-surface diagnosis. 4th edition published by Chapman and Hall. United Kingdom.

Selly, C.R., 1(1985) Elements of Petroleum Geology, W.H. Freeman and Co. New York.

Serra, O. (1986) Development in Petroleum Science: Fundamentals of Well Log Interpretation 2. The Interpretation of Logging Data, New York, Elsevier Science Publishing Company Inc., **15B**, 684.

Serra, O., (1984) Fundamentals of Well Log Interpretation The Acquisition of Logging Data: *Dev. Pet. Sci.*, 15A, 1, Amsterdam (Elsevier).

Shelton, J.W., (1984) Listric normal faults: An illustrated summary. *American Association of Petroleum Geologist (AAPG) Bulletin*, **68**, 801 - 815.

Sinclair, G., and Duguid, (1990) Laboratory induced damage – A review of the problem: *European Core Analysis Symposium*, 95 - 109.

Sneider, R.M. (1990) Introduction: reservoir description of sandstones, in J.H. Barwis, J.G. McPherson and J.R.J. Studlick, eds., Sandstone petroleum reservoirs: New York, Springer-Verlag, pp 1 - 3.

Sommer, F., (1978) Diagenesis of Jurassic sandstones in the Viking Graben. *Journal of the Geological Society*, London, **135**, 63 - 67.

Srodon, J., Clauer, N., (2001) Diagenetic history of Lower Paleozoic sediments in Pomerania (northern Poland) traced across the Teisseyre–Tornquist tectonic zone using mixed-layer illite– smectite. *Clay Minerals* **36**, 15 – 27.

Swanson, J., (2001) Weathering characteristics of sandstones for building purposes from Eastern Australia: Honours Thesis, University of New South Wales, Sydney, p. 115.

Tandon, S.K., Varshney, S.K., (1991) Origin of selective carbonate cemented (Concretionary) layers within multi-storied sandstone bodies of the Neogene Middle Siwalik Subgroup, NW Hima- P. Sanyal et al., *Sedimentary Geology* 180 (2005) 57 – 74 73 laya, India. Abstract, Birbal Sahni Birth Centenary Symposium on the Siwalik Basin, WIHG, Dehra Dun, India, pp. 45.

Theodoor W.F., (2000) Petrophysical properties from small rock samples using image analysis techniques, ISBN 90-9014-338-6.

Tucker, M.E., (2001) Sedimentary petrology: an introduction to the origin of sedimentary rocks, 3rd edition, ISBN: 978-0-632-05735-1, Blackwell publishing company.

Turrero, M.J. Fernández, A.M., Peña, J., Sánchez, M.D., Wersin, P., Bossart, P., Sánchez, M., Melón, A., Garralón, A., Yllera, A., Gómez, P., Hernán, P., (2006) Pore water chemistry of a Paleogene continental mudrock in Spain and a Jurassic marine mudrock in Switzerland: Sampling methods and geochemical interpretation, *Journal of Iberian Geology*, **2**, 233 - 258.

Turner, J.R., Grobber, N., & Sontundu, S. (2000) Geological modelling of the Aptian and Albian sequences within Block 9, the Bredasdorp Basin, offshore South Africa. *Journal of African Earth Sciences*, **31**, p. 80.

Tyrrell, E., Shellie, R. A., Hilder, E. F., Pohl, C. A., Haddad, P. R. (2009) Fast ion chromatography using short anion exchange columns. *Journal of Chromatograph A*, **1216**, 8512 – 8517.

Van de Kamp, P.C., Leake, B.E., (1985) Petrography and geochemistry of feldspathic and mafic sediments of the North-eastern Pacific margin. *Transactions of the Royal Society of Edinburgh: Earth Sciences*, **76**, 411 - 449.

Van der Plas, L., and A. C. Tobi, (1965) A Chart for judging the reliability of point counting results: *American Journal of Science*, **263**, pp. 87-901.

Van Wagoner, J.C., Posamentier, H.W., Mitchum, R.M., Vail, P.R., Sarg, J.F., Loutit, T.S., Hardenbol, J., (1988) An overview of sequence stratigraphy and key definitions. In: Wilgus, C.K., Hastings, B.S., Kendall, C.G. St. C., Posamentier, H.W., Ross, C.A., Van Wagoner, J.C. (Eds.), *Sea Level Changes—An Integrated Approach*, *Society of Sedimentary Geology (SEPM) Special Publication*, **42**, 39 - 45.

Walderhaug, O., (1994a) Precipitation rates for quartz cement in sandstones determined by fluid inclusion micro-thermometry and temperature –history modelling. *Journal of Sedimentary Research, Section A*, 324 - 333.

Walderhaug, O., (1994b) Temperatures of quartz cementation in Jurassic sandstones from Norwegian continental shelf: Evidence from fluid inclusion. *Journal of Sedimentary Research*, **64**, 311 - 324.

Watanabe, K. (1987) Inclusions in flux-grown crystals of corundum. *Crystal Research and Technology*, **22**, 345 - 355.

Weber, K.J., Klootwijk, P.H., Konieczek, J. and Van Der Vlugt, W.R., (1978) Simulation of water injection in a barrier-bar-type, oil-rim reservoir in Nigeria. *Journal of Petroleum Technology*, 1555 - 1565.

Weibel, R. and Friis, H., (2004) Opaque minerals as keys for distinguishing oxidizing and reducing diagenetic conditions in the Lower Triassic Bunter Sandstone, North German Basin. *Sedimentary Geology*, **169**, pp. 129 - 149. Wiley and Sons, 2nd Edition, pp. 273.

Weltje, G.J. & von Eynatten, H. (2004) Quantitative provenance analysis of sediments: review and outlook. *Sedimentary Geology*, **171**, 1 - 11.

Wilbur, S. (2009) Universal Quantification-The Uncelebrated Strength of ICPMS <http://spectroscopyonline.findanalytichem.com/spectroscopy/Atomic+Perspectives+Column/Universal-Quantification-mdash-The-Uncelebrated-St/ArticleStandard/Article/detail/597218>. Accessed on November 18, 2010.

Williams, L.B., Hervig, R.L., and BjØlykke, K., (1997) New evidence for the origin of quartz cements in hydrocarbon reservoirs revealed by oxygen isotope microanalysis. *Geochemica et Cosmochimica Acta*, **61**, 2529 - 2538.

Wilkinson, M., Haszeldine, R.S., (1996) Aluminum loss from arkoses produces diagenetic quartzites and secondary porosity: Fulmar Formation, North Sea. *Journal of the Geological Society* (London) **154**, 747 - 751.

Wilson, M.D., (1992) Inherited grain-rimming clays in sandstones from eolian and shelf environments: their origin and control on reservoir properties: in Houseknecht, D.W., Pittman, E.D., Keller, W.D.F. (Eds.), Origin, Diagenesis, and Petrophysics of Clay Minerals in Sandstones. *Journal of Sedimentary Geology* SEPM, Special Publication, **47**, 209 - 225.

Wood, E.M. (1995) Oil and gas development potential in Block 9, the Bredasdorp Basin, offshore South Africa. *Oil & Gas Journal*, 27th June, 2010.

Worden, R., and Morad, S, (2000) Clay mineral in sandstones: a review of critical problems. In El-Ghali, M.A.K., Morad, S., Mansurbeg, H., Ajdanlijsky, A.A.C., Ogle, N., Al-Aasm, I., and Sirat, M,: in Distribution of diagenetic alterations within depositional facies and sequence stratigraphic framework of fluvial sandstones: evidence from the Petrohan terrigenous group, lower Triassic, NW Bulgaria. *Marine and Petroleum Geology*, **xxx**, 10.

Worden, R.H and Morad, S., (2000) Quartz cementation in oil field sandstones: a review of the key controversies: in Worden, R.H, Morad, S. (Eds.), Quartz cementation in sandstones. *International Association of Sedimentologist* Special Publication **29**, 1 - 20, Blackwell Science.

Xu, Z. (1999) XAS and XRD Structural Study of Nickel Electrode Materials (Part I) and FTIR quantitative analysis of mineral mixtures (Part II), PhD Dissertation, Michigan Technological University, Houghton, MI.

Zhang, J., Qin, L., Zhang, Z., (2008) Depositional facies, diagenesis and their impact on the reservoir quality of Silurian sandstones from Tazhong area in central Tarim Basin, Western China. *Journal of Asian Earth Sciences*, **33**, 42 - 62.

Related referenced website:

<http://www.fittulsa.com/fis.php>; accessed on 6th April, 2012.

Fluid inclusion studies: Proximal to pay gas (PTPG; in-house-unpublished report, 2011)

<http://spectroscopyonline.findanalytichem.com/spectroscopy/ICP-MS/ICP-MS-AUniversally-Sensitive-GC-Detection-Method/ArticleStandard/Article/detail>; accessed on November 18, 2010.

<http://www.chem.agilent.com/en-us/products/instruments/icp-ms/pages/gp455.aspx>; accessed on 22nd December, 2011.

<http://ocw.mit.edu/courses/earth-atmospheric-and-planetary-sciences/12-110-sedimentary-geology-spring-2007/lecture-notes/ch7.pdf>: accessed on 9th June, 2012.

Douglas, J.C., <http://www.gekko.ro/files/subsurfacef.pdf>: accessed on 18th June 2012.
<http://www.chem.agilent.com/en-us/products/instruments/icp-ms/pages/gp455.aspx>
accessed on 16th December, 2011.

<http://geology.uprm.edu/MorelockSite/morelockonline/digbk/ContMarg.pdf>: accessed on 26th September, 2012.

Society of Petrophysical Wireline Log Analyst SPWLA Glossary, (1984 – 1997).

URL:

<http://www.spwla.org/publications/view/item/933> accessed: 23rd March, 2012

Appendix 1: Mineralogical composition of the F-O gas field samples from XRD.

Well name	Depth(m)	Calcite	Chlorite	Microcline	Muscovite	Plagioclase	Pyrite	Quartz	Rutile	Ankerite	
F-O1	3712	2.96	2.06	1.48	2	6.74	0.19	84.54	0.04	x	
F-O1	3717.52	2.77	1.1	3.52	2.16	8.47	0.16	81.68	0.14	x	
F-O1	3727	0.16	2.12	0.66	1.41	7.12	0.03	80.07	0.14	x	
F-O1	3720.25	2.29	1.48	5.54	3.06	8.1	0.22	79.2	0.1	x	
F-O1	3722.04	0.46	0.93	1.54	2	6.66	0.08	88.33	0	x	
F-O1	3715.01	0	0.98	1.41	1.98	6.54	0.13	88.96	0	x	
F-O1	3725	0.06	0.98	1.63	1.64	5.78	0.07	89.69	0.16	x	
Average		1.24	1.38	2.25	2.04	7.06	0.13	84.64	0.08	0	
F-O2	3620	0.18	3.68	0.85	3.61	8.03	0.15	83.28	0.21	x	
F-O2	3626.05	0.16	2.65	0.84	2.08	4.88	0.62	88.54	0.24	x	
F-O2	3630.03	0.09	1.89	0.69	2.74	6.42	0.49	87.45	0.21	x	
F-O2	3635.04	0.31	5.62	3.38	4.75	7.48	0.53	77.49	0.45	x	
F-O2	3647.01	0.13	3.43	0.9	1.84	5.94	0.05	87.45	0.26	x	
F-O2	3657.13	0.11	6.31	2.19	3.57	9.87	0.63	77.03	0.3	x	
F-O2	3665.01	0.03	4.86	3.48	4.06	11.1	0.23	76.16	0.08	x	
F-O2	3675	0.11	6.31	2.19	3.57	9.87	0.63	77.03	0.3	x	
F-O2	3727	0	4.13	4.92	2.52	7.49	0.05	80.53	0.36	x	
F-O2	3738.1	31.43	2.5	6.54	0.53	7.08	0	30.93	0	20.98	
Average		0.11	4.14	2.60	2.93	7.82	0.34	76.59	0.24	2.10	
F-O3	3705.2	0.57	12.69	5.65	18.74	17.24	1.71	42.54	0.87	x	
F-O3	3713.08	2.1	2.4	0.71	2.39	5.65	0.57	82.51	0.19	3.47	
F-O3	3717.23	5.55	1.92	4.29	1.99	6.53	0.05	79.63	0.04	x	
F-O3	3723	0.94	2.73	2.7	2.2	7.49	0.08	83.69	0.17	x	
F-O3	3725	0.23	1.66	4.49	2.95	7.13	0.07	78.78	0.16	4.55	
F-O3	3730	0.94	2.49	2.26	1.7	6.17	0.06	86.22	0.15	x	
F-O3	3735.05	0.85	4.45	2.76	2.43	7.63	0.09	81.6	0.18	x	
F-O3	3741	0.33	7.49	2.71	6.16	12.71	0.41	69.67	0.53	x	
F-O3	3755	1.85	6.54	3.87	5.85	12.84	0.61	67.98	0.48	x	
F-O3	3765	19.92	3.05	2.67	2.74	8.74	0.15	62.66	0.06	x	
Average		3.33	4.54	3.21	4.72	9.21	0.38	73.53	0.28	0.80	
F-O4	3737.97	0	4.1	2.01	2.06	6.67	0.06	84.98	0.13	x	Dolomite
F-O4	3776.9	0.18	5.69	2.92	3.3	9.62	0.71	77.29	0.28	x	
F-O4	3788.01	4.59	6.52	3.25	3.28	7.8	0.09	74.33	0.14	x	
F-O4	3791.29	7.63	1.17	3.89	1.7	3.72	0.02	81.86	0.02	x	
F-O4	3794.97	1.14	6.04	3.02	3.34	7.97	0.08	78.2	0.21	x	
F-O4	3797	16.28	1.01	3.04	0.58	4.66	0.01	74.42	0	x	
F-O4	3802.38	68.95	0.6	2.61	0	2.29	0.28	20.4	0	x	4.86
F-O4	3807.08	0.98	4.18	2.51	1.88	6.88	0.04	83.4	0.14	x	
Average		12.47	3.66	2.91	2.02	6.20	0.16	71.86	0.12	0	
F-R1	3830.02	0.45	10.07	5.28	16.86	17.07	2.34	41.02	0.74	6.17	
F-R1	3832.04	0.42	11.76	7.83	20.52	17.81	3.07	37.38	1.21	x	
F-R1	3952.04	1.44	6.09	3.26	3.66	10.57	0.22	74.46	0.31	x	
F-R1	3954	9.78	4.85	2.64	2.77	7.88	0.28	71.65	0.14	x	
F-R1	3956.01	14.52	4.39	3.44	4.45	13.65	1.31	58.01	0.22	x	
F-R1	3958.06	1.26	6.68	4.75	3.69	12.92	0.5	69.77	0.43	x	
F-R1	3960.07	2.32	6.01	3.4	3.43	13.81	0.57	70.14	0.33	x	
Average		4.31	7.12	4.37	7.91	13.39	1.18	60.35	0.48	0.88	
F-S1	3623	1.39	5.94	2.5	4.06	13.71	0.69	71.42	0.29	x	
F-S1	3630	2.44	4.82	3.3	4.06	11.82	0.27	73.25	0.05	x	
F-S1	3635.02	0.75	5.74	3.05	4.09	12.39	0.2	73.6	0.18	x	
F-S1	3660	0.18	4.76	2.89	5.44	14.05	0.77	71.58	0.33	x	
F-S1	3664	0.29	4.37	4.02	4.95	7.85	0.6	72.39	0.32	5.2	
F-S1	3668	0.03	4.72	2.61	3.47	11.28	0.37	77.23	0.28	x	
F-S1	3671	0.46	3.86	3.22	3.78	7.86	0.28	72.01	0.3	8.24	
F-S1	3677.1	6.55	3.91	6.58	3.12	12.97	1.13	65.45	0.3	x	
F-S1	3684	3.78	5.31	5.22	8.28	14.3	1.2	61.35	0.57	x	
F-S1	3687.02	5.54	6.58	3.62	5.81	14.87	1.15	62.05	0.36	x	
Average		2.14	5.00	3.70	4.71	12.11	0.67	70.03	0.30	1.34	

Appendix 2: Physico-chemical compositions of the immobile water extracts from the F-O field samples

Well Name	Depth (m)	Ca (mg/l)	Mg (mg/l)	Na (mg/l)	K (mg/l)	Cl (mg/l)	SO4 (mg/l)	Well Name	Depth (m)	Ca (mg/l)	Mg (mg/l)	Na (mg/l)	K (mg/l)	Cl (mg/l)	SO4 (mg/l)
F-01	3712	7.8	1.9	22.8	18.1	22.3	10.5	F-04	3737.97	7.4	3.5	40.9	44.6	78.4	29.4
F-01	3715.01	12.3	3.4	34.5	19.9	49.8	12.9	F-04	3776.9	17.7	3.1	41.9	41.8	60.6	86.7
F-01	3717.52	9.8	2.8	23.4	16.8	31.2	7.7	F-04	3788.01	8.2	1.5	34.1	38	63.1	11.7
F-01	3727	11.7	5.9	21.9	15	23.5	9.1	F-04	3791.29	11.5	2	24.6	27.9	45.1	14
F-01	3722.04	13.7	3.3	41	20.4	63.7	19.5	F-04	3794.97	8.2	1.7	34.5	36.4	49.4	17.7
F-01	3720.25	10.8	4.2	27	20.6	44.9	9.2	F-04	3797	10.5	1.5	19.1	20.6	29.1	5.3
F-01	3725	13.5	4.3	31	18.3	43.2	12.6	F-04	3802.38	16.5	1.8	21.7	17.5	36.8	16.7
F-02	3620	17.5	4.3	39.5	30.7	41	106.5	F-04	3807.08	7.3	1.6	30.1	28.5	45	8.5
F-02	3626.05	4.7	5.4	37.2	30.5	44.9	81.1	Well Name	Depth (m)	Ca (mg/l)	Mg (mg/l)	Na (mg/l)	K (mg/l)	Cl (mg/l)	SO4 (mg/l)
F-02	3727	7.7	2.6	49.6	23.5	87.1	14.5	F-R1	3830.02	3.3	1.2	62.7	37.7	11.9	38.5
F-02	3635.04	5.3	10.2	18.6	29	28.2	91.7	F-R1	3832.04	23.1	5	86.8	57.4	9.6	273
F-02	3647.01	10.1	2.4	66.9	25.7	125	18.2	F-R1	3960.07	15.8	2.2	40.4	32.6	31.8	69.4
F-02	3657.13	9	4.3	45.7	35.4	67.6	72.7	F-R1	3956.01	20.5	2.6	27.9	31.9	12.4	85.1
F-02	3675	7.4	1.4	37.9	22.5	56.6	9.2	F-R1	3954	13.9	2.6	25.3	24.1	22.7	34.9
F-02	3630.03	10.7	6.7	21.9	13	52.7	93.3	F-R1	3952.04	14.1	2.3	39.1	27.7	43.1	52
F-02	3665.01	10	1.4	19.7	13.9	54.9	23.6	F-R1	3958.06	12.9	1.8	35.3	29.8	28	57.3
F-02	3738.1	114	17.5	14.4	11	46.3	440	Well Name	Depth (m)	Ca (mg/l)	Mg (mg/l)	Na (mg/l)	K (mg/l)	Cl (mg/l)	SO4 (mg/l)
F-03	3705.2	2.6	0.5	49.5	33.1	12.2	48.9	F-S1	3623	8.3	1.3	46.9	32.9	58.2	30.1
F-03	3713.08	10	2.7	26.4	25.4	31.9	17.3	F-S1	3630	11	2.6	58.8	34.9	102.6	27.2
F-03	3717.23	12.1	2.5	35.1	21.3	62.3	10.8	F-S1	3635.02	15.9	3.2	113.5	40.6	261.9	19.5
F-03	3725	8.9	3	29.8	22.7	41.5	5.6	F-S1	3668	13	3	61	34.5	101.3	28.6
F-03	3723	10.2	2.9	32.3	24.1	54.4	9.9	F-S1	3664	11.9	3.5	53.2	42.5	69.6	41.2
F-03	3730	10.3	2.1	31.5	19.4	53.6	8.1	F-S1	3660	13.9	3.2	61.4	41.4	99.1	70.1
F-03	3735.05	7.4	1.7	28.3	26.7	31.5	17.5	F-S1	3671	14.5	4	61.7	35.8	100.5	31.6
F-03	3741	5.7	1.2	33	39.5	18.1	36.1	F-S1	3677.1	8.8	1.5	33.8	32.1	27.1	36.7
F-03	3755	13.2	1.6	39.5	30.5	32.5	68.6	F-S1	3684.1	7	0.9	20.5	20.3	18.1	56
F-03	3765	8.1	1	26.9	24.7	36	8.2	F-S1	3687.02	7.7	1.1	45.1	38.9	40	51.3

Appendix 3: Calculated statistical results from major oxide analysis of the F-O field samples

Well name	Depth (m)	CIA	CIW	ICV	Na ₂ O/ K ₂ O	SiO ₂ /Al ₂ O ₃	K ₂ O/Na ₂ O	Na ₂ O+K ₂ O	Well name	Depth (m)	CIA	CIW	ICV	Na ₂ O/ K ₂ O	SiO ₂ /Al ₂ O ₃	K ₂ O/Na ₂ O	Na ₂ O+K ₂ O
F-01	3712.00	37.94	151.01	2.39	0.67	31.46	1.50	1.28	F-04	3737.97	64.14	164.27	1.40	0.52	20.51	1.92	1.88
F-01	3715.01	51.59	153.05	1.84	0.74	33.95	1.35	1.24	F-04	3776.90	65.46	202.01	1.18	0.65	13.75	1.55	2.60
F-01	3717.52	37.78	143.86	2.55	0.57	33.24	1.74	1.20	F-04	3788.01	47.58	161.21	2.11	0.48	14.78	2.07	1.88
F-01	3720.25	35.94	149.98	2.96	0.55	27.40	1.82	1.41	F-04	3791.29	22.86	124.48	4.62	0.38	35.73	2.67	0.90
F-01	3722.04	50.98	155.09	1.59	0.75	33.81	1.33	1.29	F-04	3794.97	60.43	166.31	1.46	0.45	15.20	2.23	2.14
F-01	3725.00	47.94	152.03	1.93	0.65	36.07	1.53	1.32	F-04	3797.00	12.82	119.38	8.28	0.32	38.78	3.16	0.81
F-01	3727.00	40.51	174.47	2.66	0.89	27.37	1.12	1.58	F-04	3802.38	2.31	105.10	45.35	0.17	19.54	5.80	0.35
Average		43.24	154.21	2.28	0.69	31.90	1.48	1.33	F-04	3807.08	56.80	159.17	1.55	0.52	21.53	1.93	1.73
F-02	3620.00	67.57	195.89	1.08	0.76	17.21	1.31	2.21	Average		41.55	150.24	8.24	0.43	22.47	2.67	1.54
F-02	3626.05	67.24	159.17	1.23	0.59	25.15	1.71	1.60	Well name	Depth (m)	CIA	CIW	ICV	Na₂O/ K₂O	SiO₂/Al₂O₃	K₂O/Na₂O	Na₂O+K₂O
F-02	3630.06	67.38	161.21	1.24	0.55	22.99	1.82	1.72	F-R1	3830.20	68.23	195.89	1.01	0.23	3.94	4.27	5.05
F-02	3635.04	71.05	174.47	1.16	0.39	11.88	2.55	2.64	F-R1	3832.04	73.52	198.95	0.86	0.22	3.66	4.45	5.40
F-02	3647.01	65.93	162.23	1.19	0.59	24.78	1.69	1.67	F-R1	3952.04	73.51	198.95	0.86	0.22	3.67	4.45	5.40
F-02	3657.13	67.56	197.93	1.12	0.56	13.55	1.79	2.73	F-R1	3954.00	34.95	167.33	2.81	0.55	15.25	1.82	1.90
F-02	3665.01	62.79	206.09	1.16	0.62	13.98	1.63	2.78	F-R1	3956.01	35.74	243.83	2.37	0.76	9.70	1.31	3.33
F-02	3676.00	59.82	208.13	1.37	0.67	13.65	1.50	2.70	F-R1	3958.06	63.37	237.71	1.13	0.65	10.11	1.54	3.50
F-02	3727.00	66.53	185.69	1.25	0.61	17.29	1.64	2.26	F-R1	3960.07	58.72	242.81	1.22	0.71	10.49	1.40	3.43
F-02	3738.10	5.94	114.28	19.56	0.28	15.16	3.57	0.65	Average		58.29	212.21	1.46	0.48	8.12	2.75	4.00
Average		60.18	176.51	3.03	0.56	17.56	1.92	2.10	Well name	Depth (m)	CIA	CIW	ICV	Na₂O/ K₂O	SiO₂/Al₂O₃	K₂O/Na₂O	Na₂O+K₂O
F-03	3705.20	72.58	226.49	0.88	0.32	4.21	3.14	5.23	F-S1	3623.00	61.13	249.95	1.17	0.93	11.09	1.07	3.11
F-03	3717.23	34.67	156.11	2.80	0.68	25.05	1.47	1.39	F-S1	3630.00	51.79	204.05	1.55	0.70	13.98	1.42	2.52
F-03	3718.08	46.42	155.09	2.03	0.53	22.27	1.87	1.58	F-S1	3635.02	61.42	236.69	1.15	0.86	12.46	1.16	2.96
F-03	3723.00	53.43	168.35	1.57	0.72	23.38	1.39	1.63	F-S1	3660.00	65.97	245.87	0.99	0.67	9.46	1.50	3.64
F-03	3725.00	52.93	171.41	1.52	0.53	21.46	1.89	2.06	F-S1	3664.00	59.18	212.21	1.33	0.56	10.45	1.80	3.14
F-03	3730.00	53.90	154.07	1.53	0.65	30.53	1.55	1.38	F-S1	3668.10	64.60	210.17	1.12	0.66	12.83	1.51	2.76
F-03	3735.05	60.83	169.37	1.40	0.58	18.70	1.72	1.89	F-S1	3671.00	52.39	204.05	1.70	0.64	12.56	1.57	2.67
F-03	3741.00	68.99	217.31	0.97	0.47	8.56	2.12	3.66	F-S1	3677.10	47.73	220.37	1.65	0.61	10.03	1.64	3.17
F-03	3755.00	63.60	240.77	1.08	0.60	8.90	1.67	3.76	F-S1	3684.10	60.53	240.77	1.13	0.51	6.72	1.96	4.16
F-03	3765.00	26.08	191.81	3.50	0.70	14.84	1.43	2.23	F-S1	3687.02	55.35	244.85	1.28	0.61	7.94	1.63	3.80
Average		53.34	185.08	1.73	0.58	17.79	1.83	2.48	Average		58.01	226.90	1.31	0.68	10.75	1.53	3.19